VOLTAGE CONTROL IN DISTRIBUTION SYSTEM WITH DISTRIBUTED GENERATION

Ph.D. THESIS

by

NOVALIO DARATHA

DEPARTMENT OF ELECTRICAL ENGINEERING
INDIAN INSTITUTE OF TECHNOLOGY ROORKEE
ROORKEE – 247667 (INDIA)
JUNE, 2015

VOLTAGE CONTROL IN DISTRIBUTION SYSTEM WITH DISTRIBUTED GENERATION

A THESIS

Submitted in partial fulfilment of the requirements for the award of the degree

of

DOCTOR OF PHILOSOPHY

in

ELECTRICAL ENGINEERING

by

NOVALIO DARATHA

DEPARTMENT OF ELECTRICAL ENGINEERING
INDIAN INSTITUTE OF TECHNOLOGY ROORKEE
ROORKEE – 247667 (INDIA)
JUNE, 2015

INDIAN INSTITUTE OF TECHNOLOGY ROORKEE
ROORKEE

CANDIDATE'S DECLARATION

I hereby certify that the work which is being presented in the thesis entitled **VOLTAGE CONTROL IN DISTRIBUTION SYSTEM WITH DISTRIBUTED GENERATION** in partial fulfilment of the requirements for the award of the Degree of Doctor of Philosophy and submitted in the Department of Electrical Engineering of the Indian Institute of Technology Roorkee is an authentic record of my own work carried out during a period from July 2010 to June 2015 under the supervision of Dr. Jaydev Sharma (Late), Professor and Dr. Biswarup Das, Professor, Department of Electrical Engineering, Indian Institute of Technology Roorkee.

The matter presented in this thesis has not been submitted by me for the award of any other degree of this or any other Institute.

(Novalio Daratha)

This is to certify that the above statement made by the candidate is correct to the best of our knowledge.

(Biswarup Das)
Supervisor

The Ph. D. Viva-Voce Examination of Novalio Daratha, Research Scholar, has been held on 7th April 2016.

Chairman, SRC **External Examiner**

This is to certify that the students has made all the correction in the thesis.

(Biswarup Das)
Supervisor

Head of Department

Abstract

Voltage regulation in distribution system is a control effort for keeping the magnitude of all voltages in the distribution system within prescribed limits. Voltage regulation aims at avoiding two types of violations: overvoltages and undervoltages. An undervoltage (overvoltage) violation happens if magnitude of the voltage is between 80% and 90% (110% and 120%) of the nominal value for longer than one minute. Voltage regulation is usually the responsibility of the network operator. It is important since all devices are optimized to operate in rated voltages and voltage violations may reduce the performance and lifetime of those devices.

The main cause of voltage variations is the behaviour of electricity customers and distributed generations. Since the distribution system loads vary over time, the voltage drops on distribution lines also vary. Sometimes, this variation may lead to an undervoltage or an overvoltage situation. In addition, the connection of distributed generation (DG) resources in a distribution network introduces another source of fluctuations in power flow in the network. This also may introduce voltage violations. In the future, due to the environmental and economic considerations, the penetration of DG resources in the distribution system will increase. In addition, electricity consumption will also grow steadily. Consequently, the risk of violations in voltages will be higher in the future. This further emphasizes the importance of voltage regulation in distribution network.

The voltage regulation is carried out by different types of controllers such as On-load tap changer (OLTC), shunt capacitor (SC) and static var compensator (SVC). An OLTC is an autotransformer that has multiple taps and, hence, can change its voltage ratio while serving the loads. Shunt capacitors are connected to the network in shunt through appropriate switching mechanism and by varying the number of shunt capacitors the reactive power injected to the system is varied thereby varying the system voltage. At any bus, either a single capacitor or a bank of capacitors may be connected. An SVC is a combination of shunt capacitor, shunt reactor and power electronic devices, which can smoothly change its effective reactance according to the network operating condition and its control strategy. The settings of OLTC (tap setting) and SC (number of SC) are discrete in nature. On the other hand, the setting of an SVC can be discrete (slope) or continuous (reference voltage). Nevertheless, due to power electronic devices, its effective reactance can take continuous values.

For effective voltage regulation, the settings of all the above voltage regulation devices need to be determined in a coordinated manner. These settings are usually determined such that the network is operated optimally in some sense. Depending upon the preference of the network operator, different objectives (such as loss minimization, improvement of system voltage profile etc.) are adopted for optimal operation of the network. Therefore, the voltage regulation problem can be posed as an optimization problem. The solution of the optimization problem gives the optimal and coordinated settings of the controllers.

In most of the previous works on voltage regulation in distribution system, SVC has not been considered as most of the distribution networks do not have any SVC installed. Only few works have considered SVC in voltage regulation problem in distribution system. However, these works have considered only balanced network. On the other hand, distribution systems are generally unbalanced networks. Moreover, in the future, the presence of SVC in the distribution system is expected to increase because of its fast response and reduction in price. Consequently, there is a need for a model for SVC that can be used in voltage regulation problem of an unbalanced distribution system. Furthermore, the available works in voltage regulation problem use constant reactive power injection model of SVC. However, another popular operating mode of an SVC is voltage control mode. Hence, a model for SVC operating in voltage control mode for voltage regulation problem in unbalanced distribution system is also required.

To address the above issue, a constrained (involving both equality and inequality constraints), multi-objective optimisation problem has been formulated in Chapter 2 for voltage regulation in an unbalanced distribution system. The formulated problem considers single-phase and multi-phase OLTC, SC and SVC as voltage control devices. Further, the SVC is assumed to operate in voltage control mode using droop control. In this mode, the slope setting and reference voltage of the SVC need to be determined. It is to be noted that the slope setting is treated as discrete variable while the reference voltage is treated as continuous variable. The objective functions include minimization of power loss in the system and the number of switching of OLTC, SC and SVC. The equality constraints involve the nodal current balance equations and the relations between current and voltages of all elements in the network. The inequality constraints represent the regulatory and physical limits of the network and its elements. The regulatory limits include the limits on voltage magnitudes and amount of unbalance in the system. The physical limits

involve the operational limits of OLTC, SC and SVC. As the formulated optimisation problem involves both discrete (tap positions of OLTCs, number of SCs, and slope settings of SVC) and continuous (reference voltage of SVC) variables, the formulated optimization problem is a mixed integer non-linear programming (MINLP) problem.

To solve the above MINLP problem, a two-stage solution methodology has been developed. In the first stage, the original MINLP is relaxed into a non-linear programming (NLP) problem by considering all the discrete variables as continuous variables and subsequently, the relaxed NLP problem is solved by using interior point method (IPM). The major purpose of this stage is reduction in the size of the discrete search space. From the solution of the NLP relaxation, the two closest possible discrete values are selected. In this manner, the discrete search space is reduced significantly. In the second stage, from the selected discrete values, a smaller MINLP is formulated involving only binary discrete values. This smaller MINLP is solved using branch and bound (BB) method. With this two-stage approach, the formulated problem has been solved for one-hour-ahead study.

The effectiveness of the developed method has been investigated on a modified IEEE 123 bus unbalanced radial distribution system. This system has one single-phase OLTC, one two-phase OLTC, two three-phase OLTCs, three single-phase SC, one three-phase SC, and one three-phase SVC. In addition, it has many photovoltaic (PV) generations as well. Further, while solving the optimization problem, both uniform and non-uniform operations of the multi-phase control devices have been considered. When a multi-phase device operates uniformly, its settings for all its phases are kept the same. On the other hand, in non-uniform operation, the settings in different phases are allowed to be different. The performance of the developed two-stage algorithm has been investigated on several test cases in this system. It was found that to solve the formulated optimization problem for 24 one-hour periods, the proposed algorithm takes less than 10 minutes. Further, the performance of the developed algorithm has also been tested for the case of fast moving clouds. In this case, one-step-ahead optimization has been used to solve the problem and the optimal solution could be found within 2 minutes. This is a significant improvement considering that the original MINLP problem was unsolved even after 8 hours (using a branch-and-bound solver). As a result, the proposed two-step solution method has the potential for practical application.

In Chapter 2, the one-hour-ahead optimization study has been conducted assuming that the

load and generation patterns remain fixed during the one-hour period of study. However, during this one-hour period, loads and generations can vary significantly. Therefore, upon implementation of the settings of the controllers (obtained assuming fixed load and generation pattern), there may be voltage violations or suboptimal operation of the network. To avoid this possibility, it is important to consider the uncertainties in load and generation in the voltage regulation problem. In Chapter 3, application of robust optimization technique is proposed to consider these uncertainties. To apply the robust optimization (RO) technique, the property of monotonicity of the voltage magnitudes against the variation of load and generation has been used. Following this property, the extreme values of magnitudes of voltages correspond to the situations in which loads and generations are also at their corresponding extreme values. Therefore, in the robust optimization method, different extreme scenarios are considered and if the solution obtained by the RO method ensures the acceptable operation of the network in all these extreme scenarios, then it can be safely concluded that the operation of network would be acceptable under the actual load and generation variation within the limiting values.

In Chapter 3, from the extreme values of loads and generations, 32 extreme scenarios have been generated. Furthermore, the optimization problem discussed in Chapter 2 has been extended to consider all of these extreme scenarios at once. This chapter conjectures that the optimal solution of the problem corresponds to the robust settings of the controllers. The settings are robust if the network remains feasible for all possible values of load and generation as long as these values remain within the intervals defined by the extreme scenarios.

However, the robust optimization problem cannot be solved using the method described in Chapter 2. Therefore, a new two-stage approach has been proposed based on the absolute values constraint method. The first stage of Chapter 3 is same as that of Chapter 2. However, in the second stage, the binary MINLP are reformulated again. Each binary variable is replaced by a continuous variable that are constrained to have binary values using the absolute value constraints. The new problem is an NLP in which all variables are continuous. Using the new proposed methodology, the RO problem has been solved to compute the controller settings in the modified IEEE 123 bus system. Moreover, Monte Carlo Simulation (MCS) studies have been carried out to verify the above conjecture. The boundaries of magnitudes of voltages calculated using RO method have been compared with those calculated using MCS studies. It was found that the discrepancies

between the values obtained by the RO method and the MCS method are small for all practical purpose thereby validating the above conjecture. Furthermore, the performance of the proposed method has also been tested for a representative day with fast moving clouds and the performance was found to be quite satisfactory. However, as the price of the robustness, the robust solution is a little bit worse than the non-robust solution in terms of the optimal value of the objective function. Further, the best operating strategy corresponding to robust solution differs from that corresponding to non-robust solution discussed in Chapter 2.

In Chapters 2 and 3, the topology of the system has been assumed to be fixed. However, due to various reasons, such as enhancement of network efficiency, restoration of supply after the occurrence of a fault etc., the configuration of the system is altered. Because of this change in topology, the controller settings obtained in one configuration may not be feasible in other configuration(s). Therefore, it is important to ensure that the obtained controller settings remain feasible for all possible, pre-selected configurations of the network. However, in the literature, no such methodology has been proposed to consider topology variation in voltage control problem.

To address the above issue, in Chapter 4, a methodology to find the optimal settings of the controllers in voltage control problem has been proposed considering the variation in topology. The method ensures that for any configuration within a set of pre-selected topologies, all bus voltages across the network remain within their specified limits. This method assumes that network reconfiguration is carried out separately from voltage regulation studies and that topological changes of the network occur within one-day period.

The optimal settings obtained by the proposed method can be maintained at the same values even when the network changes its topology within the set of pre-selected configurations. Hence, the solution is robust against uncertainty of topologies. Simulation studies have been carried out on the modified IEEE 123 bus system to verify the efficacy of the proposed method. The results obtained show that when more than two topological changes in a day are expected, the proposed method is better than the conventional voltage regulation method that considers no topological change.

In most of the previous works in the literature and in Chapters 2-4 of this thesis, all OLTCs are assumed to operate in time-of-day mode. In this mode, the positions of a tap of an OLTC is optimized beforehand in the off-line mode and communicated to the OLTC. The OLTC will change its

tap position based on the schedule communicated to it by the network operator. However, in this mode of operation, a good forecast of future variation of load and generation is required. If the actual load and generation conditions are different from the forecasted values, the degree of optimality may be reduced. In addition, it requires communication infrastructure for communication between the central control centre and the controllers.

On the other hand, an OLTC can also be controlled in line drop compensation (LDC) mode. In this mode, the position of a tap of an OLTC is selected by the local controller based on the setting of the LDC and the measured local current and voltage. Hence, if loading condition changes significantly, the OLTC will sense it and adjust the position of its tap according to its LDC settings. However, the settings of LDC are generally chosen based on heuristics rules. Hence, coordination with other OLTCs and controllers cannot be done optimally.

Now, in the literature, no optimization model of OLTC operating in LDC mode for voltage regulation studies could be found. To address this issue, Chapter 5 proposes an optimization model of an OLTC operating in LDC mode. The developed model can be integrated into the optimization problems discussed in the previous chapters. As a result, it is possible to coordinate an OLTC operating in LDC mode with other controllers in the network.

In the LDC mode, there are four parameters corresponding to each tap of an OLTC. These are: voltage reference, voltage bandwidth, resistance setting and reactance setting. All of these are discrete quantities. Based on the values of these parameters and the measured local current and voltage, the position of a tap of the OLTC can be decided by the microprocessor of the OLTC. Hence, if an OLTC operates in LDC mode, the position of its taps is no longer a control variable as is the case in previous chapters. With the proposed optimization model, the values of the parameters of LDC of an OLTC are calculated once in every 24-hour. Conventionally, the modification of the settings of LDC is done seasonally or when there is a significant change in the loading condition of the network. Hence, the LDC mode does not need the availability of a communication network.

However, the optimization problem that considers LDC operation cannot be solved using the methods described in the previous chapters. Hence, another new two-stage method has been proposed. The first stage of Chapter 5 is same as that of Chapter 2. There are two differences between the second stage of Chapter 5 and that of Chapter 3. Firstly, from the solution of the first stage,

three closest possible discrete values are considered for voltage reference, voltage bandwidth, resistance setting, reactance setting and taps of OLTCs. However, for shunt capacitor and SVC, only two discrete values are considered. Hence, the new MINLP has ternary, binary and continuous variable. Secondly, the exact penalty function method is used to solve the new MINLP. The relaxation is applied for both equality and inequality constraints

Simulation studies have been carried out for a number of possible operating strategies of OLTC, SC, and SVC. The results indicate that the proposed model and method can be used to coordinate an OLTC operating with LDC mode with other controllers. Moreover, the computational times for 24-hour-ahead optimization are shorter than 2 minutes. Hence, the proposed model and method can be quite useful in planning and operation in unbalanced distribution system where OLTCs operate in LDC mode.

In all the previous chapters, constant power load has been assumed. However, this model is accurate only for industrial loads. On the other hand, commercial and residential loads are voltage dependent. Therefore, it is important to consider different types of loads in voltage regulation problem. Chapter 6 explores this issue in more detail. In this chapter, a polynomial model of voltage-dependent loads is considered and the obtained results have been compared with the results obtained using constant power loads. Detail comparative studies obtained with constant power loads considering multiple topology and line drop compensation have also been carried out. The optimization problem corresponding to voltage-dependent loads are harder to solve than that corresponding to constant-power loads. This is evident because the methods described in Chapters 2, 3 and 4 cannot solve the optimization problem with voltage-dependent loads. However, the method described in chapter 5 solves the problem with voltage-dependent loads successfully. However, it is to be noted that for considering the uncertainties in voltage dependent loads, it is quite difficult to find the intervals of possible values of load power of the voltage dependent loads due to the unknown voltage magnitudes at buses at which those loads are connected. Consequently, uncertainties in voltage dependent loads in voltage regulation problem could not be undertaken in this work.

In general, the optimal solution corresponding to constant-power loads differs from those corresponding to voltage-dependent loads. The significance of the difference may depend on the characteristics of each distribution system. However, the simulation studies verify the efficacy and

the efficiency of the proposed method. Thus, the proposed method has the potential to be used in planning and operation of a distribution system that serves many voltage-dependent loads such as commercial and residential customers.

Outline of the thesis

Based on the above discussion, the outline of the thesis is as follows:

- In Chapter 2, a constrained (involving both equality and inequality constraints), multi-objective optimisation problem has been formulated for voltage regulation in an unbalanced radial distribution system. The formulated problem considers single-phase and multi-phase OLTC, SC and SVC as voltage control devices. The formulated optimisation problem involves both discrete and continuous variables and therefore, it is a mixed integer non-linear programming (MINLP) problem. To solve this MINLP problem efficiently, a two-stage solution method has been developed. A large number of test cases (including a case of fast moving clouds) have been considered on the modified IEEE 123 bus unbalanced radial distribution system to validate the effectiveness of the developed solution procedure. However, the formulated optimization problem in this chapter assumes that both load and generation conditions are accurately known and, also, the topology of the system remains fixed.

- In Chapter 3, the uncertainties in both load and generation conditions are considered in the voltage control problem. For considering these uncertainties, the voltage regulation problem is formulated as a robust optimisation problem. As the two-stage solution method developed in Chapter 2 is unable to solve this RO problem satisfactorily, a new two-stage solution procedure has been developed to solve this RO problem. Again, several test cases (including fast moving clouds) have been considered on the modified IEEE 123 bus system to validate the efficacy of the developed solution procedure to solve the robust voltage control problem. However, in this chapter also, it has been assumed that the topology of the system remains fixed.

- In Chapter 4, uncertainty in topology has been considered in the voltage regulation problem. However, in this case, no uncertainty in the load and generation conditions has been considered. The solution of the formulated problem ensures that the settings of the controllers can

be maintained at the same values even when the network changes its topology within the set of pre-defined configurations. Moreover, the controller settings also ensure that the bus voltages in the network remain within the limits for any topology within the set of pre-defined configurations. As in the previous chapters, several studies on the IEEE 123 bus system have been carried out to validate the effectiveness of the proposed method.

- In Chapter 5, LDC mode of operation of an OLTC is considered (in Chapters 2-4, time-of-day mode of OLTC has been used). To integrate the LDC mode of OLTC in the voltage regulation problem and find its settings in coordination with the other control devices, a new optimisation model of LDC has been developed. Simulation studies have been carried out on the IEEE 123 bus system to investigate the comparative performances of OLTC operating in time-of-day mode and LDC mode.

- In Chapter 6, voltage dependent loads have been considered (in all the previous chapters, constant power loads have been used). To represent the voltage dependent loads, polynomial model of the load has been used. Detailed studies have been carried out on the IEEE 123 bus system to compare the obtained results with those obtained with constant power load corresponding to uncertain topology and LDC mode of operation of OLTC.

- In Chapter 7, major conclusions of this work are given and a few suggestions for future work in this field of study are also provided.

Contribution of the thesis

To summarize, the major contributions of this thesis are as follows:

- For including the SVC operating in voltage control mode in voltage regulation in unbalanced radial distribution system, a current-voltage based optimization model using Cartesian coordinate has been developed and a two-stage optimization method has been proposed to solve it.

- For considering the uncertainty of load and generation, a robust-optimization-based voltage regulation problem has been formulated and its continuous reformulation that is based on complementarity condition has been proposed.

- For considering frequent topological changes in distribution system, the exact penalty based relaxation method has been proposed to solve voltage regulation problem considering multiple topologies.

- An optimization model of line drop compensation of an OLTC has been developed. The model has been integrated into the model of voltage regulation problem. However, this model introduces an integer-valued state variable corresponding to the position of a tap of an OLTC. A modelling approach to represent the integer state variable using continuous variable has been proposed.

- A study on the effect of voltage dependent load on the performance of voltage regulation problem has been carried out to identify the strengths and weaknesses of the popular practice of using constant-power load in voltage regulation problem. The studies corresponding to multiple topology approach and line drop compensation have been carried out.

Acknowledgements

In the name of God, the infinitely Good, the All Merciful

All praise is due to God, Lord of the worlds.

I take this opportunity to express my sincere gratitude to toward both of my guides: the late Prof. Jaydev Sharma and Prof. Biswarup Das. I have been very fortunate to receive their continuous academic advice, constant encouragement, endless patience, and priceless guidance and support throughout this work. They have been training me the skill and art to identify attractive and important research problems and to propose effective solutions to them.

During my work in Roorkee, I have been served by three excellent heads of department i.e. Prof. Vinod Kumar, Prof. Pramod Agrawal and Prof. S.K. Srivastava. They have ensured my stay in Electrical Engineering Department as comfortable as possible and solve many problems I have faced. In addition, officers in the department, Mr. Manmohan and Rishab in particular, have been continuously helping me in all possible steps. Also, techinicians in Power System Simulation Laboratory, Mr. Ravinder and Mr. Kapoor, deserve my highest appreciation.

I wish also to mention the memorable conversation I have with Prof. Vinay Pant and Prof. Dewal. We had many small talks in the way or in chai shop in which I have received many attention and suggestion.

My journey in Roorkee are blessed with many friends: Pushkar Triphati, Javed Dhillon, Neeraj Gupta, Muhamad Nabab Alam, Hari Krishna Muda, Akhilesh Mathur, Haresh Shabhadia, Afroz Alam, Shuklal Sisodiya, Sajan, Sandeep Kaur, Manasa Mandala and many more. In additions, I have great neighbors in KIH such as Eka, Amanda, Ahmad Nawawi, Tursinbay, Almutaz Abdelfatah, Adrian, Mohammad Atia, Batirbek to mention a few. I have also spent many hours in tennis court with Kuldeep Singh, Javed, and Firdaus. Furthermore, there are many friends also whom I meet mainly in masjid such as Muhammad Akram, Irfan, Amir, Aslam, Muzaffar and Farhad. All of you are elements of a beautiful mozaic of my life in Roorkee.

I must not miss Mr. Rattan Lal and his team in Indian Council for Cultural Relation who pick me from airport when I arrived to Delhi for the first time. They have work very well to ensure that I have the financial support I needed as a student for almost five years.

I received a lot of support from two education attache of Indonesian Embassy in New Delhi i.e. Prof. Son kuswadi and Prof. Iwan Pranoto. Both of them have been instrumental in supporting my work in Roorkee.

Moreover, I thank all of my colleagues in Electrical Engineering Department of University of Bengkulu who support my study here in many ways. Also, I thank University of Bengkulu for granting a leave for pursuing my PhD in IIT Roorkee.

For their endless support, love, patience, and encouragement, I thank my mother, Ismawati, my father, Damhuri, and my sisters, Dian Kusumawati, Irma Nurliawati and Yulia Wulandari. I am very fortunate that my parents give me the best education, the warmest care, the righteous upbringing and the best in everything

Most importantly, I dedicated this thesis to my wife, Marisadonna Asteria, and our son, Ghatreef Zaviyar Akram. During my PhD period I have not been able to fulfil all my responsibilities as a husband and a father properly. No words can express my gratitude and appreciation to her, and my in-laws, for the kind support and tremendous care. Icha is the twin of my soul and the love of my life.

Novalio Daratha

Roorkee, June 2015

Contents

List of Tables

List of Figures

List of Abbreviations

ACOPF Alternating Current Optimal Power Flow.

AMPL A Mathematical Programming Language.

BBM Branch and Bound Method.

CVR Conservation Voltage Regulation.

DFIG Doubly-Fed Induction Generator.

DG Distributed Generation.

DNO Distribution Network Operator.

DSTATCOM Distribution Static Synchronous Compensator.

ELS Energy Loss per Strategy.

EPS Electric Power System.

Eq. Equation.

Eqs. Equations.

Fig. Figure.

GA Genetic Algorithm.

IEA International Energy Agency.

IEEE Institute of Electrical and Electronics Engineering.

IPM Interior Point Method.

IPOPT Interior Point Optimizer.

kVA kilo Volt Ampere.

kVAR kilo Volt Ampere Reactive.

kW kilo Watt.

kWh kilo Watt hour.

LDC Line Drop Compensation.

LV Low Voltage.

MCS Monte Carlo Simulation.

MINLP Mixed Integer Non Linear Programming.

MVA Mega Volt Ampere.

NLP Non-Linear Programming.

OLTC On-Load Tap Changer.

OPF Optimal Power Flow.

PCC Point of Common Connection.

PMSG Permanent Magnet Synchronous Generator.

pu per unit.

PV Photo voltaic.

RO Robust Optimization.

SC Shunt Capacitor.

SCIG Squirell Cage Induction Generator.

SG Synchronous Generator.

SR Shunt Reactor.

SVC Static Var Compensator.

SVR Step-type Voltage Regulator.

UPFC Unified Power Flow Controller.

VDMI Voltage Drop Magnitude Index.

VMI Voltage Magnitude Index.

VR Voltage Regulator.

VRP Voltage Regulation Problem.

VSC Voltage Source Conventer.

VUI Voltage Unbalance Index.

VVC Volt/Var Control.

ZIP Combination of constant-impedance (Z), constant-current (I) and constant power (P) loads.

List of Symbols

$\bar{\mathbf{A}}, \bar{\mathbf{B}}, \mathbf{C}, \mathbf{D}$ (3×3) matrices used in modeling feeder, transformer, OLTC and X_{SL}.

$\mathbf{A_x}, \mathbf{A_y}, \mathbf{B_x}, \mathbf{B_y}$ Real and imaginary part of $\bar{\mathbf{A}}$ and $\bar{\mathbf{B}}$.

b_F^r The bus at which receiving end r of feeder segment F is connected.

b_F^s The bus at which sending end r of feeder segment F is connected.

b_G The bus at which generator G is connected.

b_k Binary variable for discrete variable d_k^2, $b_k \in \{0, 1\}$.

b_k^c A continuous variable corresponding to a binary variable b_k corresponding to time t

b_{lk}, b_{uk} Two auxiliary continuous variables corresponding to k^{th} binary variable b_k

b_{lop+}^t A continuous variable associated with b_{op+}^t

b_{lop-}^t A continuous variable associated with b_{op-}^t

b_o The bus at which OLTC o is connected.

b_{op+}^t A continuous variable which is constrained to be in $\{0, 1\}$ by (5.18b)- (5.18d)

b_{op-}^t A continuous variable which is constrained to be in $\{0, 1\}$ by (5.18e)- (5.18g) corresponding to time t

b_S^r The bus at which receiving end r of series component S is connected.

b_S^s The bus at which sending end s of series component S is connected.

b_{uop+}^t A continuous variable associated with b_{op+^t}

b_{uop-}^t A continuous variable associated with b_{op-}^t

b_v The bus at which SVC v is connected.

$\mathbf{c}$ Vector of continuous variables.

c_k^1 k-th continuous variable in NLP (stage 1) corresponding to d_k^1.

c_k^{1*} The optimum value of c_k^1.

$\Delta\bar{E}_o$ The voltage error corresponding an OLTC o which operates in line drop compensation mode.

$\Delta\bar{E}_o^t$ The voltage error corresponding an OLTC o which operates in line drop compensation mode at time t.

δ_k The step size of d_k^1.

δ_{op} The step size of tap_{op}^t.

$\mathbf{d}$ Vector of discrete variables.

d_k^{lb} The nearest lower boundary. It is the d_k^1 closest to and smaller than c_k^{1*}.

D_{NC} The non-containment distance as defined in Eq. (3.23).

D_{NC}^{ipl} The non-containment distance corresponding to lower bounds at phase p of bus i as defined in Eq. (3.25).

D_{NC}^{ipu} The non-containment distance corresponding to upper bounds at phase p of bus i as defined in Eq. (3.24).

db_o Bandwidth of the line drop compensation of an OLTC o.

db_o^{max} Maximum value of the bandwidth of an OLTC o.

db_o^{min} Minimum value of the bandwidth of an OLTC o.

db_{oa} Bandwidth of the line drop compensation of an OLTC o corresponding to phase a.

db_{ob} Bandwidth of the line drop compensation of an OLTC o corresponding to phase b.

db_{oc} Bandwidth of the line drop compensation of an OLTC o corresponding to phase c.

d_k^1 k-th discrete variable in initial MINLP (stage 1).

d_k^2 k-th discrete variable in the binary MINLP (Stage 2).

d_k^{2*} The optimum value of d_k^2.

$\bar{E}^p(i)$ Complex line voltage at bus i and phase p, p.u.

$\bar{E}_{yi}^{2ts}$ Negative-sequence voltage of bus i corresponding to time t and scenario s.

$\bar{E}^{b_o pt\tau}$ The complex voltage at phase p of the secondary terminal b_o of an OLTC o corresponding to time t and topology τ.

$\bar{E}^{ipt\tau}$ The complex voltage at phase p of bus i corresponding to time t and topology τ.

$\bar{E}^{ipts}$ The complex voltage at phase p of bus i corresponding to time t and scenario s.

$\bar{E}^{ip}$ The complex voltage at phase p of bus i.

$\bar{\mathbf{E}}(m)$ (3×1) vector of complex voltage at bus m
= $[\bar{E}^a(m)\ \bar{E}^b(m)\ \bar{E}^c(m)]^T$.

E_{0x}^{ip} The real part of the rated voltage at phase p of bus i.

E_{0y}^{ip} The imaginary part of the rated voltage at phase p of bus i.

$\bar{E}_i^2$ Negative-sequence voltage of bus i.

$E_{xit\tau}^2$ Real part of negative-sequence voltage of bus i corresponding to time t and topology τ.

E_{xi}^2 Real part of negative-sequence voltage of bus i.

$E_{yit\tau}^2$ Imaginary part of negative-sequence voltage of bus i corresponding to time t and topology τ.

E_{yi}^2 Imaginary part of negative-sequence voltage of bus i.

$\bar{E}_i^{1ts}$ Positive-sequence voltage of bus i corresponding to time t and scenario s.

$\bar{E}_i^1$ Positive-sequence voltage of bus i.

$E^1_{xit\tau}$ Real part of positive-sequence voltage of bus i corresponding to time t and topology τ.

E^1_{xi} Real part of positive-sequence voltage of bus i.

$E^1_{yit\tau}$ Imaginary part of positive-sequence voltage of bus i corresponding to time t and topology τ.

E^1_{yi} Imaginary part of positive-sequence voltage of bus i.

$\bar{E}^{mea,t}_o$ The voltage measured at the secondary terminal of an OLTC o at time t.

$\bar{E}^{mea}_o$ The voltage measured at the secondary terminal of an OLTC o.

$E^{ref,max}_o$ Maximum value of the reference voltage for an OLTC o operating in LDC mode.

$E^{ref,min}_o$ Minimum value of the reference voltage for an OLTC o operating in LDC mode.

E^{ref}_o Reference voltage for OLTC o operating in LDC mode.

E^{ref}_{oa} Reference voltage at phase a for OLTC o operating in LDC mode.

E^{ref}_{ob} Reference voltage at phase b for OLTC o operating in LDC mode.

E^{ref}_{oc} Reference voltage at phase c for OLTC o operating in LDC mode.

$\bar{E}^1_v$ Positive-sequence voltage of SVC v.

$\bar{E}^{ref}_v$ Reference voltage for SVC v.

$E^{ref,t\tau}_v$ Reference voltage for SVC v corresponding to time t and topology τ.

$E^{ref,ts}_v$ Reference voltage for SVC v corresponding to time t and scenario s.

$\mathbf{E}_x(m)$ Real part of $\bar{\mathbf{E}}$.

$\mathbf{E}^{t\tau}_x(b^r_S)$ Vector of real part of the voltage at bus b^r_S corresponding to time t and τ.

$\mathbf{E}^{t\tau}_x(b^s_S)$ Vector of real part of the voltage at bus b^s_S corresponding to time t and τ.

$E^{ipt\tau}_x$ Real part of the voltage at phase p of bus i corresponding to time t and topology τ.

E_x^{ipts} Real part of the voltage at phase p of bus i corresponding to time t and scenario s.

E_x^{ipt} Real part of the voltage at phase p of bus i corresponding time t.

E_x^{ip} Real part of the voltage at phase p of bus i.

$E_x^{pt\tau}(b_v)$ Real part of the voltage at phase p of bus b_v corresponding to time t and τ.

$E_x^{p}(b_v)$ Real part of the voltage at phase p of bus b_v.

$\mathbf{E}_y(m)$ Imaginary part of $\bar{\mathbf{E}}$.

$\mathbf{E}_y^{t\tau}(b_S^r)$ Vector of imaginary part of the voltage at bus b_S^r corresponding to time t and τ.

$\mathbf{E}_y^{t\tau}(b_S^s)$ Vector of imaginary part of the voltage at bus b_S^s corresponding to time t and τ.

$E_y^{ipt\tau}$ The imaginary part of the voltage at phase p of bus i corresponding to time t and topology τ.

E_y^{ipts} The imaginary part of the voltage at phase p of bus i corresponding to time t and scenario s.

E_y^{ipt} The imaginary part of the voltage at phase p of bus i corresponding to time t.

E_y^{ip} The imaginary part of the voltage at phase p of bus i.

$E_y^{pt\tau}(b_v)$ Real part of the voltage at phase p of bus b_v corresponding to time t and τ.

$E_y^{p}(b_v)$ Imaginary part of the voltage at phase p of bus b_v.

$\mathbf{g}$ vector of functions of equality constraints

$\mathbf{g}_i$ vector of functions of equality constraints corresponding to i^{th} scenario.

g_i The i^{th} function of equality constraint.

$\mathbf{h}$ vector of functions of inequality constraints

$\mathbf{h}_i$ vector of functions of inequality constraints corresponding to i^{th} scenario.

h Discrete time index $h \in \{0, 1, ..., h^{max}\}$.

h^{max} Maximum value of h.

h_j The j^{th} function of inequality constraint.

$\bar{I}_G$ Complex current of generator G.

$I_{Gx}^{ipt\tau}$ Real current of generator G which is connected to bus i at phase p corresponding to time t and topology τ.

I_{Gx}^{ip} Real current of generator G which is connected to bus i at phase p.

$I_{Gy}^{ipt\tau}$ Reactive current of generator G which is connected to bus i at phase p corresponding to time t and topology τ.

I_{Gy}^{ip} Reactive current of generator G which is connected to bus i at phase p.

$\bar{I}_{ij}^{p\tau}(h)$ The complex current flowing in the feeder between bus i and j at phase p at h-th hour in topology τ, p.u.

$\bar{I}_{ij}^{ps}(h)$ The complex current flowing in the feeder between bus i and j at phase p at h-th hour in scenario s, p.u.

$\bar{I}_{ij}^{p}(h)$ The complex current flowing in the feeder between bus i and j at phase p at h-th hour, p.u.

$I_{Lx}^{ipt\tau}$ Real current of load L which is connected to phase p of bus i corresponding to time t and topology τ.

I_{Lx}^{ipts} Real current of load L which is connected to phase p of bus i corresponding to time t and scenario s.

I_{Lx}^{ip} Real current of load L which is connected to phase p of bus i.

$I_{Ly}^{ipt\tau}$ Reactive current of load L which is connected to phase p of bus i corresponding to time t and topology τ.

I_{Ly}^{ipts} Reactive current of load L which is connected to phase p of bus i corresponding to time t and scenario s.

I_{Ly}^{ip} Reactive current of load L which is connected to bus i at phase p.

$\bar{I}_{o}^{mea,t}$ The current measured at the secondary terminal of an OLTC o at time t.

$\bar{I}_{o}^{mea}$ The current measured at the secondary terminal of an OLTC o

$\bar{I}_S$ Complex current of series component S.

$\bar{\mathbf{I}}_S$ (3×1) vector of complex current of series component $S = [\bar{I}_S^a \ \bar{I}_S^b \ \bar{I}_S^c]^T$.

$\mathbf{I}_{Sxr}$ (3×1) vector of real component of $\bar{I}_S$ at its receiving end.

$\mathbf{I}_{Sxr}^{t\tau}$ (3×1) vector of real component of $\bar{I}_S$ at its receiving end corresponding to time t and topology τ.

$\mathbf{I}_{Sxs}$ (3×1) vector of real component of of $\bar{I}_S$ at its sending end.

$\mathbf{I}_{Sxs}^{t\tau}$ (3×1) vector of real component of $\bar{I}_S$ at its sending end corresponding to time t and topology τ.

$\mathbf{I}_{Syr}$ (3×1) vector of reactive component of $\bar{I}_S$ at its receiving end.

$\mathbf{I}_{Syr}^{t\tau}$ (3×1) vector of imaginary component of of $\bar{I}_S$ at its receiving end corresponding to time t and topology τ.

$\mathbf{I}_{Sys}$ (3×1) vector of reactive component of $\bar{I}_S$ at its sending end.

$\mathbf{I}_{Sys}^{t\tau}$ (3×1) vector of imaginary component of of $\bar{I}_S$ at its sending end corresponding to time t and topology τ.

$I_{SCx}^{ipt\tau}$ Real current of a shunt capacitor SC which is connected to bus i at phase p corresponding to time t and topology τ.

I_{SCx}^{ip} Real current of a shunt capacitor SC connected at phase p of bus i.

$I_{SCy}^{ipt\tau}$ Reactive current of a shunt capacitor SC which is connected to bus i at phase p corresponding to time t and topology τ.

I_{SCy}^{ip} Reactive current of a shunt capacitor SC connected at phase p of bus i.

$I_{SRx}^{ipt\tau}$ Real current of a shunt reactor SR connected at phase p of bus i corresponding to time t and topology τ.

I_{SRx}^{ip} Real current of a shunt reactor SR connected at phase p of bus i.

$I_{SRy}^{ipt\tau}$ Imaginary current of a shunt reactor SR connected at phase p of bus i corresponding to time t and topology τ.

I_{SRy}^{ip} Reactive current of a shunt reactor SR connected at phase p of bus i.

I_{Sxr}^{ip} Real current of series component S at its receiving end which is connected to bus i at phase p.

I_{Sxs}^{ip} Real current of series component S at its sending end which is connected to bus i at phase p.

I_{Syr}^{ip} Reactive current of series component S at its receiving end which is connected to bus i at phase p.

I_{Sys}^{ip} Reactive current of series component S at its sending end which is connected to bus i at phase p.

$I_{vx}^{ipt\tau}$ Real current of SVC v connected at phase p of bus i corresponding time t and topology τ.

I_{vx}^{ip} Real current of SVC v connected at phase p of bus i.

I_{vx}^{p} Real current of SVC v connected at phase p.

$I_{vy}^{ipt\tau}$ Reactive current of SVC v connected at phase p of bus i corresponding time t and topology τ.

I_{vy}^{ip} Reactive current of SVC v connected at phase p of bus i.

I_{vy}^{p} Reactive current of SVC v connected at phase p.

K_{ρ} Coefficient of exact penalty relaxation method.

K_{pc}^{ip} Coefficient of constant-power part of the real power of a ZIP load.

K_{pi}^{ip} Coefficient of constant-current part of the real power of a ZIP load.

K_{pz}^{ip} Coefficient of constant-impedance part of the real power of a ZIP load.

K_{qc}^{ip} Coefficient of constant-power part of the reactive power of a ZIP load.

K_{qi}^{ip} Coefficient of constant-current part of the reactive power of a ZIP load.

K_{qz}^{ip} Coefficient of constant-impedance part of the reactive power of a ZIP load.

l_{mag}^{ipt} The lower bound of the magnitude of the voltage at phase p of bus i.

l_{mcs}^{ip} The lower bound of the magnitude of the voltage at phase p of bus i calculated using Monte Carlo Simulation.

l_{rob}^{ip} The lower bound of the magnitude of the voltage at phase p of bus i calculated using robust voltage regulation.

n_{τ} Total number of topologies included in the set possible topologies $\mathbf{T}$.

n_{BUS} Total number of buses in a network.

n_c Total number of capacitor in a capacitor bank.

n_D Total number of discrete variables.

n_F Total number of feeder segments in a network.

n_g Total number of equality constraints.

n_h Total number of inequality constraints.

n_{OLTC} Total number of OLTCs in a network.

n_r Total number of reactor in a reactor bank.

n_{SC} Total number of SCs in a network.

n_{SVC} Total number of SVCs in a network.

n_S Total number of scenarios.

n_T Total number of hours.

n_t Ratio of a transformer.

$\mathbf{p}$ Vector of parameters.

P_G^{ipt} The real power of generator G at bus i and phase p and time t.

P_G^{ip} The real power of generator G at bus i and phase p.

$P_G^{ip}(h)$ The real power of generator G at bus i and phase p and time h.

P_L^{ipts} The real power of load L which is connected at phase p of bus i corresponding to time t and scenario s.

P_L^{ipt} The real power of load L which is connected at phase p of bus i corresponding to time t.

P_L^{ip} The real power of load L which is connected at phase p of bus i.

$P_{PVrated}^{ip}$ The rated power of PV generator connected at bus i and phase p.

$P_{PV}(h)$ The ratio between real output power and rated power of PV generator at time h.

P_{vp}^{spec} Specified real power of SVC v at phase p, p.u.

Q_G^{ipt} The imaginary power of generator G at bus i and phase p corresponding to time t.

Q_G^{ip} The imaginary power of generator G at bus i and phase p.

Q_L^{ipts} The reactive power of load L which is connected at phase p of bus i corresponding to time t and scenario s.

Q_L^{ipt} The reactive power of load L which is connected at phase p of bus i corresponding to time t.

Q_L^{ip} The reactive power of load L which is connected at phase p of bus i.

Q_{vp}^{max} Maximum reactive power of an SVC v connected at phase p, p.u.

Q_{vp}^{min} Minimum reactive power of an SVC v connected at phase p, p.u.

Q_v^a Reactive power of an SVC v connected at phase a, p.u.

Q_v^b Reactive power of an SVC v connected at phase b, p.u.

Q_v^c Reactive power of an SVC v connected at phase c, p.u.

Q_v^p Reactive power of an SVC v connected at phase p, p.u.

$Q_v^{pt\tau}$ Reactive power of an SVC v at phase p corresponding time t and topology τ, p.u.

Q_v^{pts} Reactive power of an SVC v at phase p corresponding time t and scenario s, p.u.

$Q_v^{at\tau}$ The reactive power of an SVC v at phase a corresponding to time t and topology τ.

$Q_v^{bt\tau}$ The reactive power of an SVC v at phase b corresponding to time t and topology τ.

$Q_v^{ct\tau}$ The reactive power of an SVC v at phase c corresponding to time t and topology τ.

ρ_{b+} A variable for relaxing the equality constraint given in Eq. (5.24).

ρ_{b-} A variable for relaxing the equality constraint given in Eq. (5.25).

ρ_b A variable for relaxing the equality constraint given in Eq. (5.23d).

ρ_{gi} A variable for relaxing the i^{th} equality constraint.

ρ_{hj} A variable for relaxing the j^{th} inequality constraint.

r_{ij}^p Phase-p resistance of the line between bus i and j, p.u.

sc The tap position of a shunt capacitor bank.

sc^{ipt} The tap position of a shunt capacitor bank connected at phase p of bus i and time t.

sc^{ip} The tap position of a shunt capacitor bank connected at phase p of bus i.

$sc_{SC}^{ip}(h)$ The tap position of a shunt capacitor bank SC connected at phase p of bus i corresponding to time h.

sr The tap position of a shunt reactor bank.

sr^{ipt} The tap position of a shunt reactor bank connected at phase p of bus i at time t.

sr^{ip} The tap position of a shunt reactor bank connected at phase p of bus i.

tap^{ts}_{mnp} The tap position of an OLTC connecting bus m and n at phase p corresponding to time t and scenario s.

tap_{oa} Tap position of OLTC o at phase a.

tap_{ob} Tap position of OLTC o at phase b.

tap_{oc} Tap position of OLTC o at phase c.

$tap_{op}(h)$ Tap position of OLTC o at phase p at h-th hour.

$tap^{lb,t}_{op}$ An estimate of tap^{t}_{op}.

tap^{max}_{op} Maximum tap position of OLTC o at phase p.

tap^{min}_{op} Minimum tap position of OLTC o at phase p.

tap^{t}_{op} Position of the tap of an OLTC o at phase p at time t.

$\mathbf{T}$ The set of possible radial topologies in which all loads can be served.

τ_i The i^{th} element of $\mathbf{T}$. $i = 1, 2, .., n_\tau$.

U^{max} Maximum value of U_i.

u^{ipt}_{bal} The upper bound of the unbalance of the voltage at phase p of bus i.

U_i Voltage unbalance index of bus i.

$U^{t\tau}_{i}$ Voltage unbalance index of bus i corresponding to time t and topology τ.

U^{ts}_{i} Voltage unbalance index of bus i corresponding to time t and scenario s.

u^{ipt}_{mag} The upper bound of the magnitude of the voltage at phase p of bus i.

u^{ip}_{mcs} The upper bound of the magnitude of the voltage at phase p of bus i calculated using Monte Carlo Simulation.

u_{rob}^{ip} The upper bound of the magnitude of the voltage at phase p of bus i calculated using robust voltage regulation.

$X_{SLv}^{pt\tau}$ Slope setting of SVC v at phase p corresponding to time t and topology τ.

X_{SLv}^{pts} Slope setting of SVC v at phase p corresponding to time t and scenario s.

$X_{SLv}^{p}(h)$ Slope setting of SVC v at phase p at h-th hour.

X_{SC}^{ip} The reactance of a capacitor bank SC connected at phase p of bus i, p.u ($X_{SC}^{ip} < 0$).

$X_{SLp}^{v,min}$, $X_{SLp}^{v,max}$ Minimum and maximum value of X_{SLp}^{v}.

X_{SLv}^{at} Slope of SVC v at phase a at time t, p.u.

X_{SLv}^{bt} Slope of SVC v at phase b at time t, p.u.

X_{SLv}^{ct} Slope of SVC v at phase c at time t, p.u.

X_{SLv}^{p} Slope of SVC v at phase p where $p \in \{a, b, c\}$, p.u.

X_{SR}^{ip} The reactance of a reactor bank SC connected at phase p of bus i, p.u ($X_{SR}^{ip} > 0$).

$\bar{Z}_t^a$ Impedance of transfomer t at phase a.

$\bar{Z}_t^b$ Impedance of transfomer t at phase b.

$\bar{Z}_t^c$ Impedance of transfomer t at phase c.

$\bar{Z}^{pq}$ An element of an impedance matrix of a feeder $p \in \{a, b, c\}$ and $q \in \{a, b, c\}$.

z_{op}^{t} A continuous variable which is constrained by Eqs. (5.18) to have integer values to have integer values.

1 — Introduction

I do not know what I may appear to the world, but to myself I seem to have been only like a boy playing on the seashore, and diverting myself in now and then finding a smoother pebble or a prettier shell than ordinary, whilst the great ocean of truth lay all undiscovered before me.

- Isaac Newton

1.1 Electric Distribution System

ELECTRIC Distribution System is a part of electrical power system that is connected to the retail consumers. As depicted in Figure 1.1, it is divided into primary and secondary network. Their topologies are generally radial and consist of a main feeder and many laterals, as shown in Figure 1.2. Only few of them are weakly meshed networks. Radial networks have several benefits such as simpler protection scheme, lower fault current as well as ease of voltage control and as a result, these are cheaper to operate as compared to weakly meshed networks.

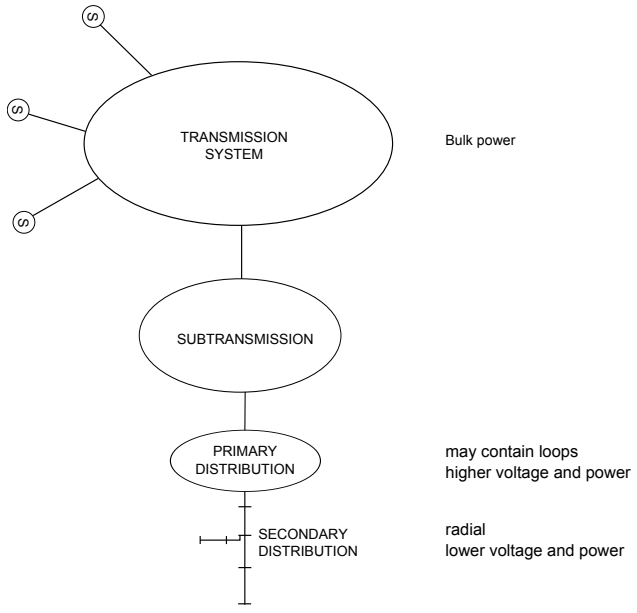

Figure 1.1: Distribution system as a subset of whole electrical system.

One of the responsibilities of an electric power company is maintaining the voltage magnitudes all over its network within prescribed limits. The European standard EN 50160 [1] specifies that

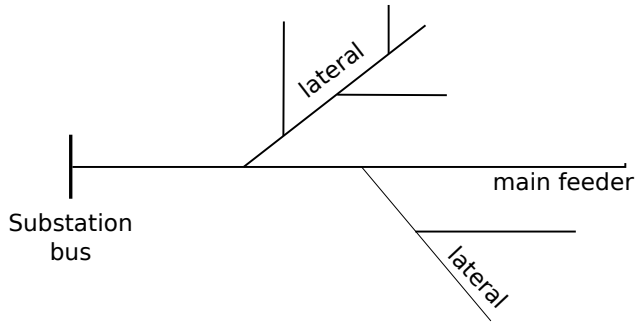

Figure 1.2: Definition of main and lateral feeder in radial network.

the voltage magnitude at lower-voltage and medium-voltage networks must be within $\pm 10\%$ of its nominal value 95% of the time in one week. The ANSI Standard C84-1 [2] defines two ranges (range A and B) of voltage magnitudes within which the voltage magnitudes are allowed to vary from a nominal value of 120 V. Range A is the optimal range and has to be maintained during normal situation. Range B is not optimal and is allowed during emergency for a short time only. In general, electric devices are designed to work optimally if supplied with a voltage at and around its nominal value.

The focus of the above standards is long-term voltage variations. These standards consider root-means-squared deviations of voltage magnitude for a period longer than one minute. There are two types of long-duration variations i.e. undervoltages and overvoltages. An undervoltage (overvoltage) situation happens if magnitude of the voltage is between 80% and 90% (110 % and 120%) of the nominal value for longer than one minute [3]. These variations are mainly caused by variation of loads over time. However, if distributed generations (DGs) are installed in a distribution network then variation of output of DGs may also lead to long-term voltage variations. It is important that the voltage magnitudes are always maintained within their limits.

As an illustration of the importance of voltage regulation, consider an incandescent lamp. The luminous flux of an incandescent lamp is given by [4, 5]

$$\frac{f}{f_n} = \left(\frac{V}{V_n}\right)^b, \tag{1.1}$$

where V and V_n are the magnitude of voltage and its nominal value, respectively; f and f_n are the luminous flux when the voltage is at V and V_n, respectively; and b is a factor equal to 3.6 for an incandescent lamp and 1.8 for discharge lamp. For an incandescent lamp, if the voltage magnitude

varies from -10% to $+10\%$, the luminous flux varies from 70% to 140%. Hence, the quality of the light is best when the lamp is supplied with the nominal voltage. Other types of devices, such as personal computer [6] and electric motors [7], also suffer degradation in performance and effective life time due to voltage violation.

In order to avoid problems related to undervoltages or overvoltages, voltage regulation in distribution system is required. Since one of the sources of voltage variations is fluctuations in loads, the voltage regulation has been a necessity since the beginning of power system [8]. Earlier in a power system, there was no distributed generation in distribution system. Hence, all loads were served by the substation only. In the beginning, the network was small enough for effective voltage regulation using load tap changer only. As the loads kept on growing, one or more shunt capacitors were installed in the substation. Furthermore, as the network grew wider, shunt capacitors were also installed in some of the feeders in the network. If a particular feeder was too long, one or more additional on-load tap changer (OLTC) might be also installed between certain two feeder segments in the network.

The evolution of voltage regulation methodology used in electrical distribution networks followed the growth of those networks. In early times, automation of voltage regulation based on local measurements was started because manual control became too expensive. The automatic control was possible due to the availability of earlier versions of OLTCs such as tap changing transformer, booster transformer with tap changer and induction regulator [9]. These were electromechanical devices. Later, the use of computer [10] and programmable logic controller (PLC) [11, 12] to control OLTC had also been explored. The benefits of using line drop compensation (LDC) had also been recognized in [13, 14]. LDC can boost the voltages when loads are high but keep the voltages close to their nominal values when loads are low [3]. In addition, LDC had been used in conservation voltage reduction (CVR) in order to save more energy [15]. In rural distribution system, long feeder may exist and multiple voltage regulators may be needed. Therefore, the interaction [16] and coordination [17] among those regulators were also studied.

After sometimes, shunt capacitors (SC) and later static var compensator (SVC) were also installed in a substation. Hence, these new controllers were needed to be coordinated with OLTCs which existed previously in the substation. A number of approaches have been proposed for coordinated control of OLTCs and SCs installed in the substation such as dynamic programming [18],

branch-and-bound algorithm [19], heuristic algorithm [20], quasi Newton method [21], and fuzzy logic [12, 22–25]. Moreover, rule based approaches were also investigated in [26, 27]. In some substation, an SVC may exist and can be coordinated with OLTCs [27, 28]. In a distribution system, some part of its network may grow faster than other parts of the same network. Hence, the need for installing additional controller beyond substation has also been identified [29].

In the next stage of evolution of voltage regulation in distribution system, the need of analysis of whole network was felt because shunt capacitors were installed in the feeders [30–34]. For example, voltage and reactive power control using OLTCs and shunt capacitors are discussed in [35–44]. It is also possible to integrate voltage regulation with topology control (network reconfiguration) in which tie-switches, OLTCs and shunt capacitors are jointly optimized [45]. Distributed control of multiple capacitors is discussed in [46]. Uncertainty in loads and network impedances were considered in [25]. In addition, the presence of harmonics due to nonlinear loads has been considered also in [47–49].

Majority of the above papers consider balanced networks [8–18, 22, 26–29, 35–43, 45]. Only in [30–34, 47, 48], unbalanced networks have been considered.

As the bus voltages are primarily controlled by reactive power compensation, the term ”voltage/reactive power control” or ”volt/var” control have also been used in the literature to refer to the control action provided by OLTCs and shunt capacitors. Further, other reactive power compensator, such as SVC and distribution synchronous static compensator (D-STATCOM [50]), may also be installed in the distribution system. In this thesis, the term ’voltage regulation’ and ”volt/var control” are used interchangeably.

Apart from fluctuations in loads, variations in output power from DGs also cause voltage variations, which is discussed next.

1.2 Distributed Generation (DG)

The aggregate rate of human energy consumption is expected to increase in the future because of exponential growth of human population as well as the per capita energy consumption. Nowadays, the main sources of energy are fossil fuels such as oil, coal and gas [51]. However, fossil energy sources are also known to contribute to climate change [52]. Therefore, many efforts had been made to reduce the amount of carbon emission related to the use of fossil fuels. One of the most

influential international effort to solve the emission problem is the United Nation Kyoto Protocol in which many governments agree to some targets on emission reduction [53]. This was further improved in the form of forward-looking decisions to secure global climate future through the Bali Road Map [54]. One of the feasible strategies to reduce the emission is the use of renewable energy sources. Therefore, the share of renewable energy in the overall portfolio of electric power is also expected to increase in the future [51]. This leads to many research efforts on renewable energy sources in general [55].

Some of the renewable energy sources can be used as distributed generation. Distributed Generation is a small generation connected to the distribution network or on the customer side of the meter [56]. A more formal definition can be found in IEEE Standard Dictionary terms as follows [57]:

> A Distributed Generation is an electric generation facility connected to an area Electric Power System (EPS) through a Point of Common Coupling (PCC); it is a subset of Distributed Resources (DR).

Furthermore, DG has several alternative names such as embedded generation and dispersed generation. Another alternative definition is provided by International Energy Agency (IEA) [58] as:

> Distributed Generation is a generating plant serving a customer on-site or providing support to a distribution network, connected to the grid at distribution-level voltages.The technologies generally include engines, small (and micro) turbines, fuel cells, and photovoltaic systems. It generally excludes wind power, since that is mostly produced on wind farms rather than for on-site power requirements.

In addition, IEA defines dispersed generation as follows [58]:

> Dispersed Generation is distributed generation plus wind power and other generation, either connected to a distribution network or completely independent of the grid.

Hence, there is no universally accepted definition of distributed generation. However, this thesis uses the simple definition as given in [56].

DG technology can be either renewable, such as wind generator, photovoltaic (PV) and micro hydro generator; or non-renewable, such as internal combustion engine (ICE) and gas turbine. In terms of their operation, they can be dispatchable, such as, ICE and gas turbine; or non-dispatchable, such as wind and PV. A dispatchable DG means that it participates in optimal dispatch performed by the system operator. A non-dispatchable DG means that its output generally is fully imported into the system without curtailment.

For their electromechanical conversion, DGs may use synchronous generator (SG), permanent magnet synchronous generator (PMSG), Squirrel Cage Induction Generator (SCIG), or Doubly-fed Induction Generator (DFIG) [59]. These electric machines can be directly connected to grid or interfaced with power electronic converter. On the other hand, in case of Photovoltaic (PV) system, 'direct' conversion from light to electrical energy is used. For fuel cell, electrochemical conversion is accomplished. Both PV and fuel cell are connected to power grid via power electronic converters. A list of distributed generation technologies along with their grid interface is shown in Table 1.1 [59].

Benefits of DG can be categorized into technical, economical and environmental ones. The major technical benefits may include reduced power losses, improved voltage profile of the network, increased energy efficiency, enhanced system reliability and security, improved power quality and relieved transmission congestion. Moreover, the major economic benefits may include deferred investment related to upgradation of facilities, reduced operation and maintenance cost for some DG technologies, enhanced productivity, reduced health-care cost due to improvement of environment, reduced reserve requirement, and increased security for critical load. Last but not the least, reduced carbon emission from a DG (with renewable energy sources) has very important environmental benefit. More discussion are available, for example, in [60, 61].

1.3 The Effects of Distributed Generation on Voltage Regulation in Distribution System

Some of the effects of distributed generation on voltage regulation are as follows [62]:

1. A DG can increase or decrease the voltage magnitude along the feeder at which it is connected depending on the feeder parameters and loading as well as the type, control method and generated power of the DG.

2. There is a possibility of "voltage hunting" between a capacitor bank and a DG if both are

Table 1.1: DGs types, electric machines, and utility interfaces

DG Type	Generator	Utility Interface	Dispatchable	Reactive Power Control
ICE	SG	directly	Yes	Able
	SCIG	directly	Yes	Unable
Gas Turbine	SG	directly	Yes	Able
Microturbines	PMSG	rectifier+inverter	Yes	Able
		AC/AC converter	Yes	Able
	SCIG	directly	Yes	Unable
Wind	DFIG	rectifier+inverter	No	Able
	SG or PMSG	rectifier+inverter	No	Able
Photovoltaic	-	inverter	No	Able
Fuel cells	-	inverter	Yes	Able
Microhydro	SG	directly	Yes	Able
	SCIG	directly	Yes	Unable

operating in voltage control mode. Reverse power flow caused by a DG may introduce overvoltage if the capacitor bank operates in reactive power control mode. Time-of-the-day and ambient-temperature control of capacitors also create the possibility of causing over voltage when DGs generate high power and a capacitor is switched on.

3. A DG can disturb the operation of voltage regulator working in the following mode: normal (active power) bidirectional, co-generation, and reactive-power bidirectional modes. It can also disturb line drop compensation (LDC) mode of operation of the regulator.

Because of these impacts, many research efforts have been made in the literature for voltage regulation in the presence of distributed generation.

1.4 Voltage Regulation with Distributed Generation

There are many works reported in the literature about voltage regulation in distribution system with distributed generation. In general, voltage regulation problem is formulated as an optimiza-

tion problem and can be considered as an optimal power flow (OPF) problem. Since voltage controllers such as OLTCs and SCs are discrete controllers, the problem becomes a mixed integer nonlinear programming problem. As a practical distribution system can be large, the problem is very challenging and difficult to solve. It is known to be non-convex and NP-hard. However, it is to be noted that few works on voltage regulation problem, such as [63, 64], may not be considered as optimization problems in formal sense.

In the literature, voltage regulation problem in the presence of distributed generation has been addressed from different aspects as follows:

1. Voltage control devices.
2. Control philosophy.
3. Uncertainties in the system.
4. Load characteristics.
5. Type of network (balanced of unbalanced)

Each of these aspects is discussed in the following subsections.

1.4.1 Voltage control devices

Different type of voltage control devices have been considered in the literature i.e. OLTC [63, 65–68], OLTC + SC [44,64,69,70] , OLTC + energy storage (ES) [71,72], OLTC + SC + energy storage (ES) [73], OLTC + SC + tie switch [74–76] and OLTC + shunt reactor (SR) + SC + SVC [77]. Participation of distributed generation is also an important topic in voltage regulation as discussed previously. Nowadays, distributed generation is allowed to operate only in unity power factor [78]. This means that DGs produce only active power. A number of studies have found that reactive power support from DGs can give benefits to operation of distribution systems [65–68, 75, 79–89]. Furthermore, joint control of both real and reactive power can give even more benefit than real or reactive power control separately [74, 90–92].

1.4.2 Control philosophy

In term of the control scheme, previous works considered centralized control scheme [44,69,70,74, 90,93,94] or localized control scheme [71,79–81,85–87,91,92,95,96]. Centralized control scheme

assumes the availability of measurement devices all over the network and communication network among the controlling devices and the measurements devices. While this may not be an accurate assumption in many present networks, it will be accurate in the context of future smart grid. On the other hand, the localized control scheme assumes that each controller has local measurements and optional minimum communication with other controlling devices. There are also some works which combine local control with minimal availability of communication network [97–100].

In addition, in most of the works on voltage regulation, an OLTC is controlled in time-of-the-day mode. In this mode, the taps positions corresponding to predefined time instances are optimized off-line and sent to the OLTC. This can be seen as feed-forward control. The other one is voltage-control mode in which two parameters are required i.e. a voltage reference and a dead band. If line drop compensation feature is used then additional parameters, i.e. R and X which represent impedance of the line between the OLTC and the controlled bus, need to be optimized as well. Few works on this topic are available in the literature [63, 101]. A method for finding the voltage and impedance settings is proposed in [63] considering the presence of DGs. In [101], dead-band control methodology is proposed for balanced distribution system. However, in this work, the voltage regulation problem has not been considered as an OPF problem. To the best of the knowledge of this author, the optimization model of OLTC operating in line drop compensation mode integrated into optimal power flow is not yet available in the literature. Since LDC is generally available for most of OLTCs, the availability of LDC model may be used in many studies in distribution system operation. Since majority of works in voltage regulation consider OLTCs operating on time-of-the-day control mode, integration of LDC model into an OPF problem allows us to optimize the operation of OLTCs in voltage-control mode. It also helps in optimizing the LDC settings against minimization of loss, number of switching and other criteria.

Another important issue is the participation of DGs in reactive power compensation. Table 1.1 shows that some of DGs have reactive power capability. Even the present standard allows DGs only to operate in unity power factor [78], the participation of DGs in reactive power support has been studied in [68, 69, 79, 92, 102, 103]. There are centralized [69, 92, 102] as well as localized [68, 79, 103] control schemes. In particular, the local reactive power compensation by the DGs can be voltage-based [68, 103] or real-power-based [79] droop control.

1.4.3 Uncertainties (load, generation and topology)

Uncertainties in loads and generations [73, 75, 84, 99, 104–120] as well as in network parameters [121, 122] and topologies of the network do exist in practical networks. The sources of these uncertainties include measurement errors, the variability of natural energy sources, consumer behaviours, faults, electricity price [123] etc. Those uncertainties had been considered in voltage regulation problem using fuzzy logic [70, 94, 95] and stochastic approaches [73, 75, 82, 84, 102, 112, 124, 125]. There are a number of alternative approaches which have been used for solving different power system problems such as reachability set [126], ellipsoid approach [110], minimax regret [127] and robust optimization technique [128, 129]. However, these methods have not been used for solving voltage regulation problem in an unbalanced radial distribution system.

Uncertainties in topology is also an important issue. Traditionally, the topology of a distribution network is decided in the planning stage and is not modified frequently [130, 131]. However, the efficiency of power delivery can be improved when flexible network topology is combined with active management of distribution network [76, 132]. In future power market, when multiple supply point and time-varying price will exist, the network reconfiguration will be more frequent to operate the distribution system optimally [133]. Furthermore, dynamic configuration can increase DG hosting capacity, improve reliability, and reduce losses in the distribution system [134–136]. Loss allocation is also affected by network configuration [137]. Moreover, real power curtailment of DGs can be reduced by changing the topology of the network [74]. These possibilities will increase the uncertainty in topology of future networks. Thus, optimal voltage regulation considering uncertain topology is an important topic which leads to two possible directions of research:

1. Finding an optimal control strategy for each new topology.

2. Finding an optimal control strategy for all feasible topologies similar to the approach of [64] (in a distribution system) or [105] (in a microgrid).

As far as voltage regulation problem is concerned, the idea of [64, 105] is not well explored.

1.4.4 Load characteristics

In a power system, some loads can be modelled as constant-power (PQ) loads (within a range of voltage magnitude) because their power consumption remains constant irrespective of the mag-

nitude of the voltage (within that range) [138]. Many other types of loads will consume different amount of power at different magnitude of the voltage [138]. Hence, the aggregate loads at a node does not behave like constant-power load. However, loads are generally considered as constant-power loads in many works in voltage regulation. This assumption introduces some errors [139–141]. In reality, at bus level, loads are not pure constant-power loads. Constant-power model is popular because it overestimates the line losses [141] in the network and, hence, introduces a sense of security. The error in estimation of loads causes error in estimation of line voltage drop. Hence, in voltage regulation problem, better accuracy in load estimation is preferred. Therefore, in IEEE distribution test feeder, other type of loads, i.e. constant-current (I) and constant-impedance (Z) loads have been introduced [142] and used in voltage regulation problems [20, 143]. On the other hand, residential and commercial loads are better modelled as ZIP loads and industrial loads as constant-power loads [138]. ZIP load model is a linear combination of constant-impedance, constant-current, and constant-power load models. Thus, using ZIP load model in a voltage regulation problem has the potential to improve the accuracy of its solution. This requirement has been previously recognized in the problems of power flow [144], optimal power flow [145], siting and sizing of DGs [146], voltage regulation [147, 148] as well as in combined network reconfiguration and voltage regulation problem [149]. The work represented in both [147, 149] consider balanced distribution system. On the other hand, the work represented in [148] considers unbalanced network without the presence of SVC. Consequently, to the best of our knowledge, the available literature does not consider voltage dependency of load characteristics in voltage regulation problem in an unbalanced distribution system with SVC.

1.4.5 Type of network

At medium voltage level, distribution networks are generally quite balanced. Hence, some works in voltage regulation considered balanced network models which are simpler and smaller than unbalanced network models [44, 64–66, 68–70, 72–75, 77, 79–95, 99, 102–104, 112, 134–136]. Since the actual distribution networks are highly unbalanced [150, 151], some works considered unbalanced networks models [59, 63, 64, 67, 71, 76, 97, 124, 143, 143, 150, 151]. In particular, at low voltage level, distribution networks are highly unbalanced. In the operation of future smart grid, modelling of low voltage networks will be required to assess the impact of single-phase DGs such

as single-phase PV generators installed at roof top.

1.5 Research Gaps in Voltage Regulation in Distribution System with Distributed Generation

Based of the literature review discussed above, the following research gaps were identified:

1. The role of static var compensator in voltage regulation of an unbalanced distribution system with distributed generation is not yet explored in the literature.

2. Regarding the uncertainties of load and generation in distribution system, fuzzy logic and probabilistic approach have been studied for voltage regulation problem. However, in fuzzy logic and probabilistic approaches, the membership function and probabilistic distribution of the uncertain quantities are required. On the other hand, in robust optimization technique, only the limits of the uncertainties are required which are comparatively easier to obtain. However, in the literature, application of robust optimization technique for voltage regulation in an unbalanced distribution system has not yet been explored.

3. While uncertainties in loads and generations in voltage regulation problem have received significant attention in the literature, the uncertainties in topology of the network have not received similar level of attention. Methodology for deciding the optimal settings of the voltage control devices which ensure the satisfactory operation of the network in multiple topologies is not explored in the literature.

4. In some of the present distribution systems, line drop compensation is used. However, an OPF-based technique for finding the optimal settings of line drop compensation in an unbalanced distribution system having distributed generation is not available in the literature. Availability of such model allows optimization of LDC parameters for various applications.

5. Most of the works in voltage regulation focus on constant-power load models. On the other hand, at bus level, composite model which consider all the three types of loads, called ZIP model, is more accurate. However, in voltage regulation problems, ZIP models have not been used extensively. Hence, there is an opportunity to study the application of ZIP model in voltage regulation problem of an unbalanced distribution system in the presence of distributed generation.

1.6 Contribution of this thesis

Based on the discussion in the previous section, the major contribution of this thesis are highlighted below:

1. Optimal coordination between OLTC and SVC in unbalanced distribution systems with distributed generation.

2. Robust voltage regulation in unbalanced distribution system with uncertain loads and generation.

3. Voltage regulation considering multiple feasible configurations.

4. Optimal settings of LDC parameters in the voltage regulation problem.

5. Voltage regulation considering voltage-dependent loads.

1.7 Thesis Outline

The rest of this thesis is outlined as follows:

1. Chapter 2 presents optimal coordination between OLTC, SC and SVC in unbalanced distribution system. In the literature, the optimal coordination between OLTC, SC and SVC is found to be available in balanced system only and only one of them considers the presence of distributed generation. For solving the resulting optimization problem, a branch and bound based approach is proposed. It uses a Cartesian modelling approach of unbalanced distribution system and proposes a set of equality and inequality constraints which models an SVC. The chapter also presents an approach to evaluate the operation of OLTC, SC, and SVC.

2. Chapter 3 presents an application of robust optimization technique to the voltage regulation problem in unbalanced distribution system. It takes into account the uncertainty in generations and loads by considering a finite number of extreme scenarios simultaneously. Hence, the size of optimization problem increases significantly and computational time becomes quite large. In order to avoid these problems, an alternative formulation is proposed which can be solved using an interior point method and reduces the computation time significantly.

3. Chapter 4 considers uncertainty in the topology of distribution networks. In this thesis, it is assumed that the information of all possible feasible configurations is already available. The proposed approach tries to find the optimum settings of the voltage controllers which are feasible for all possible feasible topologies.

4. Chapter 5 presents an OPF-based approach to find the optimal settings of LDC.

5. Chapter 6 considers voltage-dependent loads in the problem of voltage regulation. It extends the previous work on balanced radial distribution system to an unbalanced radial distribution system.

6. Chapter 7 concludes this thesis and also gives few suggestions for further work in this area.

2 — Coordination between OLTC, SC and SVC for Voltage Regulation in Unbalanced Distribution System with Distributed Generation

Every science consists in the coordination of facts;
if the different observations were entirely isolated, there would be no science.
- Auguste Comte

Abstract

Chapter 1 indicates that SVC in unbalanced radial distribution system is not well studied in the literature. Therefore, this chapter focuses on application of SVC for voltage regulation in an unbalanced radial distribution network. In particular, this chapter discusses a two-stage approach for solving the optimal voltage regulation problem in an unbalanced radial distribution system in the presence of photo-voltaic (PV) generation. The on-load tap changer (OLTC), shunt capacitor (SC) and static VAr compensator (SVC) have been considered as the voltage control devices in this chapter. The formulated voltage control problem is a mixed integer non-linear programming (MINLP) problem which remains unsolved even after 8 hours due to its computational burden. However, the proposed two-stage approach can solve this problem in less than 10 minutes. The feasibility of the proposed approach has been demonstrated on a modified IEEE 123 bus unbalanced radial distribution system.

2.1 Introduction

IT has been predicted that the amount of distributed generation (DG) connected to the distribution system will increase significantly in the near future because they can provide many technical, economic as well as environmental benefits [62]. However, it also presents new chal-

lenges to the operation of distribution networks which were initially designed without considering the presence of DGs.

In particular, DGs put significant challenges to voltage regulation in distribution systems [62]. DGs can cause voltage magnitude and power loss to increase or decrease. DGs also influence the operation of on load tap changer (OLTC), step-type voltage regulators (SVR) and Shunt Capacitor (SC) in distribution systems depending on load and generation condition, control mode and location of these devices. For example, in a system with significant photo-voltaic (PV) penetration, normal operation of OLTC along with the variation of PV generation caused by cloud movement over the system may result in an over-voltage condition [151]. In order to solve this fast variation, the use of static var compensator (SVC), distribution static synchronous compensator (D-STATCOM) [152] or voltage source converter (VSC) based DG [88, 143, 153, 154] have been proposed in the literature.

SVCs have been installed in power system before the era of DGs. Their role in fast and slow voltage regulation is well established in the literature. However, for distribution system application, operational issues of SVC have not been fully explored as yet. Only in the work represented in [77] (to the best of the knowledge of this author), the coordination issue among SVC and different voltage control devices, in the presence of DG, has been solved by employing Genetic Algorithm (GA). However, in this work, only a balanced distribution system has been considered. On the other hand, it is well recognized in the literature that for voltage control study in a distribution system, the unbalance nature of a distribution system needs to be considered [20, 21, 143, 151].

To consider unbalanced operation of distribution system for voltage regulation with SVC, in this chapter, the coordination issue between OLTC, SC and SVC is solved in an unbalanced distribution system in the presence of PV systems. To understand the role of SVC in voltage regulation in a more comprehensive way, four combinations of controllers are considered i.e. SVC only, SVC+OLTC, SVC+SC and SVC+SC+OLTC. Furthermore, SVC is considered in voltage regulation mode in such a way that the SVC's slope and voltage reference are integrated in the problem formulation. This control mode can extend the linear operating range of SVC and tends to enforce load sharing between static compensator and other similar devices [155].

All investigations have been made on a modified IEEE 123 bus unbalanced radial distribution system. This chapter is organized as follows. Section 2.2 describes the mathematical model of the

SVC. Section 2.3 formulates the voltage regulation problem in an unbalanced distribution system. Section 2.4 describes the proposed solution method for solving the formulated problem. Section 2.5 presents the main results of this chapter. Finally Section 2.6 highlights the main conclusion of this chapter.

2.2 SVC Model

There are two parameters of an SVC that can be adjusted during operation: voltage reference V_{ref} and slope X_{SL} [156, 157]. This is valid when the SVC is operating in the voltage controlled mode. Another mode is the reactive power control mode in which the reactive power reference is given. However, when its limit is reached, it can not function either in voltage control mode or in reactive power control mode. It will behave as either a fixed capacitor (during under-voltage/heavily-loaded condition) or a fixed inductor (during over-voltage/lightly-loaded/over-generated condition). For these two conditions, SVC is not controllable and therefore is not suitable for voltage regulation.

The SVC in voltage control mode can be modelled as a three-phase line with pure reactance X_{SL} in series with a voltage source. Therefore each SVC model needs an additional dummy PV bus as depicted in Fig. 2.1. The reactance of SVC v is defined as follows:

$$\begin{bmatrix} X^a_{SLv} & 0 & 0 \\ 0 & X^b_{SLv} & 0 \\ 0 & 0 & X^c_{SLv} \end{bmatrix}. \tag{2.1}$$

Without losing generality, the formulation can be simplified by assuming

$$X^a_{SLv} = X^b_{SLv} = X^a_{SLv}. \tag{2.2}$$

In addition, the following equations are also valid [158]:

$$P^{spec}_{vp} = E^p_x(b_v)I^p_{vx} + E^p_y(b_v)I^p_{vy} = 0, \forall p, \forall v \tag{2.3}$$

$$Q^p_V = E^p_y(b_v)I^p_{vx} - E^p_x(b_v)I^p_{vy} \ \ \forall p, \forall v \tag{2.4}$$

$$|\bar{E}^{ref}_v| = E^1_v \tag{2.5}$$

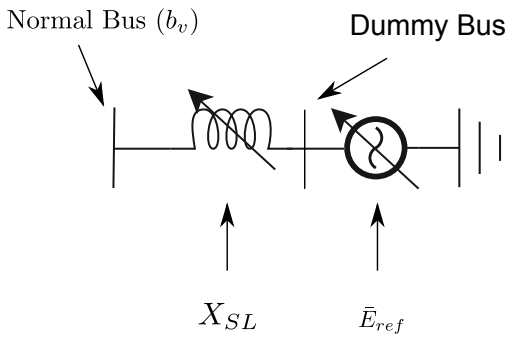

Figure 2.1: The SVC model.

$$Q_v^a = Q_v^b = Q_v^c \tag{2.6}$$

In Eq. (2.3), P_{vp}^{spec} is zero because SVC does not generate nor consume any real power.

2.3 Problem Formulation

In this chapter, the voltage regulation problem has been formulated as an optimization problem to find the optimal settings of the voltage control devices that minimize the total line losses and the number of switchings in the voltage control devices in an unbalanced radial distribution system. The optimization problem is constrained by the distribution component characteristics, power balance, as well as physical and regulatory limits. The optimization variables include bus voltages, tap position of OLTC, slope setting of SVC, settings of SC and voltage reference of SVC.

In this chapter, the DG has been assumed to operate with unity power factor. By assuming the DGs to operate with unity power factor, it has been ensured that the reactive power support is provided only by SVC or SC.

2.3.1 Objective Function

For optimal distribution system operation, one of the primary objectives is minimization of energy loss over a certain period. The energy losses over a 24-hour period can be estimated using Eq. (2.7).

$$J_1 = \sum_{h=1}^{24} \sum_{p=a}^{c} \sum_{i=1}^{n_{BUS}} \sum_{j=1, j\neq i}^{n_{BUS}} r_{ij}^p |\bar{I}_{ij}^p(h)|^2 \tag{2.7}$$

In distribution systems with high DG penetration, intermittent generation (such as wind and

photo voltaic) can increase and decrease the voltages rather frequently. Consequently, number of switchings of the voltage regulators is expected to increase.

On the other hand, utilities generally are interested in minimizing the number of switching operations due to economic and technical considerations [159]. To satisfy this requirement, this chapter proposes three more objective functions which are also to be minimized along with J_1. The objective functions for OLTC, SVC and SC are defined in Eqs. (2.8), (2.9) and (2.10), respectively.

$$J_2 = \sum_{h=1}^{24} \sum_{p=a}^{c} \sum_{o=1}^{n_{OLTC}} (tap_{op}(h) - tap_{op}(h-1))^2 \tag{2.8}$$

$$J_3 = \sum_{h=1}^{24} \sum_{p=a}^{c} \sum_{v=1}^{n_{SVC}} (X_{SLv}^{p}(h) - X_{SLv}^{p}(h-1))^2 \tag{2.9}$$

$$J_4 = \sum_{h=1}^{24} \sum_{p=a}^{c} \sum_{SC=1}^{n_{SC}} (sc_{SC}^{ip}(h) - sc_{SC}^{ip}(h-1))^2 \tag{2.10}$$

Combining the above four objective functions, the following overall objective function is formed as Eq. (2.11).

$$J = \alpha J_1 + \beta J_2 + \gamma (J_3 + J_4) \tag{2.11}$$

where α, β, and γ are non-negative weighting factor for J_1, J_2 and $J_3 + J_4$ respectively. Further, it is to be noted that $\alpha + \beta + \gamma = 1$.

2.3.2 Equality Constraints

The model of distribution system components and the circuit laws define the equality constraints required in the proposed formulation. In addition, physical and regulatory limits determine the inequality constraints.

Load constraints For a constant-power load L connected at phase p of bus i, active (P_L^{ip}) and reactive (Q_L^{ip}) power are assumed to be constant. Hence the following equality constraints must be satisfied:

$$I_{Lx}^{ip} = \frac{P_L^{ip} E_x^{ip} + Q_L^{ip} E_y^{ip}}{(E_x^{ip})^2 + (E_y^{ip})^2} \tag{2.12}$$

$$I_{Ly}^{ip} = \frac{P_L^{ip} E_y^{ip} - Q_L^{ip} E_x^{ip}}{(E_x^{ip})^2 + (E_y^{ip})^2}. \tag{2.13}$$

Distributed Generation Distributed generations are considered as negative constant power loads. For specified real and reactive power injections at bus i and phase p, real and reactive components of currents are calculated using Eqs. (2.14) and (2.15), respectively.

$$I_{Gx}^{ip} = \frac{P_G^{ip} E_x^{ip} + Q_G^{ip} E_y^{ip}}{(E_x^{ip})^2 + (E_y^{ip})^2} \tag{2.14}$$

$$I_{Gy}^{ip} = \frac{P_G^{ip} E_y^{ip} - Q_G^{ip} E_x^{ip}}{(E_x^{ip})^2 + (E_y^{ip})^2} \tag{2.15}$$

For a DG operating in constant power factor mode, both its real and reactive power are negative specified quantities. A unity power factor operation of DG implies that its specified reactive power is zero and its real power is a negative quantity. Presently for realistic PV representation, unity power factor is assumed as recommended in [78].

Shunt Capacitor and Reactor For a shunt capacitor SC connected at phase p of bus i, the following equality constraints must be satisfied:

$$I_{SCx}^{ip} = \frac{sc^{ip}}{n_c} \frac{+E_y^{ip}}{X_{SC}^{ip}}, X_{SC}^{ip} < 0 \tag{2.16}$$

$$I_{SCy}^{ip} = \frac{sc^{ip}}{n_c} \frac{-E_x^{ip}}{X_{SC}^{ip}}, X_{SC}^{ip} < 0. \tag{2.17}$$

Similarly, for a shunt reactor SR connected at phase p of bus i, the following equality constraints must be satisfied:

$$I_{SRx}^{ip} = \frac{sr^{ip}}{n_r} \frac{+E_y^{ip}}{X_{SR}^{ip}}, X_{SR}^{ip} > 0 \tag{2.18}$$

$$I_{SRy}^{ip} = \frac{sr^{ip}}{n_r} \frac{-E_x^{ip}}{X_{SR}^{ip}}, X_{SR}^{ip} > 0. \tag{2.19}$$

Note that the complex current of a shunt capacitor (reactor), $I_{SCx}^{ip} + jI_{SCy}^{ip}$ ($I_{SRx}^{ip} + jI_{SRy}^{ip}$), leads (lags) its terminal voltage, $E_x^{ip} + jE_y^{ip}$, by 90^0. However, this does not necessarily means that $I_{SCx}^{ip} = I_{SR_x}^{ip} = 0$ which happens only when $E_y^{ip} = 0$.

In case of single capacitor (reactor), the discrete variable satisfy $sc^{ip} \in \{0, 1\}$ ($sr^{ip} \in \{0, 1\}$.) On the other hand, in case of a capacitor (reactor) bank having n_c (n_r) capacitors (reactors) of equal ratings, $sc^{ip} \in \{0, 1, ..., n_c\}$ ($sr^{ip} \in \{0, 1, ..., n_r\}$).

SVC SVC's model equations are given in Eqs. (2.2), (2.3), (2.5) and (2.6).

Series Components Distribution system series components i.e. feeders, transformers, OLTCs can be mathematically described using the ABCD model [150]. Eqs. (2.20) and (2.21) represent voltage constraints of the series components.

$$\begin{aligned}\mathbf{E}_x(b_S^s) &= \mathbf{A}_x\mathbf{E}_x(b_S^r) - \mathbf{A}_y\mathbf{E}_y(b_S^r) \\ &\quad + \mathbf{B}_x\mathbf{I}_{Sxr} - \mathbf{B}_y\mathbf{I}_{Syr} \qquad (2.20)\\ \mathbf{E}_y(b_S^s) &= \mathbf{A}_x\mathbf{E}_y(b_S^r) + \mathbf{A}_y\mathbf{E}_x(b_S^r) \\ &\quad + \mathbf{B}_x\mathbf{I}_{Sxr} + \mathbf{B}_y\mathbf{I}_{Syr} \qquad (2.21)\end{aligned}$$

Similarly, Eqs. (2.22) and (2.23) represent current constraints of the series components.

$$\mathbf{I}_{Sxs} = \mathbf{C}\mathbf{E}_x(b_S^r) + \mathbf{D}\mathbf{I}_{Sxr} \qquad (2.22)$$

$$\mathbf{I}_{Sys} = \mathbf{C}\mathbf{E}_y(b_S^r) + \mathbf{D}\mathbf{I}_{Syr} \qquad (2.23)$$

For distribution feeder modelled as series impedance without shunt admittance, $\mathbf{I}_{Sxs} = \mathbf{I}_{Sxr}$ and $\mathbf{I}_{Sys} = \mathbf{I}_{Syr}$. For transformer and OLTC, generally, $\mathbf{I}_{Sxs} \neq \mathbf{I}_{Sxr}$ and $\mathbf{I}_{Sys} \neq \mathbf{I}_{Syr}$. Table 2.1 shows the matrices $\mathbf{A}$, $\mathbf{B}$, $\mathbf{C}$, and $\mathbf{D}$ for some series components.

Sequence Voltage Constratins Since voltage unbalance ratio is expressed in terms of positive and negative sequence voltages, the folowing constraints also apply for all three-phase buses:

$$E_{xi}^1 = \frac{1}{3}\left(E_x^{ia} + E_x^{ib}\cos 120^o - E_y^{ib}\sin 120^o + E_x^{ic}\cos 240^o - E_y^{ic}\sin 240^o\right) \qquad (2.24)$$

$$E_{yi}^1 = \frac{1}{3}\left(E_y^{ia} + E_y^{ib}\cos 120^o + E_x^{ib}\sin 120^o + E_y^{ic}\cos 240^o + E_x^{ic}\sin 240^o\right) \qquad (2.25)$$

$$E_{xi}^2 = \frac{1}{3}\left(E_x^{ia} + E_x^{ib}\cos 240^o - E_y^{ib}\sin 240^o + E_x^{ic}\cos 120^o - E_y^{ic}\sin 120^o\right) \qquad (2.26)$$

$$E_{yi}^2 = \frac{1}{3}\left(E_y^{ia} + E_y^{ib}\cos 240^o + E_x^{ib}\sin 240^o + E_y^{ic}\cos 120^o + E_x^{ic}\sin 120^o\right) \qquad (2.27)$$

Current Balance Further, based on Kirchhoff's law, Eqs. (2.28) and (2.29) define nodal current balance equations for all buses and phases.

$$I_{Sxr}^{ip} = \sum I_{Sxs}^{ip} + \sum I_{Lx}^{ip} + \sum I_{vx}^{ip} + \sum I_{SCx}^{ip} + \sum I_{SRx}^{ip} - \sum I_{Gx}^{ip} \qquad (2.28)$$

$$I_{Syr}^{ip} = \sum I_{Sys}^{ip} + \sum I_{Ly}^{ip} + \sum I_{vy}^{ip} + \sum I_{SCy}^{ip} + \sum I_{SRy}^{ip} - \sum I_{Gy}^{ip} \qquad (2.29)$$

$$\forall i, \forall p$$

Table 2.1: Matrices of series elements

Elements	$\mathbf{A}$	$\bar{\mathbf{B}}$	$\mathbf{C}$	$\mathbf{D}$
Feeder	$\begin{bmatrix} 1 & 0 & 0 \\ 0 & 1 & 0 \\ 0 & 0 & 1 \end{bmatrix}$	$\begin{bmatrix} \bar{Z}^{aa} & \bar{Z}^{ab} & \bar{Z}^{ac} \\ \bar{Z}^{ba} & \bar{Z}^{bb} & \bar{Z}^{bc} \\ \bar{Z}^{ca} & \bar{Z}^{cb} & \bar{Z}^{cc} \end{bmatrix}$	$\begin{bmatrix} 0 & 0 & 0 \\ 0 & 0 & 0 \\ 0 & 0 & 0 \end{bmatrix}$	$\begin{bmatrix} 1 & 0 & 0 \\ 0 & 1 & 0 \\ 0 & 0 & 1 \end{bmatrix}$
The $\mathbf{A}, \mathbf{B}$ and $\mathbf{D}$ are real matrices since the feeder's shunt admittance is neglected. [150].				
OLTC	$\begin{bmatrix} \frac{1}{tap_{oa}} & 0 & 0 \\ 0 & \frac{1}{tap_{ob}} & 0 \\ 0 & 0 & \frac{1}{tap_{oc}} \end{bmatrix}$	$\begin{bmatrix} 0 & 0 & 0 \\ 0 & 0 & 0 \\ 0 & 0 & 0 \end{bmatrix}$	$\begin{bmatrix} 0 & 0 & 0 \\ 0 & 0 & 0 \\ 0 & 0 & 0 \end{bmatrix}$	$\begin{bmatrix} tap_{oa} & 0 & 0 \\ 0 & tap_{ob} & 0 \\ 0 & 0 & tap_{oc} \end{bmatrix}$
Transformer D-Yg	$\frac{n_t}{3}\begin{bmatrix} 0 & 2 & 1 \\ 1 & 0 & 2 \\ 2 & 1 & 0 \end{bmatrix}$	$\frac{n_t}{3}\begin{bmatrix} 0 & 2\bar{Z}_t^b & \bar{Z}_t^c \\ \bar{Z}_t^a & 0 & 2\bar{Z}_t^c \\ 2\bar{Z}_t^a & \bar{Z}_t^b & 0 \end{bmatrix}$	$\begin{bmatrix} 0 & 0 & 0 \\ 0 & 0 & 0 \\ 0 & 0 & 0 \end{bmatrix}$	$\frac{1}{n_t}\begin{bmatrix} 1 & -1 & 0 \\ 0 & 1 & -1 \\ -1 & 0 & 1 \end{bmatrix}$
The matrices correspond to other type of connection can be found in [150].				
X_{SL}	$\begin{bmatrix} 1 & 0 & 0 \\ 0 & 1 & 0 \\ 0 & 0 & 1 \end{bmatrix}$	$\begin{bmatrix} jX_{SLv}^a & 0 & 0 \\ 0 & jX_{SLv}^b & 0 \\ 0 & 0 & jX_{SLv}^c \end{bmatrix}$	$\begin{bmatrix} 0 & 0 & 0 \\ 0 & 0 & 0 \\ 0 & 0 & 0 \end{bmatrix}$	$\begin{bmatrix} 1 & 0 & 0 \\ 0 & 1 & 0 \\ 0 & 0 & 1 \end{bmatrix}$
Note that the SVC slopes X_{SLv}^a,X_{SLv}^b and X_{SLv}^c are discrete control variables [156].				

2.3.3 Inequality Constraints

Based on various physical and regulatory limits, the following inequality constraints are considered:

1. Voltage magnitude limits at all buses and phases including all load and SVC's dummy bus:

$$0.95 \leq |\bar{E}^p(i)| \leq 1.05, \forall i, \forall p \tag{2.30}$$

2. Voltage magnitude limits for a node that is connected to the secondary terminal of OLTC [150]:

$$0.9 \leq |\bar{E}^p(b_o)| \leq 1.1, \forall o, \forall p \tag{2.31}$$

3. Positive-sequence voltage reference limit of SVC:

$$0.95 \leq |\bar{E}_v^{ref}| \leq 1.05, \forall v \tag{2.32}$$

4. Reactive power limit of SVC:

$$Q_{vp}^{min} \leq Q_v^p \leq Q_{vp}^{max}, \forall v, \forall p \tag{2.33}$$

5. limits on slope of SVC:

$$X_{SLp}^{v,min} \leq X_{SLv}^p \leq X_{SLp}^{v,max}, \forall v, \forall p \tag{2.34}$$

6. Limit on tap position of OLTC:

$$tap_{op}^{min} \leq tap_{op}(h) \leq tap_{op}^{max}, \forall o, \forall p \tag{2.35}$$

7. Limit on voltage balance factor U_2 for all three-phase buses:

$$0 \leq U_{2i} = 100\frac{|\bar{E}_i^2|}{|\bar{E}_i^1|} \leq U_2^{max} \tag{2.36}$$

IEC 61000-2-12 specifies that $U_2^{max} = 2\%$ [160].

2.4 Solution Method

The voltage regulation problem is a Mixed-Integer Non-Linear Programming (MINLP) of the following form,

$$\begin{aligned} &\underset{\mathbf{c},\mathbf{d}}{\text{minimize}} \quad J \\ &\text{subject to} \quad (2.2)-(2.6), (2.12)-(2.36), \end{aligned} \tag{P2.0}$$

where $\mathbf{c}$ and $\mathbf{d}$ represent continuous and discrete variables, respectively. Continuous variables are real and imaginary parts of three-phase voltages at all nodes and the voltage reference of the SVC. Discrete variables are OLTC tap positions and slope (X_{SL}) setting of the SVC. It is to be noted that the MINLP problem described in (P2.0) is essentially an optimal power flow (OPF) formulation. Now, it is well known that it is quite difficult to handle discrete variables in OPF. To circumvent this, in this chapter, a simple approach following [20] and [19] is proposed. The proposed approach is a two-stage decision making procedure: stage 1 is one-day-ahead optimization procedure that

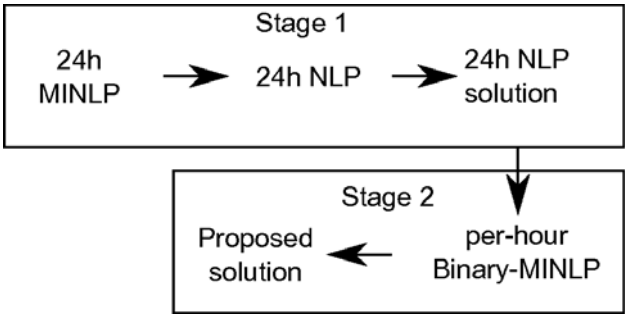

Figure 2.2: Flowchart of the proposed method.

requires forecasted values of load and generation. It provides a reduced search space for stage 2 which is a local optimization procedure that requires present load and generation levels obtained through forecasting or direct measurement. The approach contains the following steps (see Fig. 2.2):

1. Stage 1

   (a) Convert all discrete variable d_k^1 into continuous variable c_k^1. This relaxes the initial MINLP (P2.0) into a Non-Linear Programming (NLP) given by (P2.1) below.

$$\begin{aligned} &\underset{c}{\text{minimize}} \quad J \\ &\text{subject to} \quad (2.2)-(2.6), (2.12)-(2.36). \end{aligned} \tag{P2.1}$$

   (b) Solve the NLP using interior point method [161].

   (c) Let $h = 0$.

   (d) From the solution of the NLP (c_k^{1*}), find the nearest lowest boundary d_k^{lb}. If the optimum continuous value is equal to one of the discrete values, let it be the lowest boundary.

   (e) Define new discrete variable

$$d_k^2 = d_k^{lb} + b_k * \delta_k \tag{2.37}$$

   δ_k is the step size of the k^{th} variable and b_k is a binary variable corresponding to the k^{th} original discrete variable.

2. Stage 2

(a) Using the new discrete variables, another MINLP is formulated which has only binary discrete variables.

$$\begin{aligned} &\underset{c,b}{\text{minimize}} \quad J \\ &\text{subject to} \quad (2.2)-(2.6), (2.12)-(2.36). \end{aligned} \tag{P2.2}$$

(b) Solve the new MINLP using Branch-and-Bound method [162].

(c) Let $h = h + 1$.

(d) If $h <= h^{max}$, repeat 2.a) - 2.d), otherwise stop.

After both stages are completed successfully, the solution consists of the optimal values of control variables for each time step h. For k^{th} optimal discrete variables d_k^{2*}, switching operation is required when its consequtive values are different, i.e.

$$d_k^{2*}(h) \neq d_k^{2*}(h-1).$$

Otherwise, there is no need for switching operation.

2.5 Result and Discussion

2.5.1 Modified IEEE 123 Bus System

To investigate the efficacy of the proposed method, it was implemented on modified IEEE 123 bus system [142] as shown in Fig. 2.3. In this system, the three-phase base MVA is 5 while the line-to-line voltage base is 4.16 kV. Without any loss of generality, following assumptions have been made:

1. The SC which are originally located at bus 64 is moved to bus 73.
2. Each SC is assumed as a capacitor bank with $n_c = 8$ and, hence, $sc_{SC}^{ip} \in \{0, 1, 2, 3, ..., 8\}$.
3. An SVC is installed at the original location of 3-phase SC i.e. at bus 64 having a capacity of 3 x 0.12 p.u. (capacitive) and 3 x 0.12 p.u. (inductive).
4. The load given in [142] is assumed as peak loads.
5. The slope of the SVC has 6 possible tap positions corresponding to $\{0.00, 0.01, ..., 0.05\}$.

6. The taps position of an OLTC can be varied from -16 to $+16$ which constitutes 33 possible positions for each phase.

7. Residential load profiles for both real and reactive power loads have been used and are shown in Fig. 2.4.

8. A PV module is installed at every node at which constant-power load is present with a capacity of 50% of peak load at that node. For example, since there is a 40-kW constant power load at phase a of bus 4, there is also a 20-kW DG installed at phase a of bus 4. By this process, a total of 967.5 kW distributed generation has been considered in this system. Appendix B presents more details about load and generation.

9. The generated powers of PVs are assumed to follow the curve $P_{PV}(h)$ shown in Fig 2.4. From those curves of Fig. 2.4, for any particular hour, the amount of PV generation is obtained using Eq. (2.38), which, in turn, represents a negative constant power load for this particular hour.

$$P_G^{ip}(h) = P_{PV}(h) P_{PVrated}^{ip} \tag{2.38}$$

   Therefore, by following the curve shown in Fig. 2.4, the PV generation is actually represented as a variable negative constant power load on an hourly basis. For any particular value of negative constant power load, the corresponding values of I_{Gx}^{ip} and I_{Gy}^{ip} are calculated from Eqs. (2.14) and (2.15). Similarly, real and reactive loads follow the curves $P(h)$ and $Q(h)$ in Fig. 2.4, respectively. The load and generation profiles are based on [77].

10. All constant-impedance and constant-current loads are converted into constant-power load but no DG is assumed to be connected at those buses.

Initially, the optimization procedure has been carried out over a period of 24-h with 1 hour time step ($h^{max} = 24, h = 1$) following the philosophies laid down in [19, 20] . All loads have been assumed to follow the same profile. While this type of uniform behaviour is less likely in reality, it could provide a representation of possible highest rate of load variation. Residential load profile has been used for all constant power loads.

As discussed earlier, the ratings of the PV generators are 50% of the rated constant-power load connected at the same bus. While 50% PV penetration level might be over-optimistic, the

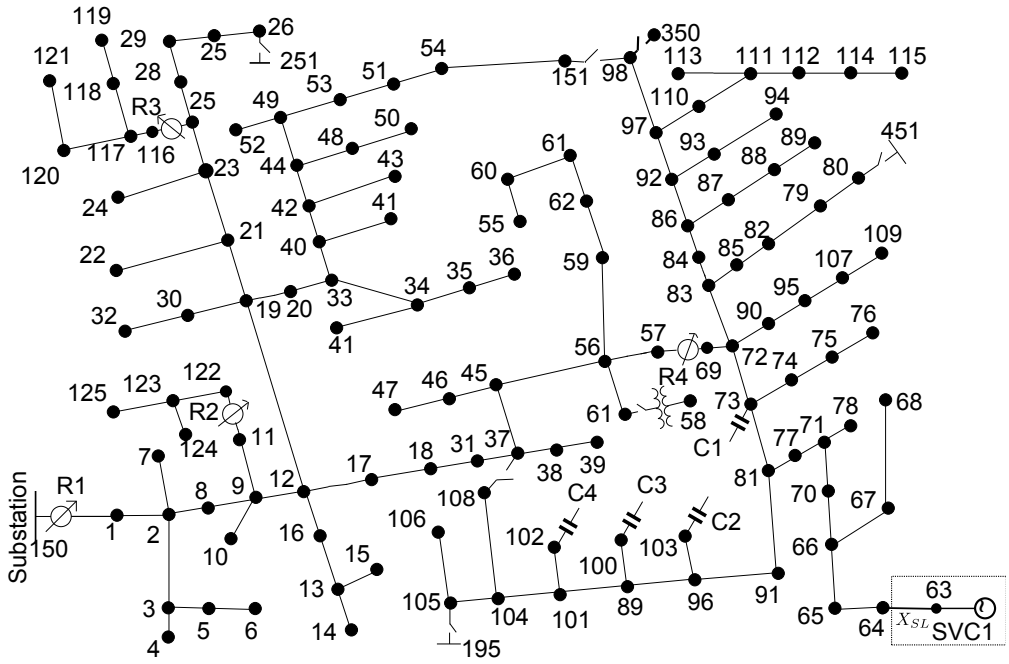

Figure 2.3: Modified IEEE 123 bus system.

value was chosen so that the rate of variation of distribution generation is significantly high. All generations have been chosen to follow the same profile for the same reason adopted for varying the load profile.

2.5.2 Simulation Studies

A number of simulation studies have been performed to study the behaviour of the system under the proposed optimization approach. Several combinations of α, β and γ have been adopted and are given in Table 2.2. It is to be noted that these weighting factors have been chosen arbitrarily. Actually, these weighting factors signify the relative importance of various objective functions, which, in turn are dependent on the perception of distribution network operator (DNO) concerned. Now, any perception is quite subjective and can vary quite widely from one DNO to another. However, the proposed algorithm should be applicable over the possible wide variation of perception of the DNOs and to validate that, the values of α, β and γ have been chosen over a wide range (between 0 and 1).

These cases have been compared using different indices i.e. total line losses, number of switchings of OLTC, SC, and SVC, bus voltage magnitude index and line voltage drop magnitude index for the system with 4 OLTCs (R1 - R4), 4 SC (C1-C4) and 1 SVC (SVC1) as shown in Fig. 2.3.

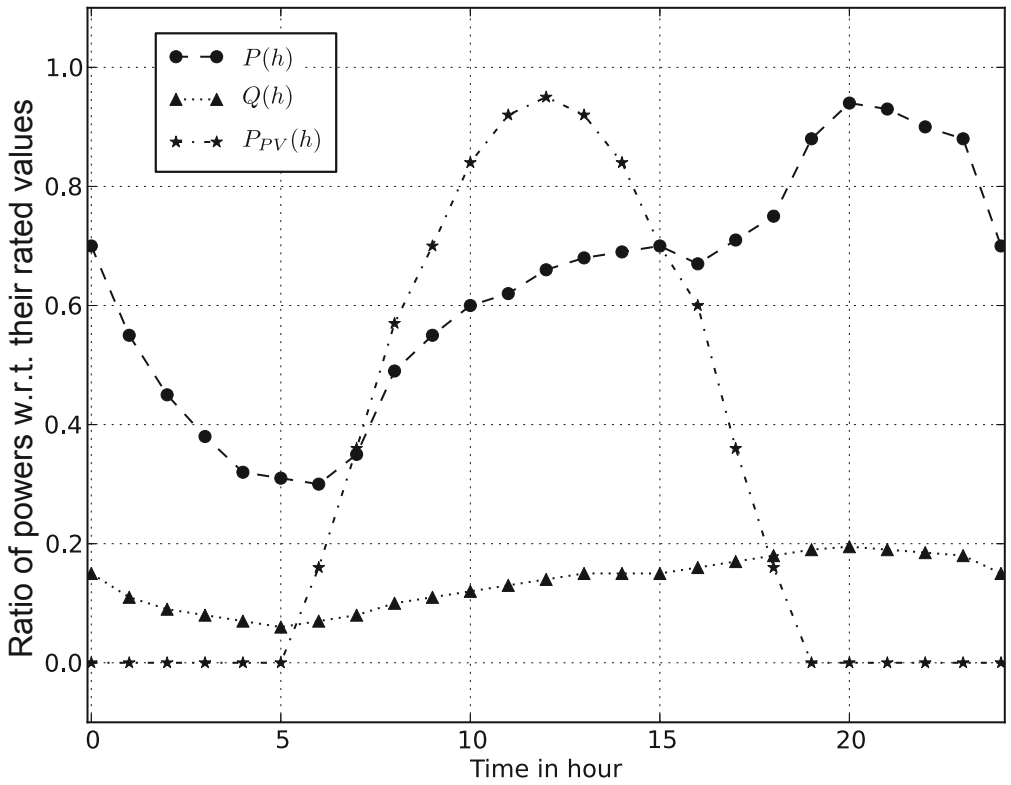

Figure 2.4: Real load ($P(h)$), reactive load ($Q(h)$) and photo-voltaic ($P_{PV}(h)$) generation profile.

It is to be noted that the SVC, the capacitor C1 and the OLTCs R1 and R4 are three-phase devices. OLTC R2, shunt capacitors C2-C4 are single-phase ones while R3 is a two-phase device.

The voltage magnitude index (VMI) as defined in Eq. (2.39) indicates the closeness of system voltages to their rated values. The smaller the value of VMI is, the closer are the bus voltage magnitudes to their rated values. As there are a number of OLTCs installed in the network (for example R2, R3, and R4), there is possibility for jumps in voltage magnitude in the voltage profile of the system. Therefore, VMI alone is not always a good index for flatness of the system voltage profile. Hence, Line Voltage Drop Magnitude Index (VDMI) as defined in Eq. (2.40) is used to represent the flatness of the voltage profile in a better way.

$$\mathit{VMI} = \sum_{h=0}^{23} \sum_{p=a}^{c} \sum_{i=1}^{n_{BUS}} (1 - |\bar{E}_i^p|)^2 \tag{2.39}$$

$$\mathit{VDMI} = \sum_{h=0}^{23} \sum_{p=a}^{c} \sum_{i=1}^{n_F} \left(|\bar{E}^p(b_F^s)| - |\bar{E}^p(b_F^r)| \right) \tag{2.40}$$

Table 2.2: Choice of α, β and γ for case studies

Cases	A	B	C	D	E	F
α	1.00	0.90	0.80	0.70	0.60	0.50
β	0.00	0.05	0.10	0.15	0.20	0.25
γ	0.00	0.05	0.10	0.15	0.20	0.25
Cases	G	H	I	J		
α	0.40	0.30	0.20	0.10		
β	0.30	0.35	0.40	0.45		
γ	0.30	0.35	0.40	0.45		

Each of the case studies shown in Table 2.2 has been carried out under eighteen control strategies as shown in Table 2.3. In uniform operation of OLTCs, SCs or SVCs, the same settings are used in all phases. When different settings among phases are allowed, OLTCs, SCs or SVCs are in non-uniform operation. It is to be noted that for uniform (non-uniform) operation of SVC, the equality relation given in Eqs. (2.2) and (2.6) are valid (non-valid).

Below, the performance of different strategies vis-a-vis different indices are discussed.

2.5.2.1 Total Line Losses

Total line losses of all cases for different strategies are given in Table 2.4 and these are also shown graphically in Fig. 2.5(a). The values of minimum, maximum, mean and standard deviation of losses over all cases and strategies are 945.76, 1058.98, 986.93, 50.78 kWh, respectively. Thus, these losses are rather close to each other.

It can be seen that the strategy with only SVC (strategies I and II) has the highest loss. Furthermore, strategies III-VI involving SVC and SC, have also higher losses than other strategies with OLTCs (strategies VII - XVIII). This is expected because strategy I-VI has only reactive power compensation while strategies VII-XVIII have both OLTC and reactive power compensation. Note that top two most efficient strategies are strategies VII and XI, respectively. In both strategies, all devices operate non-uniformly. It is also found that non-uniform operation of OLTCs corresponds to better energy efficiency than uniform operation of OLTC. In addition, when OLTCs operate non uniformly, non-uniform operation of reactive power compensators leads to lower losses than uni-

Table 2.3: Definition of Strategies of Operation of Controllers

Controller Group	Strategy	Operation*		
		OLTC	SVC	SC
SVC	I	-	NU	-
	II	-	U	-
SVC+SC	III	-	NU	NU
	IV	-	NU	U
	V	-	U	NU
	VI	-	U	U
OLTC+SVC	VII	NU	NU	-
	VIII	NU	U	-
	IX	U	NU	-
	X	U	U	-
OLTC+SVC+SC	XI	NU	NU	NU
	XII	NU	NU	U
	XIII	NU	U	NU
	XIV	NU	U	U
	XV	U	NU	NU
	XVI	U	NU	U
	XVII	U	U	NU
	XVIII	U	U	U

* NU = non- uniform, U=uniform

Table 2.4: Losses corresponding to each case and strategy in kWh.

	A	B	C	D	E	F	G	H	I	J
I	998.92	998.92	998.92	998.92	998.92	998.92	998.92	998.92	998.92	998.92
II	998.97	998.97	998.97	998.97	998.97	998.98	998.98	999.14	999.17	998.98
III	997	998.94	998.94	998.94	998.94	998.94	998.94	998.94	998.94	998.94
IV	997	998.94	998.94	998.94	998.94	998.94	998.94	998.94	998.94	998.94
V	997.52	998.99	998.99	998.99	998.99	998.99	998.99	998.99	998.99	998.99
VI	997.52	998.99	998.99	998.99	998.99	998.99	998.99	998.99	998.99	998.99
VII	891.86	891.91	892.00	891.99	892.24	892.36	892.43	892.62	893.01	894.34
VIII	892.70	892.73	892.84	893.44	893.06	893.04	893.39	893.77	894.28	896.26
IX	897.35	897.36	897.40	897.66	897.70	897.71	897.74	897.85	897.87	897.86
X	900.40	898.02	898.05	898.07	898.21	898.21	898.43	898.84	900.77	900.84
XI	890.97	891.94	892.02	892.01	892.23	892.38	892.52	892.79	893.00	894.14
XII	890.96	891.93	892.02	892.03	892.23	892.39	896.35	892.85	892.86	894.14
XIII	891.75	892.71	892.82	892.91	893.05	893.07	893.42	893.54	894.37	894.99
XIV	891.77	893.33	893.42	892.86	893.11	893.07	899.71	893.39	894.37	895.01
XV	896.39	897.36	897.42	897.66	897.71	901.19	897.74	897.86	897.83	898.15
XVI	896.37	897.36	897.42	897.66	897.69	897.71	897.74	897.85	898.11	898.14
XVII	896.94	898.01	898.05	898.07	897.69	898.11	898.33	898.55	900.81	900.87
XVII	896.92	898.01	898.05	898.06	898.20	898.21	898.44	898.82	900.80	900.86

form operation of reactive power compensators. In general, non-uniform operation gives greater freedom and hence lower losses as compared to uniform operation.

2.5.2.2 Voltage Profile

Values of voltage magnitude index for all cases under different strategies are given in Table 2.5 and are graphically shown in Fig. 2.5(b). The values of minimum, maximum, mean and standard deviation of VMI over all cases and strategies are 2.143, 18.019, 11.826, 6.825, respectively. It is to be noted that the smaller values of VMI are, the closer the voltage magnitudes to their rated values are. Fig. 2.5(b) shows that strategies I - VI which do not have OLTCs have lower values of VMIs than strategies VII - XVIII which have OLTCs. This is expected since OLTCs can increase magnitudes of voltages and thereby decreasing the total line losses. Moreover, Fig. 2.5(b) shows that strategies in which OLTCs operate non-uniformly have higher VMI than ones in which OLTCs operate uniformly (VII vs IX, VIII vs X, XI vs XV, XII vs XVI, XIII vs XVII and XIV vs XVIII.)

However, as VMI is the sum total of $(24 \times 3 \times n_B)$ squared values (Eq. 2.39), there is not

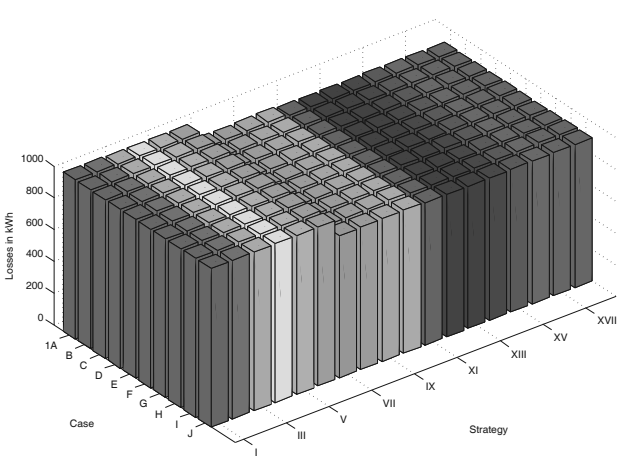

(a) Losses

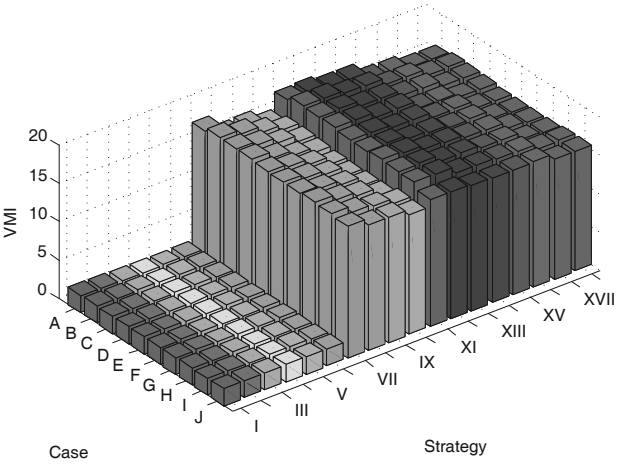

(b) VMI

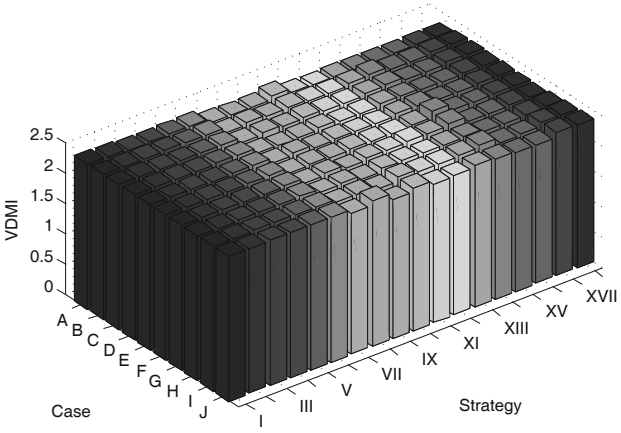

(c) VDMI

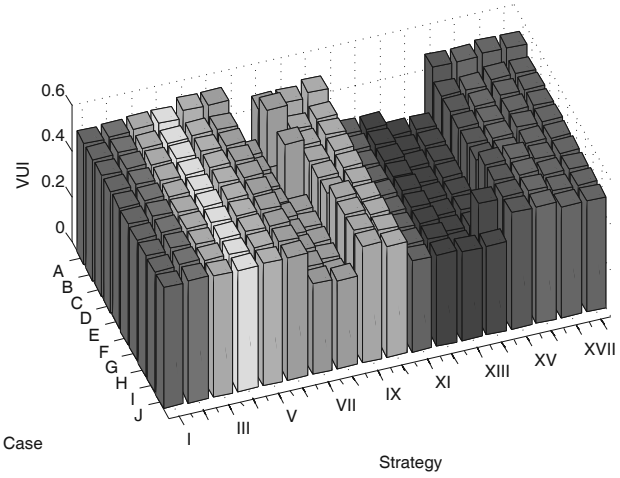

(d) VUI

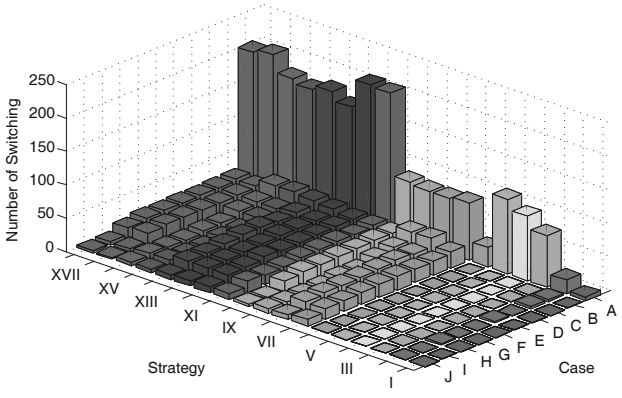

(e) number of switchings

Figure 2.5: Comparison of different combination of cases and strategies based on losses, VDMI, VMI, VUI and number of switchings.

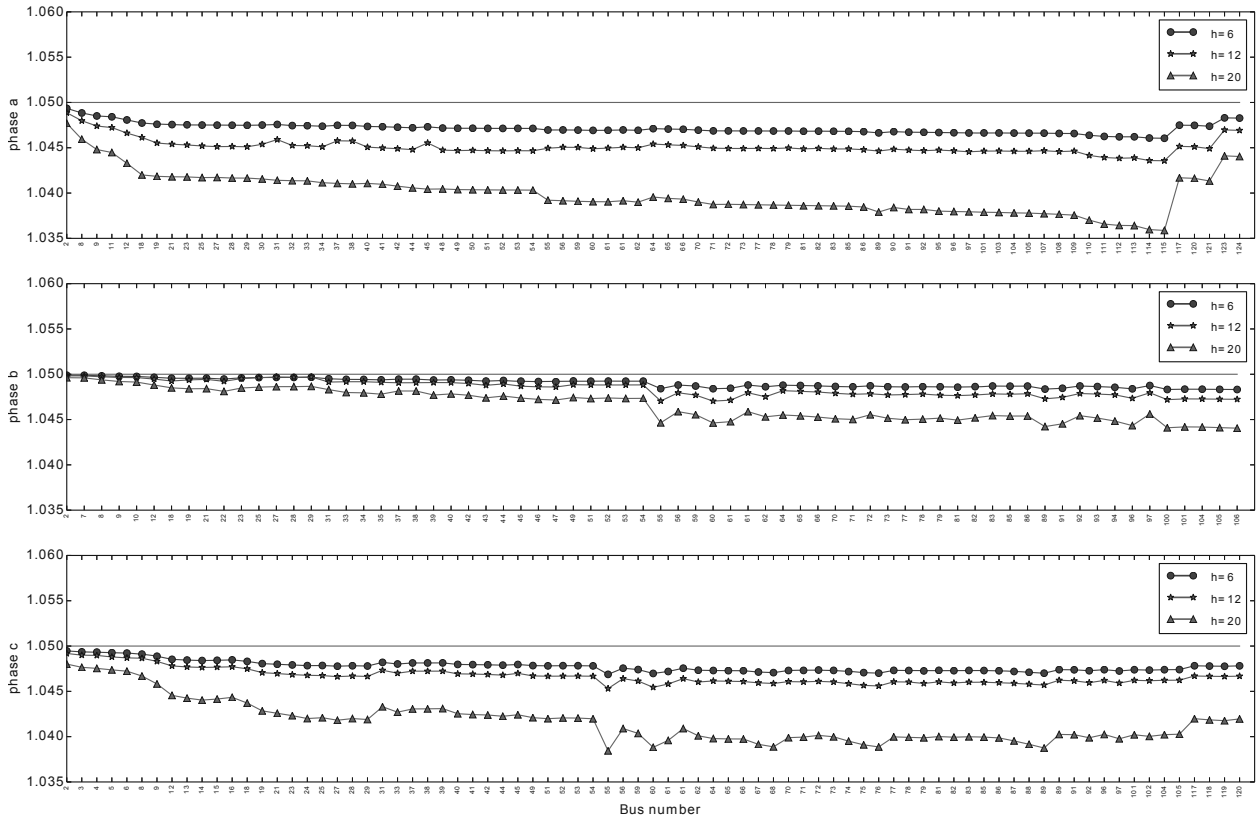

Figure 2.6: Bus voltage magnitudes at several time for strategy XV and case J (top = phase a, middle = phase b, bottom = phase c).

much difference between the voltage profiles of strategy I - VI, as the values of VMI for these six strategies do not differ much. Similar conclusion can also be drawn for strategies VII-XVIII.

Some representative bus voltage magnitude profiles of the system for strategy XV-case J is shown in Fig. 2.6. From this figure, it is observed that the bus voltage profiles for strategy XV are quite flat and close to each other.

Further, the values of VDMI for different combination of cases and strategies are shown in Fig. 2.5(c). The corresponding numerical values are given in Table 2.6. The values of minimum, maximum, mean and standard deviation of VDMI over all cases and strategies are 2.270, 2.415, 2.340, 0.039 p.u., respectively. Thus, these values of VDMIs are rather close to each other. The values of VDMI corresponding to strategies without OLTCs (I-VI) are higher than those corresponding to strategies with OLTCS. However, all values of VDMI are small and, hence, the proposed method is able to flatten the voltage profiles effectively.

Moreover, Fig. 2.5(a) shows that losses of strategies without OLTCs are higher than strategies

Table 2.5: VMI corresponding to each case and strategy.

	A	B	C	D	E	F	G	H	I	J
I	2.21987	2.21992	2.21992	2.21992	2.21992	2.21992	2.21992	2.21992	2.21992	2.21992
II	2.22522	2.22601	2.22589	2.22555	2.22379	2.22449	2.22448	2.20292	2.20255	2.22515
III	2.14285	2.21992	2.22016	2.22016	2.21992	2.21992	2.21992	2.22016	2.21992	2.21992
IV	2.14289	2.21992	2.21992	2.21992	2.21992	2.21992	2.21992	2.21992	2.21991	2.21986
V	2.15043	2.22487	2.22487	2.22487	2.22551	2.22551	2.22551	2.22486	2.22487	2.22486
VI	2.15026	2.22551	2.22551	2.22487	2.22486	2.2255	2.22486	2.22485	2.22485	2.22481
VII	17.5467	18.0155	17.9356	17.9083	17.5987	17.5204	17.4953	17.6895	17.5047	17.1745
VIII	16.0961	17.5114	17.3309	17.0676	17.1533	17.0768	17.0762	16.9792	16.7199	16.4064
IX	16.0961	16.6164	16.5771	16.2318	16.4919	16.4831	16.5092	16.4328	16.4212	16.3532
X	15.2246	15.8102	15.7939	15.644	15.4097	15.4013	15.4218	15.4222	15.7295	15.6429
XI	17.4326	18.0102	17.9244	17.8751	17.6042	17.5122	17.7071	17.5318	17.4495	16.5475
XII	17.4348	18.0185	17.9302	17.8524	17.6041	17.5017	17.5825	17.529	17.47	16.5464
XIII	17.1116	17.5453	17.3279	17.152	17.1211	17.009	17.0101	16.7948	16.6237	16.2685
XIV	17.0904	17.5126	17.3115	17.261	17.1179	16.8634	16.8632	16.8533	16.5379	16.2412
XV	16.0042	16.6142	16.5539	16.2261	16.4785	16.4732	16.4945	16.4213	16.3763	16.2658
XVI	16.0061	16.6137	16.5556	16.2261	16.4855	16.4785	16.4945	16.4283	16.3106	16.2729
XVII	15.5166	15.8028	15.7736	15.6172	15.5426	15.5356	15.5546	15.5706	15.65	15.6022
XVIII	15.4736	15.8028	15.7736	15.6295	15.394	15.3871	15.406	15.4206	15.6617	15.6147

with OLTCs. Fig. 2.5(b) supports this by showing that the values of VMIs of strategies without OLTCs are lower than the strategies with OLTCs. In addition, Figs. 2.5(a) and 2.5(c) show that losses and VDMI are highly correlated since losses of a line depends linearly on voltage drop over that line.

2.5.2.3 Voltage Unbalance

Fig. 2.5(d) shows maximum voltage unbalance index over all buses and time periods for each combination of case and strategy. The corresponding numerical values are given in Table 2.7. It is shown that these values are well within the maximum limit of 2%. Hence, in terms of unbalance of voltages, the proposed method is effective for any combination of case and strategy.

2.5.2.4 Number of Switchings

The total number of switchings for different combinations of cases and strategies are given in Fig. 2.5(e). The corresponding numerical values are shown in Table 2.8. Case A (which minimizes

Table 2.6: VDMI corresponding to each case and strategy.

	A	B	C	D	E	F	G	H	I	J
I	2.38812	2.38812	2.38812	2.38812	2.38812	2.38812	2.38812	2.38812	2.38812	2.38812
II	2.38848	2.3886	2.38848	2.38864	2.38788	2.38845	2.38845	2.37727	2.37884	2.38845
III	2.36174	2.38812	2.38812	2.38812	2.38812	2.38812	2.38812	2.38812	2.38812	2.38812
IV	2.36174	2.38812	2.38812	2.38812	2.38812	2.38812	2.38812	2.38812	2.38811	2.38809
V	2.36806	2.38862	2.38862	2.38862	2.38862	2.38862	2.38862	2.38861	2.38861	2.38861
VI	2.36806	2.38862	2.38862	2.38861	2.38861	2.38861	2.38861	2.3886	2.3886	2.38858
VII	2.29903	2.30339	2.30602	2.30513	2.30984	2.31312	2.31545	2.32748	2.32859	2.31825
VIII	2.29229	2.33288	2.33488	2.28806	2.33824	2.32748	2.3445	2.3454	2.33173	2.39701
IX	2.29229	2.30647	2.30251	2.30165	2.30483	2.30488	2.29103	2.28932	2.28935	2.28524
X	2.35131	2.33071	2.33444	2.32663	2.32167	2.32167	2.33207	2.32877	2.35285	2.35315
XI	2.2752	2.30249	2.30649	2.3056	2.30365	2.31301	2.32864	2.32862	2.32457	2.28492
XII	2.27377	2.30244	2.30512	2.30379	2.30361	2.31411	2.35874	2.32864	2.31919	2.28513
XIII	2.27135	2.33144	2.33356	2.33135	2.33692	2.32608	2.34336	2.33383	2.33076	2.32224
XIV	2.27419	2.35132	2.35153	2.33112	2.33705	2.41462	2.39012	2.33333	2.36779	2.31378
XV	2.2704	2.30574	2.30209	2.30104	2.30439	2.30441	2.29039	2.28885	2.28462	2.28443
XVI	2.2699	2.30574	2.30208	2.30104	2.30435	2.30438	2.29039	2.28882	2.2842	2.28437
XVII	2.28662	2.32941	2.33317	2.3254	2.32261	2.32265	2.30977	2.31734	2.35175	2.35432
XVIII	2.28719	2.3294	2.33317	2.32536	2.32036	2.3204	2.30751	2.32744	2.35171	2.35425

only the loss) has the highest number of switchings for all strategies. Total number of switchings in cases B-J are much smaller than that for case A.

2.5.3 Overall comparison

In order to select the best combination of strategy and case, Fig. 2.7 shows the average values of losses, VDMIs, VMIs, VUIs and numbers of switching corresponding to each case. For each case, the average is calculated over 18 strategies. Figs. 2.7(a) - 2.7(d) show that the average values of losses, VDMI, VMI and VUI do not vary much with cases. On the other hand, Fig. 2.7(e) shows that the average number of switchings varies significantly with the weights of objective functions. Hence, in this work, case J, which corresponds to $\alpha = 0.1, \beta = \gamma = 0.45$, is selected as the best case in terms of number of switchings. Since losses of each case are very close to each other, case J is concluded as the best one.

Moreover, Fig. 2.8(a) compares different strategies based on average values of the same indices. For each strategy, the average is calculated over 10 cases. Figs. 2.8(a) and 2.8(b) show that

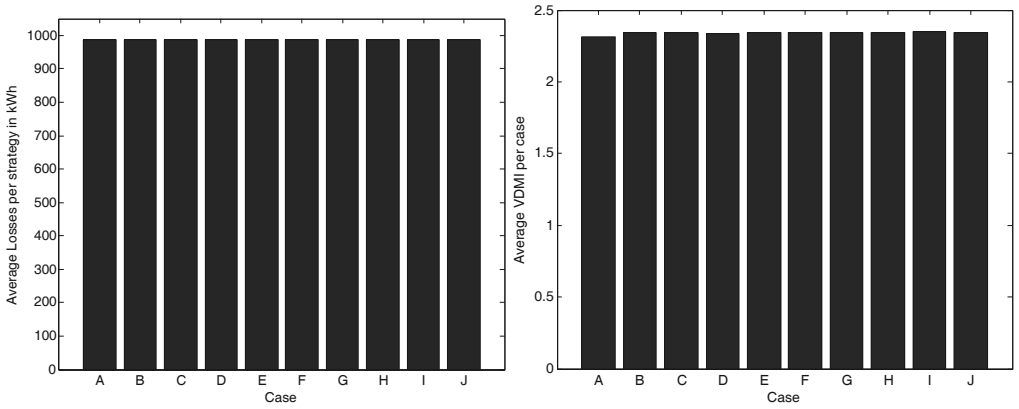

(a) Average losses

(b) Average VDMI

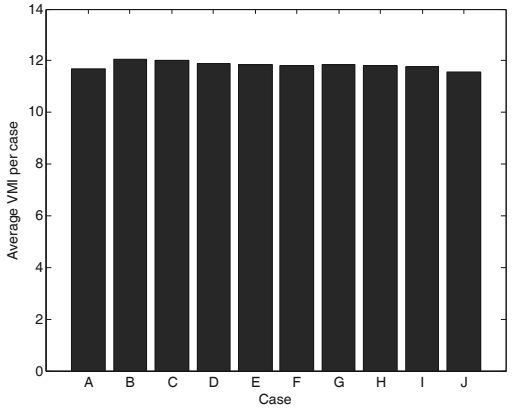

(c) Average VMI

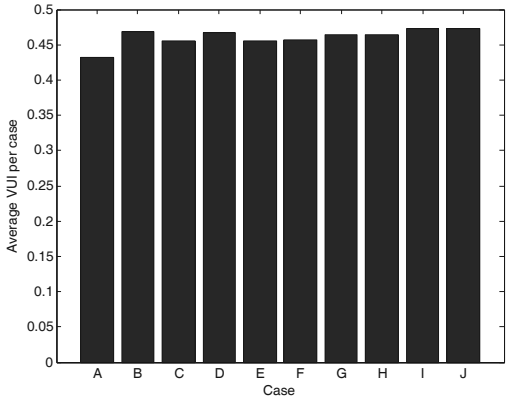

(d) Average VUI

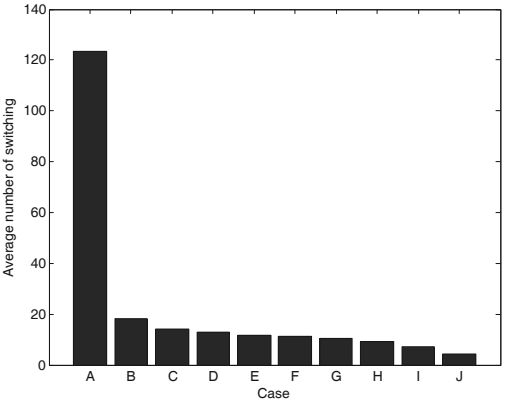

(e) Average number of switchings

Figure 2.7: Comparison of cases based on average losses, VDMI, VMI, VUI and number of switchings.

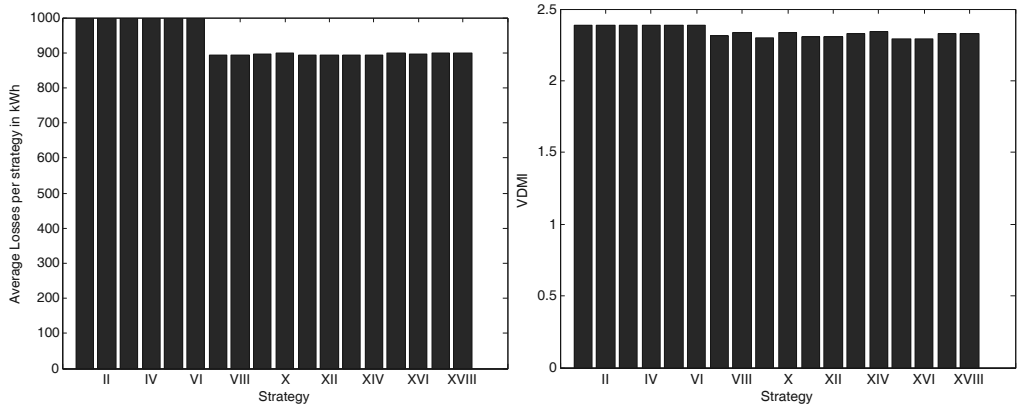

(a) Average losses

(b) Average VDMI

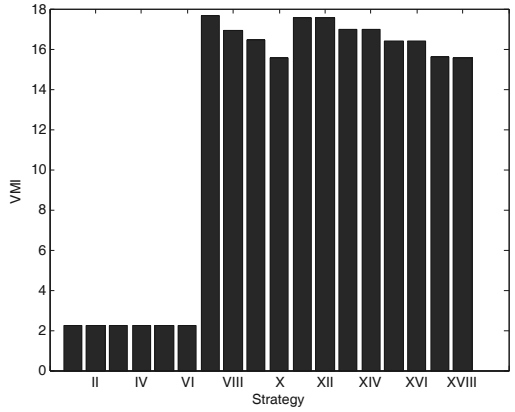

(c) Average VMI

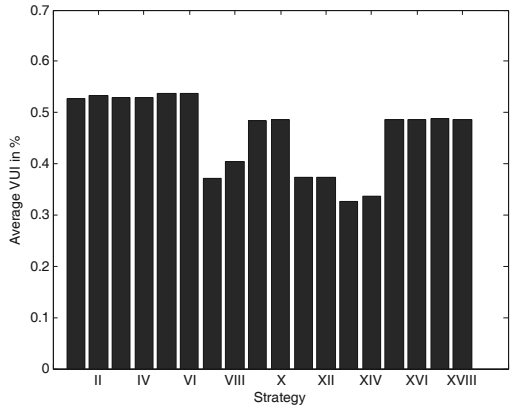

(d) Average VUI

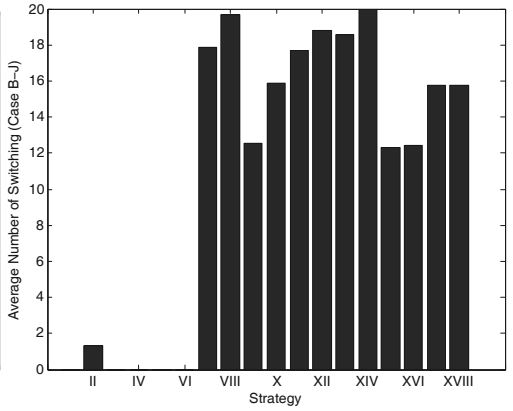

(e) Average number of switchings

Figure 2.8: Comparison of strategies based on average losses, VDMI, VMI, VUI and number of switchings. Since case A does not minimize number of switchings, it is not included in the calculation of average number of switchings.

Table 2.7: VUI corresponding to each case and strategy.

	A	B	C	D	E	F	G	H	I	J
I	0.526817	0.526817	0.526817	0.526817	0.526817	0.526817	0.526817	0.526817	0.526816	0.526809
II	0.534178	0.534177	0.534177	0.534177	0.534177	0.534177	0.534177	0.534177	0.534177	0.534177
III	0.541123	0.526817	0.526817	0.526817	0.526817	0.526817	0.526817	0.526817	0.526816	0.526809
IV	0.541123	0.526817	0.526817	0.526817	0.526817	0.526817	0.526817	0.526817	0.526816	0.526809
V	0.572913	0.534177	0.534177	0.534177	0.534177	0.534177	0.534177	0.534177	0.534177	0.534177
VI	0.572913	0.534177	0.534177	0.534177	0.534177	0.534177	0.534177	0.534177	0.534177	0.534177
VII	0.187667	0.38868	0.38868	0.38868	0.38868	0.396383	0.396399	0.396399	0.396399	0.396289
VIII	0.507032	0.570251	0.336201	0.561362	0.336201	0.336201	0.336197	0.336197	0.336197	0.385597
IX	0.507032	0.460787	0.460787	0.460787	0.460787	0.460787	0.510253	0.50839	0.50839	0.508332
X	0.526475	0.482175	0.482175	0.482175	0.482175	0.482175	0.482175	0.483823	0.483823	0.483792
XI	0.18895	0.3891	0.3891	0.3891	0.3891	0.396678	0.396694	0.396694	0.396694	0.396599
XII	0.18895	0.3891	0.3891	0.3891	0.3891	0.39781	0.396694	0.396694	0.396694	0.396599
XIII	0.182371	0.336201	0.336201	0.336201	0.336201	0.336201	0.336197	0.336197	0.336197	0.385594
XIV	0.131664	0.336201	0.336201	0.336201	0.336201	0.336201	0.336197	0.336197	0.502776	0.385594
XV	0.513904	0.460787	0.460787	0.460787	0.460787	0.460787	0.50839	0.50839	0.50839	0.508325
XVI	0.513904	0.460787	0.460787	0.460787	0.460787	0.460787	0.50839	0.50839	0.50839	0.508332
XVII	0.527099	0.482176	0.482176	0.482176	0.482176	0.482176	0.483824	0.483824	0.483824	0.483784
XVIII	0.523338	0.482176	0.482176	0.482176	0.482176	0.482176	0.483824	0.483824	0.483824	0.483792

the average values of losses and VDMI for different strategies are close to each other. Figs. 2.8(c) and 2.8(e) show that the values of VMI and number of switchings corresponding to strategies without OLTCs are lower than those corresponding to strategies with OLTCs. However, Fig. 2.8.(a) shows that strategies I-VI have higher losses than strategies VII-XVIII. Hence, strategies I-VI are not considered further.

Furthermore, Fig. 2.8(e) shows that strategy XV has the lowest number of switchings. Moreover, Fig. 2.8(d) shows that the VUI values for all strategies are well within the allowable maximum limit. Furthermore, in term of losses and VDMI, strategies VII-XVIII are very close to each other. Lastly, although strategy XV does not have the lowest values of VMI, it possesses a VMI value which is reasonably close to the lowest VMI value (among the strategies VII-XVIII). Therefore, strategy XV, in which OLTCs operate uniformly while SVC and SC operate non-uniformly, is selected as the best strategy. Furthermore, as an illustration, the voltage profiles corresponding to strategy XV at hours 6, 12 and 20 are shown in Fig. 2.9.

Table 2.8: Total number of switchings corresponding to each case and strategy.

	A	B	C	D	E	F	G	H	I	J
I	6	0	0	0	0	0	0	0	0	0
II	21	3	3	0	3	0	0	3	0	0
III	78	0	0	0	0	0	0	0	0	0
IV	96	0	0	0	0	0	0	0	0	0
V	111	0	0	0	0	0	0	0	0	0
VI	29	0	0	0	0	0	0	0	0	0
VII	86	23	20	20	20	19	18	16	15	10
VIII	83	34	21	23	21	19	18	18	16	7
IX	83	33	21	16	9	9	7	6	6	6
X	87	22	22	20	20	19	19	15	3	3
XI	210	23	20	21	20	19	16	15	16	9
XII	212	23	22	21	20	19	22	17	16	9
XIII	169	27	21	20	21	19	18	17	16	8
XIV	183	30	23	20	23	23	20	17	17	7
XV	175	33	19	16	9	9	6	6	8	5
XVI	182	33	19	16	9	9	6	6	8	6
XVII	207	22	20	19	19	19	19	17	5	2
XVIII	201	22	20	20	19	19	19	15	5	3

2.5.4 Computational Burden

All simulation studies have been carried out on a personal computer with Intel Xeon E5420 2.5 GHz CPU, 4 GB memory and windows 7 as the operation system. For solving (P2.0) and (P2.2),

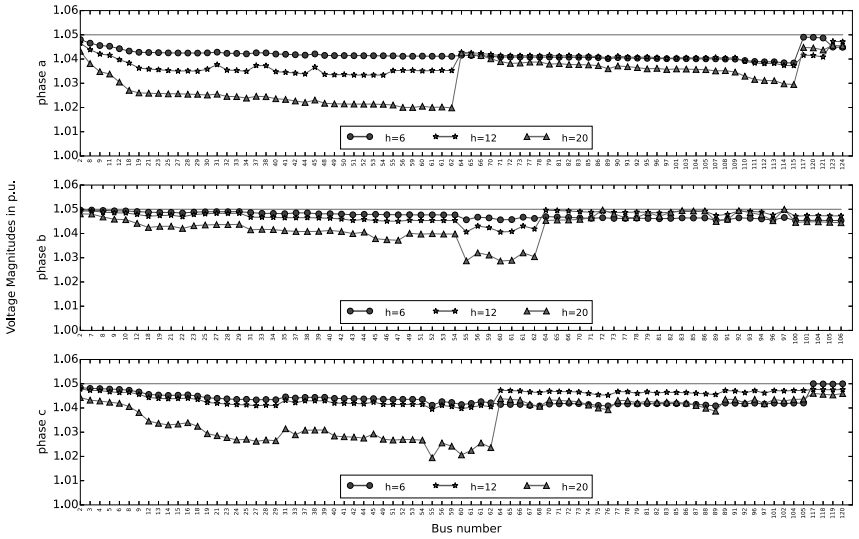

Figure 2.9: Voltage profile at hours 6 12 and 20 corresponding to strategy XV.

bonmin (Basic Open-source Nonlinear Mixed INteger programming) was used [162]. IPOPT (Interior Point OPTimizer) 3.10.1 was used for solving (P2.1) [161, 163]. The AMPL (A Mathematical Programming Language) was used as modelling language [164]. Table 2.9 shows various pertinent details of the problem addressed in this chapter. This table also shows that due to a very large search space, the original problem P2.0 was unsolved even after 8 hours. However, the proposed two-stage approach could solve the formulated problem (P2.1 and P2.2) in less than 10 minutes (for a study horizon of 24 hours).

2.5.5 Further Issues

Before concluding the chapter, several other important issues also need to be addressed as discussed below.

2.5.5.1 Optimality of the Solution

The obtained solutions described in Sections 2.5.2 and 2.5.3 above could not be checked for optimality. Actually, for checking the optimality, a Monte-carlo simulation (MCS) study, in which all the possible combinations of the positions of the voltage control devices are checked, needs to be carried out. Now, in the system under study, there are 9 (equivalent single phase) OLTCs, 3 (equivalent single phase) SVCs and 6 (equivalent single phase) SCs. Each OLTC and SC has 33 and 9 possible tap positions, respectively, while each SVC has 6 possible values of X_{SL}. Therefore,

Table 2.9: Comparison of Computational Burden

Mean computation time	P0 was unsolved after 8 hour	
	Total 1 P1 and 24 P2s	$<$ 10 minutes
Original MINLP	Continuous Variables	47950
	Binary Variables	600
NLP	Continuous Variables	48550
Binary NLP	Continuous Variables	1926
	Binary Variables	15
Search space	MINLP (24h)	2^{600+24}
	Binary-MINLP (per-hour)	2^{15}

the total number of possible combinations is $33^9 \times 6^3 \times 9^6$. Now, the average computational time for evaluating a single combination is about 0.3 seconds. Therefore, with available computational resources, the total time required for checking all the combinations would be 5.07×10^{13} years. As a result, the MCS study could not be undertaken and thus, the optimality of the obtained solution could not be checked.

2.5.5.2 Performance under different load curves

In this chapter, the load profile shown in Fig. 2.4 has been considered so far. To investigate the applicability of the proposed algorithm for different other load profiles, real and reactive load profiles shown in Fig. 2.10 and 2.11, respectively, have been furthered considered along with the same generation profile shown in Fig. 2.4 [77].

The values of total losses and number of switchings corresponding to strategy XV for all cases of different load profiles are shown in Fig. 2.12 and Fig. 2.13, respectively. Fig. 2.12 shows that the losses are close to each other. However, Fig. 2.13 shows that more switching operation are needed in case of commercial and industrial profiles as compared to the residential profile. In addition, mean computation time for solving the subproblem (P2.1) and (P2.2) over all cases are shown in Table 2.10 which shows that there is small difference in terms of computational burden for commercial and residential loads. However, for industrial loads, the computational burden is relatively high. This is due the the fact that the profile of industrial load has more drastic variations

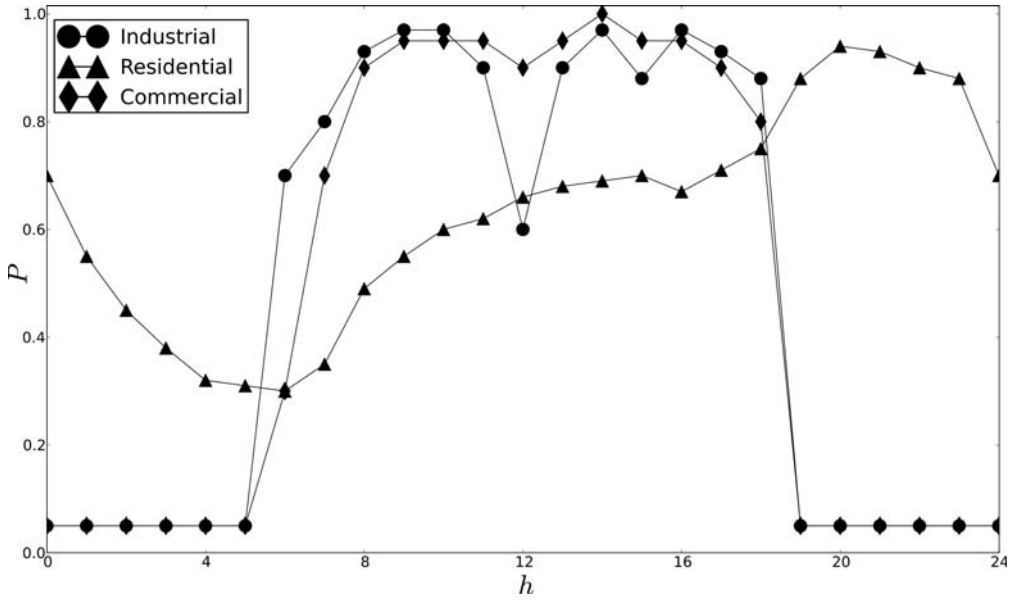

Figure 2.10: Different real power load profiles for comparison of performance of strategy XV.

Table 2.10: Comparison of Computation Time of Different Load Profiles

Profile	Mean Computation Time	
	P1 (seconds)	P2 (seconds)
Commercial	25.03	7.93
Industrial	67.70	7.68
Residential	27.32	12.95

as (compared to residential and commercial loads) and therefore, the problem P1 (which takes into account the load profile of the entire day) is harder to solve for industrial loads. However, the computational burden corresponding to P2 (which takes into account only one-hour ahead prediction) are quite similar to each other.

2.5.5.3 24-hour ahead versus 1-hour ahead optimization

In the results presented so far, the voltage regulation problem has been solved for the next 24 hours period in which the entire load (generation) variation for the next 24 hours has been considered in the optimization process. On the other hand, the voltage regulation problem can also be solved

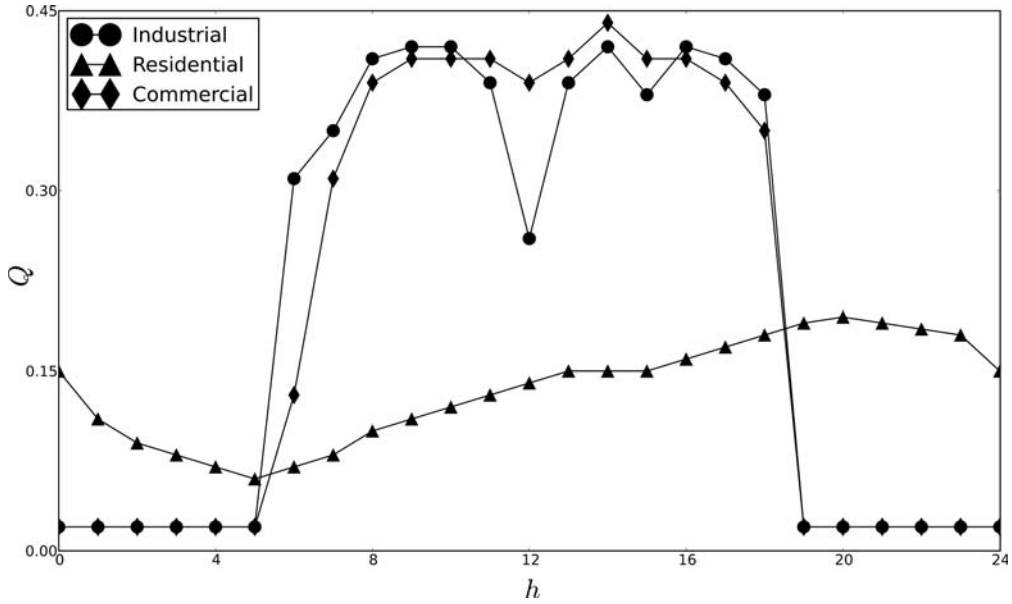

Figure 2.11: Different reactive power load profiles for comparison of performance of strategy XV.

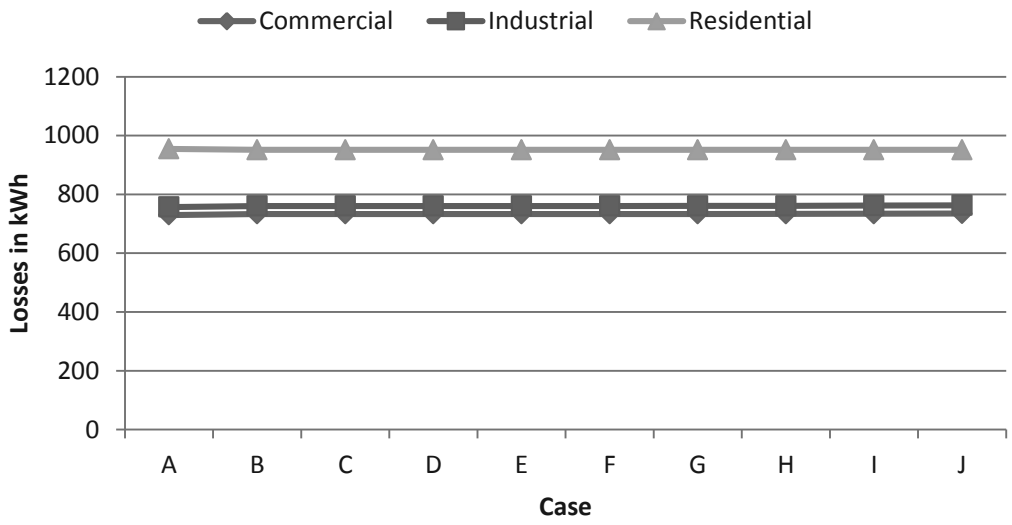

Figure 2.12: Comparison of total losses for different load profiles using strategy XV for all cases.

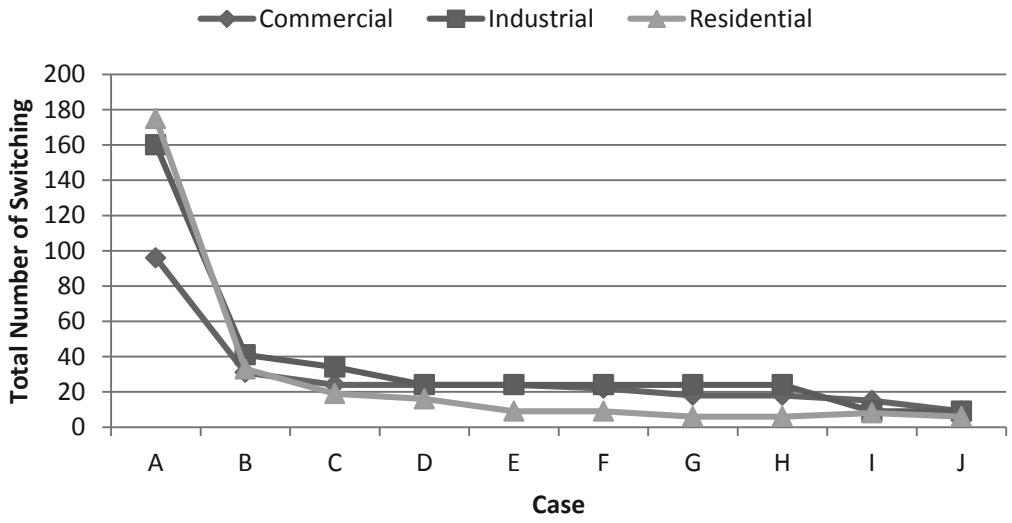

Figure 2.13: Comparison of total number of switchings for different load profiles using strategy XV for all cases.

by an hour-by-hour optimization procedure (again for the next 24 hours period). It would be instructive to compare the results of these two different approaches. Table 2.11 shows such a representative result corresponding to strategy XV, case J. From this table it is observed that the number of switchings, losses and total computation time are more with hour-by-hour technique (as compared to those for 24-hour optimization procedure). On the other hand, quality of forecasted data is high with hour-by-hour optimization procedure [119]. Therefore, neither method can be considered to be superior to the other one and, hence, depending on the objective of the DNO, the most appropriate method should be chosen.

It is to be noted that the one hour ahead dispatch can also be used effectively if there is a large difference between the forecasted and actual load and generation pattern. In case of this large difference (between the actual and the forecasted generation and load pattern), the optimum values calculated with 24-hour ahead dispatch would no longer be valid. In that case, the one hour dispatch would be adopted with one-hour ahead forecasted values of load and generation patterns (which are expected to be quite accurate) and the resulting settings of OLTCs, SCs and SVC slopes would be implemented.

Table 2.11: 1-hour versus 24-hour optimization

Simulation Interval	1-h	24-h
Losses (kWh)	980.32	951.90
number of switchings	12	5
Number of P1 runs	24	1
Number of P2 runs	24	24
Total computation time (seconds)	30.7	88.6
Forecast quality	better	worst

Table 2.12: Real and reactive power load and generation profiles

h	$P(h)$	$Q(h)$	$P_{PV}(h)$
12:00	0.95	0.8	0.95
12:01	0.95	0.8	0
12:02	0.95	0.8	0.95

2.5.5.4 Fast Moving Clouds Effects

The PV generation profile depicted in Fig. 2.4 is valid for a clear day without any clouds. In reality, many days are cloudy. In particular, when fast moving cloud is passing above a distribution network with high penetration of PV, power fluctuation with high rate of change may exist in the networks.

The proposed approach, using one time step ($h^{max} = h = 1$), can be used in this kind of situation for voltage regulation because it can be solved in less than 1 minute. The delay time of OLTC is around 2-3 minutes. Therefore, by the time the tap position of an OLTC is to be changed, one run of the proposed algorithm can be completed to obtained the settings of the control variables. For illustration, a sudden change in PV generation between 12:00 and 12:02 hour as shown in Table 2.12 has been assumed. The variation of real and reactive power loads in the same period are also shown in Table 2.12. The proposed approach was implemented by using 1-minute ahead forecast for two intervals between 12:00 and 12:02 hour corresponding to strategy XV. The maximum computation time (over all cases A-J) has been found to be approximately 10 seconds

Table 2.13: Optimal Settings of OLTCs, SCs and SVC

Time			12:00	12:01	12:02
OLTC	R1	a	8	8	8
		b	8	8	8
		c	8	8	8
	R2	a	0	0	0
	R3	a	1	1	1
		c	0	0	0
	R4	a	0	-6	-6
		b	0	-6	-6
		c	0	-6	-6
SVC	X_{SL}	a	0.01	0.01	0.01
		b	0.01	0.01	0.01
		c	0.01	0.01	0.01
	$\lvert\bar{E}_v^{ref}\rvert$		1.0486	1.0461	1.0484
SC	C1	a	0	0	0
		b	0	0	0
		c	0	0	0
	C2	a	0	0	0
	C3	b	0	0	0
	C4	c	0	0	0

which is small enough to determine the optimal values of the control variables before the next sudden change in generation takes place. The optimal values of control variables at 12:00, 12:01 and 12:02 hours are shown in Tables 2.13 for strategy XV, case J. Therefore, the proposed method is equally capable of voltage regulation in the presence of fast moving clouds. The OLTC R4 requires switching of 6 steps in less than one minute which may be a difficult task for conventional OLTC. However, with fast-response tap changer proposed in [165], this task can be accomplished easily.

Furthermore, the proposed method requires accurate network model as well as accurate information of loading and generating (from DG) conditions. At present, the required metering and communication infrastructure for transferring these information to the central station does not exist in LV network. However, with the deployment of smart grid infrastructure, these information are quite likely to be available in the central station in the near future. Moreover, for taking into account the uncertainties of network impedances, loads and generation in the optimization procedure, robust optimization technique [128] can be adopted. These aspects are discussed in the subsequent chapters.

2.6 Conclusion

In this chapter, a novel and fast two-stage approach for coordination between OLTC, SVC and SC for voltage regulation in an unbalanced distribution system has been presented. Several strategies for coordination among OLTCs, SCs and SVC have been considered. The performances of these strategies has been compared on the basis of system power loss, voltage profile, and number of switchings of OLTCs, SVC and SC. From this comparative study, it has been found that uniform operation of OLTC and non-uniform operation of SVC and SC is most beneficial to the system. Further, as the proposed approach takes less than 1 minute for solving the regulation problem before it can be implemented, it can be used for hourly dispatch of OLTCs, SVC and SCs.

In the next chapter, a procedure for taking into account the uncertainties of loads and generations into the voltage regulation problem is described.

3 — Robust Voltage Regulation in Distribution System With Uncertain Generation and Load

As far as the laws of mathematics refer to reality, they are not certain;
and as far as they are certain, they do not refer to reality.
- Albert Einstein

Abstract

The last chapter assumes that load and generation are known perfectly. However, in practice, there are always measurement as well as prediction errors. Therefore, this chapter assumes that those quantities are uncertain. It discusses a robust optimization technique to solve the voltage regulation problem in an unbalanced radial distribution system in the presence of uncertainties in loads and distributed generation. The formulated problem is also a mixed-integer nonlinear programming (MINLP). However, the two-stage approach used in Chapter 2, in particular the second stage, requires high computation time. Therefore, the second stage is modified using the absolute value constraints approach which results in a nonlinear optimization problem. Hence, the two stages now are nonlinear optimization problems and require smaller computational time than that of the approach of Chapter 2. To verify the robustness of the solution obtained by the proposed method, extensive Monte Carlo simulations studies have also been carried out. The efficacy of the proposed method has been tested in modified IEEE 123 bus unbalanced radial distribution system.

3.1 Introduction

DUE to various reasons, penetration of renewable-energy-based distributed generation (DG) in distribution system will increase in the future. These DGs, such as wind and solar energy, are highly intermittent and uncertain. Hence they can affect voltage regulation in distribution

system adversely [62].

As a result, it is important to consider these uncertainties in voltage regulation problem. Uncertainties can be considered using fuzzy logic [25, 166], stochastic approaches [73, 75, 102, 124, 125, 167], interval arithmetic [104, 107], reachability set [126] or robust optimization technique [128]. Both fuzzy logic and stochastic approaches provide no guarantee that a solution will be always feasible for all possible combinations of generations and loads. On the other hand, robust optimization technique tries to find such guaranteed feasible solution [128]. Unlike stochastic approach (which works on the basis of probability distribution of the uncertainties), robust optimization technique considers the worst scenarios and finds a solution which is feasible in all possible scenarios. It is to be further noted that the worst values of uncertain parameters are generally easier to identify than their probability distributions. In spite of these potentials, only few applications of robust optimization technique in voltage regulation problem are available in the literature.

In [168], on-load tap changer (OLTC), shunt capacitor (SC), and reactive power of distributed generation are optimized to minimize the total losses. Initially, the AC optimal power flow (ACOPF) equations are linearized and subsequently, the robust optimization technique described in [169, 170] is implemented on the linearized version of ACOPF. However, the formulation considers only uncertainty in network admittances and has been tested only in a balanced network. In [171], interval method and linear model of the network are used to consider uncertainties in a balanced system. However, it considers neither distributed generator nor SC.

For considering the uncertainties in voltage regulation problem (VRP) of unbalanced distribution system, this chapter poses the VRP in an unbalanced radial system with uncertain distributed generation and loads as a robust optimization (RO) problem based on the philosophy laid down in [107, 128] and the monotonicity of voltage magnitudes vis-a-vis the variation of line power flows in most of the normal situations [172–175]. Further, a computationally efficient two-stage approach is developed to solve the proposed optimization problem. The salient features of the proposed two-stage method are:

1. The second stage is a nonlinear optimization method, not a mixed integer nonlinear optimization technique as in [20].

2. Each discrete variable is replaced by new set of constraints which have only continuous

variables using absolute value constraint approach [176] and, therefore, the optimization problem can be solved by commonly available solvers for solving a nonlinear programming problem. This approach is different from [177] which augments the Lagrangian function by quadratic penalty function which, as a result, requires a customized solver. Similarly, the optimum multiplier technique used in [178] also requires a customized solver.

The rest of this chapter is organized as follows. Section 3.2 introduces the robust optimization method. Section 3.3 discusses in detail the formulation of the robust voltage regulation problem. Furthermore, Section 3.4 explains the two-stage approach to solve the voltage regulation problem. Section 3.5 discusses the main results of this chapter obtained in a modified IEEE 123 bus system. Finally, Section 3.6 concludes this chapter.

3.2 Robust Optimization

Mathematically, the voltage regulation problem can be formulated as,

$$\begin{aligned} \underset{\mathbf{c},\mathbf{d}}{\text{minimize}} \quad & f(\mathbf{c},\mathbf{d}) \\ \text{subject to} \quad & \mathbf{g}(\mathbf{c},\mathbf{d},\mathbf{p}) = 0 \\ & \mathbf{h}(\mathbf{c},\mathbf{d},\mathbf{p}) \leq 0 \end{aligned} \tag{P3.0}$$

where $\mathbf{c}, \mathbf{d}$ and $\mathbf{p}$ are vectors of continuous variables, discrete variables and parameters, respectively; f is the objective function; $\mathbf{g}$ is the vector of functions of equality constraints representing physical nature of the distribution system, and $\mathbf{h}$ is the vector of functions of inequality constraints representing physical and regulatory limits of variables. The details of the objective functions and various constraints are given in the next section.

In practical situation, a distribution system operator needs to calculate the optimal values of the settings of various controllers before the actual generations and loads happen. Further, these controller settings should be effective even if the actual generation and loads vary within some specified intervals such that the magnitudes of the three phase voltages as well as the amount of unbalance in the three phase voltages remain within the stipulated limits. If such controller settings are obtained, then the solution is immunized against uncertainty of loads and generations.

Mathematically, this can be done by defining a set of scenarios $\mathbf{S} = \{\mathbf{s}_1, \mathbf{s}_2, ..., \mathbf{s}_{n_S}\}$ where a scenario $\mathbf{s}_i$ includes values of fixed parameters and a possible set of values of uncertain parameters;

and n_S is the total number of scenarios. A solution is robust if it is feasible for all $\mathbf{s}_i$. In order to find the robust solution, problem (P3.0) is reformulated into problem (P3.1).

$$\begin{aligned} \underset{\mathbf{c},\mathbf{d}}{\text{minimize}} \quad & f(\mathbf{c},\mathbf{d},\mathbf{S}) \\ \text{subject to} \quad & \mathbf{g}_i(\mathbf{c},\mathbf{d},\mathbf{s}_i) = 0 \;\; \forall i \in 1,2,...,n_S \\ & \mathbf{h}_i(\mathbf{c},\mathbf{d},\mathbf{s}_i) \leq 0 \;\; \forall i \in 1,2,...,n_S \end{aligned} \tag{P3.1}$$

In problem (P3.1), since for every uncertain quantity (load or generation) there are infinite number of possibilities, there are infinite number of possible $\mathbf{s}_i$, i.e. $n_S = \infty$. Hence, solving (P3.1) for all possible $\mathbf{s}_i$ involves solving an infinitely large problem. Section 3.2.1 proposes an alternative approach to identify a finite set of scenarios ($n_S < \infty$) such that the solution of (P3.1) for these scenarios ensures that all the other scenarios are taken care of in the final solution.

In this regard, it would be informative to compare robust optimization (RO) with stochastic and non-robust (conventional) optimization (NRO) techniques. The exact values of parameters (such as load and generation) are not needed in case of robust and stochastic approaches but are needed in case of non-robust approach. Moreover, stochastic optimization requires the probability distribution of the uncertain parameters. On the other hand, robust optimization requires only the ranges of the uncertain parameters. The solution of robust optimization gives the ranges of all voltages and currents in the network. The solution of stochastic optimization includes the expected values of voltages and currents in the network. Therefore, the expected values of the output quantities depend on the probability density function (PDF) of the input quantities and, as a result, for a meaningful solution of a stochastic optimization problem, reliable information of the PDFs is necessary. Lastly, the solution of conventional optimization gives the exact value for each voltage or current in the network. Obviously, the accuracy of the exact values obtained by the deterministic approach depend on the accuracy of the exact values of the input quantities. The salient features of these three optimization methods are shown in Table 3.1.

3.2.1 Reduction of Total Number of Scenarios

The total number of scenarios can be reduced based on the monotonicity of magnitudes of voltages against variation of line power flows in most of the normal situations [172–175]. Since the grid code mandates that the voltage magnitude be maintained between 0.95 pu and 1.05 pu, the monotonicity is generally valid for both real and reactive power flows in balanced and unbalanced

Table 3.1: Qualitative Comparison among Robust, Stochastic and Conventional Optimization Techniques

	Type of Optimization		
	Robust	Stochastic	Non-Robust (Conventional)
Exact value of a parameter	Not needed	Not needed	Needed
Probability distribution of parameters	Not needed	Needed	Not needed
Ranges of parameters	Needed	Not needed	Not needed
Characteristic of an output state variable*	Range	Probability distribution	Exact value

*state variables are defined in the first paragraph of Section 3.3.

systems [175, 179]. The monotonicity property allows the calculation of the boundaries of magnitude of voltages in a balanced power system by solving two non-linear programming problems at two sets of loading condition in which all loads are set at their corresponding maximum and minimum values, respectively [107].

On the other hand, in an unbalanced network, due to the unbalance in mutual impedances, voltage magnitudes may monotonically increase or decrease when the power flow increases [172, 173, 179]. Hence, the minimum magnitude of voltage at any particular phase of a bus does not necessarily coincide with minimum magnitude of voltage of other phases of the same bus. Consequently, application of method proposed in [107] in an unbalanced network requires different sets of extreme situations.

The extreme cases can be identified by separating the generators and loads into the following:

1. Group A: three-phase DGs.
2. Group B: single-phase DGs connected at phase a.
3. Group C: single-phase DGs connected at phase b.
4. Group D: single-phase DGs connected at phase c.

5. Group E: all loads.

Each group has two extreme cases corresponding to situations in which all generations (loads) are set at their corresponding maximum and minimum values, respectively. Hence, total number of combinations of extreme situations formed by those five groups are $n_S = 2^5 = 32$. These situations are taken as possible scenarios in this chapter.

The classification of generators into groups A - D is required to ensure that the extreme effects of unbalance power injections from DGs are considered. On the other hand, group E consists of all single and three-phase loads. Off course, the loads also could have been divided into separate groups of single phase and three phase loads (similar to group A - D for DGs), but in that case, the number of possible combination would have been $n_S = 2^8 = 256$, which in turn, would make the problem (P3.1) too huge to be solved by the computational resources available during the course of the work of this chapter.

Based on the philosophy laid down in [107], this chapter conjectures that the set of extreme scenarios largely defines the boundary of voltage in all buses and hence can be utilized in robust voltage regulation problem. A robust solution satisfies all constraints of (P3.1) for all possible combinations of loads and generations within the given intervals. Upon extensive simulation studies, this conjecture was found to be true (the details are given in Section 3.5).

Note that the work described in [167] also finds a finite set of scenarios ($n_S < \infty$). However, it uses probabilistic approach which also include non-extreme cases.

3.3 Problem Formulation

Robust voltage regulation in an unbalanced radial distribution system can be formulated as an optimization problem (P3.1) to find the optimal values of control variables considering all extreme cases for minimizing certain objective function subjected to equality and inequality constraints. The set of equality constraints represents Kirchhoff law of current, physical characteristics of the distribution system elements, and consistency constraints. The set of inequality constraints represents physical and regulatory limits of the control variables and the state variables. The control variables include taps position of OLTC, SC and static var compensator (SVC) slope as well as SVC voltage reference value. The state variables include real and imaginary parts of voltages and currents in the distribution network.

3.3.1 Objective Functions

In this chapter, two objective functions have been considered. These are:

1. The total line losses, J_5, given by

$$J_5 = \sum_{s=1}^{n_S} \sum_{h=1}^{24} \sum_{p=a}^{c} \sum_{i=1}^{n_{BUS}} \sum_{j=1, j\neq i}^{n_{BUS}} r_{ij}^{p} |\bar{I}_{ij}^{ps}(h)|^2. \tag{3.1}$$

   Note that when $n_S = 1$, J_5 in Eq. (3.1) is equivalent to J_1 as defined in Eq. (2.7).

2. Total number of switchings operations over all time periods, J_6, given by

$$J_6 = J_2 + J_3 + J_4 \tag{3.2}$$

Finally, the composite objective function is formed as

$$f(\mathbf{c}, \mathbf{d}) = \alpha J_5 + \beta J_2 + \gamma (J_3 + J_4), \tag{3.3}$$

where α, β and γ are non-negative weighing factor with $\alpha + \beta + \gamma = 1$. The objective in this chapter is to minimize the function $f(\mathbf{c}, \mathbf{d})$.

3.3.2 Equality Constraints

For every time instant t, and scenario s, physical laws and characteristics of distribution system elements define the following equality constraints [20, 150]. Majority of these constraints are expanded from equality constraints of Chapter 2. In addition, a set of consistency constraints are given in Eqs. (3.6) - (3.9).

3.3.2.1 Constant power load

The current of a constant power load L connected at phase p of bus i corresponding to time t in scenario s, I_L^{ipts}, has the following real and imaginary parts:

$$I_{Lx}^{ipts} = \frac{P_L^{ipts} E_x^{ipts} + Q_L^{ipts} E_y^{ipts}}{(E_x^{ipts})^2 + (E_y^{ipts})^2} \tag{3.4}$$

$$I_{Ly}^{ipts} = \frac{P_L^{ipts} E_y^{ipts} - Q_L^{ipts} E_x^{ipts}}{(E_x^{ipts})^2 + (E_y^{ipts})^2}. \tag{3.5}$$

3.3.2.2 Other constraints

All sets of constraints in Chapter 2 must be extended in similar way as Eqs. (3.4) and (3.5).

3.3.3 Consistency Constraints

The goal of robust optimization is to find the values of the control variables which would remain constant over all scenarios such that the objective function is minimized subject to the equality and inequality constraints. This leads to the following consistency constraints for all time and scenarios.

3.3.3.1 OLTC

$$tap_{mnp}^{ts} = tap_{mnp}^{t1} \; \forall (m,n), \forall s, \forall t \tag{3.6}$$

3.3.3.2 SC

$$sc^{ipts} = sc^{ipt1} \; \forall t, \forall s \tag{3.7}$$

3.3.3.3 SVC

Slope constraints

$$X_{SLv}^{pts} = X_{SLv}^{pt1}, \forall v, \forall s, \forall t \tag{3.8}$$

and voltage reference constraints,

$$E_v^{ref,ts} = E_v^{ref,t1}, \forall t, \forall s \tag{3.9}$$

Note that the state variables, such as voltages and currents, are not subjected to consistency constraints. Their values vary according to the scenarios and the control variables but must satisfy inequality constraints discussed in the following subsection.

3.3.4 Inequality Constraints

Based on physical and regulatory limits, the following inequality constraints are considered for all time t and scenario s.

3.3.4.1 Generic bus voltage magnitude limits

$$0.95 \leq |\bar{E}^{ipts}| \leq 1.05 \; \forall i, \forall p, \forall t, \forall s \tag{3.10}$$

if phase p of bus i is *not* connected to the secondary side of an OLTC.

3.3.4.2 Voltage magnitude limits at an OLTC secondary bus

$$0.9 \leq |\bar{E}^{ipts}| \leq 1.1 \ \forall i, \forall p, \forall t, \forall s \tag{3.11}$$

if phase p of bus i is connected to the secondary side of an OLTC.

3.3.4.3 Voltage unbalance limits

For a three-phase bus i, IEC 61000-2-12 [160] specifies that

$$U_i^{ts} = 100\frac{|\bar{E}_i^{2ts}|}{|\bar{E}_i^{1ts}|} \leq 2\% \ \forall i, \forall t, \forall s \tag{3.12}$$

3.3.4.4 Limits on OLTC taps

$$tap^{min} \leq tap_{mnp}^{ts} \leq tap^{max} \ \forall (m,n), \forall p, \forall t, \forall s. \tag{3.13}$$

where tap^{min} (tap^{max}) is the minimum (maximum) value of the position of a tap of an OLTC.

3.3.4.5 SVC limits

1. Slope

$$X_{SL}^{min} \leq X_{SLv}^{pts} \leq X_{SL}^{max}, \forall v, \forall p, \forall t, \forall s \tag{3.14}$$

   where X_{SL}^{min} (X_{SL}^{max}) is the minimum (maximum) slope of an SVC,

2. Voltage reference

$$0.95 \text{ pu} \leq E_v^{ref,ts} \leq 1.05 \text{ pu}, \forall v, \forall t, \forall s \tag{3.15}$$

3. Reactive power

$$Q_v^{min} \leq Q_v^{pts} \leq Q_v^{max}, \forall v, \forall t, \forall s \tag{3.16}$$

   where Q_v^{min} and Q_v^{max} are the minimum and maximum reactive power of an SVC v, respectively.

In conclusion, the robust voltage regulation problem (P3.1) can be rewritten as

$$\begin{aligned} \underset{\mathbf{c},\mathbf{d}}{\text{minimize}} \quad & f(\mathbf{c},\mathbf{d}) \\ \text{subject to} \quad & (3.4) - (3.16). \end{aligned} \tag{P3.2}$$

3.4 Methodology

The optimization problem (P3.2) is essentially a mixed integer nonlinear programming (MINLP) problem involving both continuous and discrete variables. The continuous variables include the voltage reference of an SVC, real and reactive voltage at all buses, real and reactive currents of all loads, generators, SCs, SVCs, and lines. The discrete variables include tap positions of all OLTCs and all SCs, as well as slopes of all SVCs. To solve this MINLP problem, a two stage optimization approach which is based on [20] has been developed in this chapter.

1. Stage I

   (a) Chose a time period t for which the voltage regulation problem is to be solved. This time period t represents a time interval between $t-1$:00 hour and t:00 hour.

   (b) Assume each discrete variables d_i as a continuous variables c_i^1.

   (c) The modified problem is now a non-linear programming (NLP) problem and is solved using an interior point method [161].

   (d) From the optimum values of relaxed discrete variables (denoted as c_k^{I*}), find the closest possible discrete value that is lower than c_k^{I*} and chose this value as the lower bound d_k^{lb}.

2. Stage II

   (a) For each k^{th} discrete variable, define a new discrete variable d_k^2

   $$d_k^2 = d_k^{lb} + b_k \delta_k,\ b_k \in \{0, 1\} \tag{3.17}$$

   where δ_k is the discrete step size of the k^{th} discrete variable; and b_k is the binary variable associated with the k^{th} discrete variable[1]. As a result, each discrete variable has only two possible values which significantly reduces the discrete search space. Even after this reduction, computational time can be significantly high for a moderate-sized system such as IEEE 123 bus system or any larger system. To reduce the computational burden further, a technique described below has been adopted.

[1] Note that Eq.(3.17) is equivalent to Eq. (2.37)

(b) Using the approach of [176], each binary constraint given in Eq. (3.17) is replaced by set of continuous constraints as given below:

$$d_k^c = d_k^{lb} + b_k^c \delta_k, \tag{3.18a}$$

$$b_k^c - \frac{1}{2} = b_{uk} - b_{lk}, \tag{3.18b}$$

$$\frac{1}{2} = b_{uk} + b_{lk}, \tag{3.18c}$$

$$b_{uk} b_{lk} = 0, b_{uk} \geq 0, b_{lk} \geq 0, \tag{3.18d}$$

where d_k^c is the continuous variable replacing the discrete variable d_k^2; the complementary constraints given in Eq. (3.18d) ensure that either b_{lk} or b_{uk} or both are zero [180]. In addition, the constraint given in Eq. (3.18c) ensures that either b_{lk} or b_{uk} is equal to $1/2$. Hence, *strict* complementarity is ensured [180]. Consequently, the value of b_k^c is zero (one) if $b_{lk} = 1/2$ and $b_{uk} = 0$ ($b_{lk} = 0$ and $b_{uk} = 1/2$). Thus, the constraints given in Eq. (3.18) use only continuous variable but still satisfy the constraint given in Eq. (3.17).

(c) Thus, the modified problem is an NLP as shown below in (P3.3) which is solved using an interior point method [161].

$$\begin{aligned} \underset{\mathbf{c}}{\text{minimize}} \quad & f(\mathbf{c}) \\ \text{subject to} \quad & (3.4) - (3.16) \text{ and } (3.18). \end{aligned} \tag{P3.3}$$

(d) Let $t = t + 1$.

(e) If $t \leq t^{max} = n_T$ then repeat steps 1a) - 2d), otherwise stop.

The use of constraints given in Eq. (3.18) (instead of (3.17)) significantly reduces the computational time for practical voltage regulation application.

Furthermore, proper initial values can significantly improve the performance of an interior point method. The following values have been used in this chapter. Initial values of real (imaginary) voltage at each bus are 1, -0.5 and 0.86603 (0, -0.86603 and 0.5) pu for phase a, b, and c respectively; The lower bounds of OLTC taps, SC positions, SVC slope and reactive power of the DGs have been used as their respective initial values. Initial values of auxiliary variables b_i, b_{li} and b_{ui} are 0, 0.5 and 0, respectively and the initial value of voltage reference of SVC is 1 pu.

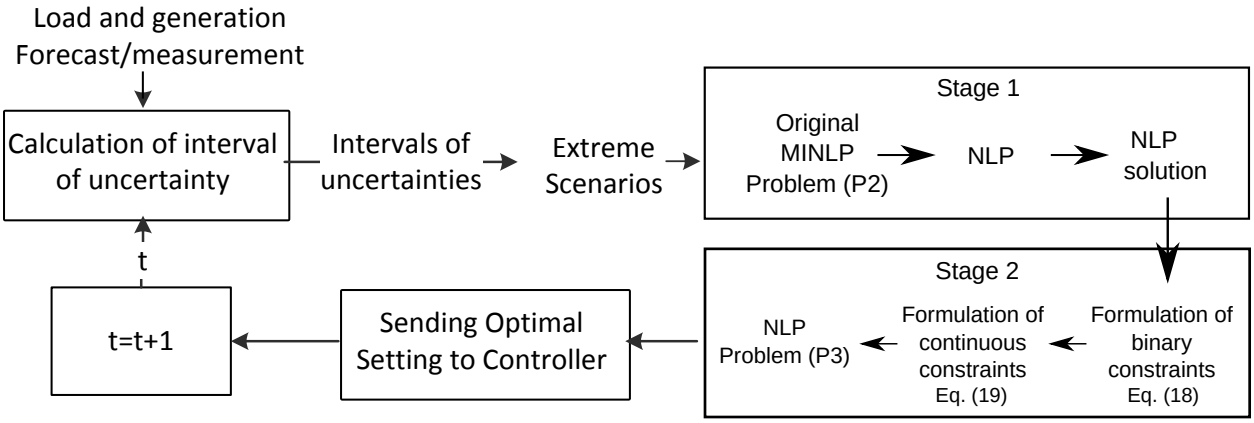

Figure 3.1: The proposed implementation approach.

3.4.1 Implementation Issues

The robust VRP is using the flowchart shown in Fig. 3.1. In a particular hour, the central controller computes the optimized control settings for the next hour based on the forecasted values of load and generation. At the beginning of the next hour, these computed controller settings are sent to the controllers (SVC, OLTC, and SC) for implementation through dedicated communication channels. These settings are kept fixed throughout the hour. As the proposed method requires forecasted values, the accuracies of the solution depends on the accuracies of the forecasted values. However, the quality of modern day short term (one hour ahead) forecasting techniques is quite high and, therefore, the quality of the obtained solution is also expected to be quite high. Note that the expected errors of the forecasted quantities are considered in calculating the intervals of uncertainties and, hence, are considered in the extreme scenarios.

In addition, in case of PV generation with fast moving clouds, if excessive power ramp is detected or forecasted [181], the interval of uncertainties is updated and the proposed method recalculates the new robust settings which, in turn, are resent to all controllers. It is to be further noted that in this work, the local controllers have been assumed to be rendered ineffective as these controllers, when acting alone (without coordination with other controllers), may not always guarantee the voltages to be within the limits.

3.5 Result and Discussion

3.5.1 Modified IEEE 123 Bus System

The proposed method was implemented in a modified IEEE 123 bus system shown in Fig. 2.3. The following modification were made.

1. The given load values are assumed to be peak values.

2. At each phase of a bus with a constant-power load, there is a photo voltaic (PV) generation with capacity of 50% of the rated load of the node. For example, since there is a 40-kW constant power load at phase a of bus 4, there is also a 20-kW DG installed at phase a of bus 4. By this process, a total of 967.5 kW distributed generation has been considered in this system. Appendix B presents more details about load and generation.

3. Constant-impedance and constant-current loads are converted into constant-power loads. Further, no DG is assumed to be present at these buses.

4. The base profiles of loads and generations are given in Fig. 2.4. For considering uncertainties, it is assumed that all loads and generations vary within $\pm 10\%$ from the values given in Fig. 2.4.

5. An SVC is installed at bus 64 having a capacity of 3×250 kVAR (capacitive) and 3×250 kVAR (inductive).

6. A 3 x 250 kVAR three-phase capacitor is installed at bus 73.

7. Three 200 kVAR single-phase capacitors are installed at buses 100 (phase b), 102 (phase c) and 103 (phase a), respectively.

8. Each SC is assumed as a capacitor bank with $n_c = 8$ and, hence, $sc_{SC}^{ip} \in \{0, 1, 2, 3, ..., 8\}$.

9. The slope of an SVC has 6 possible discrete values corresponding to $\{0, 0.01, ..., 0.05\}$.

10. The position of an OLTC has 33 possible values corresponding to $\{-16, -15, ..., +15, +16\}$.

3.5.2 Bounds of Voltage Magnitudes and Unbalance Indices

It is to be noted that the objective of robust optimization is to calculate the upper and lower bounds of the variables of interest in the presence of given amount of uncertainties in load and generation profile. If all of these bounds are feasible then the solution is robust. These bounds are calculated as described below.

For each bus i, phase p and time t, the upper (lower) bound of voltage magnitude u_{mag}^{ip} (l_{mag}^{ip}) is calculated using

$$u_{mag}^{ipt} = \max_{s=1}^{n_S} |\bar{E}^{ipts}| \quad \forall i, p, t, \tag{3.19}$$

and

$$l_{mag}^{ipt} = \min_{s=1}^{n_S} |\bar{E}^{ipts}| \quad \forall i, p, t, \tag{3.20}$$

respectively.

In addition, the upper bound of VUI, u_{bal}^{i}, is calculated using

$$u_{bal}^{it} = \max_{s=1}^{n_S} U_i^{ts} \quad \forall i, t. \tag{3.21}$$

Eq. (3.12) indicates that if upper bound of VUI is feasible then all VUIs are also feasible.

3.5.3 Scope of The Study and Results

For voltage regulation problem, both 24-hour ahead optimization and one-hour ahead optimization have been studied in the literature. However, in this chapter, one-hour ahead optimization has been chosen instead of 24-hour optimization due to the fact that nowadays, in comparison to medium-term (24-hour ahead) forecasting error, the short-term (one-hour ahead) forecasting errors are quite less and, therefore, more accurate solution can be obtained for one-hour ahead optimization.

In the last chapter, strategy XV was found to be the best one among strategies including all voltage control devices. i.e. OLTC, SVC and SC. Therefore, in this chapter also, all these three voltage control devices have been considered. In addition, Chapter 2 shows that the strategies XI-XVIII have lower energy losses than other strategies and case J has lower number of switchings as compared to other cases. Therefore, results corresponding to case J and strategies XI-XVIII are presented below.

Furthermore, these strategies have been compared based on total number of switchings ($J_2 +$

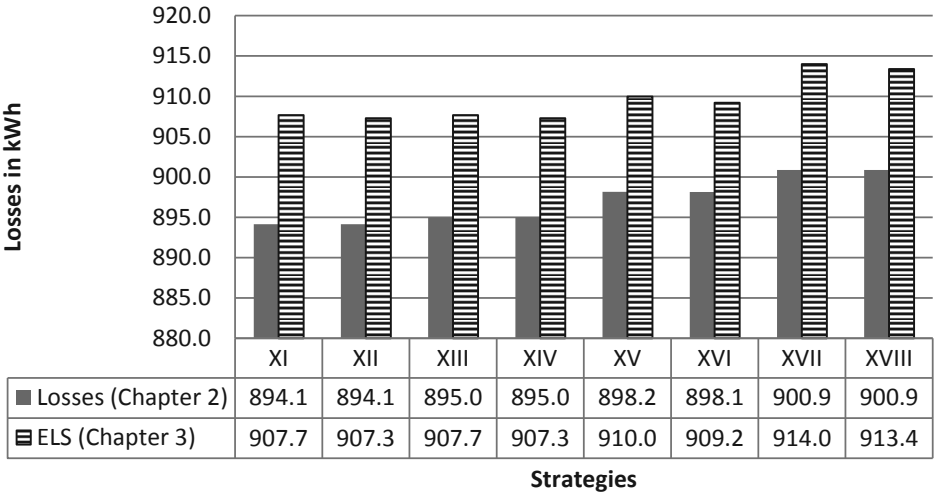

	XI	XII	XIII	XIV	XV	XVI	XVII	XVIII
Losses (Chapter 2)	894.1	894.1	895.0	895.0	898.2	898.1	900.9	900.9
ELS (Chapter 3)	907.7	907.3	907.7	907.3	910.0	909.2	914.0	913.4

Figure 3.2: Comparison of ELS and losses corresponding case J for strategies XI - XVIII using approaches described in Chapter 2 and 3.

$J_3 + J_4$) and average energy loss per scenario (ELS) defined as

$$ELS = \frac{J_5}{N_S}; N_S = 32. \tag{3.22}$$

The values of ELS for these eight strategies corresponding to case J are shown in Fig. 3.2. This figure shows that strategy XII (XVII) has the smallest (highest) average energy loss among all strategies. Strategies in which OLTCs operate non-uniformly (XI-XIV) are associated with lower losses than strategies in which OLTC operates uniformly (XV-XVII). Note that the mean and standard deviation of ELS (corresponding to these eight cases) are 909.6 kWh and 2.5 kWh, respectively. Thus, the values of those losses are arguably very close to each other. In addition, the values of losses based on non-robust approach described in Chapter 2 are also shown in Fig. 3.2. It is obvious that the robust solutions correspond to higher losses than non-robust solutions.

In addition, Fig. 3.3 shows the total number of switchings ($J_2+J_3+J_4$) for those eight strategies corresponding to case J using robust and non-robust approaches. The values of ($J_2 + J_3 + J_4$) when OLTC operates non-uniformly (Strategies XI - XIV) are lower than when OLTCs operate uniformly (Strategies XV - XVIII). Fig. 3.3 also shows that strategies XI and XIII (XVI) have (has) the smallest (highest) total number of switchings among all strategies in case of robust approach. On the other hand, strategy XVII (XI) has the lowest (highest) number of switchings in case of non-robust approach.

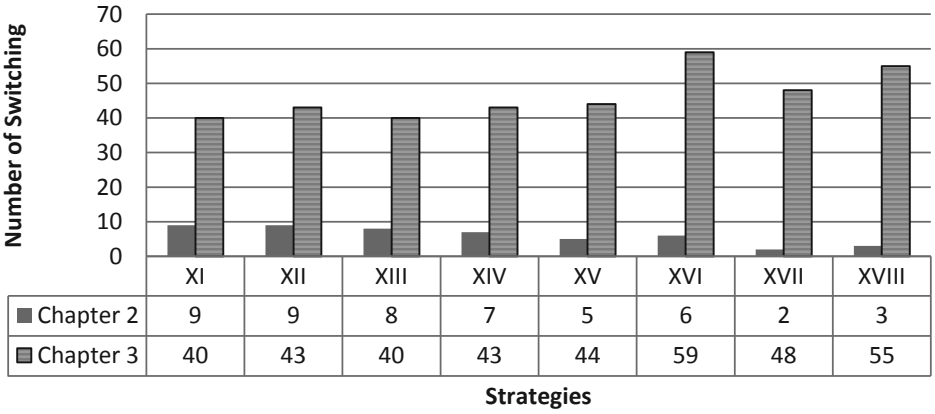

Figure 3.3: Comparison of total number of switchings of different controllers corresponding to the strategies XI-XVIII and case J using approach described in Chapter 2 and 3.

The mean and standard deviation of the total number of switchings are 46.5 and 6.5, respectively. Hence, its standard deviation is higher than that of ELS. Therefore the selection of the best strategies can be based on total number of switchings. Since strategies XI and XIII have the lowest number of switchings, any of the two can be selected as the best strategy. In addition, Fig. 3.2 shows that the two strategies have the same ELS but strategy XI has lower losses in non-robust case. Therefore, Strategy XI is selected as the best strategy.

In addition, as an illustration, Figure 3.4 shows some examples of voltage profiles in the system corresponding to strategy XI at hours 6, 12, and 20. As can be seen in the figure, profiles are moving as the load and generation are changing. However, the proposed method is capable in maintaing the profiles within limits.

3.5.4 Validation of The Proposed Method

For cross-validating the bounds calculated by the proposed method, these bounds have also been calculated through Monte Carlo Simulation (MCS) technique. If the differences between the bounds calculated by the proposed method and MCS technique are within some acceptable tolerance, then the proposed solution can be considered as robust and acceptable. The MCS was performed with OpenDSS 7.6.3.22 [182] and Python 2.7.5 [183]. Since OpenDSS does not have

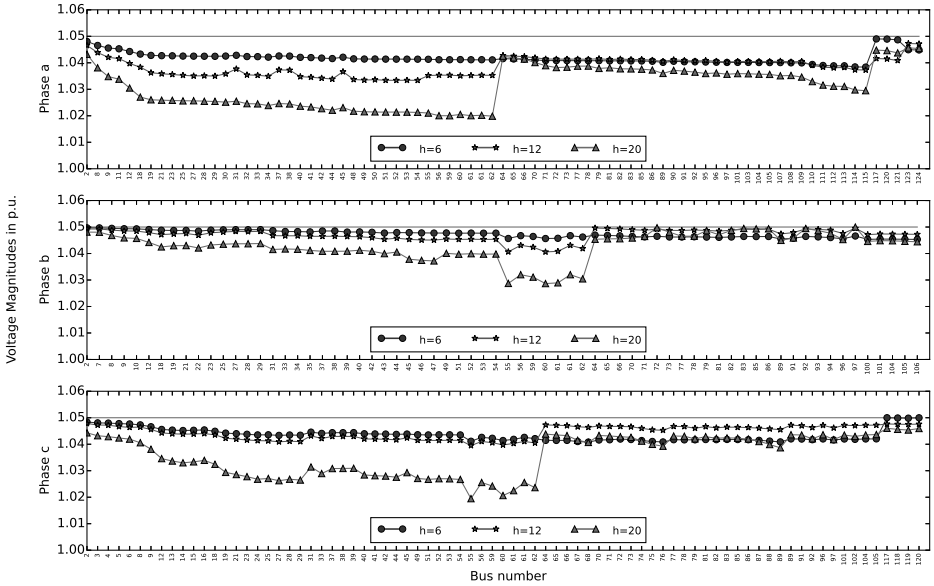

Figure 3.4: Voltage profiles of the system using strategy Xi at hours 6, 12, 20

a model for SVC, for simplicity and without loss of generality, only OLTCs and SCs have been considered in the verification process.

The boundary values of voltage magnitudes of phase a, b, and c (calculated using the proposed method and MCS) for strategy XI and Case J are shown in Figs. 3.5, 3.6, and 3.7, respectively. The upper (lower) bounds obtained by the proposed method and MCS are indicated by u_{rob} and u_{mcs} (l_{rob} and l_{mcs}), respectively. These figures show that the upper and lower bounds of voltage magnitudes obtained by the proposed method and MCS are all feasible and quite close to each other. The maximum difference between the lower (upper) bounds calculated by the proposed method and MCS are 0.79%, 0.19%, 0.23% (0.76%, 0.22%, and 0.35%) for phase a, b, and c, respectively (calculated with respect to the bounds calculated by MCS). These results can be considered to be quite acceptable for all practical purposes.

Similarly, Fig. 3.8 shows the upper bound of voltage unbalance index for strategy XI and Case J. All values are below the upper limit of 2%. The robust bounds differ from the MCS bounds with maximum error of 0.27% (calculated as absolute value of difference between robust and MCS bounds).

Figure 3.5: Bounds of bus voltage magnitude (in pu) for phase a corresponding to the time interval between 12:00 and 13:00 hours.

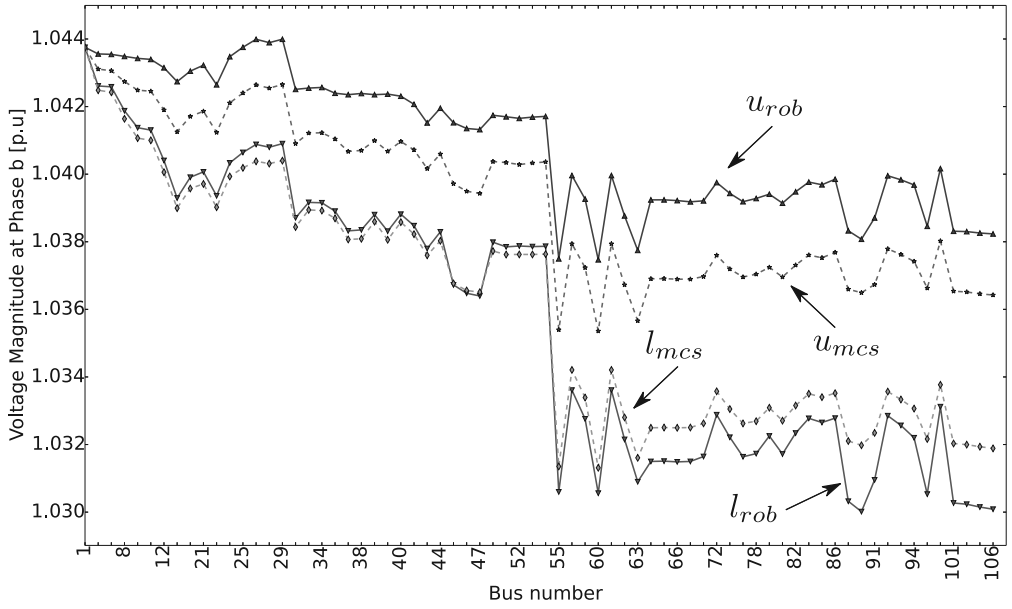

Figure 3.6: Bounds of bus voltage magnitude (in pu) for phase b corresponding to the time interval between 12:00 and 13:00 hours.

From Figs. 3.5-3.8, it is observed that most of the robust bounds contain their corresponding MCS bounds. However, there are a number of MCS bounds which are not contained by the corresponding robust bounds. To quantify these cases, a metric called non-containment distance (D_{NC})

Figure 3.7: Bounds of bus voltage magnitude (in pu) for phase c corresponding to the time interval between 12:00 and 13:00 hours.

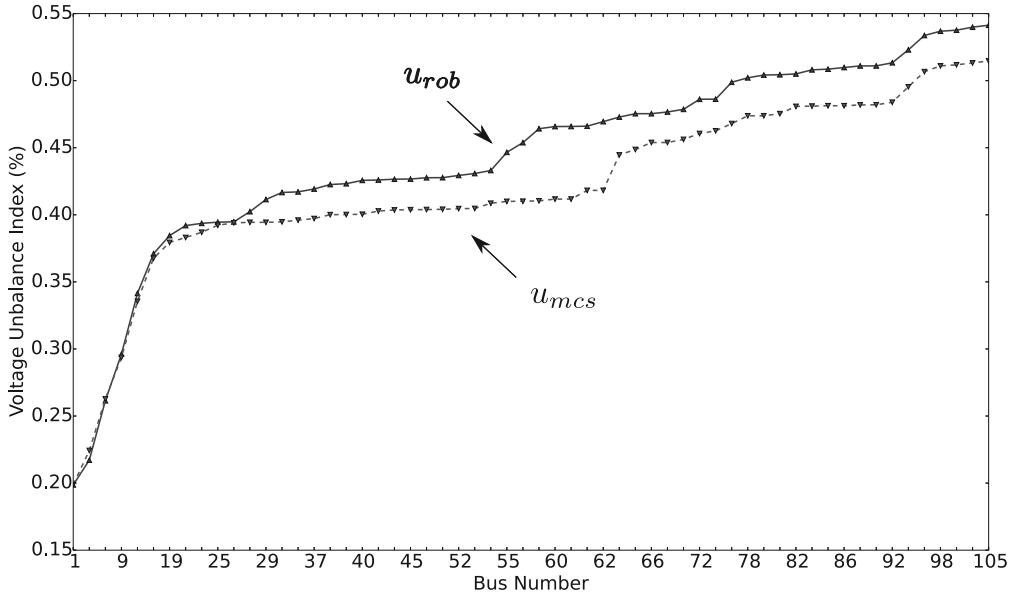

Figure 3.8: Upper bounds of bus voltage unbalance index (in %) corresponding to the time interval between 12:00 and 13:00 hours.

is defined as the maximum distance of an MCS bound from its robust bound. This is formulated as

$$D_{NC} = \max_{i,p} \left[D_{NC}^{ipl}, D_{NC}^{ipu} \right], \tag{3.23}$$

Table 3.2: Non-containment Distances corresponding to Figs. 3.5 - 3.8

Figure	Unit	Max D_{NC}^{ipl}	MaxD_{NC}^{ipu}	D_{NC}
Fig. 3.5	pu	0.0055	0.0040	0.0055
Fig. 3.6	pu	0	0.0005	0.0005
Fig. 3.7	pu	0	0.0	0.00
Fig. 3.8	%	not relevant	0.0072	0.0072

where its upper component D_{NC}^{ipu} and lower component D_{NC}^{ipl} are defined as follow

$$D_{NC}^{ipu} = \begin{cases} u_{mcs}^{ip} - u_{rob}^{ip} & \text{if } u_{mcs}^{ip} > u_{rob}^{ip} \\ 0 & \text{otherwise} \end{cases} \tag{3.24}$$

and

$$D_{NC}^{ipl} = \begin{cases} l_{rob}^{ip} - l_{mcs}^{ip} & \text{if } l_{mcs}^{ip} < l_{rob}^{ip} \\ 0 & \text{otherwise} \end{cases} \tag{3.25}$$

respectively. The smaller the value of D_{NC} is, the robust bounds contain the MCS bounds better . If $D_{NC} = 0$, the robust bounds contain all MCS bounds. Note that $D_{NC} \geq 0$.

The values of D_{NC} corresponding to Figs. 3.5 - 3.8 are shown in Table 3.2. The value of D_{NC} corresponding to the robust bounds of voltage magnitude at phase a and b are non-zeros because they do not contain all their respective MCS bounds as shown in Figs. 3.5, 3.6, respectively. On the other hand, the value of D_{NC} corresponding to the robust bounds of voltage magnitude at phase c is zero because the robust bounds contain all their respective MCS lower bounds as shown in Fig. 3.7. Furthermore, the value of D_{NC} of voltage unbalance bounds is also non-zero.

Further, from these figures, it is observed that bounds (of voltage magnitudes and unbalance indices) obtained by the proposed method are very close to the corresponding bounds obtained by MCS. In addition, the values of D_{NC} are small and the bounds are quiet far from their corresponding limits. Therefore, if the voltage bounds obtained by RO are within limits, then after practical implementation of the controller settings, the actual voltage bounds (taking place in the system) on account of variation of load and generation uncertainties are guaranteed to be within the prescribed

limits with good accuracies. Thus, the conjecture described in the Section 3.2.1 is verified with very small amount of error. Hence, the proposed method gives a very good approximation of the robust solution and is still useful for practical purposes.

3.5.5 Fast Moving Clouds

Fast moving clouds can be forecasted using full sky imagery technology [181]. Assume that the required forecast for the next hour is available and that the generation profile in Fig. 2.4 is replaced by a new PV profile shown in Fig. 3.9. This profile is based on an actual PV output at a site located at UQ Centre, St. Lucia, Queensland, Australia measured on 13 December 2013 [184]. The corresponding robust VRP, using strategy S3, has been solved and the obtained solution has been compared with the solution corresponding to generation profile shown in Fig. 2.4. The comparative results are shown in Table 3.3. As observed from Table 3.3, the total number of switchings on the day with fast moving cloud is more than that on the day with no cloud. However, the difference in ELS is quite small. Therefore, Table 3.3 indicates that rapid variation of generation corresponds to higher price (in term of number of switchings and ELS) to achieve robust solution.

As an illustration, voltage profile at selected nodes in the network are shown in Fig. 3.10 (corresponding to the generation profile shown in Fig. 3.9). For the sake of brevity, the results corresponding to the interval between 12:00 and 13:00 hour only is presented. The full profile is available at [184]. Figure 3.10 shows the voltage profiles at three nodes i.e. phase a of bus 115, phase b of bus 29 and phase c of bus 68. From Fig. 3.10 it is observed that all these three voltages are within limits. Fluctuation of generation shown in Fig. 3.9 are reflected also in the profiles shown in Fig. 3.10. Note that those three nodes are located at different parts of the studied network. Hence, the voltage profile of the whole network is within the prescribed limits.

Note that in solving the robust voltage regulation problem considering fast moving clouds, for some one-hour intervals, use of constraints shown in Eqs. (3.18) makes the optimization problem unsolvable. However, after introducing two inequality constraints as shown in Eq. (3.26) for each equality constraint given in Eq. (3.18),

$$g(\mathbf{c}) = 0 \rightarrow g(\mathbf{c}) \leq 0 \text{ and } g(\mathbf{c}) \geq 0 \tag{3.26}$$

the optimization problem could be solved. The results shown in Fig. 3.10 have been obtained following this approach.

Table 3.3: Performaces of The Proposed Method for Different Situation

Situation	ELS	Number of Switching			
	(kWh)	OLTC	SC	SVC	all
no cloud	907.7	20	20	0	40
fast moving cloud	1002	31	43	0	74

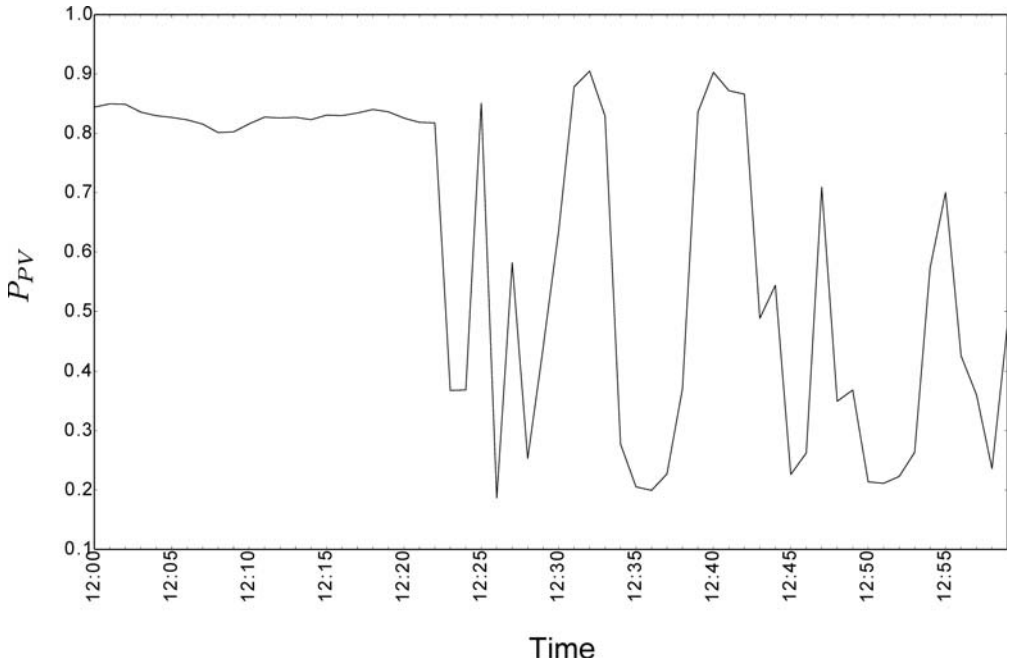

Figure 3.9: PV output profile of a sunny day with fast moving clouds based on an actual per-minute measurement in Queensland, Australia between 12:00 and 13:00 hours.

.

3.5.6 Computational Burden Analysis

Table 3.4 shows an overview of the computational burden of each stage of the proposed method corresponding to strategy XI and Case J for 24 one-hour RO problem for a day. Other strategies have fewer number of variables and constraints than strategy XI and hence the analysis of com-

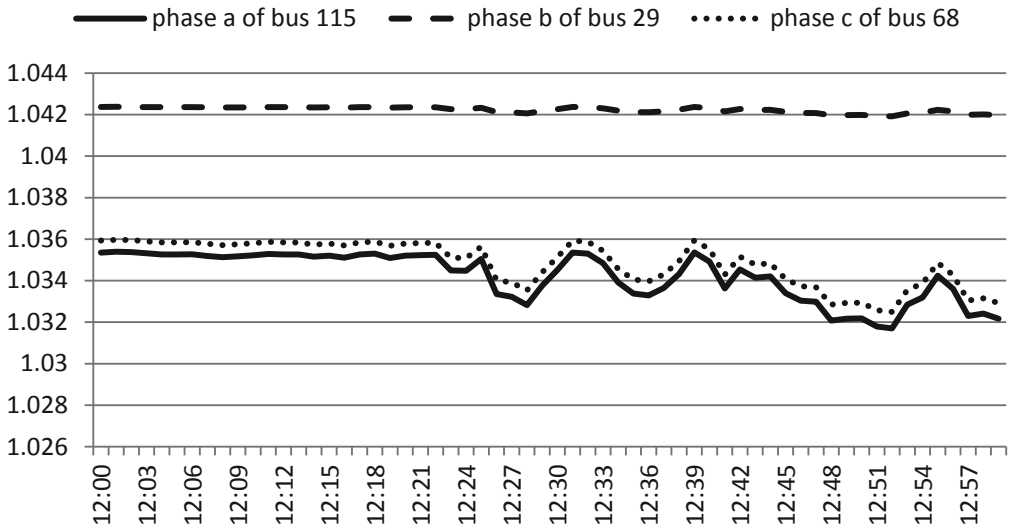

Figure 3.10: Voltage profiles between 12:00 and 13:00 hours at three different nodes in the network.

Table 3.4: Computational Burden for Strategi XI and Case J

	Stage I	Stage II
Number of runs	24	24
Number of variables	46419	46455
Number of constraints	64800	64854

putational burden for these strategies are not presented here. As the proposed method is capable of solving the robust optimization problem in approximately one minute (the maximum computational time recorded was 60.14 sec out of 24 RO runs) even with large number of constraints and variables (as shown in Table 3.4), this has the potential of future real-life application.

3.6 Conclusion

This chapter proposes a voltage regulation method in unbalanced radial distribution systems under uncertainty in loads and generations based on robust optimization technique. The effectiveness of the proposed method has been tested on 123 bus unbalanced radial network. Based on the detailed simulation studies carried out in this chapter, following conclusion can be drawn:

1. The proposed method guarantees that the bounds of magnitude and unbalance ratio of voltages taking place in the system network will always remain within the prescribed limits even in the presence of generation and load uncertainties.

2. The proposed method is fast enough for practical implementation, even under the condition of fast moving clouds.

In the next chapter, uncertainty in the network configurations would be considered in the voltage regulation problem.

4 — Voltage Regulation considering Multiple Network Topologies

A child's first geometrical discoveries are topological.
If you ask him to copy a square or a triangle, he draws a closed circle.
- Jean Piaget

Abstract

Chapter 2 assumes no uncertainty and Chapter 3 focuses on uncertainty in load and generation but neglects the uncertainty of topology of a distribution network. This chapter considers uncertain network topology. While maintaining radial topology and serving all the customers, a number of possible topologies may exist in a distribution system. Applying the approach discussed in Chapter 3, this chapter proposes a way to find the optimal setting of controllers which are feasible for any of the pre-selected possible topologies of an unbalanced radial distribution network.

4.1 Introduction

IN addition to uncertainty in loads and generations, there is also uncertainty in topology of distribution networks. The causes of the uncertainty may include the error in topology estimation or dynamic network reconfiguration due to the change in prices of electricity, or uncertainty in loads and generation in distribution networks. In future power market, it is possible to have multiple supply point and time-varying price for a distribution network. In this situation, the network reconfiguration would become more frequent to operate the distribution network at minimum cost [133]. In addition, dynamic reconfiguration in which network topology is optimized based on variation of loads and generation can increase the hosting capacity for distributed generation, increase reliability and decrease losses in distribution network [132, 134–136]. Hence, uncertainty in topology may increase significantly in the future. Moreover, the uncertainty of topology of a distribution network significantly affects the probability density function of magnitudes of voltages in the network [75]. Hence, it is important to consider the change in topology of a network in

operation and control of distribution system in general and in voltage regulation in particular.

The importance of considering the topology in voltage regulation problem is recognized in [76, 185] which study voltage regulation problem and network reconfiguration problem together. Note that the topology of a network is one of the control variables in these works. Hence, these works do not consider network topology as an uncertainty.

There are few efforts in consideration of uncertainty of topology in operation of power systems. For example, control strategies which are not dependent on the network topology has been studied in distribution network [64] or microgrid [105]. The method proposed in [64] is not an optimization-based approach and, hence, does not seek an optimality. Moreover, an optimization method is used in [105]. However, it does not include OLTCs nor SCs in their formulation. As far as voltage regulation in distribution system with distributed generation is concerned, to the best of the knowledge of this author, there has been no work in the available literature which considers the uncertainty in topology.

Therefore, this chapter considers uncertain topology in voltage regulation problem of an unbalanced radial distribution system with distributed generation. Following the approach of [105], it finds a solution which is optimal over all pre-selected finite number of credible topologies in which the system serves all the loads and operates in radial fashion. In this way, the solution will be always feasible irrespective of the prevailing configuration of the network. The proposed approach is useful when voltage regulation and network reconfiguration operate independently from each other either intentionally or by accident.

4.2 Voltage regulation considering multiple credible topologies

Assume that there is a set $\mathbf{T}$ of n_τ number of possible radial topologies in which all loads can be served,

$$\mathbf{T} = \{\tau_1, \tau_2, ..., \tau_{n_\tau}\}$$

where τ_i is the i^{th} credible topology. A credible topology is one which is able to support all loads. The optimization problem (P4.0) considers n_τ topologies at the same time and is formulated as the following:

$$\begin{aligned} \underset{\mathbf{c},\mathbf{d}}{\text{minimize}} \quad & f(\mathbf{c},\mathbf{d},\mathbf{T}) \\ \text{subject to} \quad & \mathbf{g}_i(\mathbf{c},\mathbf{d},\tau_i) = 0 \;\; \forall i \in 1,2,...,n_\tau \\ & \mathbf{h}_i(\mathbf{c},\mathbf{d},\tau_i) \leq 0 \;\; \forall i \in 1,2,...,n_\tau. \end{aligned} \tag{P4.0}$$

The solution of Problem (P4.0) gives the optimal settings of the controllers that are feasible for any topology $\tau_i \in \mathbf{T}$ and, hence, is robust against uncertainty in topology. In the following, we refer the approach used in this chapter as multiple-topology approach. Accordingly, we refer the approach used in the previous chapters as single-topology approach.

4.3 Problem Formulation

Here, the voltage regulation problem is formulated as an optimization problem to minimize the total line losses and number of switchings of controllers. All the constraints defined in Chapter 2 must be satisfied for all topologies $\tau_i \in \mathbf{T}$. The state variables considered here are the real and imaginary parts of currents and voltages at all phases of all lines and buses of all topologies. The control variables include OLTC taps position, values shunt capacitor, as well as SVC voltage and droop settings.

4.3.1 Objective Functions

In this chapter, two objective functions have been considered. The objective function J_1 defined in Eq. (2.7) is now modified to consider multiple topology and becomes J_7 as defined in Eq. (4.1).

$$J_7 = \sum_{\tau=1}^{n_\tau} \sum_{h=1}^{24} \sum_{p=a}^{c} \sum_{i=1}^{n_{BUS}} \sum_{j=1, j\neq i}^{n_{BUS}} r_{ij}^{p} |\bar{I}_{ij}^{p\tau}(h)|^2. \tag{4.1}$$

Moreover, objective functions J_2, J_3 and J_4 remain the same. Hence, the new objective function for multiple topology case is now

$$J_8 = \alpha J_7 + +\beta J_2 + \gamma(J_3 + J_4) \tag{4.2}$$

where α, β and γ are non-negative weighing factors with $\alpha + \beta + \gamma = 1$. The objective of this chapter is to minimize the function J_8.

4.3.2 Equality Constraints

Similar to the constraints described in Chapter 3, the constraints in this chapter are modified versions of the constraints in Chapter 2. For example, real and imaginary parts of the currents of a

constant-power load L are given by Eqs. (4.3) and (4.4):

$$I_{Lx}^{ipt\tau} = \frac{P_L^{ipt} E_x^{ipt\tau} + Q_L^{ipt} E_y^{ipt\tau}}{(E_x^{ipt\tau})^2 + (E_y^{ipt\tau})^2} \tag{4.3}$$

$$I_{Ly}^{ipt\tau} = \frac{P_L^{ipt} E_y^{ipts} - Q_L^{ipt} E_x^{ipt\tau}}{(E_x^{ipt\tau})^2 + (E_y^{ipt\tau})^2}. \tag{4.4}$$

where $I_{Lx}^{ipt\tau}$ and $I_{Ly}^{ipt\tau}$ are real and imaginary parts of load currents connected at phase p of bus i corresponding to time t and topology τ; $E_x^{ipt\tau}$ and $E_y^{ipt\tau}$ are real and imaginary parts of voltages at phase p of bus i corresponding to time t and topology τ; P_L^{ipt} and Q_L^{ipt} are real and imaginary parts of load power connected at phase p of bus i corresponding to time t. It is to be noted that, for a time period t, the quantities P_L^{ipt} and Q_L^{ipt} are constant, as these are dependent on the load curve, but not on topology.

Distributed Generation Distributed generations are considered as negative constant power loads. For specified real and reactive power injections at bus i and phase p, real and reactive components of currents are calculated using Eqs. (4.5) and (4.6), respectively.

$$I_{Gx}^{ipt\tau} = \frac{P_G^{ipt} E_x^{ipt\tau} + Q_G^{ipt} E_y^{ipt\tau}}{(E_x^{ipt\tau})^2 + (E_y^{ipt\tau})^2} \tag{4.5}$$

$$I_{Gy}^{ipt\tau} = \frac{P_G^{ipt} E_y^{ipt\tau} - Q_G^{ipt} E_x^{ipt\tau}}{(E_x^{ipt\tau})^2 + (E_y^{ipt\tau})^2} \tag{4.6}$$

where $I_{Gx}^{ipt\tau}$ and $I_{Gy}^{ipt\tau}$ are real and imaginary generator currents connected at phase p of bus i corresponding to time t and topology τ; P_G^{ipt} and Q_G^{ipt} are real and imaginary parts of DG power connected at phase p of bus i corresponding to time t.

Shunt Capacitor and Reactor For a shunt capacitor SC connected at phase p of bus i, the following equality constraints must be satisfied:

$$I_{SCx}^{ipt\tau} = \frac{sc^{ipt}}{n_c} \frac{+E_y^{ipt\tau}}{X_{SC}^{ip}}, X_{SC}^{ip} < 0 \tag{4.7}$$

$$I_{SCy}^{ipt\tau} = \frac{sc^{ipt}}{n_c} \frac{-E_x^{ipt\tau}}{X_{SC}^{ip}}, X_{SC}^{ip} < 0. \tag{4.8}$$

Similarly, for a shunt reactor SR connected at phase p of bus i, the following equality constraints must be satisfied:

$$I_{SRx}^{ipt\tau} = \frac{sr^{ipt}}{n_r} \frac{+E_y^{ipt\tau}}{X_{SR}^{ip}}, X_{SR}^{ip} > 0 \tag{4.9}$$

$$I_{SRy}^{ipt\tau} = \frac{sr^{ipt}}{n_r} \frac{-E_x^{ipt\tau}}{X_{SR}^{ip}}, X_{SR}^{ip} > 0. \tag{4.10}$$

Note that the complex current of a shunt capacitor (reactor), $I_{SCx}^{ipt\tau} + jI_{SCy}^{ipt\tau}$ ($I_{SRx}^{ipt\tau} + jI_{SRy}^{ipt\tau}$), leads (lags) its terminal voltage, $E_x^{ipt\tau} + jE_y^{ipt\tau}$, by 90^0. However, this does not necessarily means that $I_{SCx}^{ipt\tau} = I_{SR_x}^{ipt\tau} = 0$ which happens only when $E_y = 0$.

SVC Based on the model of SVC described in Section 2.2, the following equality constraints are must be satisfied:

$$X_{SLv}^{at} = X_{SLv}^{bt} = X_{SLv}^{ct}. \tag{4.11}$$

$$P_{vp}^{spec} = E_x^{pt\tau}(b_v) I_{vx}^{pt\tau} + E_y^{pt\tau}(b_v) I_{vy}^{pt\tau} = 0, \forall p, \forall v, \forall t, \forall \tau \tag{4.12}$$

$$Q_V^{pt\tau} = E_y^{pt\tau}(b_v) I_{vx}^{pt\tau} - E_x^{pt\tau}(b_v) I_{vy}^{pt\tau} \quad \forall p, \forall v \tag{4.13}$$

$$|\bar{E}_v^{ref,t\tau}| = E_v^{1,t\tau} \tag{4.14}$$

$$Q_v^{at\tau} = Q_v^{bt\tau} = Q_v^{ct\tau} \tag{4.15}$$

It is noteworthy that Eqs. (4.11) and (4.15) is valid (non-valid) when SVC operates uniformly (non-uniformly).

Series Components Distribution system series components i.e. feeders, transformers, OLTCs can be mathematically described using the ABCD model [150]. Eqs. (4.16) and (4.17) represent voltage constraints of the series components.

$$\begin{aligned} \mathbf{E}_x^{t\tau}(b_S^s) = \mathbf{A}_x \mathbf{E}_x^{t\tau}(b_S^r) - \mathbf{A}_y \mathbf{E}_y^{t\tau}(b_S^r) \\ + \mathbf{B}_x \mathbf{I}_{Sxr}^{t\tau} - \mathbf{B}_y \mathbf{I}_{Syr}^{t\tau} \end{aligned} \tag{4.16}$$

$$\begin{aligned} \mathbf{E}_y^{t\tau}(b_S^s) = \mathbf{A}_x \mathbf{E}_y^{t\tau}(b_S^r) + \mathbf{A}_y \mathbf{E}_x^{t\tau}(b_S^r) \\ + \mathbf{B}_x \mathbf{I}_{Sxr}^{t\tau} + \mathbf{B}_y \mathbf{I}_{Syr}^{t\tau} \end{aligned} \tag{4.17}$$

Similarly, Eqs. (4.18) and (4.19) represent current constraints of the series components.

$$\mathbf{I}_{Sxs}^{t\tau} = \mathbf{CE}_{x}^{t\tau}(b_S^r) + \mathbf{DI}_{Sxr}^{t\tau} \tag{4.18}$$

$$\mathbf{I}_{Sys}^{t\tau} = \mathbf{CE}_{y}^{t\tau}(b_S^r) + \mathbf{DI}_{Syr}^{t\tau} \tag{4.19}$$

Sequence Voltage Constratins Since voltage unbalance ratio is expressed in terms of positive and negative sequence voltages, the folowing constraints also apply for all three-phase buses:

$$E_{xit\tau}^{1} = \frac{1}{3}\left(E_{x}^{iat\tau} + E_{x}^{ibt\tau}\cos 120^o - E_{y}^{ibt\tau}\sin 120^o + E_{x}^{ict\tau}\cos 240^o - E_{y}^{ict\tau}\sin 240^o\right) \tag{4.20}$$

$$E_{yit\tau}^{1} = \frac{1}{3}\left(E_{y}^{iat\tau} + E_{y}^{ibt\tau}\cos 120^o + E_{x}^{ibt\tau}\sin 120^o + E_{y}^{ict\tau}\cos 240^o + E_{x}^{ict\tau}\sin 240^o\right) \tag{4.21}$$

$$E_{xit\tau}^{2} = \frac{1}{3}\left(E_{x}^{iat\tau} + E_{x}^{ibt\tau}\cos 240^o - E_{y}^{ibt\tau}\sin 240^o + E_{x}^{ict\tau}\cos 120^o - E_{y}^{ict\tau}\sin 120^o\right) \tag{4.22}$$

$$E_{yit\tau}^{2} = \frac{1}{3}\left(E_{y}^{iat\tau} + E_{y}^{ibt\tau}\cos 240^o + E_{x}^{ibt\tau}\sin 240^o + E_{y}^{ict\tau}\cos 120^o + E_{x}^{ict\tau}\sin 120^o\right) \tag{4.23}$$

Current Balance Further, based on Kirchhoff's law, Eqs. (4.24) and (4.25) define nodal current balance equations for all buses and phases.

$$I_{Sxr}^{ipt\tau} = \sum I_{Sxs}^{ipt\tau} + \sum I_{Lx}^{ipt\tau} + \sum I_{vx}^{ipt\tau} + \sum I_{SCx}^{ipt\tau} + \sum I_{SRx}^{ipt\tau} - \sum I_{Gx}^{ipt\tau} \tag{4.24}$$

$$I_{Syr}^{ipt\tau} = \sum I_{Sys}^{ipt\tau} + \sum I_{Ly}^{ipt\tau} + \sum I_{vy}^{ipt\tau} + \sum I_{SCy}^{ipt\tau} + \sum I_{SRy}^{ipt\tau} - \sum I_{Gy}^{ipt\tau} \tag{4.25}$$

$$\forall i, \forall p, \forall t, \forall \tau$$

4.3.3 Consistency Constraints

The goal of optimization is to find the values of the control variables which would remain constant over all topologies such that the objective function is minimized subject to the equality and inequality constraints. This leads to the following consistency constraints for all time and topologies.

4.3.3.1 OLTC

$$tap_{op}^{t\tau} = tap_{op}^{t1}\ \forall o, \forall \tau, \forall t \tag{4.26}$$

4.3.3.2 SC

$$sc^{ipt\tau} = sc^{ipt1}\ \forall t, \forall \tau \tag{4.27}$$

4.3.3.3 SVC

Slope constraints

$$X_{SLv}^{pt\tau} = X_{SLv}^{pt1}, \forall v, \forall \tau, \forall t \tag{4.28}$$

and voltage reference constraints,

$$E_{v}^{ref,t\tau} = E_{v}^{ref,t1}, \forall v, \forall t, \forall \tau \tag{4.29}$$

Note that the state variables, such as voltages and currents, are not subjected to consistency constraints. Their values vary according to the topology and control variables and must be within the corresponding limits.

4.3.4 Inequality Constraints

Based on various physical and regulatory limits, the following inequality constraints are considered:

1. Voltage magnitude limits at all buses and phases including all load and SVC's dummy bus:

$$0.95 \leq |\bar{E}^{ipt\tau}| \leq 1.05, \forall i, \forall p, \forall t, \forall \tau \tag{4.30}$$

2. Voltage magnitude limits for node that is connected to secondary terminal of OLTC [150]:

$$0.9 \leq |\bar{E}^{b_o pt\tau}| \leq 1.1, \forall o, \forall p, \forall t, \forall \tau \tag{4.31}$$

3. Positive-sequence voltage reference limit of SVC:

$$0.95 \leq |\bar{E}_{v}^{ref,t\tau}| \leq 1.05, \forall v, \forall t, \forall \tau \tag{4.32}$$

4. Reactive power limit of SVC:

$$Q_{vp}^{min} \leq Q_{v}^{pt\tau} \leq Q_{vp}^{max}, \forall v, \forall p, \forall t, \forall \tau \tag{4.33}$$

5. limits on slope of SVC:

$$X_{SLp}^{v,min} \leq X_{SLv}^{pt\tau} \leq X_{SLp}^{v,max}, \forall v, \forall p, \forall t, \forall \tau \tag{4.34}$$

6. Limit on tap position of OLTC:

$$tap_{op}^{min} \leq tap_{o}^{pt} \leq tap_{op}^{max}, \forall o, \forall p, \forall t, \forall \tau \tag{4.35}$$

7. Limit on voltage balance factor $U_2^{ipt\tau}$ for all three-phase buses:

$$0 \leq U_2^{ipt\tau} = 100\frac{E_{it\tau}^2}{E_{it\tau}^1} \leq U_2^{max}, \forall i, \forall t, \forall \tau \tag{4.36}$$

IEC 61000-2-12 specifies that $U_2^{max} = 2\%$ [160].

Finally, voltage regulation problem in radial unbalanced distribution system considering uncertain topology can be stated as,

$$\begin{aligned} &\underset{\mathbf{c},\mathbf{d}}{\text{minimize}} \quad J_8 \\ &\text{subject to} \quad (4.3) - (4.36). \end{aligned} \tag{P4.1}$$

where $\mathbf{c}$ and $\mathbf{d}$ represent continuous and discrete variables, respectively.

4.4 Solution Method

The optimization problem (P4.1) is solved using a 2-stage approach explained below.

1. Stage 1

   (a) Change Eq. (4.30)

   $$0.95 \leq |\bar{E}^{ipt\tau}| \leq 1.05, \forall i, \forall p, \forall t, \forall \tau \tag{4.30}$$

   into

   $$0.95 - \rho_e \leq |\bar{E}^{ipt\tau}| \leq 1.05 + \rho_e, \forall i, \forall p, \forall t, \forall \tau, \tag{4.37}$$

   where $\rho_e \geq 0$ is an auxiliary variable which must be minimized. This approach is called the *exact penalty function based relaxation method* [116]. It can reduce the number of iterations significantly.

   (b) Neglect the voltage unbalance constraints given in Eq. (4.36). Note that in Stage 2, these constraints are considered again. Since the final solution is taken from the solution of stage 2, the unbalance constraints are considered in the final solution.

   In addition, the more balanced a network is, the lesser the line losses is. Since one of the objectives is minimization of losses, the optimization process is also reducing the amount of unbalance in the network.

(c) Convert all discrete variables d_k^1 into continuous variables c_k^1. This relaxes the initial MINLP (P4.1) into a Non-Linear Programming (NLP) given by (P4.2a) below

$$\begin{aligned} \underset{\mathbf{c}}{\text{minimize}} \quad & J_8 + K_\rho \rho_e \\ \text{subject to} \quad & (4.3) - (4.29), (4.31) - (4.35) \end{aligned} \tag{P4.2a}$$

where $K_\rho \geq K_\rho^{min} > 0$ is a sufficiently large constant. Since there is only one value of ρ_e in a solution, it represents the maximum violation of magnitude of voltages over all i, p, t and τ. Therefore, if $\rho_e \leq 10^{-6}$, it can be concluded that there is no voltage magnitude violation. In [116], the value of K_ρ^{min} is calculated by solving a bi-level optimization problem. However, the actual value of K_ρ^{min} is not required here. Therefore, repeated simulation studies were performed to find that $K_\rho = 1000$ is sufficient.

(d) Solve the NLP (P4.2a) using interior point method [161] for 24-hour period.

(e) From the solution of the NLP (P4.2a) (c_k^{1*}), find the nearest lowest boundary d_k^{lb}. If the optimum continuous value is equal to one of the discrete value, let it be the lowest boundary.

(f) Define new discrete variable

$$d_k^2 = d_k^{lb} + b_k * \delta_k \tag{4.38}$$

where δ_k is the step size of the k^{th} variable and b_k is a binary variable corresponding to k^{th} original discrete variable.

(g) Using the new discrete variables, another MINLP (P4.2b) is formulated which has binary variables.

$$\begin{aligned} \underset{\mathbf{c},\mathbf{b}}{\text{minimize}} \quad & J_8 + K_\rho \rho_e \\ \text{subject to} \quad & (4.3) - (4.29), (4.31) - (4.35), (4.38), \end{aligned} \tag{P4.2b}$$

Chapter 2 indicates that solving the binary MINLP (P4.2b) for 24-hour period is computationally very expensive. Therefore, in stage 2, all the binary variables are converted into continuous variables.

2. Stage 2

(a) Convert each integer variable b_k into continuous variable b_k^c and use the constraints given in Eqs. (4.39).

$$d_k^c = d_k^{lb} + b_k^c \delta_k, \tag{4.39a}$$

$$b_k^c - \frac{1}{2} = b_{uk} - b_{lk}, \tag{4.39b}$$

$$\frac{1}{2} = b_{uk} + b_{lk}, \tag{4.39c}$$

$$b_{uk} b_{lk} = 0, b_{uk} \geq 0, b_{lk} \geq 0, \tag{4.39d}$$

(b) Now the Problem (P4.3) can be converted into another NLP

$$\begin{aligned} \underset{\mathbf{c}}{\text{minimize}} \quad & J_8 + K_\rho \rho_e \\ \text{subject to} \quad & (4.3) - (4.29), (4.31) - (4.37), (4.39) \end{aligned} \tag{P4.3}$$

(c) Solve the new NLP for a period of 24 hour.

4.5 Result And Discussion

4.5.1 Modified IEEE 123 Bus System

Consider a modified IEEE 123 bus distribution system shown in Fig. 2.3 which is redrawn in Fig. 4.1 to show the location of switches. It has nine (9) switches. However, in this work, only four switches (S1 - S4) out of these nine switches have been considered for illustration. Fig. 4.1 also defines three zones A, B and C which cover all lines and buses between switches S1-S3, S3-S4 and S2-S4, respectively. Note that only zone A has an OLTC. The four switches determine whether or not those zones are connected to the substation. Moreover, all modifications describe in Section 3.5.1 are also considered in this chapter.

Furthermore, Table 4.1 shows statuses of these switches in four topologies using which substation can supply all loads. Actually, there are, in total, 16 possible combinations of those four switches. However, they represent situations in which some part of the network can not be served by the substation or the network become meshed. Note that the last column of Table 4.1 shows

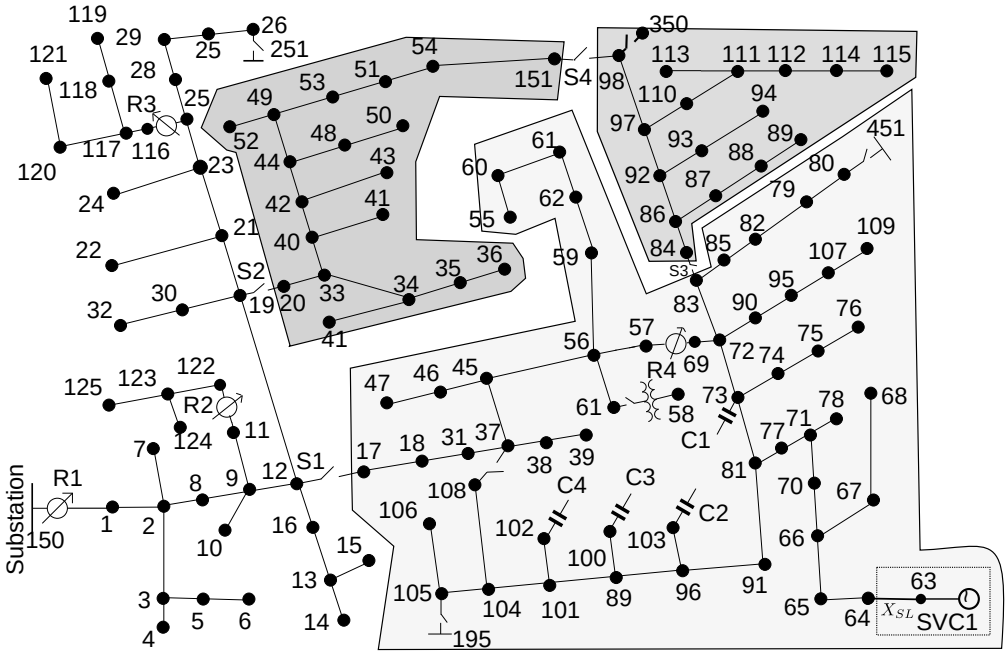

Figure 4.1: Modified IEEE 123 bus system.

Table 4.1: Statuses of Switches in Four Configurations of IEEE 123 bus system in which all loads are served

Topologies	Switch Status				Solvability
	S1	S2	S3	S4	
τ_1 (nominal)	ON	ON	ON	OFF	Yes
τ_2	ON	ON	OFF	ON	Yes
τ_3	ON	OFF	ON	ON	Yes
τ_4	OFF	ON	ON	ON	No

whether an individual topology can be solved for voltage regulation using the method of this chapter or not. Individually, configurations τ_1, τ_2 and τ_3 can be solved. However, configuration τ_4 is not feasible because OLTC R4 is too far from the substation. Therefore, in this work, the set of feasible topologies considered is

$$\mathbf{T} = \{\tau_1, \tau_2, \tau_3\}.$$

Note that configuration τ_1 corresponds to the original topology given in [186].

The proposed method can find a solution which is feasible for any topology in $\mathbf{T}$. In order to evaluate the performance of the proposed method, the performance of the each topology is compared in term of total line loss, voltage magnitude index (VMI, see Eq. (2.39)), voltage drop magnitude index (VDMI, see Eq. (2.40)) and total number of switchings The weights of objective functions are $\alpha = 0.1$ and $\beta = \gamma = 0.45$ (which corresponds to Case J in Chapter 2). The results corresponding to the multiple-topology approach are compared with those corresponding to single-topology approach. For the comparison, the following situations have been studied:

1. MT1: A situation in which the solution obtained by solving the VVC problem for multiple topologies is applied to the network using topology τ_1.

2. MT2: A situation in which the solution obtained by solving the VVC problem for multiple topologies is applied to the network using topology τ_2.

3. MT3: A situation in which the solution obtained by solving the VVC problem for multiple topologies is applied to the network using topology τ_3.

4. ST1: A situation in which the VVC problem is solved for the network having topology τ_1 using the approach of Chapter 2.

5. ST2: A situation in which the VVC problem is solved for the network having topology τ_2 using the approach of Chapter 2.

6. ST3: A situation in which the VVC problem is solved for the network having topology τ_3 using the approach of Chapter 2.

It is to be noted that for MT1 - MT3 and ST1 - ST3 the VVC problem has been solved for 24 hour period. Moreover, in solving the Problem (P4.0) the values of the weights of objective functions given in Eq. (4.2) are $\alpha = 0.1$ and $\beta = \gamma = 0.45$ based on the results of Chapter 2. The comparative assessment for all these six situations are given below.

4.5.2 Losses

Table 4.2 shows the losses corresponding to strategies XI - XVIII for MT1-MT3 and ST1-ST3. For topologies τ_1, in general, multiple-topology approach corresponds to lower losses than single-

topology approach and vice versa for topology τ_2 and τ_3. Nevertheless, Table 4.2 shows that the losses of a particular topology corresponding to both approaches are close to each other.

Furthermore, Table 4.2 shows that losses corresponding to strategies in which OLTCs operate non-uniformly (XI-XIV) are lower than those corresponding to strategies in which OLTCs operate uniformly (XV-XVIII). Moreover, for a combination of a strategy and a topology, the values of losses corresponding to both approaches are close to each other. Hence, the multiple-topology approach provides a solution which is very close to the solution taken from the single-topology approach.

Table 4.2: Total line losses in kWh for several strategies.

	Total Line Losses in kWh					
	Multiple Topology			Single Topology		
	MT1	MT2	MT3	ST1	ST2	ST3
Strategy	τ_1	τ_2	τ_3	τ_1	τ_2	τ_3
XI	888.319	869.761	1229.62	888.848	869.34	1225.92
XII	888.309	869.844	1229.33	888.64	869.34	1225.81
XIII	888.404	869.857	1229.85	888.938	869.358	1226.37
XIV	888.342	869.864	1229.63	888.692	869.368	1226.03
XV	890.823	872.002	1234.01	891.171	872.058	1231.25
XVI	890.82	872.034	1233.82	892.153	872.102	1231.8
XVII	891.427	872.565	1235.7	891.463	872.078	1232.2
XVIII	891.42	872.602	1235.41	892.194	872.175	1230.66

Table 4.3: Voltage Magnitude Index for Several Strategies

	VMI					
	Multiple Topology			Single Topology		
Strategy	τ_1	τ_2	τ_3	τ_1	τ_2	τ_3
XI	7.87419	7.56394	7.18818	8.33587	7.91128	7.72224
XII	7.92532	7.61009	7.24277	8.33833	7.91128	7.76134
XIII	7.83707	7.5441	7.16439	8.28088	7.91295	7.65838
XIV	7.84125	7.5474	7.15572	8.29899	7.90274	7.697
XV	7.94396	7.72014	7.23152	7.69705	7.60886	7.19587
XVI	7.64205	7.43818	6.92691	7.53837	7.60287	6.82619
XVII	7.81694	7.61279	7.10619	7.7375	7.61414	7.57132
XVIII	7.39088	7.18811	6.6992	7.53741	7.55819	7.55885

4.5.3 Voltage Magnitude Index

Table 4.3 shows the values of VMI corresponding to strategies XI - XVIII for MT1-MT3 and ST1-ST3. The values of VMI for different topologies are quite close to each other. Furthermore, for ST1-ST3, Table 4.3 shows that the values of VMI corresponding to non-uniform operation of OLTCs (strategies XI - XIV) are in general higher than those corresponding to uniform operation of OLTCs (strategies XV - XVIII). Moreover, similar to line losses, for a combination of a strategy and a topology, there is small difference between values of VMI corresponding to multiple-topology and single-topology approaches. Hence, in terms of VMI, both approaches have similar performance.

4.5.4 Voltage Drop Magnitude Index

Table 4.4 shows the values of VDMI corresponding to strategies XI - XVIII for MT1-MT3 and ST1-ST3. The values of VDMI of topology τ_1 and τ_2 corresponding to multiple-topology approach are higher than those corresponding to single-topology approach and vice versa in case of topology

Table 4.4: VDMI for Several Strategies

	VDMI					
	Multiple Topology			Single Topology		
Strategy	τ_1	τ_2	τ_3	τ_1	τ_2	τ_3
XI	2.28	2.48	2.57	2.25	2.38	2.68
XII	2.28	2.47	2.56	2.25	2.38	2.68
XIII	2.28	2.47	2.57	2.25	2.38	2.69
XIV	2.28	2.47	2.57	2.25	2.38	2.68
XV	2.28	2.47	2.57	2.26	2.38	2.69
XVI	2.29	2.48	2.58	2.26	2.38	2.69
XVII	2.28	2.48	2.58	2.26	2.38	2.69
XVIII	2.28	2.47	2.57	2.26	2.38	2.69

τ_3.

Furthermore, Table 4.4 shows that the values of VDMI are quite close to each other. Moreover, for a combination of a strategy and a topology, the values of VDMI corresponding to multiple-topology and single-topology approaches are close to each other. Hence, the difference of performance between both of the approaches in terms of VDMI is small.

4.5.5 Maximum Voltage Unbalance Index

Table 4.5 shows the maximum values of VUI over all buses and times corresponding to strategies XI - XVIII for MT1 - MT3 and ST1 - ST3. All values are well below the limit of 2%. For any particular topology, the values which correspond to multiple-topology approach and single-topology approach are close to each other. However, Table 4.5 indicates that topology τ_3 is more unbalanced than topologies τ_1 and τ_2.

Furthermore, Table 4.5 shows that, for topologies τ_1 and τ_2, the values of maximum VUI corresponding to non-uniform operation of OLTCs (strategies XI - XIV) are lower than those correspond to uniform operation of OLTCs (strategies XV - XVIII). This is expected since the

Table 4.5: Maximum Voltage Unbalance Index

	Maximum VUI (%)					
	Multiple Topology			Single Topology		
Strategy	τ_1	τ_2	τ_3	τ_1	τ_2	τ_3
XI	0.71	0.68	1.36	0.72	0.68	1.35
XII	0.71	0.68	1.36	0.72	0.68	1.35
XIII	0.90	0.78	1.56	0.77	0.68	1.36
XIV	0.89	0.78	1.55	0.77	0.68	1.36
XV	0.86	0.87	1.34	0.86	0.87	1.33
XVI	0.85	0.87	1.33	0.85	0.87	1.32
XVII	0.89	0.88	1.41	0.89	0.88	1.39
XVIII	0.87	0.87	1.38	0.86	0.87	1.36

former group has more degree of freedom than the later group. However, for topology τ_3, there is no clear pattern. In conclusion, in terms of voltage unbalance, both approaches give similar results.

4.5.6 Number of switchings

4.5.6.1 Without Topology Change

Table 4.6 compares total number of switchings corresponding to strategies XI-XVIII for MT1 - MT3 and ST1 - ST3. It shows that the use of multiple-topology approach leads to higher number of switchings than the use of single-topology approach in case of topologies τ_1 and τ_2 and vice versa for topology τ_3. Note that for multiple-topology approach, the same control strategy is used for all topologies. Therefore, all topologies have exactly the same number of switchings On the other hand, for single-topology approach, each topology corresponds to different control strategy and, hence, number of switchings.

Moreover, Table 4.6 shows that number of switchings correspond to MT1-MT3 and ST3 are higher than those corresponding to ST1 and ST2. This indicates that topology has an important

Table 4.6: Total number of switchings

	Total number of switchings			
	Multiple Topology	Single Topology		
	MT1 / MT2 / MT3	ST1	ST2	ST3
Strategy	τ_1/τ_2/ τ_3	τ_1	τ_2	τ_3
XI	16	9	9	17
XII	15	9	9	17
XIII	16	11	9	18
XIV	16	11	8	18
XV	13	3	6	21
XVI	19	3	6	21
XVII	7	3	3	9
XVIII	16	3	3	9

effect on number of switchings. Depending on the strategy being used, the topology with lowest number of switchings are either τ_1 or τ_2.

On one hand, for topologies τ_1 and τ_2, there are significant differences between the number of switchings values corresponding to multiple-topology and single-topology approaches. On the other hand, for topology τ_3 and most of the strategies, there are less significant differences in number of switchings between both approaches.

An important conclusion is that if there is no need of topological change, the single-topology approach seems to be better than the multiple-topology approach. However, when topological change is expected, the strength of multiple-topology approach becomes prevalent as will be discussed in the following subsection.

Table 4.7: Number of Switchings for transition from one topology to other topology corresponding to Strategy XIII and XVII.

hour	number of switchings for Each Topological Change					
	Strategy XIII			Strategy XVII		
	$\tau_1 \leftrightarrow \tau_2$	$\tau_2 \leftrightarrow \tau_3$	$\tau_1 \leftrightarrow \tau_3$	$\tau_1 \leftrightarrow \tau_2$	$\tau_2 \leftrightarrow \tau_3$	$\tau_1 \leftrightarrow \tau_3$
1	3	12	9	2	9	7
2	3	14	11	2	10	8
3	3	15	12	2	10	8
4	3	13	10	2	10	8
5	2	13	11	2	7	5
6	2	13	11	2	7	5
7	1	12	11	2	7	5
8	1	12	11	2	7	5
9	2	12	10	2	7	5
10	1	12	11	2	10	8
11	1	12	11	2	10	8
12	1	13	12	2	10	8
13	1	13	12	2	10	8
14	2	14	12	2	10	8
15	1	13	12	2	7	5
16	2	13	11	2	7	5
17	2	13	11	2	7	5
18	1	12	11	2	10	8
19	2	12	10	2	10	8
20	2	14	12	2	10	8
21	2	15	13	2	10	8
22	2	14	12	2	10	8
23	3	15	12	2	10	8
24	3	15	12	2	10	8

4.5.7 With Topology Change

Table 4.7 shows the number of switchings required due to change of topology of the network at different hours of a day for strategies XIII and XVII. As shown in Table 4.6, in case of S1 - S3,

strategy XIII is one of the worst one while strategy XVII is the best one. These two strategies are discussed in detail because these two strategies represent two extreme cases. Hence, it can be a good illustration about possible cost of change of topology.

In Table 4.7, it is assumed that the positions of discrete control settings are based on single-topology approach. Since three topologies are considered, there are three possible transitions i.e. $\tau_1 \leftrightarrow \tau_2$, $\tau_2 \leftrightarrow \tau_3$, and $\tau_1 \leftrightarrow \tau_3$ where $\tau_m \leftrightarrow \tau_n$ indicates the transition between τ_m and τ_n. Table 4.7 shows that the transitions between topologies τ_2 and τ_3 require the highest number of switchings among all these three possible transitions. On the other hand, when multiple-topology approach is used, the control variables do not change their values in the face of topology changes.

As further illustration, the optimal values of discrete variables at hour 03:00 corresponding to strategy XIII are given in Table 4.8. It can be observed that SC1 and SVC1 operate uniformly and OLTCs operate non-uniformly. Furthermore, the details of the number of switchings for all discrete variables are given in Table 4.9. The total number of switchings are also given in the last row of this table. Consequently, if topological change is required, the use of strategy XIII is not recommended.

Strategy XVII has the least number of switchings if no topology change is required. For comparison, its transition cost in terms of number of switchings are also shown in Table 4.7 which shows that the number of switchings for transitions $\tau_2 \leftrightarrow \tau_3$ and $\tau_1 \leftrightarrow \tau_3$ corresponding to Strategy XVII is smaller than those corresponding to strategy XIII. Hence, if single-topology approach is used and *only* one or two topological changes are expected, this strategy may be considered for real life application. However, if topological change is more frequent the multiple-topology approach is recommended since the transition cost is zero i.e. no switching is required for any transition. Hence, the approach developed in this chapter is useful in situation in which frequent topological change is required.

4.5.8 Overall Comparison

It is interesting to determine the best strategy among strategies XI - XVIII. Tables 4.2, 4.3, 4.4 and 4.5 show that the performance of these strategies are very close to each other. On the other hand, Tables 4.6 shows that those strategies have significant variation in total number of switchings. It shows that strategy XVII has the lowest number of switchings among all strategies. Therefore,

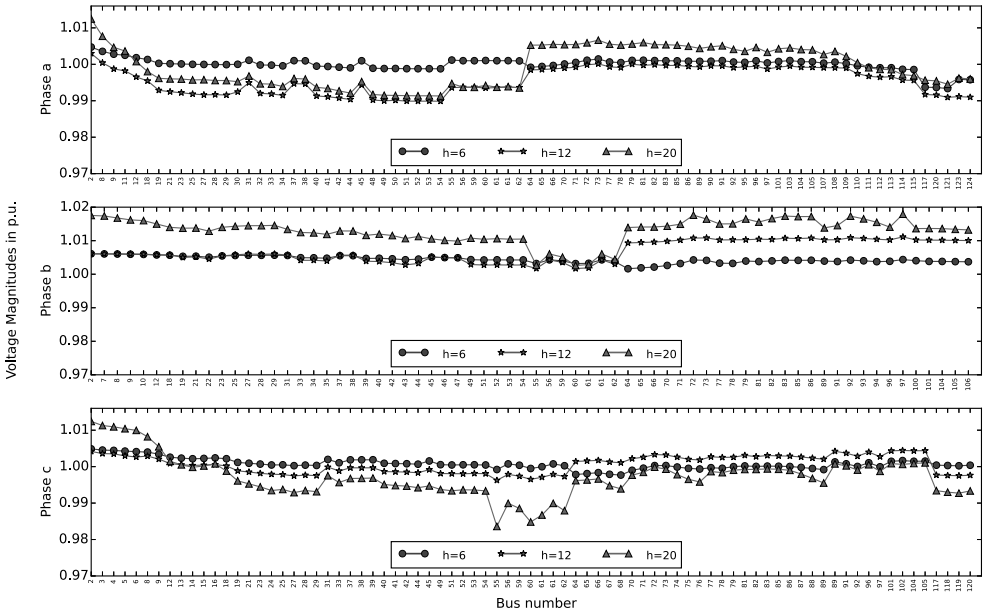

Figure 4.2: Voltage profiles at hour 6, 12 and 20 corresponding to Strategy XVII and topology τ_1.

XVII are selected as the best strategies.

Furthermore, as an illustration, Fig. 4.2 shows nine voltage profiles of the system if the topology is τ_1 and strategy XVII is used. For each phase, there are three profiles corresponding to hours 6, 12 and 20. It can be seen that all profiles at all phases are quite flat and all within limits hence the method performs satisfactorily.

4.5.9 Computational Time

Table 4.10 shows the computational time corresponding to case J for strategies XI-XVIII using multiple-topology approach. It shows that the maximum computational time is around 220 seconds. The computational times are all below 5 minutes and hence are fast enough for practical 24-hour ahead application.

4.6 Conclusion

This chapter proposes an approach to consider uncertainty of topology in voltage regulation of an unbalanced distribution system with distributed generation. It is assumed that there is a set of finite number of feasible radial topologies which can serve all loads. The proposed method considers

Table 4.8: Optimal settings of discrete control variables for Strategy XIII at hour 3:00 using multiple and single topology approaches.

Discrete Variable			Condition			
			MT1/MT2/MT3	ST1	ST2	ST3
OLTC	R1	a	7	7	7	7
		b	6	7	7	6
		c	7	7	7	7
	R2	c	0	0	0	0
	R3	a	0	0	0	0
		b	0	0	0	0
	R4	a	1	1	1	2
		b	0	0	0	1
		c	0	0	0	0
SC	C1	a	2	1	1	2
		b	2	1	1	2
		c	2	1	1	2
	C2	a	1	1	0	1
	C3	b	1	1	1	1
	C4	c	0	0	0	0
SVC	SVC1	a	0.04	0.02	0.02	0.00
		b	0.04	0.02	0.02	0.00
		c	0.04	0.02	0.02	0.00

all topologies in this set at the same time and hence called multiple-topology approach. Based on the simulation studies on the modified IEEE 123 bus system, the efficacy and efficiency of the proposed approach has been verified. Hence, the proposed method has the potential for real life application considering uncertainty in topology. It is also found that the benefit of the proposed method is evident if frequent topological changes are expected.

In the next chapter, line drop compensation (LDC) of OLTCs will be considered.

Table 4.9: Number of Switchings for transition from one topology to other topology corresponding to Case J and Strategy XIII at hour 3:00.

Discrete Variable			Transition		
			$\tau_1 \leftrightarrow \tau_2$	$\tau_2 \leftrightarrow \tau_3$	$\tau_1 \leftrightarrow \tau_3$
OLTC	R1	a	0	0	0
		b	0	1	1
		c	0	0	0
	R2	a	0	0	0
	R3	a	0	0	0
		c	0	0	0
	R4	a	1	2	1
		b	0	1	1
		c	1	1	0
SC	C1	a	0	1	1
		b	0	1	1
		c	0	1	1
	C2	a	1	1	0
	C3	b	0	0	0
	C4	c	0	0	0
SVC		a	0	2	2
		b	0	2	2
		c	0	2	2
Total			3	15	12

Table 4.10: Computational time for case J and several strategies involving OLTCs, SCs and SVC corresponding to multiple-topology and single-topology approaches.

	Computation time in seconds		
Strategy	Stage 1	Stage 2	Total
XI	48.963	122.392	171.355
XII	57.794	112.492	170.286
XIII	38.162	62.907	101.069
XIV	38.672	43.645	82.317
XV	45.307	175.832	221.139
XVI	47.796	120.309	168.105
XVII	39.126	43.451	82.577
XVIII	38.875	39.232	78.107

5 — Line Drop Compensation of OLTC

The indescribable pleasure - which pales the rest of life's joys- is abundant compensation for the investigator who endures the painful and persevering analytical work that precedes the appearance of the new truth, like the pain of childbirth.

- Santiago Ramn y Cajal in *Advice for a Young Investigator*

Abstract

Previous chapters assume that OLTCs operate in time-of-the-day mode. However, an OLTC can also operate in line drop compensation (LDC) mode. This chapter proposes an OPF-based approach to find the optimal settings of the LDC of an OLTC. In this way, the settings of the LDC of an OLTC can be coordinated with other OLTCs, SC and SVC. In addition, this chapter proposes a fast two-stage solution method employing the exact penalty function approach and a continuous representation of integer variables.

5.1 Introduction

An OLTC can be controlled in the following modes:

1. **Time of the day mode** in which the position of OLTC taps for each hour is optimized and sent to the OLTC controller. At a particular time, the controller of the OLTC ensures that the tap position is maintained according to the information it receives from the central controller. This mode has been assumed in Chapters 2 - 4.

2. **Local voltage control mode** in which the position of the taps of OLTC is locally controlled within specified band with the help of local measurements. This mode is further divided into two groups:

   (a) Voltage control without line drop compensation

   (b) Voltage control with line drop compensation. This is further called as *LDC mode*.

   This chapter focuses on the later one.

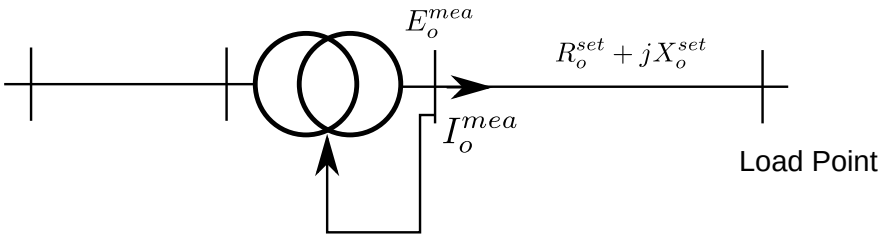

Figure 5.1: OLTC with line drop compensation

There are some benefits of the LDC mode. Firstly, the LDC mode requires relatively less amount of communication infrastructure as compared to the time-of-the-day mode. Secondly, proper choice of the value of $|E^{ref}|$ can reduce losses in a distribution system [89].

Optimal selection of LDC settings has been studied in the literature [63, 187, 188]. The work reported in [63] proposes an application of heuristic method for finding optimal settings of LDC of OLTCs in distribution system with distributed generation. The work reported in [187] uses support vector machine to find the settings of line drop compensator. Moreover, the work described in [188] proposes a heuristic method which considers maximum and minimum loading condition as well as possible future load growth. None of these uses OPF in finding the settings of LDC.

What are the possible benefits in integrating LDC into an OPF? One possible benefit is the coordination with other controllers such as SCs and SVCs. This chapter explores this issue in more detail. In previous chapters, all controllers are operated in time-of-a-day mode. Here, OLTCs operate in voltage control mode. However, since this chapter focuses on OLTCs, SCs and SVCs are assumed to operate in time-of-the-day mode. When an OLTC o operates in voltage control mode, the following discrete settings are available [150, 189, 190]:

1. Voltage magnitude reference $|\bar{E}_o^{ref}|$ in Volts. It is also called bandcenter.

2. Dead band db_o in Volts. It is also called bandwidth.

3. Impedance setting $R_o^{set} + jX_o^{set}$ in Volts. Note that it is a common practice by the manufacturers of OLTCs to use Volts for values of R_o^{set} and Z_o^{set}. They represent the voltage drop from OLTC and the virtual load point at which voltage are supposed to be controlled by the OLTC as shown in Fig. 5.1. One advantage of this practice is that the per-unit impedance between the virtual load point and the secondary terminal of OLTC, R_o^{set} and X_o^{set}, can be

Table 5.1: Typical Upper and lower limits of parameters of LDC with $V_{base}^{LDC} =$ 120 V

Parameter	symbol	limit		stepsize
		lower	upper	
		(in Volts)		
Voltage reference	$\|E_o^{ref}\|$	100	135	0.1
Bandwidth	db_o	1	6	0.1
Resistance	R_o^{set}	-24	24	0.1
Reactance	X_o^{set}	-24	24	0.1

calculated easily using [150]:

$$R_o^{set}(\text{ in p.u.}) = \frac{R_o^{set}}{V_{base}^{LDC}} \tag{5.1}$$

$$X_o^{set}(\text{ in p.u.}) = \frac{X_o^{set}}{V_{base}^{LDC}}, \tag{5.2}$$

where V_{base}^{LDC} is the base voltage of the LDC of the OLTC which is decided by its manufacturer. This chapter assumes that $V_{base}^{LDC} = 120$ V, a value commonly used in US. Similarly, the per-unit value of reference voltage $|\bar{E}_o^{ref,pu}|$ and bandwidth db_o^{pu} can also be calculated.

4. Time delay dt_o in seconds

If an OLTC operates without line drop compensation then $R_o^{set} = X_o^{set} = 0$. If an OLTC operates with line drop compensation then $R_o^{set} \neq 0 \vee X_o^{set} \neq 0$. Table 5.1 shows typical upper and lower limits of those settings in Volts [189]. It is to be noted than from here onwards, all parameters of an LDC are assumed to be in pu.

Based on the values of those settings, an OLTC's functionality is generally described by the following logic [191]:

$$\mathcal{A}(t) = \begin{cases} 1 & |\Delta\bar{E}_o| > \frac{db_o}{2} \text{ and } tap^t < tap^{max} \text{ for longer than } dt_o \text{ seconds.} \\ -1 & |\Delta\bar{E}_o| < -\frac{db_o}{2} \text{ and } tap^t > tap^{min} \text{ for longer than } dt_o \text{ seconds.} \\ 0 & otherwise \end{cases} \tag{5.3}$$

$$|\Delta\bar{E}_o| = |\bar{E}_o^{mea,t} - \bar{I}_o^{mea,t}(R_o^{set} + jX_o^{set})| - |\bar{E}_o^{ref}| \tag{5.4}$$

$$tap^{t_0+dt} = tap^{t_0} + \mathcal{A}(t_0) \tag{5.5}$$

where t represents time, $\mathcal{A}$ is the action variable, $|\Delta\bar{E}_o|$ is the voltage error in p.u., $db_o^{pu} > 0$ is the dead band in p.u., $tap \in \{-16, -15, ..., 15, 16\}$ represents the position of tap, $tap^{max} = 16$ is the maximum allowable tap position, and $tap^{min} = -16$ is the minimum tap position. The values of $\mathcal{A}$, 1, -1, and 0 represent the actions which increases the tap position by one, reduces the tap position by one and maintains the current tap position, respectively. Further, the voltage error $|\Delta\bar{E}_o|$ depends on voltage reference $\bar{E}_o^{ref}$, measured voltage $\bar{E}_o^{mea,t}$ and current $\bar{I}_o^{mea,t}$, resistance setting R_o^{set} and reactance setting X_o^{set} as given by Eq. (5.4). The impedance setting R_0^{set} and X_o^{set} represent the electrical distance between the OLTC and the regulated point.

The OLTC observes local voltage $\bar{E}^{mea,t}$ and current $\bar{I}^{mea,t}$ and decides whether to raise the tap position, lower the tap position or maintain its tap position to the present value using Eq. (5.3). If at time t_0 $\mathcal{A}(t_0) \neq 0$, then tap changing may be required. However, the OLTC must wait for a delay time dt_o before executing the switching action. Otherwise, there would be no switching action.

When an OLTC o operates in voltage control mode, the position of its tap at phase p and time t, tap_{op}^t, is determined by the values of voltage reference $\bar{E}_o^{ref}$, measured voltage $\bar{E}_o^{mea,t}$ and current $\bar{I}_o^{mea,t}$, resistance setting R_o^{set} and reactance setting X_o^{set}. The position of the tap of the OLTC (tap_{op}^t) is not selected in the optimization process the way it is done in the previous chapters. In other words, when LDC mode is considered tap_{op}^t is not a control variable but a state variable.

If the variable tap_{op}^t is considered as an integer variable, multiperiod OPF considering LDC mode may be intractable for solution of large system. For example, in the modified IEEE 123 bus system there are 9 OLTCs each of which has 33 possible values. For a 24-hour optimization, the size of discrete search space would be $33^9 \times 24 > 10^{15}$. Hence, the corresponding MINLP would be intractable.

Furthermore, in Chapters 3 and 4, binary variables have been modelled using a set of continuous variables. Since any integer variable can be represented as a sum of binary variables, it follows

that any integer variable can be modelled using a set of continuous variables. Section 5.3 explores this idea in more details.

5.2 Optimization Model of LDC

The mathematical model for the controller of an OLTC are given in Eqs. (5.3) - (5.5). They cannot be directly integrated into the formulation for voltage regulation problem because of the following reasons:

1. The logic within Eq. (5.3) poses a great challenge since logical constraints is not supported in conventional algorithms such as interior point method. However, it is possible to avoid using Eq. (5.3) in its entirety if OLTC's taps are not allowed to touch their limits unnecessarily as discussed in [67]. If this assumption is accepted then the simpler model of LDC can be formulated.

2. Eq. (5.5) includes the notion of time. Since our study is a static study, Eq. (5.5) is neglected further.

With these two assumptions, it is possible to derive a model that can be integrated into an OPF model to find optimal settings of db_o, $\bar{E}_o^{ref}$, R_o^{set} and X_o^{set}.

For any time t, the tap position of an OLTC o at phase p, tap_{op}^t, which operate in LDC mode must satisfy the following constraints:

$$|\Delta \bar{E}_o^t| = |\bar{E}_o^{mea,t} - \bar{I}_o^{mea,t}(R_o^{set} + jX_o^{set})| - |\bar{E}_o^{ref}| \tag{5.6}$$

$$-\frac{db_o}{2} \leq |\Delta \bar{E}_o^t| \leq +\frac{db_o}{2} \tag{5.7}$$

$$tap^{min} \leq tap_{op}^t \leq tap^{max} \tag{5.8}$$

$$db_o^{min} \leq db_o \leq db_o^{max} \tag{5.9}$$

$$E^{ref,min} \leq |E_o^{ref}| \leq E^{ref,max} \tag{5.10}$$

$$R_o^{set,min} \leq R_o^{set} \leq R_o^{set,max} \tag{5.11}$$

$$X_o^{set,min} \leq X_o^{set} \leq X_o^{set,max} \tag{5.12}$$

Moreover, if an OLTC o operates uniformly (non-uniformly), the following constraints are valid (invalid)

$$\bar{E}_{oa}^{ref} = \bar{E}_{ob}^{ref} = \bar{E}_{oc}^{ref}, \tag{5.13a}$$

$$R_{oa}^{set} = R_{ob}^{set} = R_{oc}^{set}, \tag{5.13b}$$

$$X_{oa}^{set} = X_{ob}^{set} = X_{oc}^{set}, \tag{5.13c}$$

and

$$db_{oa} = db_{ob} = db_{oc}. \tag{5.13d}$$

Furthermore, the position of the tap of an OLTC o at phase p at time t, tap_{op}^t does not depend directly on whether the OLTC o operates uniformly or not. Note that the LDC settings db_o, $\bar{E}_o^{ref}$, R_o^{set} and X_o^{set} do not change over time. On the other hand the tap position tap_{op}^t changes over time.

The model of line drop compensation introduces new control variables i.e. db_o, $\bar{E}_o^{ref}$, R_o^{line} and X_o^{line}. All of these new control variables are discrete. They can be reformulated into continuous variables using Eqs. (3.18). In addition, tap_{op}^t is also discrete. However, the variable tap_{op}^t is also a state variable and hence must be modelled differently as discussed in Section 5.3.

5.3 Representation of Integer Variables using Continuous Variables

Following Eq. (2.37) the variable tap_{op}^t can be written as

$$tap_{op}^t = tap_{op}^{lb,t} + z_{op}^t * \delta_{op}. \tag{5.14}$$

where

$$z_{op}^t \in \mathcal{Z} = \{-1, 0, 1\} \tag{5.15}$$

$$tap_{op}^t \subseteq \mathcal{T} = \{-16, 15, ..., 16\}. \tag{5.16}$$

Table 5.2: Values of z_{op}^t for different values of b_{op+}^t and b_{op-}^t .

b_{op+}^t	b_{op-}^t	z_{op}^t
0	0	0
0	1	-1
1	0	1
1	1	0

and

$$tap_{op}^{lb,t} \subseteq \mathcal{T} = \{-16, 15, ..., 16\}. \tag{5.17}$$

is a good estimate of tap_{op}^t.

The constraints given in Eq. (5.15) is reformulated into a set of continuos constraints given below

$$z_{op}^t = b_{op+}^t - b_{op-}^t \tag{5.18a}$$

$$\begin{aligned} b_{op+}^t - \frac{1}{2} &= b_{uop+}^t - b_{lop+}^{it} && (5.18b)\\ \frac{1}{2} &= b_{uop+}^t + b_{lop+}^t && (5.18c)\\ b_{uop+}^t b_{lop+}^t &= 0, b_{uop+}^t \geq 0, b_{lop+}^t \geq 0 && (5.18d) \end{aligned}$$

$$\begin{aligned} b_{op-}^t - \frac{1}{2} &= b_{uop-}^t - b_{lop-}^t && (5.18e)\\ \frac{1}{2} &= b_{uop-}^t + b_{lop-}^t && (5.18f)\\ b_{uop-}^t b_{lop-}^t &= 0, b_{uop-}^t \geq 0, b_{lop-}^t \geq 0 && (5.18g) \end{aligned}$$

where $b_{op+}^t, b_{uop+}^t, b_{lop+}^t, b_{op-}^t, b_{uop-}^t$ and b_{lop-}^t are all continues variables. Note that $b_{op+}^i \in \{0, 1\}$ ($b_{op-}^t \in \{0, 1\}$) due to the constraints given in Eqs. (5.18b) - (5.18d) ((5.18e) - (5.18g)). Hence, eqs. (5.18) satisfy Eq. (5.15) as shown in Table 5.2.

By using the constraints given in Eq. (5.18), the state variable tap_{op}^t is now represented as a continuous variable and the IPM-IPM method of Chapter 3 can be applied to solve the voltage regulation problem with OLTC operating in LDC mode.

Note that with the addition of new variables and constraints, the approach proposed in this chapter enables 24-hour optimization of voltage regulation problem. As shown in Chapter 2, the corresponding MINLP alternative is more intensive computationally than that of the proposed approach. Note that in Eqs. (5.6) - (5.12), the settings of LDC (db_o, $\bar{E}_o^{ref}$, R_o^{set} and X_o^{set}) do not change over time. Actually, it is also possible to optimized those settings hourly. However, the conventional operation of LDC generally does not change the values of those settings frequently because the required communication system generally is not available. Therefore, it is quite reasonable to optimize just 24-hour-ahead to increase the applicability of the proposed method.

5.4 Problem Formulation

The above line drop compensation model can easily be integrated into the optimization problem discussed in the previous chapters. For example, the Problem (P2.0) can be expanded to include LDC and becomes Problem (P5.0). In this way, new control variables, i.e. bandwidth db_o, voltage reference $\bar{E}_o^{ref}$, resistance R_o^{set} and reactance X_o^{set} of LDC, are added into the problem formulation.

$$\begin{aligned} \underset{\mathbf{c},\mathbf{d}}{\text{minimize}} \quad & J \\ \text{subject to} \quad & (2.2)-(2.6), (2.12)-(2.36), (5.6)-(5.13) \end{aligned} \tag{P5.0}$$

As discussed in the last paragraph of Section 5.3, Problem (P5.0) should be solved as a 24-hour ahead optimization. Since the problem is an MINLP, it is very difficult to solve it as it is. Therefore, the MINLP is reformulated as an NLP. Furthermore, the later problem is still very difficult to solve. Therefore, the exact penalty function approach [116] is applied to make the problem easily solvable. The approach is discussed below.

5.4.1 Exact Penalty Relaxation Method

Consider a generic optmization problem written in the following form:

$$\begin{aligned} \underset{\mathbf{c},\mathbf{d}}{\text{minimize}} \quad & f(\mathbf{c},\mathbf{d}) \\ \text{subject to} \quad & g_i(\mathbf{c},\mathbf{d},\mathbf{p}) = 0, i = 1,2,...,n_g \\ & h_j(\mathbf{c},\mathbf{d},\mathbf{p}) \leq 0, j = 1,2,...,n_h. \end{aligned} \tag{P5.0a}$$

After the exact penalty approach is applied to Problem (P5.0a), a new problem is formulated as

$$\begin{aligned} \underset{\mathbf{c},\mathbf{d}}{\text{minimize}} \quad & f(\mathbf{c},\mathbf{d}) + K_\rho \left(\sum_{i=1}^{n_g} (\rho_{gi})^2 + \sum_{j=1}^{n_h} \rho_{hj} \right) \\ \text{subject to} \quad & g_i(\mathbf{c},\mathbf{d},\mathbf{p}) = 0 + \rho_{gi}, i = 1,2,...n_g \\ & h_j(\mathbf{c},\mathbf{d},\mathbf{p}) \leq 0 + \rho_{hj}, j = 1,2,...n_h \\ & \rho_{hj} \geq 0. \end{aligned} \tag{P5.0b}$$

The Problem (P5.0b) is in general easier to solve than Problem (P5.0a). If

$$|\rho_{g_i}| \leq 10^{-7}, i = 1,2,...,n_g \tag{5.19}$$

and

$$|\rho_{h_j}| \leq 10^{-7}, j = 1,2,...,n_h \tag{5.20}$$

then the solution of Problem (P5.0b) is also the solution of the original problem (P5.0a). The coefficient of $K_\rho \geq K_\rho^{min} > 0$ must be a sufficiently large constant. In [116], the value of K_ρ^{min} is calculated by solving a bilevel optimization problem. However, the actual value of K_ρ^{min} is not required here. Therefore, repeated simulation studies were performed to find that $K_\rho = 10^9$ is sufficient.

Note that ρ_{gi} and ρ_{hi} represent new continuous variables which relax equality and inequality constraints, respectively. At the solution of Problem (P5.0b), these variables should be effectively zeros. On one hand, the function g_i may approach zero from both negative or positive values. Therefore, the variable ρ_{gi}, which corresponds to an equality constraint, is allowed to have any real value during the iterations of the algorithm. On the other hand, the function h_j must not be positive. Thus, a negative value of variable ρ_{hj} will tighten (instead of relaxing) the corresponding inequality constraints. Therefore, the variable ρ_{hj}, which corresponds to an inequality constraint, is only allowed to have non-negative value.

5.5 Solution Method

The problem (P5.0) is solved using a two-stage approach presented in this subsection. In the first stage, all discrete variables are assumed to be continuous variables. The corresponding optimization problem is then solved using interior point methods. Using the optimal solution of the first stage, another MINLP is formulated which has significantly smaller discrete search space. In the

second stage, the MINLP is further reformulated into another NLP based on the method described previously in Eqs. (2.37) and (5.18).

1. Stage 1

   (a) Convert all discrete variable d_k^1 into continuous variable c_k^1 and apply the method described in Subsection 5.4.1. This relaxes the initial MINLP (P5.0) into a Non-Linear Programming (NLP) given by (P5.1) below

$$\begin{aligned} \underset{\mathbf{c}}{\text{minimize}} \quad & J + K_\rho \left(\sum_{i=1}^{n_g} (\rho_{gi})^2 + \sum_{j=1}^{n_h} \rho_{hj} \right) \\ \text{subject to} \quad & (2.2) - (2.6), (2.12) - (2.36), (5.6) - (5.13). \end{aligned} \tag{P5.1}$$

   (b) Solve the NLP using interior point method for 24-hour period.

   (c) From the solution of the NLP (c_k^{1*}), find the nearest lowest boundary d_k^{lb}. If the optimum continuous value is equal to one of the discrete value, let it be the lowest boundary.

   (d) For all discrete variables but those corresponding to taps of OLTCs, define new discrete variable

$$d_k^{2t} = d_k^{lb,t} + b_k^t * \delta_k \tag{5.21}$$

   where δ_k is the step size of the k^{th} variable and b_k^t is an binary variable corresponding to k^{th} original discrete variable and time t.

   (e) For all discrete variables corresponding to taps of OLTCs

$$d_k^{2t} = d_k^{lb,t} + z_k^t * \delta_k \tag{5.22}$$

   where z_k^t is an integer variable corresponding to k^{th} discrete variable and time t.

   (f) Using the new discrete variables, another MINLP (P5.2) is formulated which has integer discrete variables.

$$\begin{aligned} \underset{\mathbf{c},\mathbf{z}}{\text{minimize}} \quad & J + K_\rho \left(\sum_{i=1}^{n_g} (\rho_{gi})^2 + \sum_{j=1}^{n_h} \rho_{hj} \right) \\ \text{subject to} \quad & (2.2) - (2.6), (2.12) - (2.36), (5.6) - (5.13) \\ & (5.21) - (5.22) \end{aligned} \tag{P5.2}$$

2. Stage 2

(a) For all discrete variables other than taps of OLTCs, convert each binary variable b_k^t into a continuous variable b_k^{ct} and use the constraints given in Eqs. 5.23.

$$\begin{aligned} d_k^{ct} &= d_k^{lb,t} + b_k^{ct}\delta_k, && (5.23a)\\ b_k^{ct} - \frac{1}{2} &= b_{uk}^t - b_{lk}^t, && (5.23b)\\ \frac{1}{2} &= b_{uk}^t + b_{lk}^t, && (5.23c)\\ b_{uk}^t b_{lk}^t &= \rho_b, b_{uk}^t \geq 0, b_{lk}^t \geq 0, && (5.23d) \end{aligned}$$

(b) For all discrete variables corresponding to OLTCs, apply the constraints given in Eqs. (5.18) with the following modification:

i. Change Eq. (5.18d) into

$$b_{uop+}^t b_{lop+}^t = \rho_{b+}, b_{uop+}^t \geq 0, b_{lop+}^t \geq 0, \rho_{b+} \geq 0 \quad (5.24)$$

ii. Change Eq. (5.18g) into

$$b_{uop-}^t b_{lop-}^t = \rho_{b-}, b_{uop-}^t \geq 0, b_{lop-}^t \geq 0, \rho_{b-} \geq 0 \quad (5.25)$$

(c) Note that now ρ_b, ρ_{b+} and ρ_{b-} are also variables that relax equality constraints similar to ρ_{gi}.

(d) Now the Problem (P5.2) can be converted into another NLP (P5.3).

$$\begin{aligned} \underset{\mathbf{c},\mathbf{z}}{\text{minimize}} \quad & J + K_\rho \left(\rho_b^2 + \rho_{b+}^2 + \rho_{b-}^2 + \sum_{i=1}^{n_g} \rho_{gi}^2 + \sum_{j=1}^{n_h} \rho_{hj} \right) \\ \text{subject to} \quad & (2.2) - (2.6), (2.12) - (2.36), (5.6) - (5.13) \\ & (5.18a) - (5.18c), (5.18e), (5.18f), (5.21) - (5.22), (5.23) - (5.25) \end{aligned} \quad (P5.3)$$

(e) Solve the new NLP (P5.3) for a period of 24 hour.

(f) If Eqs. (5.19), (5.20) and

$$\rho_b \leq 10^{-7}, \rho_{b+} \leq 10^{-7}, \rho_{b-} \leq 10^{-7}$$

are satisfied then the solution of (P5.3) can also be considered as the solution of (P5.0). Otherwise, the problem is assumed to be unsolvable by the proposed method.

5.6 Results and Discussion

Here, the system discussed in Subsection 3.5.1 is considered again. However, there are significant differences which should be mentioned here. Unlike Chapter 2, all OLTCs are assumed to operate in LDC mode in this chapter. In addition, the settings of LDC are optimized for period of 24 hours. Moreover, the weights of objective function J are $\alpha = 0.1, \beta = \gamma = 0.45$ which correspond to Case J as defined in Table 2.2. Note that in Chapter 2, Case J was selected as the best case.

The optimal solution taken from this chapter is compared with the results of Chapter 2 based on line losses, VMI, VDMI, VUI and total number of switchings. The detailed discussion about each of them are given below.

5.6.1 Line Losses

Fig. 5.2 compares total line losses for strategies XI - XVIII corresponding to time-of-the-day mode and LDC mode operation of OLTCs. The losses corresponding to LDC mode are lower than those corresponding to time-of-the-day mode. The maximum (minimum) difference in losses between the two modes is 12.2 (5.2) kWh. Hence, in terms of losses, the LDC mode of the OLTCs is slightly better than the time-of-the-day mode of the OLTCs.

The reason for the time-of-the-day mode having higher losses as compared to the LDC mode is the choice of the values of the weights of the objective functions. As mention earlier, $\alpha = 0.1 < \beta = \gamma = 0.45$. Hence, there is higher priority in reducing the number of switchings than reducing the total losses. It will be shown later that the time-of-the-day mode has, indeed, lower number of switchings than the LDC mode.

5.6.2 Voltage Magnitude Index

Fig. 5.3 shows the values of VMIs for strategies XI - XVIII corresponding to time-of-the-day and LDC mode of operation of OLTCs. It highlights the significant discrepancies among VMIs

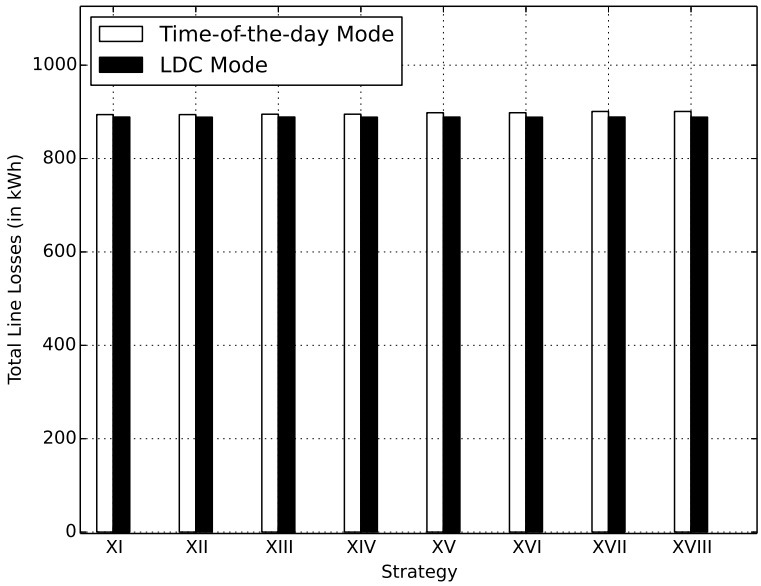

Figure 5.2: Losses

corresponding to these two modes. In case of LDC mode, the values of VMIs are lower than 10. On the other hand, in case of time-of-the-day mode, the values of VMIs are higher than 15. This means that voltages are significantly closer to their rated values in LDC mode than in time-of-the-day mode.

From the point of view of customer, VMI should be as low as possible since most of devices are designed to be optimal at rated values. Therefore, the lower the VMI is, the better the devices operate. In conclusion, in term of VMI, the LDC mode is better than the time-of-the-day mode.

The reason for the time-of-the-day mode having higher values of VMIs than the LDC mode is related to the characteristics of these modes. In the time-of-the-day mode, the magnitude of the voltages can be easily optimized by directly adjusting the position of the taps of the OLTCs. On the other hand, in the LDC mode, only one value of reference voltage $|E_o^{ref}|$ is used for the whole day. As the loads vary significantly during the day, it is not possible to have high value of reference voltage and hence, the values of VMIs corresponding to LDC mode are not as high as those corresponding to the time-of-the-day mode.

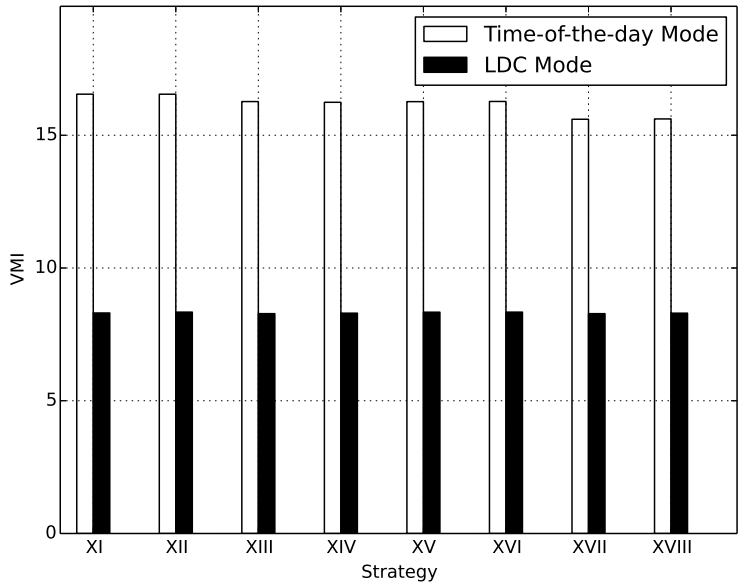

Figure 5.3: VMI

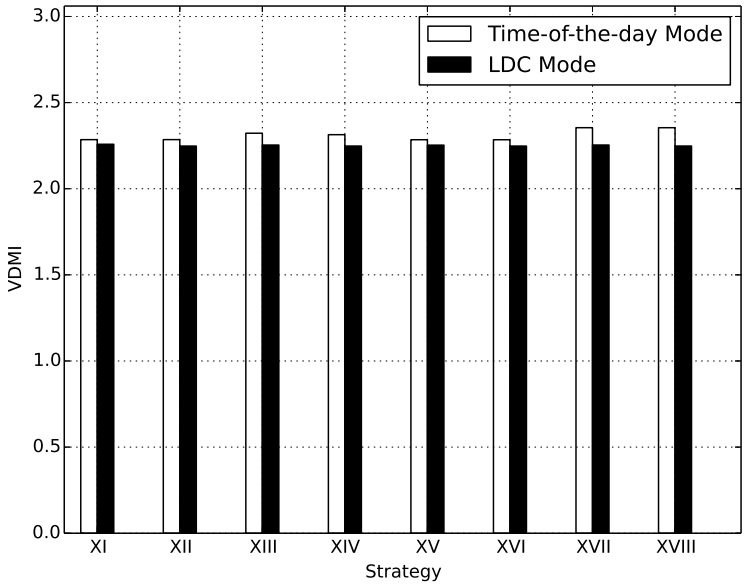

Figure 5.4: VDMI

5.6.3 Voltage Drop Magnitude Index

Fig. 5.4 compares the values of VDMI for strategis XI-XVIII corresponding to time-of-the-day and LDC mode of operation of OLTCs. The values corresponding to time-of-the-day mode are higher

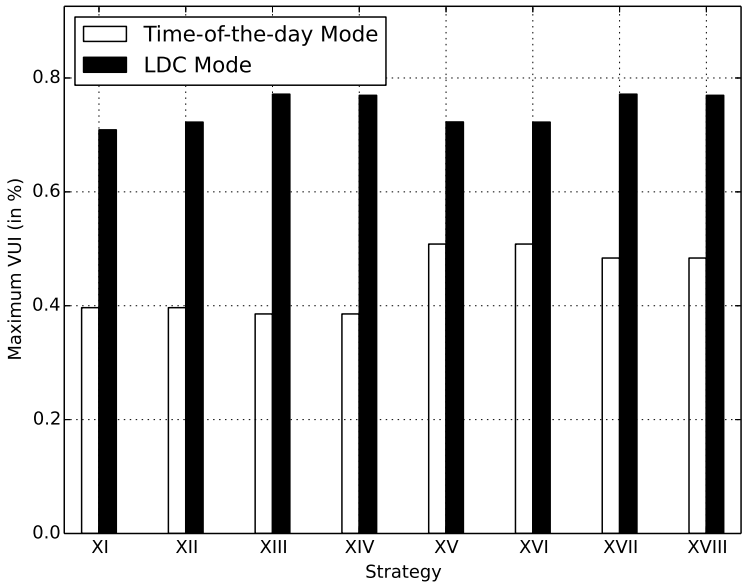

Figure 5.5: VUI

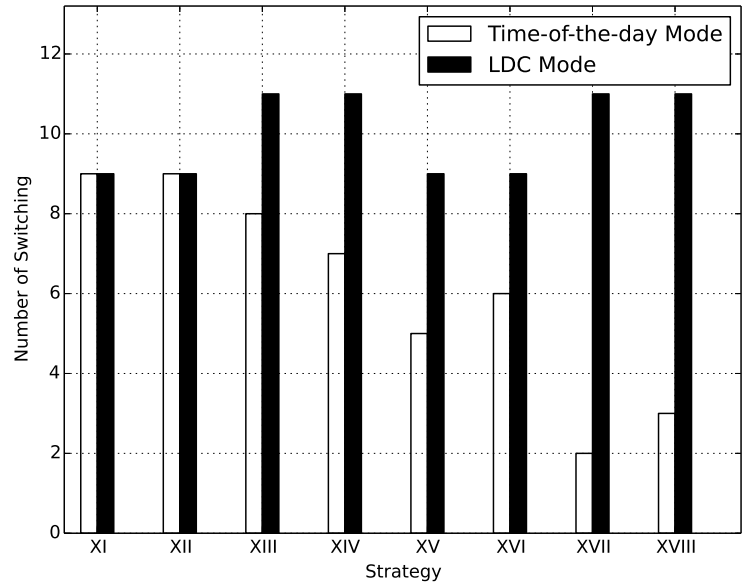

Figure 5.6: Number of switching

than those corresponding to LDC mode. This means that the flatness of the profiles of voltages corresponding to the LDC mode are better than those corresponding to the time-of-the-day mode.

Hence, in terms of VDMI, the LDC mode is generally better than the time-of-the-day mode.

The reason that the LDC mode is better than the time-of-the-day mode in term of VDMI is related to the characteristic of LDC mode. The LDC controller maintains the voltages within a small bandwidth around its reference voltage. Hence, the LDC mode is designed to flatten the voltage profile of the network. The time-of-the-day mode is not designed in this manner and hence has more freedom to find the optimal solution. Since the dominant objective function corresponds to total number of switchings, the solution of the time-of-the-day mode is not as flat as that corresponding to LDC mode.

5.6.4 Voltage Unbalance Index

Fig. 5.5 compares the maximum values of VUI for strategy XI - XVIII corresponding to time-of-the-day and LDC modes of operation of OLTCs. All of them are below the upper limits of 2%. The maximum values of VUI corresponding to LDC mode, in general, are higher than those corresponding to time-of-the-day mode. Hence, in term of voltage unbalance, the time-of-the-day mode is better than the LDC mode.

The reason that the LDC mode corresponds to higher voltage unbalance than the time-of-the-day mode is related to the characteristics of these modes of operation of OLTC. In the LDC mode, the taps of an OLTC are state variables. On the other hand, in the time-of-the-day mode, taps of an OLTC are control variables which can be optimized directly. Consequently, balancing the voltages in the network is easier in the time-of-the-day mode than the LDC mode.

5.6.5 Total Number of Switching

Fig. 5.6 compares the total number of switchings for strategy XI-XVIII corresponding to time-of-the-day and LDC modes of operation of OLTCs. It can be seen that the number of switchings corresponding to LDC mode are higher that those corresponding to time-of-the-day mode. The minimum and maximum differences are 0 and 9, respectively.

The reason that the LDC mode has higher number of switchings is related to the operating characteristics of these two modes of operation. As we discussed previously, the time-of-the-day mode corresponds to direct control of the position of the tap of an OLTC which is not the case in the LDC mode of operation. Hence, the time-of-the-day mode has more freedom in minimization of the number of switchings than the LDC mode.

Table 5.3: Computational Time for both stages for different strategies using LDC mode.

	Computational Time in Seconds							
Strategy	XI	XII	XIII	XIV	XV	XVI	XVII	XVIII
Stage 1	20	63	14	40	83	120	111	111
Stage 2	44	15	26	18	15	14	21	16
Both Stage	64	78	40	58	98	144	274	205

5.6.6 Computational Time

Table 5.3 shows the computational time required to solve the optimization problem corresponding to LDC mode for strategies XI-XVIII. The longest time is 274 seconds which corresponds to strategy XVII. Hence, the proposed method is able to solve the voltage regulation problem considering LDC operation of OLTC in less than 5 minutes. As a result, the proposed method is quite useful for real life application.

5.7 Overall Comparison

It is important to generally compare the two modes of control of OLTCs. In terms of losses, VMI and VDMI, the LDC mode is better than the time-of-the-day mode. However, in term of VUI and number of switchings, the LDC mode is worse than the time-of-the-day mode. In addition, the LDC mode requires less communication infrastructure than the time-of-the-day mode. Hence, it is not easy to say which alternative is better than the other one. Nevertheless, the method developed in this chapter may help in real life decision making process when more information is available.

Furthermore, in case of LDC mode, it is important to identify the best strategy to be implemented. In terms of losses, VMI and VDMI, all those strategies perform similarly. Moreover, Figs. 5.5 and 5.6 shows that strategies XI, XII, XV and XVI are the best ones in terms of VUI and number of switchings, respectively.

Since losses and number of switchings have rather direct financial consequences, these two indicators are used to decide the best strategy. Fig. 5.2 shows that all strategies are almost equal in terms of losses. Moreover, Fig. 5.6 shows that strategies XI, XII, XIV and XV have the lowest number of switchings. Among these four strategies, in case of the time-of-the-day mode, strategy

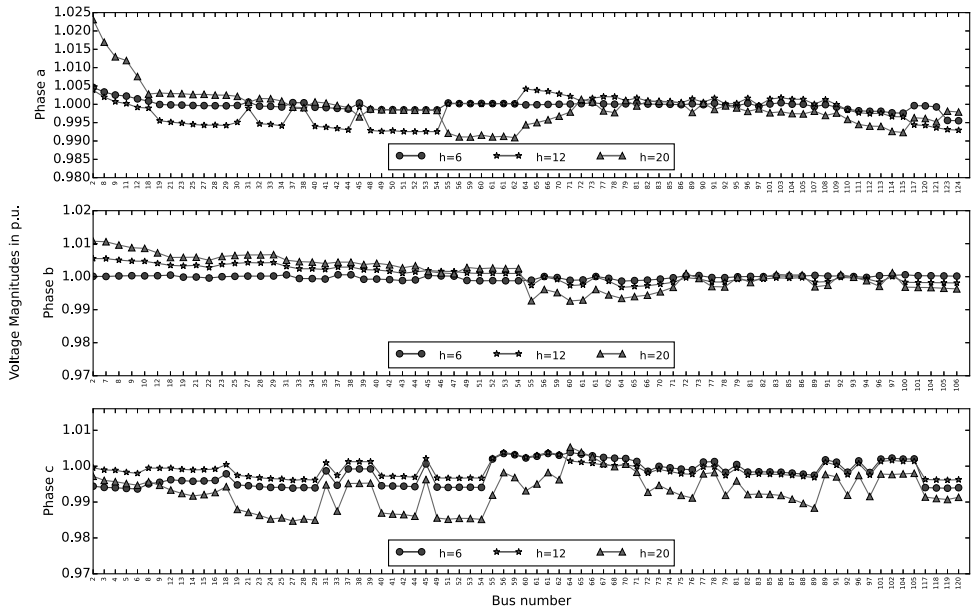

Figure 5.7: Voltage profiles corresponding to hours 6, 12, 20 and strategy XV.

XV has the lowest number of switchings. Hence, this chapter selects strategy XV as the best strategy corresponding to LDC mode.

Furthermore, as an illustration, Fig. 5.7 shows voltage profiles of the system corresponding to strategy XV and hours 6, 12, and 20. It can be seen that all voltages are well within limits and that those profiles are quite flat.

Table 5.4 compares optimal settings of LDCs of all OLTCs considering strategy XV. It is shown that some of the reactance settings are negative. This negativity desensitized the LDC against variation of reactive power flow. If the reactance setting is positive, an increase of reactive power loads may lead to an upward movement of the position of the taps of an OLTC. The negative reactance setting means that the OLTC will not increase the position of its tap when reactive load increases. This is useful since the value of reference voltage $|\bar{E}_o^{ref}|$ is closer to its upper limits than its lower limits. In other words, the negative reactance setting reduces the probability of over voltage. In this regard, the reactance settings of OLTC R4 are zeros. This is because of the fact that for OLTC R4 there are many SCs and SVC which compensate the increase in reactive loads.

On the other hand, the values of resistance setting R_o^{set} can also be negative in case of OLTCs which are located in the feeder i.e. R2-R4. Referring to Fig. 5.1, the negative values of resistance and reactance settings can be considered as selection of virtual load point in the negative direction

(direction of substation). Since real power flow is the dominant power flow in distribution network, the negative resistance setting indicates that the load point is in upward direction. In other words, it is better to regulate the upstream side (substation side) voltage instead of the downstream side voltage of the network. This is a valid situation for OLTCs installed on feeder such as R2-R4. On the other hand, the upstream side of OLTC R1 is connected to a strong bus which is assumed to be constant for all durations of simulation. Hence, there is no need for negative value of resistance settings of R1.

Furthermore, Table 5.5 also shows that the time-of-the-day mode is better than the LDC mode in term of VUI and number of switchings. On the other hand, the time-of-the-day mode is worse than the LDC mode in term of losses, VMI and VDMI. Since the weight of minimization of number of switchings is higher than the weight of minimization of losses, the time-of-the-day mode has lower number of switchings than the LDC mode.

On the other hand, the reference voltage of the LDC is closer to its upper limit (135 V) than its lower limit (100 V). This indicates that the OLTCs tries to maintain the magnitudes of the voltages at higher side of the allowed interval. Hence, the corresponding losses can be lower. Consequently, the number of switchings corresponding to LDC mode is higher than that corresponding to time-of-day mode.

In real life application, the increase in losses and number of switchings may be acceptable if the required communication infrastructure to implement time-of-the-day mode is not yet available. Hence, during the process of selection, these two alternatives should be studied properly to find the best solution for a particular implementation.

5.8 Conclusion

This chapter proposes an optimization model of the line drop compensation mode of operation of OLTCs. The model has been integrated into the voltage regulation optimization problem discussed in the previous chapters. The optimization problem has been compared with the problem discussed in Chapter 2 in terms of losses, VMI, VDMI, VUI and number of switchings. On one hand, time-of-the-day mode is better than the LDC mode in term of VUI and number of switchings. On the other hand, the time-of-the-day mode is worse than the LDC mode in term of losses, VMI and VDMI.

Table 5.4: Optimal Settings of LDC of OLTCs using strategy XV

OLTC	Phase	R_o^{set}	X_o^{set}	$\lvert\bar{E}_o^{ref}\rvert$	db_o
		(Volts)			
R1	a	1.3	-0.4	125	5.8
	b	1.3	-0.4	125	5.8
	c	1.3	-0.4	125	5.8
R2	a	-1.8	-0.2	125	5.8
R3	a	-4.1	-0.4	124.6	5.8
	c	-4.1	-0.4	124.6	5.8
R4	a	-1.6	0	125.3	5.8
	b	-1.6	0	125.3	5.8
	c	-1.6	0	125.3	5.8

Table 5.5: Comparison between Time-of-the-day Mode and LDC Mode ($\alpha = 0.1$, $\beta = \gamma = 0.45$, strategy XV)

	Time-of-the-day mode	LDC mode
Problem	(P2.0)	(P5.0)
Loss (kWh)	894.14	888.85
VMI	16.55	8.34
VDMI	2.28	2.25
VUI	0.4	0.72
Number of Switching	5	9

In real life application, the proposed modeling may be helpful in comparing these two alternatives. Since time-of-the-day mode has higher communication requirements than LDC mode, the work described in this chapter may help distribution system engineers in planning and control of voltage of radial distribution networks.

In the next chapter, voltage-dependent loads will be considered. In particular, ZIP model is integrated into the voltage regulation optimization problem.

6 — Voltage-Dependent Loads

See, I am very dependent... on beauty and peace of the world... on loyalty of friends... on love in families... on happiness and health of children. And I do not want to be free as long as I have it all..

- Galina Nelson

Abstract

In many previous works on voltage regulation of distribution networks, all loads are assumed to be constant-power loads. This can be caused by lack of data or difficulty in solving the corresponding optimization problem. This chapter explores the incorporation of voltage-dependent loads in voltage regulation problem.

6.1 Introduction

MOST of electrical loads are voltage dependent [138]. In the literature, two different models have been suggested to represent this voltage dependency: measurement -based [140, 192] and component-based [138] model. The measurement-based approach requires measurement devices, communication network and continuous adjustment as the loads change. The component-based approach requires no continuous measurement and the load model needs to be identified only once for the whole system based on the assumption that the load characteristics and compositions do not vary.

Since most of the operating networks do not have measurement and communication infrastructures required for measurement-based approach, this chapter uses component-based approach. Nevertheless, it is possible to include the measurement based model in the solution approach if these are available in future smart grids. Different component-based models available in the literature are discussed below.

Polynomial Model [193]

$$\frac{P}{P_0} = K_{pz}\left(\frac{V}{V_0}\right)^2 + K_{pi}\left(\frac{V}{V_0}\right) + K_{pc} \tag{6.1a}$$

$$+ K_{p1}\left(\frac{V}{V_0}\right)^{npv1}(1 + K_{pf1}\Delta f) \tag{6.1b}$$

$$+ K_{p2}\left(\frac{V}{V_0}\right)^{npv2}(1 + K_{pf2}\Delta f) \tag{6.1c}$$

$$K_{pz} = 1 - (K_{pi} + K_{pc} + K_{p1} + K_{p2}) \tag{6.1d}$$

$$\frac{Q}{Q_0} = K_{qz}\left(\frac{V}{V_0}\right)^2 + K_{qi}\left(\frac{V}{V_0}\right) + K_{qc} \tag{6.2a}$$

$$+ K_{q1}\left(\frac{V}{V_0}\right)^{npv1}(1 + K_{qf1}\Delta f) \tag{6.2b}$$

$$+ K_{q2}\left(\frac{V}{V_0}\right)^{npv2}(1 + K_{qf2}\Delta f) \tag{6.2c}$$

$$K_{qz} = 1 - (K_{qi} + K_{qc} + K_{p1} + K_{q2}) \tag{6.2d}$$

In the above equations, P and Q are real and reactive power of a load when its voltage is V. The coefficients K_{pz} and K_{qz} are the constant-impedance parts of the total load and the coefficients K_{pi} and K_{qi} are the constant-current part of the total load; the coefficients K_{pc} and K_{qc} are the constant-power part of the total load. Fourth and fifth terms in both the active and reactive power expressions are the two frequency dependent terms. P_0, Q_0 and V_0 are the rated values of active power, reactive power and magnitude of voltage of a load, respectively.

Generally, frequency variation is neglected and hence the generic model in Eqs. (6.1) and (6.2) reduces into Eqs. (6.1a) and (6.2a) (by setting $K_{p1} = K_{p2} = K_{q1} = K_{q2} = 0$) which is popularly named "ZIP model". The parameters of ZIP model,$\{K_{pz}, K_{pi}, K_{pc}, K_{qz}, K_{qi}, K_{qc}\}$, can be estimated based on component-based [138] or measurement-based [192] approaches.

Some representative values of these ZIP coefficients corresponding to different classes of loads are given in Table 6.1 [139]. Among the corresponding four classes considered in Table 6.1, only industrial loads have zero values for coefficients corresponding to constant-impedance and constant-current model. In other words, only industrial loads are constant-power loads. Con-

Table 6.1: ZIP Coefficients for various types of load class

Class	K_{pz}	K_{pi}	K_{pc}	K_{qz}	K_{qi}	K_{qc}
Large Commercial	0.47	-0.53	1.06	5.30	-8.73	4.43
Commercial	0.43	-0.06	0.63	4.06	-6.65	3.59
Residential	0.85	-1.12	1.27	10.96	-18.73	8.77
Industrial	0	0	1	0	0	1

sequently, in a network which serves commercial and residential loads, ZIP model is the more accurate approach than constant-power model.

Exponential Model [193]

$$P = P_0 \left(\frac{V}{V_0}\right)^{K_{pv}} [1 + K_{pf}(f - f_0)] \tag{6.3}$$

$$Q = Q_0 \left(\frac{V}{V_0}\right)^{K_{qv}} [1 + K_{qf}(f - f_0)] \tag{6.4}$$

In the above equations, the coefficient K_{pv} is the voltage coefficient for active power while K_{qv} is the voltage coefficient for reactive power; The coefficient K_{pf} and K_{qf} are the frequency coefficient for active power and reactive power, respectively; P and Q are active and reactive power at voltage V and frequency f, respectively; P_0 and Q_0 are initial (or rated) active and reactice power at voltage V_0 and frequency f_0, respectively.

Linear Model A linear model was proposed in [144] which is an estimate of more accurate ZIP model. Using this model, it is possible to have linear model of power flow which, consequently, requires less computational resource than the ZIP model. The integration of the linear model into optimal power flow is also easy.

Importance of using voltage-dependent loads in voltage regulation The importance of using the voltage-dependent model has been emphasized in the literature [139–141]. In addition, many of the loads are neither pure constant-power type nor constant-impedance type nor constant-current type [138]. Hence, the use of ZIP model increases the accuracy of the computation and improves

the quality of decision on operation and planning of distribution system.

Furthermore, the work reported in [194] shows that the performance of volt-var optimization are highly dependent on the type of load models. However, most of the works on voltage regulation use constant-power load models which stems from the observation that it provides most conservative result in comparison with the other two models (constant-impedance and constant-current). This can be seen in the following example.

When the ratio $\frac{V}{V_0} < 1.0$ a constant-power model gives an overestimated value of load power as compared to the constant-current and constant-impedance model. For example, for $\frac{V}{V_0} = 0.95$, the values of load power are P_0, $0.95P_0$ and $0.9025P_0$ for constant-power, constant-current and constant-impedance models, respectively. On the other hand, for $\frac{V}{V_0} > 1.0$, a constant-power load model gives a lower value of load power as compared to those given by constant-current and constant-impedance models. For example, for $\frac{V}{V_0} = 1.05$, the values of power are P_0, $1.05P_0$ and $1.1025P_0$ for constant-power, constant-current and constant-impedance loads, respectively. Finally, when $\frac{V}{V_0} = 1$, all three models give the same value of P_0. Therefore, to improve the accuracy of the solution of the voltage regulation problem, consideration of voltage dependent load model is preferable.

There are few works in voltage regulation problem which consider voltage dependent loads. The work described in [147] uses exponential load model in voltage regulation problem. However, it was tested in balanced network only. Some works, such as [20, 143], consider voltage regulation problem in an unbalanced distribution system in which a load is represented as either constant-impedance (Z), constant-current (I) or constant-power (P) load. However, these works do not consider polynomial or exponential model. Moreover, the work in [149] proposes voltage regulation in distribution system using voltage-dependent linear model proposed in [144].

The use of ZIP model for voltage regulation in unbalanced distribution systems is explored in [148] in which the corresponding optimization problem has been tested on IEEE 13 bus system. In [148], the voltage regulation problem is formulated as an MINLP similar to problem (P6.0) described in the next subsection. The results in Chapter 2 indicate that solving the corresponding MINLP problem for a system as big as IEEE 123 bus system for a period of 24 hour requires very high computational time. The solution method proposed in this chapter, however, reformulates the MINLP into NLP. This, in turn, allows the method to solve a modified IEEE 123 bus system easily.

6.1.1 Problem Formulation

This chapter considers voltage regulation problem in which loads are modeled as ZIP loads. For comparison purpose, the problem in Chapter 2 is modified by assuming all loads as ZIP loads. Note that in Chapter 2 all loads are assumed to be constant-power loads. Hence, voltage regulation problem considerering ZIP loads can be represented as Problem (P6.0).

$$\begin{aligned} &\underset{\mathbf{c},\mathbf{d}}{\text{minimize}} \quad J \\ &\text{subject to} \quad (2.2)-(2.6), (2.12)-(2.36), (6.5)-(6.7). \end{aligned} \tag{P6.0}$$

where Eqs. (6.5)-(6.7) represent ZIP loads and are explained below.

6.1.1.1 Voltage-Dependent Loads

For each ZIP load L connected to phase p of bus i, at a time t, the real and reactive power consumed by this load are given by

$$P_L^{ipt} = P_{L0}^{ipt}\left(K_{pz}^{i,p}(\mathcal{E}^{ipt})^2 + K_{pi}^{i,p}(\mathcal{E}^{ipt}) + K_{pc}^{i,p}\right) \tag{6.5}$$

$$Q_L^{ipt} = Q_{L0}^{ipt}\left(K_{qz}^{i,p}(\mathcal{E}^{ipt})^2 + K_{qi}^{i,p}(\mathcal{E}^{ipt}) + K_{qc}^{i,p}\right) \tag{6.6}$$

$$\mathcal{E}^{ipt} = \frac{|\bar{E}^{ipt}|}{|\bar{E}_0^{ip}|} = \frac{\sqrt{(E_x^{ipt})^2 + (E_y^{ipt})^2}}{\sqrt{(E_{0x}^{ip})^2 + (E_{0y}^{ip})^2}} \tag{6.7}$$

In the above equations, $\bar{E}_0^{ip}$ represents the rated voltage at bus i and phase p. With these values of load real and reactive power, the real and reactive current drawn by the load are calculated from Eqs. (2.12) and (2.13).

6.2 Solution Method

This chapter uses the solution method decribed in Chapter 5.

6.3 Results and Discussion

6.3.1 Modified IEEE 123 Bus System

Consider the modified IEEE 123 Bus system shown in Fig. 2.3. The modifications described in Subsection 3.5.1 are also considered here. However, all loads are now considered as residential

ZIP loads. The values of coefficients of those residential ZIP loads are given in Table 6.1. The following cases have been investigated to study the effects of voltage dependency of loads on voltage regulation problem:

1. Case 1: The situation described in Chapter 2 i.e. all loads are constant-power loads.

2. Case 2: All loads are residential ZIP loads.

The values of weights of objective functions are $\alpha = 0.1, \beta = 0.45$ and $\gamma = 0.45$ which correspond to Case J described Chapter 2. In the following sub-subsections, various indices such as losses, number of switchings, VMI, VDMI and VUI are compared for the above two cases.

6.3.1.1 Line Losses Comparison

Fig. 6.1 compares the total losses of strategies XI-XVIII corresponding to constant power loads and ZIP loads. The constant-power model suggests higher losses than those of ZIP load model in all strategies. However, the differences between these two groups are arguably small. Hence, in term of losses, the two models perform quite similarly.

The losses corresponding to ZIP loads are lower than those corresponding to constant-power loads. This is due to the fact that voltages at the load buses are usually less than 1 p.u. As a result, the total amount of power consumed by the loads become less than the rated value. As the actual amount of load power decreases, the loss in the system also decreases in the presence of voltage-dependent loads.

6.3.1.2 Voltage Magnitude Index

Fig. 6.2 compares the values of VMIs of strategies XI-XVIII corresponding to constant-power loads and ZIP loads. The values of VMIs corresponding to constant-power model are higher than those corresponding to ZIP model. The lower the value of VMI is, the closer the magnitudes of the voltages are to their rated values are, and therefore, the better the voltage profile of the network is. Hence, in term of VMIs, the ZIP model performs better than the constant-power model.

In case of constant-power loads, the algorithm tries to increase the voltage magnitude as much as possible to reduce the loss. Therefore, the VMI for constant-power loads is relatively higher. In case of ZIP loads, the algorithm tries to reduce the losses by reducing the effective amount of power. As the effective amount of power is dependent on the voltage magnitudes, essentially, the

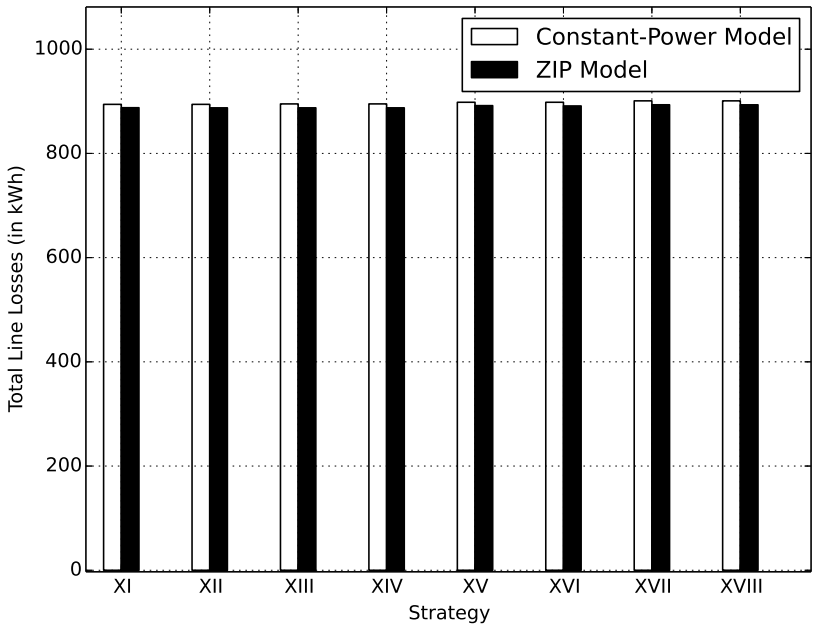

Figure 6.1: Losses

algorithm tries to reduce the loss by reducing the voltage magnitude, thereby making the VMI relatively lower.

6.3.1.3 Voltage Drop Magnitude Index

Fig. 6.3 shows the values of VDMIs corresponding to constant-power loads and ZIP loads. The values of VDMIs corresponding to these two groups are quite close to each other. However, the values corresponding to the constant-power model are higher than those corresponding to ZIP model. The smaller the VDMIs are, the flatter the voltage profile is. Hence, these two models correspond to similar level of flatness of voltage profile. In a nutshell, in term of VDMIs, the ZIP model is a little bit better than the constant-power model.

The load powers corresponding to ZIP models are less than those corresponding to constant-power models. As a result the line flows corresponding to ZIP models are lower than those corresponding to constant-power models. This further means that the voltage drop of the lines corresponding to ZIP loads are less than those corresponding to constant-power loads. Hence, the voltage drops corresponding to ZIP loads are also lower than those corresponding to constant-power loads. Consequently, the values of VDMI corresponding to ZIP loads are lower than those

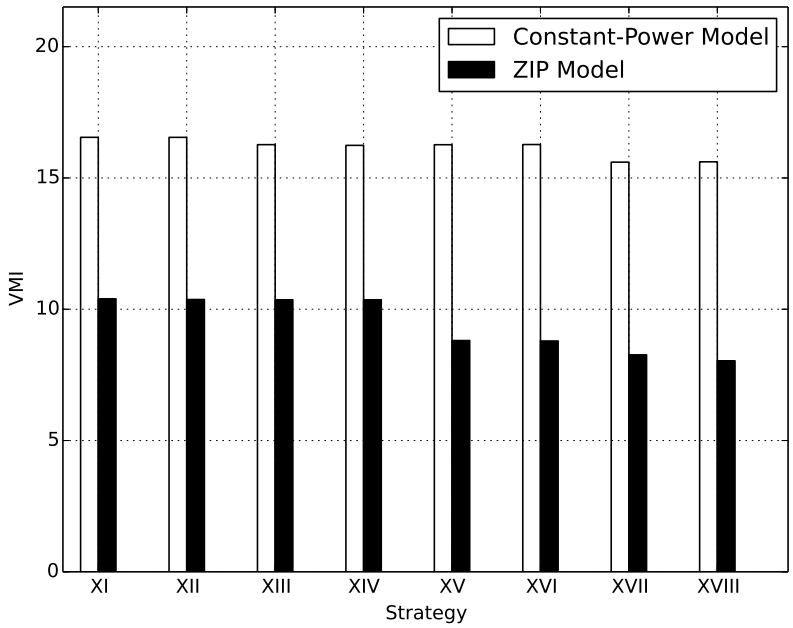

Figure 6.2: VMI

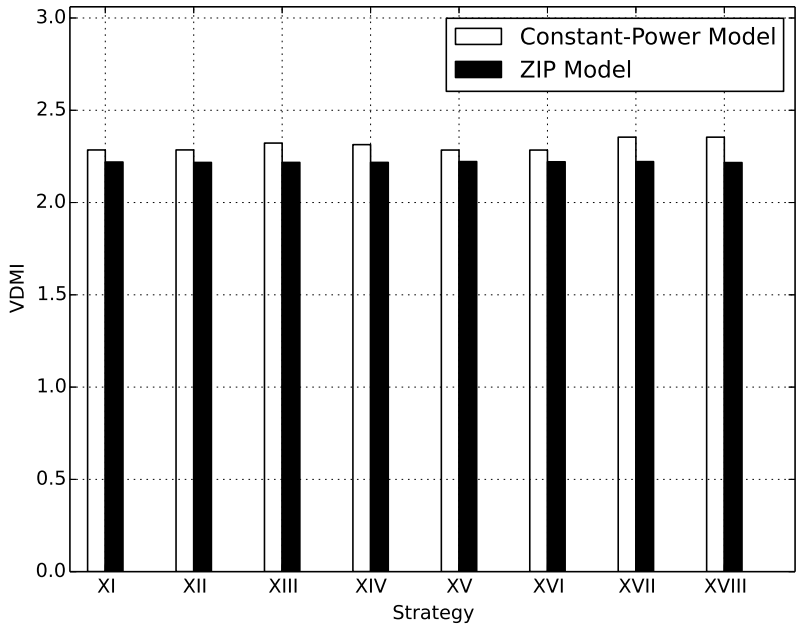

Figure 6.3: VDMI

corresponding to the constant-power loads.

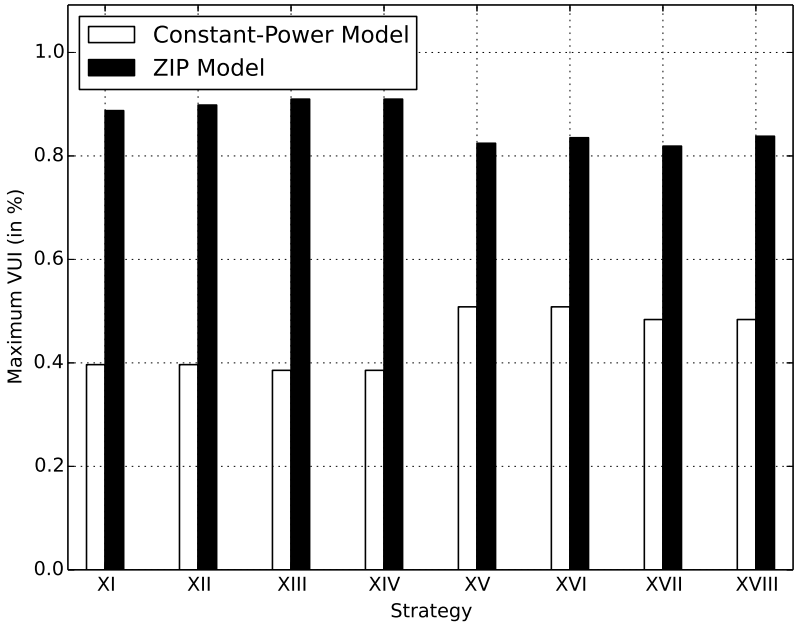

Figure 6.4: Maximum VUI

6.3.1.4 Voltage Unbalance Index

Fig. 6.4 shows that the values of maximum VUIs of strategies XI-XVIII corresponding to constant-power and ZIP loads. Fig. 6.4 shows that the values of maximum VUIs corresponding to constant-power model are lower than the ones corresponding to ZIP model. Hence in terms of VUIs, the constant-power model is better than the ZIP model.

In an unbalanced three phase line, when there is a reduction of loads in a particular phase, the voltage drop of the other two phase change differently. If the voltage drop is increasing at one phase then the voltage drop is decreasing the other phase. This behaviour has been reported in the literature [151, 172]. In case of ZIP loads, the bus voltages become more uneven (i.e. unbalanced) due to interaction between the effective amount of power and voltage magnitudes, as compared to the case with constant-power loads. As a result, the values of VUI are more for ZIP loads as compared to the case with constant-power loads. However, in both cases, the values of VUI are reasonably close to each other and are well below the upper limit of 2%.

6.3.1.5 Number of switchings

Fig. 6.5 compares the optimum total number of switchings corresponding to constant power loads and ZIP loads. The total number of switchings corresponding to constant-power loads are significantly lower than those corresponding to ZIP loads. This indicates that the use of constant-power model corresponds to better optimal total number of switchings.

As discussed previously, in the case of constant-power loads, majority of the magnitudes of the voltages are relatively higher. Thus, there is a high risk of an overvoltage during a light loading period. However, during heavy loading period, there is a small risk of an undervoltage. Therefore, the switching operation is mainly required during the light loading period and therefore, the number of switching operations for constant-power loads are relatively lower. In case of ZIP loads, the algorithm makes the OLTC R1 to maintain the voltages of buses served by it at a relatively higher level so that the voltages at the buses served by OLTCs R2-R4 can be maintained at a lower level to reduce the loss. Therefore, during a light loading (and/or high generation) period, there is a high risk of overvoltage at the buses served by OLTC R1. On the other hand, during heavy load (and/or low generation), there is a high risk of undervoltage at the buses served by OLTCs R2-R4. Thus, for both cases (light and heavy loading) appropriate switching actions need to be performed to maintain the voltages within limits. As a result, the number of switching operations with ZIP loads is relatively higher.

6.3.1.6 Overall Comparison

It is important to have overall comparison between the two load models. On one hand, in terms of losses, VMI and VDMI, the constant-power loads correspond to higher values than the ZIP loads do. On the other hand, in terms of VUI and number of switching operations, the constant power loads correspond to lower values than the ZIP loads.

In addition, the amount of differences in performances of both models should also be considered. In terms of losses and VDMI, the differences of performances are arguably small. In terms of VMI, maximum VUI, and number of switchings, the differences of performance are significant. This has an important consequence if the actual loads in the networks are voltage dependent but assumed to be constant-power loads.

Furthermore, it is also interesting to know the best strategy among these eight strategies. In

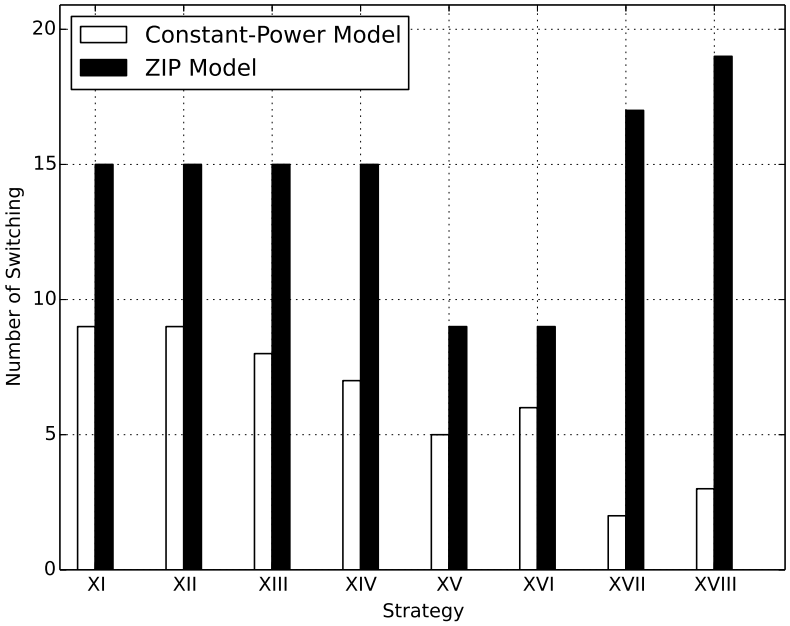

Figure 6.5: Total number of switchings

terms of losses and VDMIs, these strategies are very close to each other. In terms of VMI, VUI and number of switchings, there are significant differences. However, note that in terms of VUI and VMI, voltages are all within regulatory limits. Hence, from the point of the operator of the network, it is sufficient to consider the total number of switchings. As shown in Fig. 6.5, the two best strategies in term of number of switchings are strategy XVII and XVIII in case of constant-power loads and strategies XV and XVI in case of ZIP loads. Moreover, strategy XV is also the third best in term of number of switchings in case of constant-power loads. Therefore, considering both of the cases, strategy XV (in which the OLTCs operate uniformly; and the SVC and SCs operate non-uniformly) is selected as the best one among all strategies under study.

Note that in real life application, the comparison generally will be based on financial aspect as well. In this case, the seemingly small loss reduction gained by using the ZIP loads model may become more significant and different conclusion can be reached. Nevertheless, the approach described in this chapter can be useful in the decision making process under such situation.

Table 6.2: Comparison between the approaches of Chapters 2 and 6.

	Chapter 2	Chapter 6
Load model	Constant Power	ZIP
Stage 1 time horizon	24-hour ahead	24-hour ahead
Stage 2 time horizon	1-hour ahead	1-hour ahead
Stage 1 problem type	NLP	NLP
Stage 2 problem type	MINLP	NLP
Stage 1 solver	IPOPT	IPOPT
Stage 2 solver	BONMIN	IPOPT

Table 6.3: Computational time in seconds for $\alpha = 0.1, \beta = \gamma = 0.45$

	Strategy							
Load Model	XI	XII	XIII	XIV	XV	XVI	XVII	XVIII
Constant Power	111	108	120	109	89	82	118	141
ZIP	44	47	47	50	48	50	35	41

6.3.1.7 Computational Burden

Table 6.2 compares the approaches of Chapters 2 and this chapter in terms of several aspects. From this table, it is observed that each approach complements each other. In real situation, an expert can use any of these two approaches according to the availability of data and other considerations.

Moreover, Table 6.3 shows the computational time for strategies XI-XVIII. Maximum computational time are 50 seconds and 141 seconds for ZIP and constant-power model, respectively. Hence, both model can be solved efficiently. The computation times corresponding to ZIP model is smaller than those corresponding to constant-power model because of the difference in type of the optimization problem as indicated in Table 6.2.

Based on the above discussion, the solution method proposed in this chapter is able to solve the optimization problem corresponding to ZIP loads in relatively short time. It is also faster than the method describe in Chapter 2. Hence, the method has the potential for real life application.

Moreover, Table 6.2 shows that the time horizon of the second stage of the method proposed in this chapter is one hour. Note that the second stage can also be solved as 24-hour ahead optimization. Table 6.4 compares one-hour and 24-hour ahead optimization of stage 2 corresponding to ZIP load and strategy XV. In terms of losses, VMI, VDMI, VUI and number of switching operations, the two approaches are very close to each other. However, in terms of computation time, the one-hour ahead optimization is faster than the 24-hour optimization. Nevertheless, the computational time for both of them are all less than 2 minutes. Hence, both options are practically fast enough for real life application. Therefore, other considerations such as the availability of quality forecast would be a more decisive factor in application.

6.3.2 Comparison between constant-power loads and ZIP loads in voltage regulation with multiple topologies

This section compares voltage regulation with multiple topologies considering constant power loads with those considering ZIP loads in terms of losses, VMI, VDMI, maximum VUI, and number of switchings. The results corresponding to constant-power loads are taken from Chapter 4. The results corresponding to ZIP loads have been obtained by repeating the work in Chapter 4 by assuming that all loads are residential ZIP loads.

The voltage regulation problem in a radial unbalanced distribution system considering uncertain topology has been be stated as Problem (P4.1). It can be extended to consider ZIP loads and becomes Problem (P6.3).

$$\begin{aligned} \underset{\mathbf{c},\mathbf{d}}{\text{minimize}} \quad & J_8 \\ \text{subject to} \quad & (4.3)-(4.36), (6.5)-(6.7). \end{aligned} \tag{P6.3}$$

where $\mathbf{c}$ and $\mathbf{d}$ represent continuous and discrete variables, respectively. This subsection compares the solution of Problems (P4.1) and (P6.3).

Firstly, Table 6.5 compares the losses considering multiple topologies and constant power loads with those considering multiple topologies and ZIP loads. The losses corresponding to ZIP loads are higher than those corresponding to constant-power loads. The maximum difference is 4.2%

Table 6.4: Comparison between one-hour and 24-hour ahead optimization corresponding to Case 2 and Strategy XV.

	One-hour ahead	24-hour ahead
Load model	ZIP	ZIP
Stage 1 time horizon	24-hour ahead	24-hour ahead
Stage 2 time horizon	1-hour ahead	24-hour ahead
Stage 1 problem type	NLP	NLP
Stage 2 problem type	NLP	NLP
Stage 1 solver	IPOPT	IPOPT
Stage 2 solver	IPOPT	IPOPT
Losses (kWh)	891.72	891.73
VMI	8.81	9.12
VDMI	2.22	2.34
Max VUI (%)	0.82	0.82
Number of Switching	9	9
Computation Time (seconds)	48	70

with respect to the values corresponding to constant-power loads (Strategy XIV and topology τ_2). The mean losses corresponding to constant power and ZIP loads for each topology are also shown in the last row of Table 6.5. The differences between mean values of losses corresponding to both types of loads in percentage are 1.61%, 2.19%, 0.44% for topology τ_1, τ_2 and τ_3, respectively (calculated with respect to the values corresponding to constant power loads). In general, the ZIP loads correspond to slightly higher losses than the constant-power loads. Hence, in terms of losses, the voltage regulation considering ZIP loads is slightly worse than that corresponding to constant-power loads.

Furthermore, Fig. 6.1 shows that ZIP loads correspond to lower losses than constant-power loads. On the other hand, Table 6.5 shows reverse pattern. This difference indicate that higher losses corresponds to the cost of robustness against uncertainty in topology.

Table 6.5: Total line losses in kWh for several strategies.

	Line Losses in kWh					
	Constant-Power Load			ZIP Load		
	MT1	MT2	MT3	MT1	MT2	MT3
Strategy	τ_1	τ_2	τ_3	τ_1	τ_2	τ_3
XI	888.319	869.761	1229.62	895.438	884.435	1225.46
XII	888.309	869.844	1229.33	895.491	884.495	1225.29
XIII	888.404	869.857	1229.85	922.168	904.872	1260.27
XIV	888.342	869.864	1229.63	924.762	906.481	1265.87
XV	890.823	872.002	1234.01	895.575	883.106	1227.31
XVI	890.82	872.034	1233.82	895.506	882.927	1227.54
XVII	891.427	872.565	1235.7	901.428	887.385	1233.86
XVIII	891.42	872.602	1235.41	902.06	887.725	1234.77
Average	889.73	871.07	1232.17	904.05	890.18	1237.55

Secondly, Table 6.6 compares the values of VMI considering multiple topologies and constant-power loads with those considering multiple topologies and ZIP loads. The mean values of VMIs corresponding to constant-power loads and ZIP loads are also shown in the last row of Table 6.6. The differences between mean values of VMIs corresponding to both types of loads in percentage are 3.92%, 0.89%, 30.78% for topology τ_1, τ_2 and τ_3, respectively (calculated with respect to the

Table 6.6: Voltage Magnitude Index for Several Strategies

	VMI					
	Constant-Power Load			ZIP Load		
Strategy	τ_1	τ_2	τ_3	τ_1	τ_2	τ_3
XI	7.87	7.56	7.19	9.15	8.40	10.87
XII	7.93	7.61	7.24	9.13	8.39	10.83
XIII	7.84	7.54	7.16	8.81	8.27	10.11
XIV	7.84	7.55	7.16	8.81	8.25	10.16
XV	7.94	7.72	7.23	7.73	7.29	8.76
XVI	7.64	7.44	6.93	7.62	7.16	8.64
XVII	7.82	7.61	7.11	6.81	6.61	7.45
XVIII	7.39	7.19	6.70	6.66	6.41	7.35
Average	7.78	7.53	7.09	8.09	7.60	9.27

values corresponding to constant-power loads). Hence, the constant-power loads correspond to lower values of VMI than the ZIP loads. Consequently, in terms of VMI, voltage regulation with multiple topologies corresponding to ZIP loads is worse than those corresponding to constant-power loads.

Furthermore, Fig. 6.2 shows that ZIP loads correspond to lower values of VMIs than constant-power loads. On the other hand, Table 6.6 shows a contradicting pattern. This again indicates another price of robustness against uncertainty of topology.

Thirdly, Table 6.7 compares the values of VDMIs obtained by considering multiple topologies and constant power loads with those considering multiple topologies and ZIP loads. The mean value of VMIs corresponding to constant-power loads and ZIP loads are also shown in the last row of Table 6.7. On average, the ZIP loads correspond to lower values of VDMIs than the constant-power loads. This means than the voltage profile corresponding to ZIP loads is generally more flat than that corresponding to constant-power loads. The differences between mean values of VDMIs

Table 6.7: VDMI for Several Strategies

	VDMI					
	Constant-Power Load			ZIP Load		
Strategy	τ_1	τ_2	τ_3	τ_1	τ_2	τ_3
XI	2.28	2.48	2.57	2.24	2.43	2.53
XII	2.28	2.47	2.56	2.24	2.44	2.53
XIII	2.28	2.47	2.57	1.95	2.14	2.24
XIV	2.28	2.47	2.57	1.92	2.11	2.21
XV	2.28	2.47	2.57	2.35	2.55	2.64
XVI	2.29	2.48	2.58	2.35	2.55	2.64
XVII	2.28	2.48	2.58	2.28	2.47	2.57
XVIII	2.28	2.47	2.57	2.26	2.46	2.55
Average	2.28	2.47	2.57	2.20	2.39	2.49

corresponding to both types of loads in percentage are -3.58%, -3.25%, -3.19% for topology τ_1, τ_2 and τ_3, respectively (calculated with respect to the values corresponding to constant power loads). However, those differences are arguably small. Hence, in term of VDMI, the voltage regulation corresponding to ZIP loads is slightly better than that corresponding to constant-power loads.

Furthermore, both Fig. 6.3 and Table 6.7 agree that ZIP loads correspond to lower values of VDMI than the constant-power loads. This situation is unlike that corresponding to losses and VMI.

Fourthly, Table 6.8 shows the values of maximum values of VUI considering multiple topologies for both constant-power and ZIP loads. The mean value of those quantities are also shown in the last row of the same table. The differences between mean values of maximum of VUIs corresponding to both types of loads in percentage are -4.54%, 3.46%, -3.92 % for topology τ_1, τ_2 and τ_3, respectively (calculated with respect to the values corresponding to constant power loads). On average, the ZIP loads are better than constant-power loads for topologies τ_1 and τ_3 and vice

Table 6.8: Maximum Voltage Unbalance Index

	Maximum VUI (%)					
	Constant-Power Load			ZIP Load		
Strategy	τ_1	τ_2	τ_3	τ_1	τ_2	τ_3
XI	0.71	0.68	1.36	0.69	0.76	1.28
XII	0.71	0.68	1.36	0.70	0.82	1.28
XIII	0.9	0.78	1.56	0.81	0.82	1.35
XIV	0.89	0.78	1.55	0.81	0.82	1.35
XV	0.86	0.87	1.34	0.84	0.85	1.41
XVI	0.85	0.87	1.33	0.84	0.86	1.41
XVII	0.89	0.88	1.41	0.85	0.85	1.40
XVIII	0.87	0.87	1.38	0.84	0.85	1.36
Average	0.84	0.80	1.41	0.80	0.83	1.36

versa for topology τ_2. This pattern differs from the patterns correspond to loss, VMI and VDMI. However, these values are rather close to each other. Hence, the voltage regulation problem corresponding to ZIP loads loads is slightly better than that corresponding to constant-power loads in case of topology τ_1 and τ_3 and vice versa for topology τ_2.

Furthermore, Fig. 6.4 shows that the ZIP loads correspond to higher values of maximum VUIs than the constant-power loads. A similar similar trend is valid only with those corresponding to topology τ_2. In case of topologies τ_1 and τ_3, on average, ZIP loads correspond to lower maximum VUIs than constant-power loads.

Finally, Table 6.9 shows the number of switching operations corresponding to voltage regulation with multiple topologies considering constant-power loads and ZIP loads for different strategies and topologies. The maximum number of switchings corresponding to constant-power loads and ZIP loads are 19 and 34, respectively. Thus, in all cases, total number of switching operations is acceptable. Moreover, the average number of switching operations corresponding to constant-

power loads and ZIP loads are 14.75 and 29.00, respectively. Hence, in term of number of switching operations, the voltage regulation with multiple topologies and ZIP loads is worse than the voltage regulation with multiple topologies and constant-power loads.

Overall, on average, the multiple-topology approach with ZIP loads is better than that corresponding to constant-power loads in terms of VDMI and maximum VUI and vice versa in terms of losses, VMI and number of switching operations. Moreover, in terms of losses, VDMI, VUI, and majority of VMI (topologies τ_1 and τ_2), these two alternatives are very close to each other. On the other hand, in terms of number of switching operations and some of VMIs (topology τ_3), they differ from each other significantly. These observations indicate that the difference in solution corresponding to different load models can be significant.

6.3.3 Comparison between constant-power and ZIP loads when OLTCs operate in LDC mode

It is also interesting to compare the performance of OLTCs operating in LDC mode of control when loads are modeled as ZIP loads. It is to be noted that in Chapter 5 all loads are constant-power loads. In this subsection, the solution corresponding to LDC mode of operation with constant-power loads will be compared with LDC mode of operation with ZIP loads in terms of losses, VMI, VDMI, VUI and number of switching operations.

Firstly, Fig. 6.6 compares total line losses for different strategies corresponding to LDC with constant-power (CP) loads and ZIP loads. The losses corresponding to ZIP loads are higher than those corresponding to constant-power loads. However, the maximum (minimum) difference in term of losses between these two modes is 19.5 (12.1) kWh. Consequently, these differences are arguably small. Hence, in terms of line losses, the LDC with ZIP loads is slightly worse than the constant-power loads. Table 6.5 also shows similar pattern while Fig. 6.1 shows the reverse pattern.

In order to understand the situation better, one needs to consider the magnitude of voltage at which the real power and reactive power of a ZIP load are at their minima. It can be shown that the magnitude of voltage corresponding to minimum real power loads, $\mathcal{E}^{ipt}_{min,p}$, can be calculated using the following equation

$$\frac{\partial P^{ipt}_{L}}{\partial \mathcal{E}^{ipt}} = P^{ipt}_{L0}\left(2K^{i,p}_{pz}(\mathcal{E}^{ipt}_{min,p}) + K^{i,p}_{pi}\right) = 0. \tag{6.8}$$

Table 6.9: Total number of switchings

	Total Number of switching	
	Constant-Power Load	ZIP load
	MT1 / MT2 / MT3	MT1 / MT2 / MT3
Strategy	τ_1/τ_2/ τ_3	τ_1/τ_2/ τ_3
XI	16	26
XII	15	27
XIII	16	26
XIV	16	26
XV	13	31
XVI	19	28
XVII	7	34
XVIII	16	34
Average	14.75	29.00

Using the values of coefficients of residential loads given in Table 6.1,

$$\mathcal{E}^{ipt}_{min,p} = -\frac{K^{i,p}_{pi}}{2K^{i,p}_{pz}} = -\frac{-1.12}{2 \times 0.85} = 0.654 \text{ p.u.} < 0.95 \text{ p.u.} \tag{6.9}$$

Similarly, it can be shown that the magnitude of voltage corresponding to minimum reactive power loads, $\mathcal{E}^{ipt}_{min,q}$, can be calculated as follows (also using the values corresponding to residential loads given in Table 6.1)

$$\mathcal{E}^{ipt}_{min,q} = -\frac{K^{i,p}_{qi}}{2K^{i,p}_{qz}} = -\frac{-18.73}{2 \times 10.96} = 0.854 \text{ p.u.} < 0.95 \text{ p.u.} \tag{6.10}$$

Note that both $\mathcal{E}^{ipt}_{min,p}$ and $\mathcal{E}^{ipt}_{min,q}$ are lower than 0.95 p.u. Hence in order to minimize the loads, the magnitudes of all voltages must be as close as possible to 0.95 p.u. since all loads are assumed

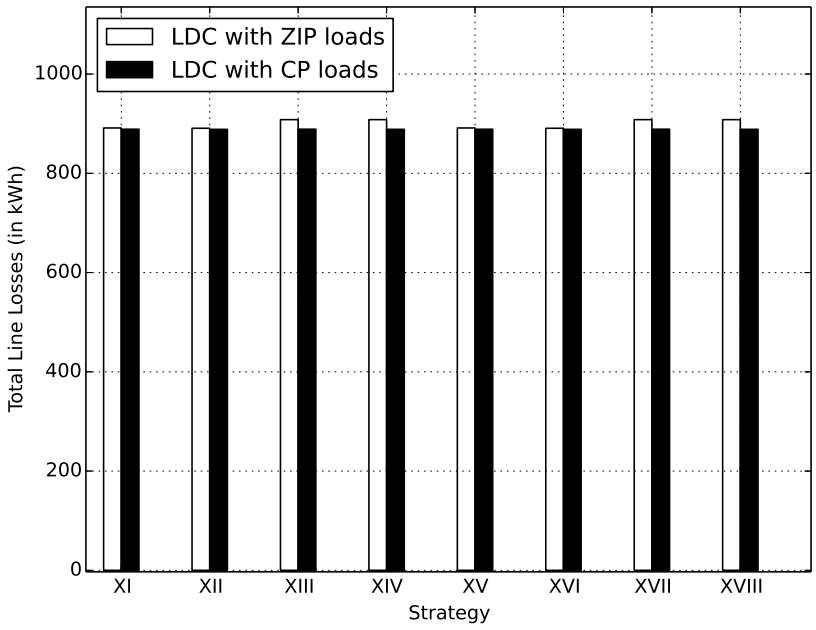

Figure 6.6: Comparison of losses corresponding to ZIP and CP loads considering LDC.

to be residential ZIP loads. In LDC mode, this can be achieved by lowering the reference voltage setting $|\bar{E}_o^{ref}|$.

However, in the modified IEEE 123 bus system under study, only R2-R4 can accomplish this. OLTC R1 which is located at the substation are forced to operate at high reference voltage so that other OLTCs (R2-R4) can have lower reference voltage. Hence, all loads which are served by OLTCs R2 - R4 operate at magnitudes of voltage which are close 0.95 p.u. On the other hand, all loads which are served by R1 (i.e. located between R1 and other OLTCs) operate at magnitudes of voltages which are close to 1.05 p.u.

Table 6.10 shows optimal settings of LDC for all OLTCs corresponding to constant-power and ZIP loads using strategy XV. For example, the reference voltage of OLTC R4 is $115.2\,\text{V} = 115.2/120 = 0.96$ p.u. This means all loads below R4 operate at magnitudes of voltages which are close to 0.95. Furthermore, note that reference voltage of R1 is $125\,\text{V} = 1.042$ p.u. This means that all loads between OLTC R1 and R2-R4 operate at magnitudes of voltages which are close to 1.05 pu. As a result, the effective loads are much more as compared to their corresponding

Table 6.10: Optimal Settings of LDC of OLTCs using strategy XV

OLTC	Phase	Constant Power				ZIP			
		R_o^{set}	X_o^{set}	$\lvert\bar{E}_o^{ref}\rvert$	db_o	R_o^{set}	X_o^{set}	$\lvert\bar{E}_o^{ref}\rvert$	db_o
		(Volts)				(Volts)			
R1	a	1.3	-0.4	125	5.8	1.3	-0.4	125	5.8
	b	1.3	-0.4	125	5.8	1.3	-0.4	125	5.8
	c	1.3	-0.4	125	5.8	1.3	-0.4	125	5.8
R2	a	-1.8	-0.2	125	5.8	-1.5	-0.2	115.2	5.8
R3	a	-4.1	-0.4	124.6	5.8	-2.3	-0.3	115.3	5.8
	c	-4.1	-0.4	124.6	5.8	-4.1	-0.3	115.5	5.8
R4	a	-1.6	0	125.3	5.8	1.3	0.4	115.2	5.8
	b	-1.6	0	125.3	5.8	1.3	0.4	115.2	5.8
	c	-1.6	0	125.3	5.8	1.3	0.4	115.2	5.8

minimum values. This is one of the possible reasons that losses corresponding to ZIP loads are higher than those corresponding to constant-power loads.

On the other hand, in case of constant-power loads, the higher the magnitudes of voltages are, the lower the line losses are. Hence, all of the reference voltages are closer to 1.05 p.u. as shown in Table 6.10. Therefore, all loads draw lower current. Consequently, line losses are also lower. This is another explanation that losses corresponding to ZIP loads are higher than those corresponding to constant-power loads.

Secondly, Fig. 6.7 compares the values of VMI corresponding to LDC with ZIP loads and constant-power loads. The values of VMI corresponding to ZIP loads are higher than those corresponding to constant-power loads. Hence, in terms of VMI, the LDC with constant power loads is better than the LDC with ZIP loads. In case of constant-power loads, the magnitudes of voltages are close to their upper limits. These buses contribute to VMI more during light loading situation than during heavy loading situation. In case of ZIP loads, the magnitudes of voltages at buses served by OLTC R1 are close to their upper limits. At buses served by OLTCs R2-R4, the magnitudes of voltages are close to their lower limits. During light loading condition, the magnitudes

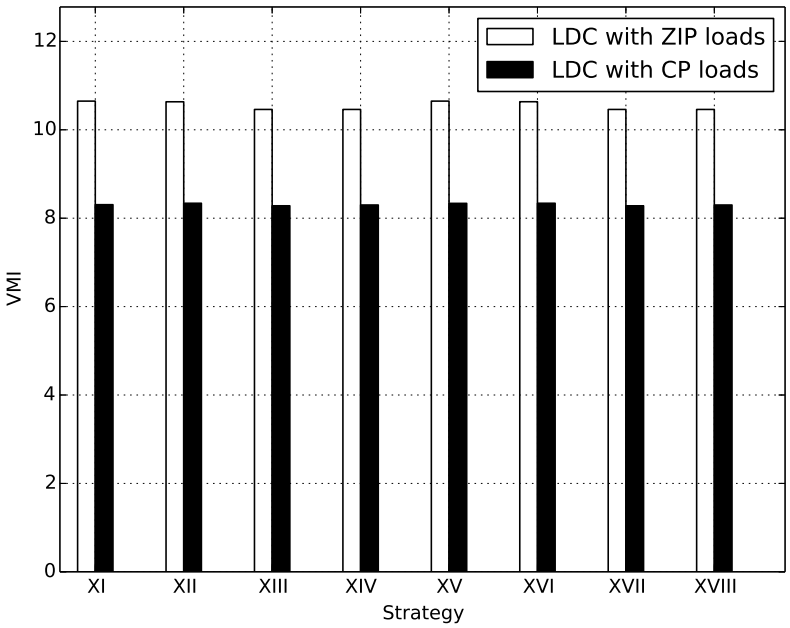

Figure 6.7: Comparison of VMI corresponding to ZIP and CP loads considering LDC.

of voltages at buses served by R1 contribute more to VMI than those served by R2-R4. During heavy loading condition, the magnitudes of voltages at buses served by R2-R4 contribute more to VMI than those served by R1. Hence, in both conditions, there are significant number of buses whose magnitudes of voltages are far from their rated values. Consequently, ZIP loads correspond to higher VMI than constant-power loads.

Thirdly, Fig. 6.8 compares the values of VDMI corresponding to ZIP loads and those corresponding to constant-power loads. The values of VDMI corresponding to ZIP loads are higher (lower) than those corresponding to constant-power loads for strategies XI, XII, XV and XVI (XII, XIV, XVII and XVIII). Note that strategies XI, XII, XV, and XVI correspond to non-uniform operation of SVC while strategies XIII, XIV, XVII and XVIII correspond to uniform operation of SVC. This means that the values of VDMI depend on operation of SVC. However, in case of constant-power loads, Fig. 6.8 shows that the values of VDMI are very close to each other among all strategies. However, in case of ZIP loads, the values of VDMI depend on the operating strategy. This issue is discussed in the following paragraph.

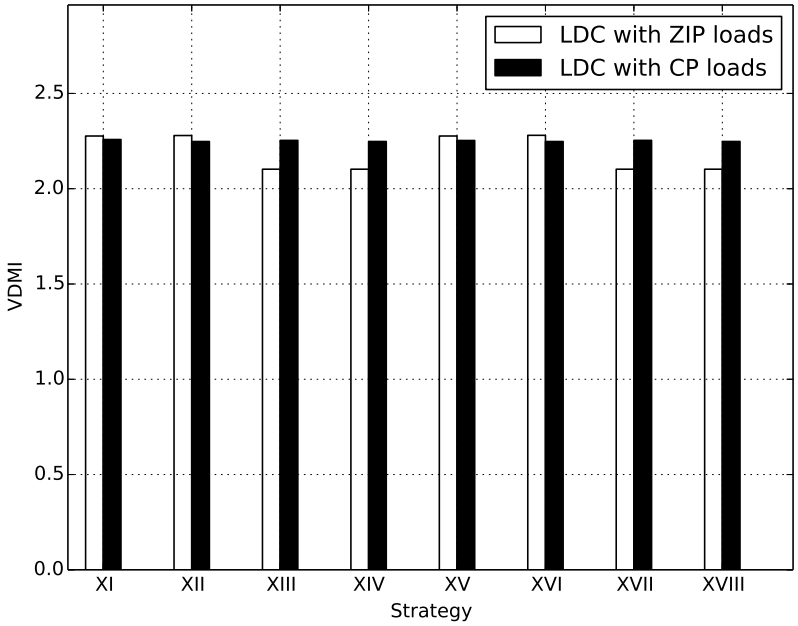

Figure 6.8: Comparison of VDMI corresponding to ZIP and CP loads considering LDC.

When the SVC operates non-uniformly, the ZIP loads correspond to higher VDMIs than constant-power loads. When the SVC operates uniformly, the ZIP loads correspond to lower VDMI than the constant-power loads. It is generally accepted that OLTCs alone can not flatten the voltage profile of a distribution network. Reactive power compensation may also be required in some part of a network. In the modified IEEE 123 bus system, this part is located around buses bus 73 , 100, 102, 103 and 63 in Fig. 2.3 where SCs and SVC are installed.

In case of ZIP loads, discrete compensation provided by those SCs can cause large change in reactive power flow. As shown in Table 6.1, the ZIP coefficients of reactive power are significantly higher than those of real power. This means that reactive power of those loads are much more sensitive to voltage variation than real power of those loads. The step size of the shunt capacitor may be large enough to introduce significant change in the magnitudes of the voltages at and nearby buses where the capacitor is located. In this situation, the smooth output of an SVC becomes important.

When the SVC operates uniformly, the voltages are more balanced than when it operates non-

uniformly. A balanced situation generally corresponds to lower losses and flatter voltage profile than an unbalanced situation. Fig. 6.8 supports this conclusion by showing that the values of VDMI of ZIP loads are lower than those of constant power loads corresponding to strategies XIII, XIV, XVII and XVIII. On the other hand, if the SVC operates non-uniformly then the voltages are less balanced as compared to the case when the SVC operates uniformly. The non-uniform operation correspond to higher values of VDMIs than the uniform operation. Fig. 6.8 shows this situation in values of VDMI corresponding to strategies XI, XII, XV and XVI. Hence, in terms of VDMI, ZIP loads are better than constant-power loads for one half of all strategies and vice versa for another half of all strategies.

Fourthly, Fig. 6.9 compares the values of VUI corresponding to ZIP and constant-power loads. The values of maximum VUIs corresponding to ZIP loads are higher than those corresponding to constant-power loads. Hence, in terms of VUI, the LDC with constant-power loads is better than the LDC with ZIP loads.

The following reasoning can be followed to explain the results of Fig. 6.9. As discussed previously, in case of ZIP loads, the magnitudes of voltages at the buses which are served by OLTC R1 are close to their upper limits. This means that ZIP loads connected to those buses draw high current. The higher the load currents of loads are, the larger the voltage drops of lines are, then the higher unbalance of voltages is.

Finally, Fig. 6.10 compares the total number of switching operations corresponding to LDC with ZIP loads and constant-power loads. The number of switching operations corresponding to ZIP loads are higher than those corresponding to constant-power loads. Hence, in terms of number of switchings, the LDC with ZIP loads is worse than the LDC with constant-power loads.

In case of constant-power loads, the reference voltages of OLTCs are close to their upper limits. Hence, there is a high risk of overvoltage when loads are light. When loads are heavy, there is much lower risk of undervoltage due to the value of the reference voltages. Hence, the switching operations mostly happen during light loading condition.

On the other hand, in case of ZIP loads, Table 6.10 shows that the reference voltage of substation OLTC R1 is close to its upper limit while reference voltages of feeder OLTCs (R2-R4) are close to their lower limits. When loads are light, there is high risk of overvoltage at buses corresponds to R1. When loads are heavy, there is high risk of undervoltage at buses corresponds to

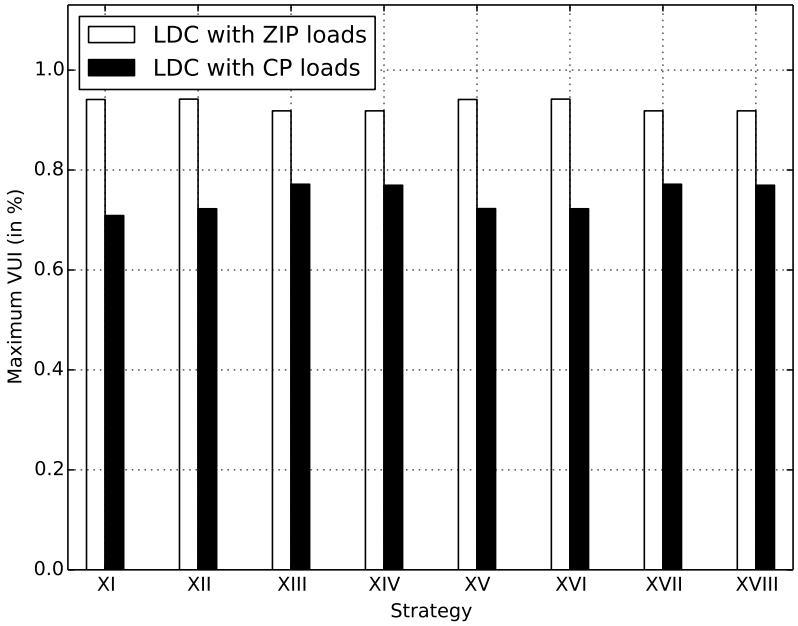

Figure 6.9: Comparison of VUI corresponding to ZIP and CP loads considering LDC.

R2-R4. Hence, in case of ZIP loads, switching operations may be required in both the situations. Consequently, ZIP loads correspond to higher number of switching operations as compared to the constant-power loads.

Overall, based on the above discussions, the LDC with ZIP loads is worse than LDC with constant-power loads in terms of losses, VMI, VUI and number of switching operations. In addition, there is no clear winner in terms of VDMI.

Moreover, selection of the best strategy is not trivial. Table 6.11 lists the best strategies based on losses, VMI, VDMI, maximum VUI and number of switchings, respectively, corresponding to LDC with ZIP loads and the LDC with constant-power loads. It is shown that each alternative is different from the other one in each of the indicators. Hence, voltage dependency of the loads is very important in selection of best strategy in case the OLTCs operate in LDC mode.

6.3.3.1 Time-of-the-day versus LDC mode

It is also interesting to compare the performance of OLTCs operating in time-of-the-day and LDC mode of control when loads are modelled as ZIP loads. It is to be noted that in Chapter 5 all loads

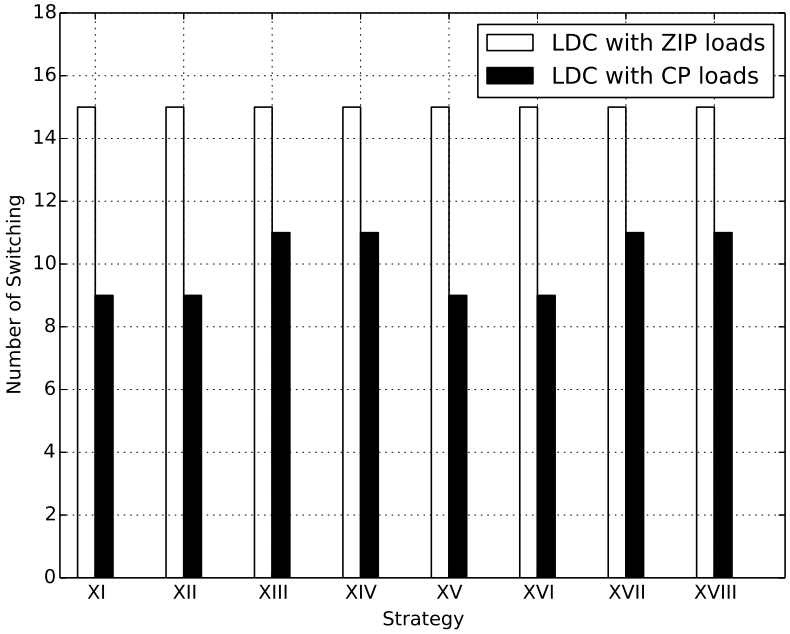

Figure 6.10: Comparison of number of switchings corresponding to ZIP and CP loads considering LDC.

are constant-power loads. The voltage regulation problem considering OLTCs operating in LDC mode and ZIP loads can be posed as the following optimization problem:

$$\begin{aligned} &\underset{\mathbf{c},\mathbf{d}}{\text{minimize}} \quad J \\ &\text{subject to} \quad (2.2)-(2.6), (2.12)-(2.36), (5.6)-(5.13), (6.5)-(6.7). \end{aligned} \tag{P6.4}$$

Table 6.12 compares both the modes when strategy XV is implemented. In terms of losses, the time-of-the-day mode is worse than the LDC mode. However, in terms of VMIs and VDMIs, VUIs and number of switching operations, the time-of-the-day mode is better than the LDC mode. Furthermore, the computational time corresponding to both these modes are less than two minutes which is quite fast. Thus, the solution method proposed here is also capable of solving the optimization problem considering both ZIP loads and OLTCs with line drop compensation.

Moreover, Fig. 6.11 shows voltage profiles of the system when strategy XV is used and OLTCs operate in LDC mode for hours 6, 12 and 20. It can be seen that all magnitudes of voltages are within limit and that those profiles are quite flat. Hence the method is still effective when voltage

Table 6.11: The best strategy per performance indicator correspondting to LDC with ZIP loads and constant-power loads.

	Best Strategy	
	ZIP	Constant Power
Loss	XII and XVI	XII and XVI
VMI	XIII, XVI, XVII and XVIII	XVII
VDMI	XIII, XVI, XVII and XVIII	XII and XVI
VUI	XI and XV	XI
Number of switching	XI - XVIII	XI, XII, XV and XVI
Overall		

dependent load are considered.

6.4 Conclusion

This chapter considers voltage-dependent loads. It also compares the results obtained by using ZIP loads with those obtained by using constant-power loads. Each of these two cases corresponds to different optimal solution. The results obtained by using ZIP loads are better (worse) than those obtained by using constant-power loads in terms of losses, VMIs and VDMIs (VUIs and number of switchings)

Furthermore, the comparison is repeated in case of voltage regulation considering topology uncertainty. The results obtained by using ZIP loads are better (worse) than those obtained by using constant-power loads in terms VDMI and VUI (losses, VMI and number of switchings).

Moreover, comparison of the results obtained by using the two load models in a network where OLTC operate in LDC mode also has been carried out. The results obtained by using ZIP loads are worse than those obtained by using constant power loads in terms of loss, VMI, VUI and number of switchings. In terms of VDMIs, the results obtained by using ZIP loads are better in 4 strategies but worse in other strategies than those obtained by using constant-power loads.

In general, the use of each load model corresponds to different optimal solution. Therefore, when the required data are available, it is important to consider voltage dependency of loads in daily operation of distribution systems. From computational point of few, the optimization studies

Table 6.12: Comparison between time-of-the-day mode and LDC mode of OLTCs considering ZIP loads corresponding to Strategy XV.

	time-of-the-day mode	LDC Mode
Load model	ZIP	ZIP
Optimization problem	(P6.0)	(P6.4)
Stage 1 time horizon	24-hour ahead	24-hour ahead
Stage 2 time horizon	1-hour ahead	24-hour ahead
Stage 1 problem type	NLP	NLP
Stage 2 problem type	NLP	NLP
Stage 1 solver	IPOPT	IPOPT
Stage 2 solver	IPOPT	IPOPT
Losses (kWh)	891.72	891.38
VMI	8.81	10.65
VDMI	2.22	2.28
Max VUI (%)	0.82	0.94
Number of Switching	9	15
Computation Time (seconds)	48	89

can be solved in few minutes. Hence the proposed method can be considered quite efficient.

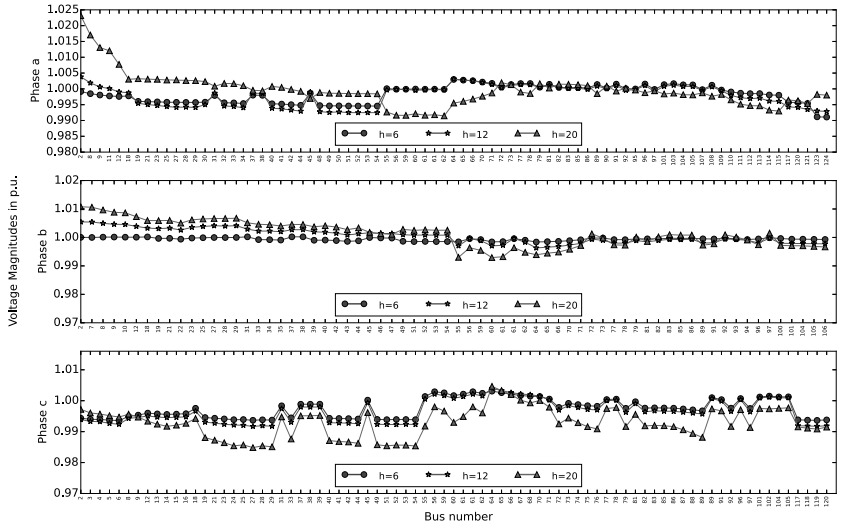

Figure 6.11: Voltage Magnitudes at different phases corresponding to LDC operation and voltage dependent loads at hours 6, 12 and 20.

7 — Conclusion

'Would you tell me, please, which way I ought to go from here?'
'That depends a good deal on where you want to get to,' said the Cat.
'I don't much care where -' said Alice.
'Then it doesn't matter which way you go,' said the Cat.
'- so long as I get SOMEWHERE,' Alice added as an explanation.
'Oh, you're sure to do that,' said the Cat, 'if you only walk long enough.
- Lewis Carroll, *Alice in Wonderland*

7.1 General

The operator of a distribution network is responsible in maintaining the magnitudes of all voltages within a certain limits. This task is called voltage regulation. As both of the loads and penetration of distributed generation are expected to continuously increase in the future, the voltage fluctuation caused by them will become more intensive. Therefore, the voltage regulation problem will be more difficult and, hence, important in the future.

This chapter highlights the major findings in the works included in this thesis and suggests a number of possible future works in the area of voltage regulation in distribution systems.

7.2 Summary of Significant Findings

The important contributions in the area of voltage regulation in distribution system with the presence of distributed generation can be summarized as follows:

A current-voltage based optimization model using Cartesian coordinate has been developed to include a static var compensator operating in voltage control mode using droop control into the voltage regulation problem in unbalanced radial distribution system. The voltage regulation problem is posed as a constrained multi-objective optimization problem considering OLTC, SC, SVC as voltage controllers. The objective functions include minimization of power loss in the system and the number of switching operations of OLTC, SC and SVC. The equality constraints involve the nodal current balance equations and the relations between currents and voltages of all elements in the network. The inequality constraints include regulatory and physical limits of the network and its elements. The physical limits involve the operational limits of OLTC, SC, and

SVC. The regulatory limits consider the limits on voltage magnitude and the amount of unbalance in the system. There are both discrete and continuous variables. Hence the problem is a mixed integer nonlinear programming (MINLP). However, solving the problem is computationally very expensive due to a very large discrete search space.

Therefore, a two-stage solution methodology has been developed to solve the above MINLP. The first stage reduces the discrete search space into a binary search space. The second stage solves the binary MINLP problem as a one-hour-ahead optimization. The effectiveness of the developed method has been investigated on a modified IEEE 123 bus unbalanced radial distribution system. The system has OLTCs, SCs, an SVC and many PV generations. Comparing the proposed method with a branch-and-bound method, the following conclusions have been drawn:

- the proposed method is computationally efficient in comparison with the branch-and-bound method.
- the proposed method can be used to optimally coordinate the operation of OLTC, SC and SVC in an unbalance radial distribution system.

For considering the uncertainty of load and generation, a robust-optimization-based voltage regulation problem has been formulated and its continuous reformulation based on complementarity condition has been proposed. Robust optimization approach follows worst-case-scenario philosophy and tries to find a robust solution. For a given sets of intervals of possible values of loads and generations, a solution is robust if the system remains feasible for any values of loads and generations within those intervals. Since there are infinitely many possible values of load and generation, considering all possibilities render the optimization problem intractable. Based on the monotonicity of relation between the magnitudes of voltages and power flows in a distribution network, this thesis conjectures that it is sufficient to consider only finite numbers of extreme cases to find the robust solution. In order to verify the conjecture, Monte Carlo simulation study has been carried out and it has been found out that the discrepancies between the results of robust optimization and Monte Carlo simulations are small. Hence, the solution is robust for all practical purposes. Since the robust voltage regulation problem is several times bigger than deterministic (non-robust) problem, the second stage of the two-stage method previously discussed was not able to solve the problem. Therefore, in the second stage, continuous reformulation has been utilized. Hence, both

of the stages are now nonlinear programming problems which can be solved in few minutes. Comparing the robust optimization and deterministic optimization, the following conclusion have been drawn:

- The monotonicity behaviour of the magnitudes of the voltages against the variation of line power flows can be used in identification of extreme scenarios. These extreme scenarios further can be used to find a robust solution of the voltage regulation problem in an unbalance radial system.

- The continuous reformulation of the second stage of the previous two-stage approach allows one to solve the robust voltage regulation problem in few minutes.

Furthermore, due to some possible benefits, topological change in in future distribution system may be more frequent. While topology optimization and voltage regulation can be integrated, this thesis assumes that they are independent from each other. Hence, the topology of a network become uncertain from the point of view of voltage regulation. If all loads must be served, there are finite number of credible topologies of a network. Hence, it may be possible to consider all of them at once and to formulate robust voltage regulation problem against uncertainty in topology. To verify its efficacy, the proposed method is implemented in a modified IEEE 123 bus system. The following conclusion can be drawn:

- Due to the radiality of the network, the number of topologies which can serve all loads are relatively smaller than meshed networks.

- For solving the problem, the exact relaxation function has been applied to voltage magnitude and unbalance constraints as well as the complementarity constraint.

In addition, most of the works in voltage regulation in the available literature assume that OLTCs operate in time-of-the-day mode. In this mode, the positions of the taps of an OLTC at each hour for a 24-hour ahead is optimized and, then, are sent to the controller of the OLTC. The controller of the OLTC will ensure that the positions of the taps are as scheduled. When the actual loading condition differs from the forecasted one, there is a possibility of violations as well as suboptimal operation of the network. On the other hand, an OLTC can also operate in the LDC mode. In this mode, the position of a tap of an OLTC is controlled based on the local measurements

of current and voltage and the settings of the LDC. This thesis proposes a model of the LDC of an OLTC which can be integrated into the previously available optimization formulation. Comparing the time-of-the-day and LDC modes, the following conclusion can be drawn:

- The proposed method enables optimal coordination of an OLTC operating in LDC mode with other controllers.
- The previous methods proposed in this thesis could not solve the corresponding optimization. In order to solve the problem, the exact relaxation method has been applied to all constraints.
- the strength of the LDC mode relies on its adaptability and less requirements in communication network.
- The LDC mode, however, has more losses and number of switching than the time-of-the-day mode.

Due to its simplicity or the lack of data, many works in the literature assume that all loads are constant-power loads. This thesis also has assumed the same in chapters considering SVC, uncertainty in loads, generation and topology, as well as the LDC mode. As significant part of loads, such as commercial and residential loads, are voltage dependent, this thesis also consider this dependency, this thesis compares the results corresponding to constant-power loads and ZIP loads considering the SVC, topological uncertainty and LDC operation. The comparison corresponding to uncertainty in loads and generation is not done due to difficulty in determining the interval of uncertainty of the voltage-dependent loads. From those comparisons, the following conclusions can be drawn:

- In general, the use of each load model corresponds to different optimal solution.
- The method with full exact function relaxation was able to solve the optimizations problems considering voltage-dependent loads.

7.3 Further Works

1. As the penetration of photo voltaic generators in distribution networks is increasing, it may be useful to install an SVC as a voltage regulation device in distribution system. The model

of SVC proposed in Chapter 2 may be used to determine the location and rating of SVC in distribution system.

2. It is predicted that the number of electric vehicles connected to the distribution network will be significant in the future. Therefore, voltage regulation considering the presence of electric vehicle can be explored.

3. In this thesis, SCs are always controlled centrally using time-of-the-day mode. However, there are other modes of operation of SCs, such as voltage-control mode, temperature-control VAR-control modes, which have not been modelled as a part of optimal power flow.

4. This thesis assumes that the voltage at the substation remains constant for the whole period of optimization. However, there are situations in which this assumption is not valid. Hence, the voltage regulation considering variation of voltages in transmission system should also be investigated.

5. In future smart grid, the application of demand response management will be more popular. This will certainly effect the voltage regulation of distribution networks. Combined voltage regulation and demand response should be also investigated further.

Publications from the research work

1. N. Daratha, B. Das, J. Sharma, ”Coordination Between OLTC and SVC for Voltage Regulation in Unbalanced Distribution System Distributed Generation,” IEEE Transactions on Power Systems, vol.29, no.1, pp.289-299, Jan. 2014.

2. N. Daratha, B. Das, J. Sharma, ”Robust voltage regulation in unbalanced radial distribution system under uncertainty of distributed generation and loads”, International Journal of Electrical Power & Energy Systems, vol. 73, Pages 516-527, Dec. 2015

Bibliography

[1] CENELEC, "Voltage characteristics of electricity supplied by public distribution networks," *European Standard EN 50160*, 1999.

[2] American National Standard Institute, "American national standard voltage ratings (60hz) for electric power systems and equipment,," *ANSI Std. C84.1*, 1989.

[3] R. Dugan, S. Santoso, M. McGranaghan, and H. Beaty, *Electrical power systems quality*, ser. McGraw-Hill professional engineering. McGraw-Hill, 2003.

[4] H. Markiewicz and A. Kaljn, *Power Quality Application Guide: 5.4.2. Voltage Disturbances*. Leonardo Power Quality Initiative, July 2004.

[5] D. D. V. Horn, "Mathematical and physical bases for incandescent lamp exponents," *Illuminating Engineering*, pp. 196–202, Apr. 1965.

[6] S. Djokic, J. Desmet, G. Vanalme, J. Milanovic, and K. Stockman, "Sensitivity of personal computers to voltage sags and short interruptions," *IEEE Transactions on Power Delivery*, vol. 20, no. 1, pp. 375–383, Jan 2005.

[7] J. R. Linders, "Effects of power supply variations on ac motor characteristics," *IEEE Transactions on Industry Applications*, vol. IA-8, no. 4, pp. 383–400, July 1972.

[8] H. C. Forbes and H. R. SEARING, "Voltage regulation and load control," *Transactions of the American Institute of Electrical Engineers*, vol. 53, no. 6, pp. 903–909, June 1934.

[9] W. Kidd and J. Carr, "The application of automatic voltage and switch control to electrical distribution systems," *Journal of the Institution of Electrical Engineers*, vol. 74, no. 448, pp. 285–297, Apr. 1934.

[10] R. Grondin, "Computer-dedicated voltage regulation method for distribution substations," *IEEE Transactions on Power Apparatus and Systems*, vol. PAS-100, no. 5, pp. 2184–2188, May 1981.

[11] D. Bassett, "Control of tap change under load transformers through the use of programmable logic controllers," *IEEE Transactions on Power Delivery*, vol. 8, no. 4, pp. 1759–1765, Oct 1993.

[12] B. Kasztenny, E. Rosolowski, J. Izykowski, M. Saha, and B. Hillstrom, "Fuzzy logic controller for on-load transformer tap changer," *IEEE Transactions on Power Delivery*, vol. 13, no. 1, pp. 164–170, Jan 1998.

[13] F. M. Starr, "Operation of load-ratio control transformers connected in parallel and in networks," *Electrical Engineering*, vol. 60, no. 12, pp. 1274–1280, Dec 1941.

[14] H. L. Prescott, "Line-drop compensation on single-phase regulators," *Electrical Engineering*, vol. 70, no. 11, pp. 983–983, Nov 1951.

[15] D. M. Lauria, "Conservation voltage reduction (CVR) at northeast utilities," *IEEE Transactions on Power Delivery*, vol. 2, no. 4, pp. 1186–1191, Oct 1987.

[16] N. Yorino, M. Danyoshi, and M. Kitagawa, "Interaction among multiple controls in tap change under load transformers," *IEEE Transactions on Power Systems*, vol. 12, no. 1, pp. 430–436, Feb 1997.

[17] M. Larsson, "Coordination of cascaded tap changers using a fuzzy-rule-based controller," *Fuzzy Sets and Systems*, vol. 102, no. 1, pp. 113 – 123, Feb. 1999.

[18] F.-C. Lu and Y.-Y. Hsu, "Reactive power/voltage control in a distribution substation using dynamic programming," *IEE Proceedings - Generation, Transmission and Distribution*, vol. 142, no. 6, pp. 639–645, Nov 1995.

[19] M. Liu, C. Canizares, and W. Huang, "Reactive power and voltage control in distribution systems with limited switching operations," *IEEE Transactions on Power Systems*, vol. 24, no. 2, pp. 889 –899, May 2009.

[20] S. Paudyal, C. Canizares, and K. Bhattacharya, "Optimal operation of distribution feeders in smart grids," *IEEE Transactions on Industrial Electronics*, vol. 58, no. 10, pp. 4495 –4503, Oct. 2011.

[21] S. Bruno, S. Lamonaca, G. Rotondo, U. Stecchi, and M. La Scala, "Unbalanced three-phase optimal power flow for smart grids," *IEEE Transactions on Industrial Electronics*, vol. 58, no. 10, pp. 4504 –4513, Oct. 2011.

[22] F.-C. Lu and Y.-Y. Hsu, "Fuzzy dynamic programming approach to reactive power/voltage control in a distribution substation," *IEEE Transactions on Power Systems*, vol. 12, no. 2, pp. 681–688, May 1997.

[23] B. de Souza and A. de Almeida, "Multiobjective optimization and fuzzy logic applied to planning of the volt/var problem in distributions systems," *IEEE Transactions on Power Systems*, vol. 25, no. 3, pp. 1274–1281, Aug 2010.

[24] D. Spatti, I. da Silva, W. Usida, and R. Flauzino, "Real-time voltage regulation in power distribution system using fuzzy control," *IEEE Transactions on Power Delivery*, vol. 25, no. 2, pp. 1112 –1123, Apr. 2010.

[25] G. Viswanadha Raju and P. R. Bijwe, "Reactive power/voltage control in distribution systems under uncertain environment," *IET Generation, Transmission Distribution*, vol. 2, no. 5, pp. 752–763, Sept. 2008.

[26] M. Baran and M.-Y. Hsu, "Volt/var control at distribution substations," *IEEE Transactions on Power Systems*, vol. 14, no. 1, pp. 312–318, Feb 1999.

[27] M. Abdel-Rahman, F. Youssef, and A. Saber, "New static var compensator control strategy and coordination with under-load tap changer," *IEEE Transactions on Power Delivery*, vol. 21, no. 3, pp. 1630–1635, July 2006.

[28] K. Son, K. Moon, S. Lee, and J. Park, "Coordination of an SVC with a ULTC reserving compensation margin for emergency control," *IEEE Transactions on Power Delivery*, vol. 15, no. 4, pp. 1193 –1198, Oct. 2000.

[29] P. E. Benner, "Regulation beyond the distribution substation," *Transactions of the American Institute of Electrical Engineers*, vol. 54, no. 8, pp. 832–837, Aug 1935.

[30] J.-C. Wang, H.-D. Chiang, K. Miu, and G. Darling, "Capacitor placement and real time control in large-scale unbalanced distribution systems: loss reduction formula, problem formulation, solution methodology and mathematical justification," *IEEE Transactions on Power Delivery*, vol. 12, no. 2, pp. 953–958, Apr 1997.

[31] J.-C. Wang, Hsiao-Dong-Chiang, K. Miu, and G. Darling, "Capacitor placement and real time control in large-scale unbalanced distribution systems: numerical studies," *IEEE Transactions on Power Delivery*, vol. 12, no. 2, pp. 959–964, Apr 1997.

[32] K. Miu, H.-D. Chiang, and G. Darling, "Capacitor placement, replacement and control in large-scale distribution systems by a ga-based two-stage algorithm," *IEEE Transactions on Power Systems*, vol. 12, no. 3, pp. 1160–1166, Aug 1997.

[33] M. Baran and F. Wu, "Optimal sizing of capacitors placed on a radial distribution system," *IEEE Transactions on Power Delivery*, vol. 4, no. 1, pp. 735 –743, Jan. 1989.

[34] ——, "Optimal capacitor placement on radial distribution systems," *IEEE Transactions on Power Delivery*, vol. 4, no. 1, pp. 725 –734, Jan. 1989.

[35] J. Grainger and S. Civanlar, "Volt/var control on distribution systems with lateral branches using shunt capacitors and voltage regulators part I: The overall problem," *IEEE Transactions on Power Apparatus and Systems*, vol. PAS-104, no. 11, pp. 3278 –3283, Nov. 1985.

[36] S. Civanlar and J. J. Grainger, "Volt/var control on distribution systems with lateral branches using shunt capacitors and voltage regulators part II: The solution method," *IEEE Transactions on Power Apparatus and Systems*, vol. PAS-104, no. 11, pp. 3284–3290, Nov 1985.

[37] ——, "Volt/var control on distribution systems with lateral branches using switched capacitors and voltage regulators part III: The numerical results," *IEEE Power Engineering Review*, vol. PER-5, no. 11, pp. 54–54, Nov 1985.

[38] R.-H. Liang and Y.-S. Wang, "Fuzzy-based reactive power and voltage control in a distribution system," *IEEE Transactions on Power Delivery*, vol. 18, no. 2, pp. 610–618, Apr. 2003.

[39] R.-H. Liang and C.-K. Cheng, "Dispatch of main transformer ULTC and capacitors in a distribution system," *IEEE Transactions on Power Delivery*, vol. 16, no. 4, pp. 625–630, Oct 2001.

[40] R.-H. Liang and Y.-S. Wang, "Main transformer ULTC and capacitors scheduling by simulated annealing approach," *International Journal of Electrical Power & Energy Systems*, vol. 23, no. 7, pp. 531 – 538, Oct. 2001.

[41] Y. Liu, P. Zhang, and X. Qiu, "Optimal volt/var control in distribution systems," *International Journal of Electrical Power & Energy Systems*, vol. 24, no. 4, pp. 271 – 276, May 2002.

[42] J. young Park, S.-R. Nam, and J.-K. Park, "Control of a ULTC considering the dispatch schedule of capacitors in a distribution system," *IEEE Transactions on Power Systems*, vol. 22, no. 2, pp. 755–761, May 2007.

[43] E. Atmaca, "An ordinal optimization based method for power distribution system control," *Electric Power Systems Research*, vol. 78, no. 4, pp. 694 – 702, Apr. 2008.

[44] A. Mohapatra, P. Bijwe, and B. Panigrahi, "An efficient hybrid approach for volt/var control in distribution systems," *IEEE Transactions on Power Delivery*, vol. 29, no. 4, pp. 1780–1788, Aug 2014.

[45] A. Augugliaro, L. Dusonchet, S. Favuzza, and E. Sanseverino, "Voltage regulation and power losses minimization in automated distribution networks by an evolutionary multi-objective approach," *IEEE Transactions on Power Systems*, vol. 19, no. 3, pp. 1516–1527, Aug 2004.

[46] M. Kleinberg, K. Miu, N. Segal, H. Lehmann, and T. Figura, "A partitioning method for distributed capacitor control of electric power distribution systems," *IEEE Transactions on Power Systems*, vol. 29, no. 2, pp. 637–644, March 2014.

[47] A. Ulinuha, M. A. S. Masoum, and S. Islam, "Optimal scheduling of LTC and shunt capacitors in large distorted distribution systems using evolutionary-based algorithms," *IEEE Transactions on Power Delivery*, vol. 23, no. 1, pp. 434–441, Jan. 2008.

[48] A. Ulinuha, M. Masoum, and S. Islam, "Hybrid genetic-fuzzy algorithm for volt/var/total harmonic distortion control of distribution systems with high penetration of non-linear loads," *IET Generation, Transmission Distribution*, vol. 5, no. 4, pp. 425 –439, Apr. 2011.

[49] T. Ghose and S. Goswami, "Effects of unbalances and harmonics on optimal capacitor placement in distribution system," *Electric Power Systems Research*, vol. 68, no. 2, pp. 167 – 173, 2004.

[50] T. Aziz, M. Hossain, T. Saha, and N. Mithulananthan, "Var planning with tuning of statcom in a dg integrated industrial system," *IEEE Transactions on Power Delivery*, vol. 28, no. 2, pp. 875–885, April 2013.

[51] IEA, *World Energy Outlook 2013*. International Energy Agency, 2013.

[52] M. Höök and X. Tang, "Depletion of fossil fuels and anthropogenic climate change – a review," *Energy Policy*, vol. 52, pp. 797 – 809, 2013.

[53] U. Nations, "Kyoto protocol to the united nations framework convention on climate change," [online] available at http://unfccc.int/resource/docs/convkp/kpeng.pdf, 1998.

[54] ——, "Report of the conference of the parties on its thirteenth session," [online] available at http://unfccc.int/resource/docs/2007/cop13/eng/06a01.pdf, Dec. 2007.

[55] F. Manzano-Agugliaro, A. Alcayde, F. Montoya, A. Zapata-Sierra, and C. Gil, "Scientific production of renewable energies worldwide: An overview," *Renewable and Sustainable Energy Reviews*, vol. 18, pp. 134 – 143, 2013.

[56] T. Ackermann, G. Andersson, and L. Sder, "Distributed generation: a definition," *Electric Power Systems Research*, vol. 57, no. 3, pp. 195 – 204, Apr. 2001.

[57] IEEE Standards Publishing Programs, *IEEE 100 The Authoritative Dictionary of IEEE Standards Terms Seventh Edition*. New York: IEEE Press, 2000.

[58] *Distributed Generation in Liberalised Electricity Markets*. Paris: IEA, 2002.

[59] S. Moghaddas-Tafreshi and E. Mashhour, "Distributed generation modeling for power flow studies and a three-phase unbalanced power flow solution for radial distribution systems considering distributed generation," *Electric Power Systems Research*, vol. 79, no. 4, pp. 680 – 686, Apr. 2009.

[60] W. El-Khattam and M. Salama, "Distributed generation technologies, definitions and benefits," *Electric Power Systems Research*, vol. 71, no. 2, pp. 119 – 128, Oct. 2004.

[61] G. Pepermans, J. Driesen, D. Haeseldonckx, R. Belmans, and W. Dhaeseleer, "Distributed generation: definition, benefits and issues," *Energy Policy*, vol. 33, no. 6, pp. 787 – 798, Apr. 2005.

[62] R. Walling, R. Saint, R. Dugan, J. Burke, and L. A. Kojovic, "Summary of distributed resources impact on power delivery systems," *IEEE Transactions on Power Delivery*, vol. 23, no. 3, pp. 1636–1644, July 2008.

[63] M. Kim, R. Hara, and H. Kita, "Design of the optimal ULTC parameters in distribution system with distributed generations," *IEEE Transactions on Power Systems*, vol. 24, no. 1, pp. 297 –305, Feb. 2009.

[64] J. Hambrick and R. Broadwater, "Configurable, hierarchical, model-based control of electrical distribution circuits," *IEEE Transactions on Power Systems*, vol. 26, no. 3, pp. 1072–1079, Aug 2011.

[65] S. Salih, P. Chen, and O. Carlson, "The effect of wind power integration on the frequency of tap changes of a substation transformer," *IEEE Transactions on Power Systems*, vol. 28, no. 4, pp. 4320–4327, Nov 2013.

[66] M. El Moursi, H. Zeineldin, J. Kirtley, and K. Alobeidli, "A dynamic master/slave reactive power-management scheme for smart grids with distributed generation," *IEEE Transactions on Power Delivery*, vol. 29, no. 3, pp. 1157–1167, June 2014.

[67] Y. Agalgaonkar, B. Pal, and R. Jabr, "Distribution voltage control considering the impact of pv generation on tap changers and autonomous regulators," *IEEE Transactions on Power Systems*, vol. 29, pp. 182–192, 2014.

[68] Z. Ziadi, M. Oshiro, T. Senjyu, A. Yona, N. Urasaki, T. Funabashi, and C.-H. Kim, "Optimal voltage control using inverters interfaced with PV systems considering forecast error in a distribution system," *IEEE Transactions of Sustainable Energy*, vol. 5, no. 2, pp. 682–690, Apr. 2014.

[69] A. Borghetti, "Using mixed integer programming for the volt/var optimization in distribution feeders," *Electric Power Systems Research*, vol. 98, pp. 39 – 50, May 2013.

[70] M. Zare and T. Niknam, "A new multi-objective for environmental and economic management of volt/var control considering renewable energy resources," *Energy*, vol. 55, pp. 236 – 252, June 2013.

[71] F. Marra, G. Yang, C. Traeholt, J. Ostergaard, and E. Larsen, "A decentralized storage strategy for residential feeders with photovoltaics," *IEEE Transactions on Smart Grid*, vol. 5, no. 2, pp. 974–981, March 2014.

[72] X. Liu, A. Aichhorn, L. Liu, and H. Li, "Coordinated control of distributed energy storage system with tap changer transformers for voltage rise mitigation under high photovoltaic penetration," *IEEE Transactions on Smart Grid*, vol. 3, no. 2, pp. 897–906, June 2012.

[73] T. Niknam, M. Zare, and J. Aghaei, "Scenario-based multiobjective volt/var control in distribution networks including renewable energy sources," *IEEE Transactions on Power Delivery*, vol. 27, no. 4, pp. 2004–2019, Oct. 2012.

[74] F. Capitanescu, I. Bilibin, and E. Romero Ramos, "A comprehensive centralized approach for voltage constraints management in active distribution grid," *IEEE Transactions on Power Systems*, vol. 29, no. 2, pp. 933–942, March 2014.

[75] C.-L. Su, "Stochastic evaluation of voltages in distribution networks with distributed generation using detailed distribution operation models," *IEEE Transactions on Power Systems*, vol. 25, no. 2, pp. 786–795, May 2010.

[76] H. Mostafa, R. El-Shatshat, and M. Salama, "Multi-objective optimization for the operation of an electric distribution system with a large number of single phase solar generators," *IEEE Transactions on Smart Grid*, vol. 4, no. 2, pp. 1038–1047, June 2013.

[77] T. Senjyu, Y. Miyazato, A. Yona, N. Urasaki, and T. Funabashi, "Optimal distribution voltage control and coordination with distributed generation," *IEEE Transactions on Power Delivery*, vol. 23, no. 2, pp. 1236 –1242, Apr. 2008.

[78] Standards Coordinating Committee 21, "IEEE standard for interconnecting distributed resources with electric power systems," *IEEE Std 1547-2003*, pp. 1–28, July 2003.

[79] A. Samadi, R. Eriksson, L. Soder, B. Rawn, and J. Boemer, "Coordinated active power-dependent voltage regulation in distribution grids with PV systems," *IEEE Transactions on Power Delivery*, vol. 29, no. 3, pp. 1454–1464, June 2014.

[80] A. Di Fazio, G. Fusco, and M. Russo, "Decentralized control of distributed generation for voltage profile optimization in smart feeders," *IEEE Transactions on Smart Grid*, vol. 4, no. 3, pp. 1586–1596, Sept. 2013.

[81] P. Jahangiri and D. Aliprantis, "Distributed volt/var control by pv inverters," *IEEE Transactions on Power Systems*, vol. 28, no. 3, pp. 3429–3439, Aug 2013.

[82] A. Rueda-Medina and A. Padilha-Feltrin, "Distributed generators as providers of reactive power support – a market approach," *IEEE Transactions on Power Systems*, vol. 28, no. 1, pp. 490–502, Feb 2013.

[83] G. Mokhtari, G. Nourbakhsh, and A. Ghosh, "Smart coordination of energy storage units (ESUs) for voltage and loading management in distribution networks," *IEEE Transactions on Power Systems*, vol. 28, no. 4, pp. 4812–4820, Nov 2013.

[84] Y.-Y. Hong, F.-J. Lin, Y.-C. Lin, and F.-Y. Hsu, "Chaotic PSO-Based VAR control considering renewables using fast probabilistic power flow," *IEEE Transactions on Power Delivery*, vol. 5, no. 5, pp. 2412–2420, Sept 2014.

[85] H.-G. Yeh, D. Gayme, and S. Low, "Adaptive var control for distribution circuits with photovoltaic generators," *IEEE Transactions on Power Systems*, vol. 27, no. 3, pp. 1656–1663, Aug 2012.

[86] E. Demirok, P. Casado Gonza andlez, K. Frederiksen, D. Sera, P. Rodriguez, and R. Teodorescu, "Local reactive power control methods for overvoltage prevention of distributed solar inverters in low-voltage grids," *IEEE Journal of Photovoltaics*, vol. 1, no. 2, pp. 174 –182, Oct. 2011.

[87] A. Cagnano, E. De Tuglie, M. Liserre, and R. Mastromauro, "Online optimal reactive power control strategy of PV inverters," *IEEE Transactions on Industrial Electronics*, vol. 58, no. 10, pp. 4549–4558, Oct 2011.

[88] F. Viawan and D. Karlsson, "Voltage and reactive power control in systems with synchronous machine-based distributed generation," *IEEE Transactions on Power Delivery*, vol. 23, no. 2, pp. 1079 –1087, Apr. 2008.

[89] ——, "Combined local and remote voltage and reactive power control in the presence of induction machine distributed generation," *IEEE Transactions on Power Systems*, vol. 22, no. 4, pp. 2003–2012, Nov 2007.

[90] E. Dall'Anese, S. Dhople, and G. Giannakis, "Optimal dispatch of photovoltaic inverters in residential distribution systems," *IEEE Transactions of Sustainable Energy*, vol. 5, no. 2, pp. 487–497, Apr. 2014.

[91] V. Calderaro, G. Conio, V. Galdi, G. Massa, and A. Piccolo, "Optimal decentralized voltage control for distribution systems with inverter-based distributed generators," *IEEE Transactions on Power Systems*, vol. 29, no. 1, pp. 230–241, Jan. 2014.

[92] T. Stetz, F. Marten, and M. Braun, "Improved low voltage grid-integration of photovoltaic systems in germany," *IEEE Transactions of Sustainable Energy*, vol. 4, no. 2, pp. 534–542, Apr. 2013.

[93] A. Borghetti, M. Bosetti, S. Grillo, S. Massucco, C. Nucci, M. Paolone, and F. Silvestro, "Short-term scheduling and control of active distribution systems with high penetration of renewable resources," *IEEE Systems Journal*, vol. 4, no. 3, pp. 313–322, Sept 2010.

[94] R.-H. Liang, Y.-K. Chen, and Y.-T. Chen, "Volt/var control in a distribution system by a fuzzy optimization approach," *International Journal of Electrical Power & Energy Systems*, vol. 33, no. 2, pp. 278 – 287, 2011.

[95] M. Azzouz, H. Farag, and E. El-Saadany, "Real-time fuzzy voltage regulation for distribution networks incorporating high penetration of renewable sources," *IEEE Systems Journal*, to be published.

[96] M. Bahadornejad and N.-K. Nair, "Intelligent control of on-load tap changing transformer," *IEEE Transactions on Smart Grid*, vol. 5, no. 5, pp. 2255–2263, Sept 2014.

[97] M. Baran and I. El-Markabi, "A multiagent-based dispatching scheme for distributed generators for voltage support on distribution feeders," *IEEE Transactions on Power Systems*, vol. 22, no. 1, pp. 52 –59, Feb. 2007.

[98] R. Bottura and A. Borghetti, "Simulation of the volt/var control in distribution feeders by means of a networked multi-agent system," *IEEE Transactions on Industrial Informatics*, vol. 10, no. 4, pp. 2340–2353, Nov 2014.

[99] F. Ren, M. Zhang, and D. Sutanto, "A multi-agent solution to distribution system management by considering distributed generators," *IEEE Transactions on Power Systems*, vol. 28, no. 2, pp. 1442–1451, May 2013.

[100] M. Elkhatib, R. El-Shatshat, and M. Salama, "Novel coordinated voltage control for smart distribution networks with DG," *IEEE Transactions on Smart Grid*, vol. 2, no. 4, pp. 598–605, Dec 2011.

[101] J.-H. Choi and S.-I. Moon, "The dead band control of LTC transformer at distribution substation," *IEEE Transactions on Power Systems*, vol. 24, no. 1, pp. 319–326, Feb 2009.

[102] M. Kabir, Y. Mishra, G. Ledwich, Z. Dong, and K. Wong, "Coordinated control of grid-connected photovoltaic reactive power and battery energy storage systems to improve the voltage profile of a residential distribution feeder," *IEEE Transactions on Industrial Informatics*, vol. 10, no. 2, pp. 967–977, May 2014.

[103] M. H. J. Bollen and A. Sannino, "Voltage control with inverter-based distributed generation," *IEEE Transactions on Power Delivery*, vol. 20, no. 1, pp. 519–520, Jan 2005.

[104] M. Pirnia, C. Canizares, K. Bhattacharya, and A. Vaccaro, "A novel affine arithmetic method to solve optimal power flow problems with uncertainties," *IEEE Transactions on Power Systems*, vol. 29, no. 6, pp. 2775–2783, Nov 2014.

[105] M. Abdelaziz, H. Farag, and E. El-Saadany, "Optimum droop parameter settings of islanded microgrids with renewable energy resources," *IEEE Transactions of Sustainable Energy*, vol. 5, no. 2, pp. 434–445, April 2014.

[106] Y. Zhang, N. Gatsis, and G. Giannakis, "Robust energy management for microgrids with high-penetration renewables," *IEEE Transactions of Sustainable Energy*, vol. 4, no. 4, pp. 944–953, Oct 2013.

[107] A. Vaccaro, C. Canizares, and K. Bhattacharya, "A range arithmetic-based optimization model for power flow analysis under interval uncertainty," *IEEE Transactions on Power Systems*, vol. 28, no. 2, pp. 1179–1186, May 2013.

[108] A. Martinez-Mares and C. Fuerte-Esquivel, "A robust optimization approach for the interdependency analysis of integrated energy systems considering wind power uncertainty," *IEEE Transactions on Power Systems*, vol. 28, pp. 3964–3976, Nov. 2013.

[109] A. Korad and K. Hedman, "Robust corrective topology control for system reliability," *IEEE Transactions on Power Systems*, vol. 28, no. 4, pp. 4042–4051, Nov 2013.

[110] X. Jiang, Y. Chen, and A. Dominguez-Garcia, "A set-theoretic framework to assess the impact of variable generation on the power flow," *IEEE Transactions on Power Systems*, vol. 28, no. 2, pp. 855–867, May 2013.

[111] H. Yu and W. Rosehart, "An optimal power flow algorithm to achieve robust operation considering load and renewable generation uncertainties," *IEEE Transactions on Power Systems*, vol. 27, no. 4, pp. 1808–1817, Nov. 2012.

[112] Y.-Y. Hong and Y.-F. Luo, "Optimal var control considering wind farms using probabilistic load-flow and gray-based genetic algorithms," *IEEE Transactions on Power Delivery*, vol. 24, no. 3, pp. 1441–1449, July 2009.

[113] D. Das and P. Satpathy, "A fuzzy set theory approach to handle parameter uncertainties in saddle node bifurcation analysis," *Electric Power Components and Systems*, vol. 34, no. 12, pp. 1295–1312, 2006.

[114] S. Ganguly, N. Sahoo, and D. Das, "Multi-objective particle swarm optimization based on fuzzy-pareto-dominance for possibilistic planning of electrical distribution systems incorporating distributed generation," *Fuzzy Sets and Systems*, vol. 213, pp. 47–73, 2013.

[115] S. Surender Reddy, P. Bijwe, and A. Abhyankar, "Optimal posturing in day-ahead market clearing for uncertainties considering anticipated real-time adjustment costs," *IEEE Systems Journal*, vol. PP, no. 99, pp. 1–14, 2013.

[116] T. Ding, R. Bo, F. Li, Y. Gu, Q. Guo, and H. Sun, "Exact penalty function based constraint relaxation method for optimal power flow considering wind generation uncertainty," *IEEE Transactions on Power Systems*, vol. PP, no. 99, pp. 1–3, 2014.

[117] N. Jain, S. Singh, and S. Srivastava, "PSO based placement of multiple wind DGs and capacitors utilizing probabilistic load flow model," *Swarm and Evolutionary Computation*, vol. 19, no. 0, pp. 15 – 24, 2014.

[118] K. Bhaskar and S. Singh, "AWNN-assisted wind power forecasting using feed-forward neural network," *Sustainable Energy, IEEE Transactions on*, vol. 3, no. 2, pp. 306–315, April 2012.

[119] T. Senjyu, H. Takara, K. Uezato, and T. Funabashi, "One-hour-ahead load forecasting using neural network," *IEEE Transactions on Power Systems*, vol. 17, no. 1, pp. 113–118, Feb 2002.

[120] N. Jain, S. Singh, and S. Srivastava, "A generalized approach for DG planning and viability analysis under market scenario," *Industrial Electronics, IEEE Transactions on*, vol. 60, no. 11, pp. 5075–5085, Nov 2013.

[121] B. Das, "Consideration of input parameter uncertainties in load flow solution of three-phase unbalanced radial distribution system," *IEEE Transactions on Power Systems*, vol. 21, no. 3, pp. 1088–1095, Aug 2006.

[122] G. Sivanagaraju, S. Chakrabarti, and S. Srivastava, "Uncertainty in transmission line parameters: Estimation and impact on line current differential protection," *Instrumentation and Measurement, IEEE Transactions on*, vol. 63, no. 6, pp. 1496–1504, June 2014.

[123] S. Mishra, D. Das, and S. Paul, "Active loss allocation systems in radial distribution systems," *Cogeneration and Distributed Generation Journal*, vol. 25, no. 3, pp. 26–43, 2010.

[124] Y. Cao, Y. Tan, C. Li, and C. Rehtanz, "Chance-constrained optimization-based unbalanced optimal power flow for radial distribution networks," *IEEE Transactions on Power Delivery*, vol. 28, no. 3, pp. 1855–1864, July 2013.

[125] D. McQueen, P. Hyland, and S. Watson, "Application of a monte carlo simulation method for predicting voltage regulation on low-voltage networks," *IEEE Transactions on Power Systems*, vol. 20, no. 1, pp. 279–285, Feb. 2005.

[126] M. Althoff, "Formal and compositional analysis of power systems using reachable sets," *IEEE Transactions on Power Systems*, vol. 29, no. 5, pp. 2270–2280, Sept 2014.

[127] R. Jiang, J. Wang, M. Zhang, and Y. Guan, "Two-stage minimax regret robust unit commitment," *IEEE Transactions on Power Systems*, vol. 28, no. 3, pp. 2271–2282, Aug 2013.

[128] A. Ben-Tal, L. El Ghaoui, and A. Nemirovski, *Robust Optimization*, ser. Princeton Series in Applied Mathematics. New Jersey: Princeton University Press, October 2009.

[129] D. Bertsimas, E. Litvinov, X. Sun, J. Zhao, and T. Zheng, "Adaptive robust optimization for the security constrained unit commitment problem," *IEEE Transactions on Power Systems*, vol. 28, no. 1, pp. 52–63, Feb 2013.

[130] S. Singh, T. Ghose, and S. Goswami, "Optimal feeder routing based on the bacterial foraging technique," *IEEE Transactions on Power Delivery*, vol. 27, no. 1, pp. 70–78, Jan 2012.

[131] A. Samui, S. Singh, T. Ghose, and S. Samantaray, "A direct approach to optimal feeder routing for radial distribution system," *IEEE Transactions on Power Delivery*, vol. 27, no. 1, pp. 253–260, Jan 2012.

[132] F. Pilo, G. Pisano, and G. Soma, "Optimal coordination of energy resources with a two-stage online active management," *IEEE Transactions on Industrial Electronics*, vol. 58, no. 10, pp. 4526 –4537, oct. 2011.

[133] O. Fajardo and A. Vargas, "Reconfiguration of MV distribution networks with multicost and multipoint alternative supply, Part II: Reconfiguration plan," *IEEE Transactions on Power Systems*, vol. 23, no. 3, pp. 1401–1407, Aug 2008.

[134] F. Capitanescu, L. Ochoa, H. Margossian, and N. Hatziargyriou, "Assessing the potential of network reconfiguration to improve distributed generation hosting capacity in active distribution systems," *IEEE Transactions on Power Systems*, vol. PP, no. 99, pp. 1–11, 2014.

[135] D. Bernardon, A. Mello, L. Pfitscher, L. Canha, A. Abaide, and A. Ferreira, "Real-time reconfiguration of distribution network with distributed generation," *Electric Power Systems Research*, vol. 107, pp. 59 – 67, Feb. 2014.

[136] E. Lopez, H. Opazo, L. Garcia, and P. Bastard, "Online reconfiguration considering variability demand: Applications to real networks," *IEEE Transactions on Power Systems*, vol. 19, no. 1, pp. 549–553, Feb 2004.

[137] J. Savier and D. Das, "Impact of network reconfiguration on loss allocation of radial distribution systems," *IEEE Transactions on Power Delivery*, vol. 22, no. 4, pp. 2473–2480, 2007.

[138] A. Bokhari, A. Alkan, R. Dogan, M. Diaz-Aguilo, F. de Leon, D. Czarkowski, Z. Zabar, L. Birenbaum, A. Noel, and R. Uosef, "Experimental determination of the ZIP coefficients for modern residential, commercial, and industrial loads," *IEEE Transactions on Power Delivery*, vol. 29, no. 3, pp. 1372–1381, June 2014.

[139] M. Diaz-Aguilo, J. Sandraz, R. Macwan, F. de Leon, D. Czarkowski, C. Comack, and D. Wang, "Field-validated load model for the analysis of CVR in distribution secondary networks: Energy conservation," *IEEE Transactions on Power Delivery*, vol. 28, no. 4, pp. 2428–2436, Oct 2013.

[140] Z. Wang and J. Wang, "Time-varying stochastic assessment of conservation voltage reduction based on load modeling," *IEEE Transactions on Power Systems*, vol. 29, no. 5, pp. 2321–2328, Sept 2014.

[141] W. Rosehart, C. Canizares, and V. Quintana, "Effect of detailed power system models in traditional and voltage-stability-constrained optimal power-flow problems," *IEEE Transactions on Power Systems*, vol. 18, no. 1, pp. 27–35, Feb 2003.

[142] Distribution System Analysis Subcommittee, "IEEE 13 node test feeder," [online] http://ewh.ieee.org/soc/pes/dsacom/testfeeders/feeder13.zip. Accessed at 1 July 2013.

[143] S. Deshmukh, B. Natarajan, and A. Pahwa, "Voltage/var control in distribution networks via reactive power injection through distributed generators," *IEEE Transactions on Smart Grid*, vol. 3, no. 3, pp. 1226–1234, Sept 2012.

[144] J. Marti, H. Ahmadi, and L. Bashualdo, "Linear power-flow formulation based on a voltage-dependent load model," *IEEE Transactions on Power Delivery*, vol. 28, no. 3, pp. 1682–1690, July 2013.

[145] D. Molzahn, B. Lesieutre, and C. DeMarco, "Approximate representation of ZIP loads in a semidefinite relaxation of the OPF problem," *IEEE Transactions on Power Systems*, vol. 29, no. 4, pp. 1864–1865, July 2014.

[146] D. Hung, N. Mithulananthan, and K. Lee, "Determining PV penetration for distribution systems with time-varying load models," *IEEE Transactions on Power Systems*, vol. 29, no. 6, pp. 3048–3057, Nov 2014.

[147] Z. Wang, J. Wang, B. Chen, M. Begovic, and Y. He, "MPC-based voltage/var optimization for distribution circuits with distributed generators and exponential load models," *IEEE Transactions on Smart Grid*, vol. 5, no. 5, pp. 2412–2420, Sept 2014.

[148] E. A. Paaso, Y. Liao, and A. M. Cramer, "Formulation and solution of distribution system voltage and VAR control with distributed generation as a mixed integer non-linear programming problem," *Electric Power Systems Research*, vol. 108, pp. 164 – 169, 2014.

[149] H. Ahmadi and J. Marti, "Distribution system optimization based on a linear power-flow formulation," *IEEE Transactions on Power Delivery*, vol. PP, no. 99, pp. 1–1, 2014.

[150] W. Kersting, *Distribution system modeling and analysis*, ser. Electric power engineering series. Boca Raton: CRC Press, 2002.

[151] R. Yan and T. K. Saha, "Voltage variation sensitivity analysis for unbalanced distribution networks due to photovoltaic power fluctuations," *IEEE Transactions on Power Systems*, vol. 27, no. 2, pp. 1078–1089, May 2012.

[152] T. Lee, S. Hu, and Y. Chan, "D-STATCOM with positive-sequence admittance and negative-sequence conductance to mitigate voltage fluctuations in high-level penetration of distributed generation systems," *IEEE Transactions on Industrial Electronics*, vol. 60, pp. 1417–1428, Apr. 2013.

[153] R. Varma, V. Khadkikar, and R. Seethapathy, "Nighttime application of PV solar farm as STATCOM to regulate grid voltage," *IEEE Transactions on Energy Conversion*, vol. 24, no. 4, pp. 983 –985, Dec. 2009.

[154] Y.-R. Mohamed and E. El-Saadany, "A control scheme for PWM voltage-source distributed-generation inverters for fast load-voltage regulation and effective mitigation of unbalanced voltage disturbances," *IEEE Transactions on Industrial Electronics*, vol. 55, no. 5, pp. 2072 –2084, May 2008.

[155] N. Hingorani and L. Gyugyi, *Understanding FACTS: concepts and technology of flexible AC transmission systems*. New York: IEEE Press, 2000.

[156] *IEEE guide for the functional specification of transmission static var compensators*, IEEE Std. 1031-2011.

[157] P. Preedavichit and S. Srivastava, "Optimal reactive power dispatch considering FACTS devices," *Electric Power Systems Research*, vol. 46, no. 3, pp. 251 – 257, 1998.

[158] W.-M. Lin, C.-H. Huang, and T.-S. Zhan, "A hybrid current-power optimal power flow technique," *IEEE Transactions on Power Systems*, vol. 23, no. 1, pp. 177–185, Feb. 2008.

[159] T. Malakar and S. Goswami, "Active and reactive dispatch with minimum control movements," *International Journal of Electrical Power & Energy Systems*, vol. 44, no. 1, pp. 78 – 87, 2013.

[160] IEC 61000-2-12 Ed. 1.0 b, "Compatibility levels for low-frequency conducted disturbances and signalling in public medium-voltage power supply systems," 2003.

[161] A. Wchter and L. T. Biegler., "On the implementation of a primal-dual interior point filter line search algorithm for large-scale nonlinear programming," *Mathematical Programming*, vol. 106(1), pp. 25–27, Apr. 2006.

[162] P. Bonami, L. T. Biegler, A. R. Conn, G. Cornujols, I. E. Grossmann, C. D. Laird, J. Lee, A. Lodi, F. Margot, N. Sawaya, and A. Wchter, "An algorithmic framework for convex mixed integer nonlinear programs," *Discrete Optimization*, vol. 5, no. 2, pp. 186 – 204, May 2008.

[163] P. R. Amestoy, A. Guermouche, J.-Y. L'Excellent, and S. Pralet, "Hybrid scheduling for the parallel solution of linear systems," *Parallel Computing*, vol. 32, no. 2, pp. 136–156, 2006.

[164] AMPL (a modelling language for mathematical programming). [Online] http://ampl.com/.

[165] H. Jiang, R. Shuttleworth, B. A. T. Al Zahawi, X. Tian, and A. Power, "Fast response gto assisted novel tap changer," *IEEE Transactions on Power Delivery*, vol. 16, no. 1, pp. 111–115, Jan 2001.

[166] K. H. Abdul-Rahman and S. M. Shahidehpour, "Application of fuzzy sets to optimal reactive power planning with security constraints," *IEEE Transactions on Power Systems*, vol. 9, no. 2, pp. 589–597, May 1994.

[167] S. Alnaser and L. Ochoa, "Advanced network management systems: A risk-based AC OPF approach," *IEEE Transactions on Power Systems*, vol. PP, no. 99, pp. 1–10, 2014.

[168] A. Saric and A. Stankovic, "A robust algorithm for volt/var control," in *Power Systems Conference and Exposition, 2009. PSCE '09. IEEE/PES*, 2009, pp. 1–8.

[169] D. Bertsimas and M. Sim, "The price of robustness," *Operations Research*, vol. 52, no. 1, pp. 35–53, Feb. 2004.

[170] D. Bertsimas and A. Thiele, "A robust optimization approach to inventory theory," *Operations Research*, vol. 54, no. 1, pp. 150–168, 2006.

[171] A. Viehweider, H. Schichl, D. de Castro, S. Henein, and D. Schwabeneder, "Smart robust voltage control for distribution networks using interval arithmetic and state machine concepts," in *Innovative Smart Grid Technologies Conference Europe (ISGT Europe), 2010 IEEE PES*, 2010, pp. 1–8.

[172] K. Miu and H.-D. Chiang, "Existence, uniqueness, and monotonic properties of the feasible power flow solution for radial three-phase distribution networks," *IEEE Transactions on Circuits and Systems I: Fundamental Theory and Applications*, vol. 47, no. 10, pp. 1502 – 1514, Oct. 2000.

[173] R. Yan and T. Saha, "Investigation of voltage imbalance due to distribution network unbalanced line configurations and load levels," *IEEE Transactions on Power Systems*, vol. 28, no. 2, pp. 1829–1838, May 2013.

[174] P. Kundur, *Power System Stability and Control*. New York: Tata McGraw-Hill, 1994.

[175] X.-P. Zhang, P. Ju, and E. Handschin, "Continuation three-phase power flow: A tool for voltage stability analysis of unbalanced three-phase power systems," *IEEE Transactions on Power Systems*, vol. 20, no. 3, pp. 1320–1329, Aug. 2005.

[176] T. Ding, R. Bo, W. Gu, Q. Guo, and H. Sun, "Absolute value constraint based method for interval optimization to SCED model," *IEEE Transactions on Power Systems*, vol. 29, no. 2, pp. 980–981, March 2014.

[177] M. Liu, S. Tso, and Y. Cheng, "An extended nonlinear primal-dual interior-point algorithm for reactive-power optimization of large-scale power systems with discrete control variables," *IEEE Transactions on Power Systems*, vol. 17, no. 4, pp. 982 – 991, nov 2002.

[178] S. Patra and S. Goswami, "Handling inequalities and discrete variables in newton optimal power flow using optimal multiplier and fuzzy based limit enforcement and relaxation technique," *International Journal of Electrical Power & Energy Systems*, vol. 42, no. 1, pp. 359 – 366, 2012.

[179] H. Sheng and H.-D. Chiang, "CDFLOW: A practical tool for tracing stationary behaviors of general distribution networks," *IEEE Transactions on Power Systems*, vol. 29, no. 3, pp. 1365–1371, May 2014.

[180] W. Rosehart, C. Roman, and A. Schellenberg, "Optimal power flow with complementarity constraints," *IEEE Transactions on Power Systems*, vol. 20, no. 2, pp. 813–822, May 2005.

[181] C. W. Chow, B. Urquhart, M. Lave, A. Dominguez, J. Kleissl, J. Shields, and B. Washom, "Intra-hour forecasting with a total sky imager at the UC san diego solar energy testbed," *Solar Energy*, vol. 85, no. 11, pp. 2881 – 2893, 2011.

[182] OpenDSS. [Online] http://sourceforge.net/projects/electricdss/.

[183] Python. [Online] https://www.python.org/.

[184] UQ solar photovoltaic data. [Online] http://solar.uq.edu.au/. The University of Queensland.

[185] A. Mendes, N. Boland, P. Guiney, and C. Riveros, "Switch and tap-changer reconfiguration of distribution networks using evolutionary algorithms," *IEEE Transactions on Power Systems*, vol. 28, no. 1, pp. 85–92, Feb 2013.

[186] W. Kersting, "Radial distribution test feeders," in *Power Engineering Society Winter Meeting, 2001. IEEE*, vol. 2, 2001, pp. 908 –912 vol.2.

[187] H. Kikusato, N. Takahashi, J. Yoshinaga, Y. Fujimoto, Y. Hayashi, S. Kusagawa, and N. Motegi, "Method for determining line drop compensator parameters of low voltage regulator using support vector machine," in *Innovative Smart Grid Technologies Conference (ISGT), 2014 IEEE PES*, Feb 2014, pp. 1–5.

[188] W. Kersting, "Distribution feeder voltage regulation control," *IEEE Transactions on Industry Applications*, vol. 46, no. 2, pp. 620–626, March 2010.

[189] *GE-2011 Digital Tapchanger Control*, General Electric, 2002.

[190] "IEEE 123 node distributio test feeder," [online] http://ewh.ieee.org/soc/pes/dsacom/testfeeders/., Accessed at 1 July 2013.

[191] F. Milano, "Hybrid control model of under load tap changers," *IEEE Transactions on Power Delivery*, vol. 26, no. 4, pp. 2837–2844, Oct 2011.

[192] S. Son, S. H. Lee, D.-H. Choi, K.-B. Song, J.-D. Park, Y.-H. Kwon, K. Hur, and J.-W. Park, "Improvement of composite load modeling based on parameter sensitivity and dependency analyses," *IEEE Transactions on Power Systems*, vol. 29, no. 1, pp. 242–250, Jan 2014.

[193] IEEE Task Force on Load Representation for Dynamic Performance, "Bibliography on load models for power flow and dynamic performance simulation," *IEEE Transactions on Power Systems*, vol. 10, no. 1, pp. 523–538, Feb 1995.

[194] V. Dabic, C. Siew, J. Peralta, and D. Acebedo, "BC hydro's experience on voltage var optimization in distribution system," in *Transmission and Distribution Conference and Exposition, 2010 IEEE PES*, Apr. 2010, pp. 1–7.

A — Simple Network

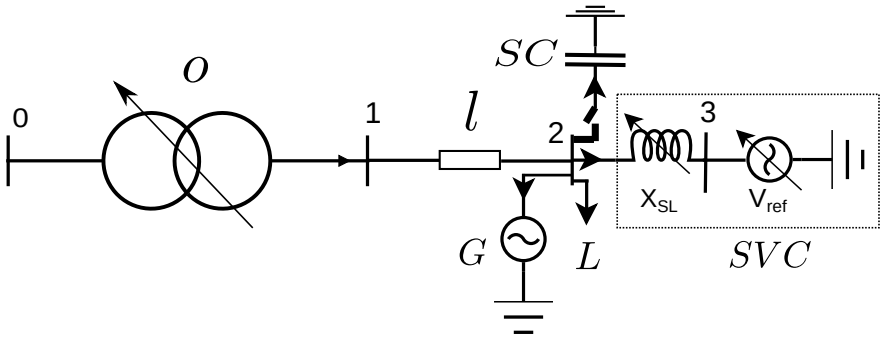

Figure A.1: A simple network with an OLTC o, a line l, a load L, a distributed generation G, a shunt capacitor SC and and svc v

Consider a simple radial network shown in Fig. A.1. The network has a OLTC o, a line l, an SVC v, a Load L, a generation G and a shunt capacitor SC. For simplicity all of those devices are three-phase devices and all shunt elements are wye connected. The constraints corresponding to the network are given below. The equality constraints correspond to

A.1 Nodal Current Balance

The nodal current balance law applies to bus 1 and 2 only. Bus 0 is the slack bus and Bus 3 is a dummy bus. Hence, for bus 0 and 3, the law does not apply. Since buses 1 and 2 have three phases, in total there are 6 nodes. For each node, there are two equations corresponding to real and imaginary current, respectively. Hence, in total, there $6\times2 = 12$ equality constraints corresponding to nodal current balance.

$$I^{ip}_{oxr} = \sum I^{ip}_{lxs} + \sum I^{ip}_{Lx} + \sum I^{ip}_{vx} + \sum I^{ip}_{SCx} - \sum I^{ip}_{Gx} \tag{A.1}$$

$$I^{ip}_{oyr} = \sum I^{ip}_{lys} + \sum I^{ip}_{Ly} + \sum I^{ip}_{vy} + \sum I^{ip}_{SCy} - \sum I^{ip}_{Gy} \tag{A.2}$$

$$\forall i \in \{1,2\}, \forall p \in \{a,b,c\}$$

A.2 OLTC

For OLTC o, there are four matrix relations given in eqs. (A.3) - (A.6) which must be satisfied. Since OLTC o is a three-phase device, from each matrix relation, there are three complex relations. From each of those complex relations, there are two real relations. Hence, in total, there are $4 \times 3 \times 2 = 24$ equality constraints corresponding to OLTC o.

$$\begin{aligned} \mathbf{E}_x(b_S^s) &= \mathbf{A}_x\mathbf{E}_x(b_S^r) - \mathbf{A}_y\mathbf{E}_y(b_S^r) \\ &+ \mathbf{B}_x\mathbf{I}_{Sxr} - \mathbf{B}_y\mathbf{I}_{Syr} \end{aligned} \tag{A.3}$$

$$\begin{aligned} \mathbf{E}_y(b_S^s) &= \mathbf{A}_x\mathbf{E}_y(b_S^r) + \mathbf{A}_y\mathbf{E}_x(b_S^r) \\ &+ \mathbf{B}_x\mathbf{I}_{Sxr} + \mathbf{B}_y\mathbf{I}_{Syr} \end{aligned} \tag{A.4}$$

$$\mathbf{I}_{Sxs} = \mathbf{C}\mathbf{E}_x(b_S^r) + \mathbf{D}\mathbf{I}_{Sxr} \tag{A.5}$$

$$\mathbf{I}_{Sys} = \mathbf{C}\mathbf{E}_y(b_S^r) + \mathbf{D}\mathbf{I}_{Syr} \tag{A.6}$$

where $S = o, b_S^s = 0, b_S^r = 1$,

$$\bar{\mathbf{A}} = \begin{bmatrix} \frac{1}{tap_{oa}} & 0 & 0 \\ 0 & \frac{1}{tap_{ob}} & 0 \\ 0 & 0 & \frac{1}{tap_{oc}} \end{bmatrix}, \bar{\mathbf{B}} \begin{bmatrix} 0 & 0 & 0 \\ 0 & 0 & 0 \\ 0 & 0 & 0 \end{bmatrix},$$

$$\mathbf{C} = \begin{bmatrix} 0 & 0 & 0 \\ 0 & 0 & 0 \\ 0 & 0 & 0 \end{bmatrix}, \mathbf{D} = \begin{bmatrix} tap_{oa} & 0 & 0 \\ 0 & tap_{ob} & 0 \\ 0 & 0 & tap_{oc} \end{bmatrix}$$

A.3 Line

Similar to OLTC o, line l is a three-phase element of distribution system. Therefore, there 24 equality constraints corresponding to line l.

$$\begin{aligned}\mathbf{E}_x(b_S^s) &= \mathbf{A}_x\mathbf{E}_x(b_S^r) - \mathbf{A}_y\mathbf{E}_y(b_S^r) \\ &+ \mathbf{B}_x\mathbf{I}_{Sxr} - \mathbf{B}_y\mathbf{I}_{Syr} \qquad \text{(A.7)} \\ \mathbf{E}_y(b_S^s) &= \mathbf{A}_x\mathbf{E}_y(b_S^r) + \mathbf{A}_y\mathbf{E}_x(b_S^r) \\ &+ \mathbf{B}_x\mathbf{I}_{Sxr} + \mathbf{B}_y\mathbf{I}_{Syr} \qquad \text{(A.8)}\end{aligned}$$

$$\mathbf{I}_{Sxs} = \mathbf{C}\mathbf{E}_x(b_S^r) + \mathbf{D}\mathbf{I}_{Sxr} \qquad \text{(A.9)}$$

$$\mathbf{I}_{Sys} = \mathbf{C}\mathbf{E}_y(b_S^r) + \mathbf{D}\mathbf{I}_{Syr} \qquad \text{(A.10)}$$

where $S = l, b_S^s = 1, b_S^r = 2$ $\bar{\mathbf{A}} = \begin{bmatrix}1 & 0 & 0\\ 0 & 1 & 0\\ 0 & 0 & 1\end{bmatrix}$, $\bar{\mathbf{B}} = \begin{bmatrix}\bar{Z}^{aa} & \bar{Z}^{ab} & \bar{Z}^{ac}\\ \bar{Z}^{ba} & \bar{Z}^{bb} & \bar{Z}^{bc}\\ \bar{Z}^{ca} & \bar{Z}^{cb} & \bar{Z}^{cc}\end{bmatrix}$, $\mathbf{C} = \begin{bmatrix}0 & 0 & 0\\ 0 & 0 & 0\\ 0 & 0 & 0\end{bmatrix}$,$\mathbf{D} = \begin{bmatrix}1 & 0 & 0\\ 0 & 1 & 0\\ 0 & 0 & 1\end{bmatrix}$.

A.4 Load

The load L is a three-phase load connected at bus 2. It has three equations for real currents given in eq. (A.11) and three equations for imaginary currents given in eqs. (A.12). Therefore, it corresponds to six equality constraints.

$$I_{Lx}^{ip} = \frac{P_L^{ip}E_x^{ip} + Q_L^{ip}E_y^{ip}}{(E_x^{ip})^2 + (E_y^{ip})^2} \qquad \text{(A.11)}$$

$$I_{Ly}^{ip} = \frac{P_L^{ip}E_y^{ip} - Q_L^{ip}E_x^{ip}}{(E_x^{ip})^2 + (E_y^{ip})^2}. \qquad \text{(A.12)}$$

$$\forall i \in \{2\}, \forall p \in \{a, b, c\}$$

A.5 Generator

Similar to load L, generator G is a three phase devices. It has three equations corresponding to real currents given in eqs. (A.13) and three imaginary currents given in eqs. (A.14). Hence, it corresponds to six equality constraints.

$$I_{Gx}^{ip} = \frac{P_G^{ip} E_x^{ip} + Q_G^{ip} E_y^{ip}}{(E_x^{ip})^2 + (E_y^{ip})^2} \tag{A.13}$$

$$I_{Gy}^{ip} = \frac{P_G^{ip} E_y^{ip} - Q_G^{ip} E_x^{ip}}{(E_x^{ip})^2 + (E_y^{ip})^2} \tag{A.14}$$

$$\forall i \in \{2\}, \forall p \in \{a, b, c\}$$

A.6 Shunt Capacitor

Shunt capacitor SC is also a three-phase device connected to bus 2. It corresponds to six equality constraints.

$$I_{SCx}^{ip} = \frac{sc^{ip}}{n_c} \frac{+E_y^{ip}}{X_{SC}^{ip}}, X_{SC}^{ip} < 0 \tag{A.15}$$

$$I_{SCy}^{ip} = \frac{sc^{ip}}{n_c} \frac{-E_x^{ip}}{X_{SC}^{ip}}, X_{SC}^{ip} < 0. \tag{A.16}$$

$$\forall i \in \{2\}, \forall p \in \{a, b, c\}$$

A.7 SVC

The SVC v corresponds to three real power balance equations

$$P_{vp}^{spec} = E_x^p(b_v) I_{vx}^p + E_y^p(b_v) I_{vy}^p = 0, \forall p, \forall v \tag{A.17}$$

three reactive power balance equations

$$Q_V^p = E_y^p(b_v) I_{vx}^p - E_x^p(b_v) I_{vy}^p \;\; \forall p, \forall v \tag{A.18}$$

and one voltage reference equation

$$|\bar{E}_v^{ref}| = E_v^1 \tag{A.19}$$

where

$$b_v = 2, \forall p \in \{a, b, c\}.$$

The slope of SVC v, X_{SL}, is modeled as a series element similar to OLTC o and line l. Hence, there are 24 equality constraints corresponding to the slope of SVC v.

$$\begin{aligned}\mathbf{E}_x(b_S^s) = \mathbf{A}_x\mathbf{E}_x(b_S^r) - \mathbf{A}_y\mathbf{E}_y(b_S^r) \\ + \mathbf{B}_x\mathbf{I}_{Sxr} - \mathbf{B}_y\mathbf{I}_{Syr}\end{aligned} \tag{A.20}$$

$$\begin{aligned}\mathbf{E}_y(b_S^s) = \mathbf{A}_x\mathbf{E}_y(b_S^r) + \mathbf{A}_y\mathbf{E}_x(b_S^r) \\ + \mathbf{B}_x\mathbf{I}_{Sxr} + \mathbf{B}_y\mathbf{I}_{Syr}\end{aligned} \tag{A.21}$$

$$\mathbf{I}_{Sxs} = \mathbf{C}\mathbf{E}_x(b_S^r) + \mathbf{D}\mathbf{I}_{Sxr} \tag{A.22}$$

$$\mathbf{I}_{Sys} = \mathbf{C}\mathbf{E}_y(b_S^r) + \mathbf{D}\mathbf{I}_{Syr} \tag{A.23}$$

where $S = X_{SL}, b_S^s = 2, b_S^r = 3$

$$\bar{\mathbf{A}}\begin{bmatrix}1 & 0 & 0\\ 0 & 1 & 0\\ 0 & 0 & 1\end{bmatrix}, \bar{\mathbf{B}}\begin{bmatrix}jX_{SLv}^a & 0 & 0\\ 0 & jX_{SLv}^b & 0\\ 0 & 0 & jX_{SLv}^c\end{bmatrix}, \mathbf{C}\begin{bmatrix}0 & 0 & 0\\ 0 & 0 & 0\\ 0 & 0 & 0\end{bmatrix}, \mathbf{D}\begin{bmatrix}1 & 0 & 0\\ 0 & 1 & 0\\ 0 & 0 & 1\end{bmatrix}$$

Hence, in total, SVC v corresponds to $3 + 3 + 1 + 24 = 31$ equality constraints.

A.8 Uniform Operation Constraints

If OLTC o or shunt capacitor SC or SVC v operate uniformly the following constraints must also be satisfied:

1. OLTC o

$$tap_{oa} = tap_{ob} = tap_{oc} \tag{A.24}$$

2. SC

$$sc^{2a} = sc^{2b} = sc^{2c} \tag{A.25}$$

3. SVC v

$$X^a_{SLv} = X^b_{SLv} = X^a_{SLv}. \tag{A.26}$$

$$Q^a_v = Q^b_v = Q^c_v \tag{A.27}$$

A.9 Sequence Voltage Constratins

Since voltage unbalance ratio is expressed in terms of positive and negative sequence voltages, the folowing constraints also apply for bus 1 and 2:

$$\begin{aligned}
E^1_{xi} &= \frac{1}{3}\left(E^{ia}_x + E^{ib}_x \cos 120^o - E^{ib}_y \sin 120^o + E^{ic}_x \cos 240^o - E^{ic}_y \sin 240^o\right) && \text{(A.28)}\\
E^1_{yi} &= \frac{1}{3}\left(E^{ia}_y + E^{ib}_y \cos 120^o + E^{ib}_x \sin 120^o + E^{ic}_y \cos 240^o + E^{ic}_x \sin 240^o\right) && \text{(A.29)}\\
E^2_{xi} &= \frac{1}{3}\left(E^{ia}_x + E^{ib}_x \cos 240^o - E^{ib}_y \sin 240^o + E^{ic}_x \cos 120^o - E^{ic}_y \sin 120^o\right) && \text{(A.30)}\\
E^2_{yi} &= \frac{1}{3}\left(E^{ia}_y + E^{ib}_y \cos 240^o + E^{ib}_x \sin 240^o + E^{ic}_y \cos 120^o + E^{ic}_x \sin 120^o\right) && \text{(A.31)}\\
& i \in \{1, 2\}
\end{aligned}$$

There only 2 three-phase buses in the network. Hence, in total, there are eight equality constraints correspond to sequence voltage of three-phase buses.

A.10 Inequality Constraints

Based on various physical and regulatory limits, the following inequality constraints are considered:

1. Voltage magnitude limits at all buses and phases including all load and SVC's dummy bus:

$$0.95 \leq |\bar{E}^{ip}| \leq 1.05, i \in \{2, 3\}, \forall p \in \{a, b, c\} \tag{A.32}$$

Hence, there are six inequalities corresponding to voltage magnitude limits.

2. Voltage magnitude limits for a node that is connected to the secondary terminal of OLTC [150]:

$$0.9 \leq |\bar{E}^p(b_o)| \leq 1.1, b_o = 1, \forall p \in \{a, b, c\} \tag{A.33}$$

Hence, there are three inequalities constraints correspond to the limits of magnitude of voltages at an OLTC's secondary terminal.

3. Positive-sequence voltage reference limit of SVC v:

$$0.95 \leq |\bar{E}_v^{ref}| \leq 1.05. \tag{A.34}$$

Hence, there is one inequality corresponding to the voltage reference of SVC v.

4. Reactive power limit of SVC:

$$Q_{vp}^{min} \leq Q_v^p \leq Q_{vp}^{max}, p \in \{a, b, c\} \tag{A.35}$$

Hence, there are three inequalities corresponding to the reactive power of SVC v.

5. limits on slope of SVC:

$$X_{SLp}^{v,min} \leq X_{SLv}^p \leq X_{SLp}^{v,max}, p \in \{a, b, c\} \tag{A.36}$$

Hence, there are three inequalities corresponding to the slope of SVC v.

6. Limit on tap position of OLTC:

$$tap_{op}^{min} \leq tap_{op}(h) \leq tap_{op}^{max}, p \in \{a, b, c\} \tag{A.37}$$

Hence, there are three inequalities corresponding to the position of the taps of OLTC o.

7. Limit on voltage balance factor U_2 for all three-phase buses:

$$0 \leq U_{2i} = 100\frac{|\bar{E}_i^2|}{|\bar{E}_i^1|} \leq U_2^{max}, i \in \{1, 2\} \tag{A.38}$$

Hence, there are two inequalities corresponding to voltage unbalance factor in the network.

Table A.1: Number of Equality Constraints

Equality Constraints		
Name	Number	Section
Nodal current balance	12	A.1
OLTC	24	A.2
Line	24	A.3
Load	6	A.4
Generator	6	A.5
Shunt capacitor	6	A.6
SVC	31	A.7
Uniform operation	4	A.8
Sequence Voltage	8	A.9
Total	127	

Finally, the voltage regulation problem of the network shown in Fig. A.1 can be formulated as Problem (P:simple). The corresponding number of equality and inequality constraints are given in Tables A.1 and A.2, respectively.

$$\begin{aligned} \underset{\mathbf{c},\mathbf{d}}{\text{minimize}} \quad & J \\ \text{subject to} \quad & (A.1) - (2.36), \end{aligned} \tag{P:simple}$$

Table A.2: Number of Inequality Constraints

Inequality Constraints		
Name	Number	Section
Voltage Magnitude	6	A.10
Voltage Magnitude of OLTC o	3	
Reference Voltage of SVCv	1	
Reactive Power of SVCv	3	
Slope of SVC v	3	
Position of taps of OLTC o	3	
Voltage unbalance factor	2	
Total	21	

B — Load and Generation Data for modified 123 bus

Table B.1: Load Data

	Load	P_L^{ia}	Q_L^{ia}	P_L^{ib}	Q_L^{ib}	P_L^{ic}	Q_L^{ic}
Bus (i)	Model	kW	kVAr	kW	kVAr	kW	kVAr
2	Y-PQ	40	20	0	0	0	0
4	Y-PR	0	0	0	0	40	20
5	Y-I	0	0	0	0	20	10
6	Y-Z	0	0	0	0	40	20
7	Y-PQ	0	0	20	10	0	0
8	Y-PQ	20	10	0	0	0	0
10	Y-PQ	0	0	20	10	0	0
11	Y-PQ	40	20	0	0	0	0
14	Y-PQ	0	0	0	0	40	20
15	Y-PQ	0	0	0	0	20	10
16	Y-Z	0	0	0	0	40	20
18	Y-PQ	40	20	0	0	0	0
22	Y-Z	0	0	40	20	0	0
24	Y-PQ	0	0	0	0	40	20
27	Y-PQ	0	0	0	0	40	20
28	Y-I	40	20	0	0	0	0
29	Y-Z	40	20	0	0	0	0
30	Y-PQ	40	20	0	0	0	0

to be continued in next page

	Load	P_L^{ia}	Q_L^{ia}	P_L^{ib}	Q_L^{ib}	P_L^{ic}	Q_L^{ic}
Node (i)	Model	kW	kVAr	kW	kVAr	kW	kVAr
31	Y-PQ	40	20	0	0	0	0
32	Y-I	40	20	0	0	0	0
33	D-PQ	40	20	0	0	0	0
35	Y-I	0	0	20	10	0	0
38	Y-Z	20	10	0	0	0	0
39	Y-PQ	0	0	20	10	0	0
39	Y-PQ	0	0	20	10	0	0
41	Y-Z	40	20	0	0	0	0
41	Y-PQ	0	0	0	0	20	10
42	Y-PQ	20	10	0	0	0	0
43	Y-Z	0	0	40	20	0	0
46	Y-I	0	0	20	10	0	0
47	Y-PQ	0	0	20	10	0	0
48	Y-I	20	10	0	0	0	0
49	Y-I	35	25	35	25	35	25
50	Y-PQ	20	10	0	0	0	0
51	Y-PQ	0	0	0	0	40	20
52	Y-Z	70	50	70	50	70	50
53	Y-PQ	35	25	70	50	35	20
54	Y-PQ	20	10	0	0	0	0
55	Y-PQ	0	0	0	0	75	35
56	Y-PQ	20	10	0	0	0	0
59	Y-Z	0	0	0	0	40	20
60	D-Z	35	25	35	25	70	50
62	Y-PQ	40	20	0	0	0	0
63	Y-I	0	0	75	35	0	0

to be continued in next page

	Load	P_L^{ia}	Q_L^{ia}	P_L^{ib}	Q_L^{ib}	P_L^{ic}	Q_L^{ic}
Node (i)	Model	kW	kVAr	kW	kVAr	kW	kVAr
64	Y-PQ	0	0	0	0	20	10
65	Y-PQ	40	20	0	0	0	0
67	Y-PQ	0	0	0	0	20	10
68	Y-PQ	0	0	0	0	40	20
70	Y-PQ	0	0	40	20	0	0
74	Y-PQ	0	0	0	0	40	20
75	Y-Z	0	0	0	0	40	20
76	Y-PQ	0	0	0	0	40	20
77	Y-PQ	0	0	40	20	0	0
78	Y-Z	40	20	0	0	0	0
79	Y-Z	0	0	0	0	40	20
81	D-I	105	80	70	50	70	50
82	Y-PQ	0	0	40	20	0	0
85	Y-PQ	40	20	0	0	0	0
87	Y-PQ	0	0	0	0	20	10
88	Y-PQ	0	0	0	0	40	20
89	Y-PQ	0	0	0	0	40	20
90	Y-PQ	20	10	0	0	0	0
91	Y-PQ	0	0	20	10	0	0
93	Y-PQ	0	0	40	20	0	0
94	Y-PQ	0	0	40	20	0	0
95	Y-PQ	40	20	0	0	0	0
96	Y-PQ	0	0	40	20	0	0
100	Y-I	0	0	40	20	0	0
102	Y-PQ	0	0	0	0	40	20
103	Y-PQ	40	20	0	0	0	0

to be continued in next page

	Load	P_L^{ia}	Q_L^{ia}	P_L^{ib}	Q_L^{ib}	P_L^{ic}	Q_L^{ic}
Node (i)	Model	kW	kVAr	kW	kVAr	kW	kVAr
105	Y-PQ	0	0	20	10	0	0
106	Y-PQ	0	0	20	10	0	0
107	Y-PQ	20	10	0	0	0	0
108	Y-PQ	40	20	0	0	0	0
109	Y-PQ	40	20	0	0	0	0
110	Y-PQ	40	20	0	0	0	0
112	Y-I	20	10	0	0	0	0
113	Y-PQ	20	10	0	0	0	0
114	Y-Z	40	20	0	0	0	0
115	Y-PQ	20	10	0	0	0	0
118	Y-PQ	0	0	0	0	20	10
119	Y-PQ	0	0	0	0	20	10
121	Y-I	40	20	0	0	0	0
124	Y-I	20	10	0	0	0	0
125	Y-Z	40	20	0	0	0	0
		1420	775	915	515	1155	630

Table B.2: Generation Data

	P_G^{ia}	P_G^{ib}	P_G^{ic}
Node (i)	kW	kW	kW
2	20	0	0
4	0	0	20
7	0	10	0
8	10	0	0
10	0	10	0

to be continued in next page

Bus (i)	P_G^{ia}	P_G^{ib}	P_G^{ic}
11	20	0	0
14	0	0	20
15	0	0	10
18	20	0	0
24	0	0	20
27	0	0	20
30	20	0	0
31	20	0	0
33	20	0	0
39	0	10	0
39	0	10	0
41	0	0	10
42	10	0	0
47	0	10	0
50	10	0	0
51	0	0	20
53	17.5	35	17.5
54	10	0	0
55	0	0	37.5
56	10	0	0
62	20	0	0
64	0	0	10
65	20	0	0
67	0	0	10
68	0	0	20
70	0	20	0
74	0	0	20

to be continued in next page

Bus (i)	P_G^{ia}	P_G^{ib}	P_G^{ic}
76	0	0	20
77	0	20	0
82	0	20	0
85	20	0	0
87	0	0	10
88	0	0	20
89	0	0	20
90	10	0	0
91	0	10	0
93	0	20	0
94	0	20	0
95	20	0	0
96	0	20	0
102	0	0	20
103	20	0	0
105	0	10	0
106	0	10	0
107	10	0	0
108	20	0	0
109	20	0	0
110	20	0	0
113	10	0	0
115	10	0	0
118	0	0	10
119	0	0	10
Total	387.5	235	345

C — Load Models in Cartesian Coordinates

This appendix presents equations for constant-power, constant-impedance and constant-current load models in Cartesian coordinate system. It is based on [150] which presents the same results using polar coordinate system. For easy reference, the main results are given in Table C.1.

C.1 Wye-Connected Loads

A complex load connected at phase p of bus i can represented as

$$\bar{S}^{ip} = |\bar{S}^{ip}|\angle\theta^{ip} = P^{ip} + jQ^{ip}$$

where $\bar{S}^{ip}$ is the complex power of load connected at phase p of bus i; θ^{ip} is its power factor angle; P^{ip} is its real part and Q^{ip} is its reactive part. Irrespective of their types, loads are often given in terms of their rated power $\bar{S}_0 = P_0 + jQ_0$.

C.1.1 Constant-Power Load

In a constant power load model, $\bar{S} = P + jQ$, real P and reactive Q power are assumed to be constant.

$$\bar{I}_{CP} = \left(\frac{\bar{S}}{\bar{E}}\right)^* = \left(\frac{P+jQ}{E_x+jE_y}\right)^* = \frac{P-jQ}{E_x-jE_y} = \left(\frac{P-jQ}{E_x-jE_y}\right)\left(\frac{E_x+jE_y}{E_x+jE_y}\right)$$

$$\begin{aligned}
\bar{I} &= \frac{(P-jQ)(E_x+jE_y)}{E_x^2+E_y^2} \\
&= \frac{(PE_x+QE_y)+j(PE_y-QE_x)}{E_x^2+E_y^2} \\
&= \frac{(PE_x+QE_y)}{E_x^2+E_y^2} + j\frac{(PE_y-QE_x)}{E_x^2+E_y^2} \\
&= I_x + jI_y
\end{aligned}$$

Table C.1: Equality constraints of various load types.

Load Types	Equality Constraints	parameters
Constant power	$I_{x,CP} = \frac{P_{CP}E_x + Q_{CP}E_y}{E_x^2+E_y^2}$ $I_{y,CP} = \frac{P_{CP}E_y - Q_{CP}E_x}{E_x^2+E_y^2}$	P_{CP}, Q_{CP}
Constant impedance	$I_{x,CZ} = \frac{E_x r + E_y x}{r^2+x^2}$ $I_{y,CZ} = \frac{E_y r - E_x x}{r^2+x^2}$	$r = \frac{P_{CZ0}\lvert\bar{E}_0\rvert^2}{{P_{CZ0}}^2+{Q_{CZ0}}^2}$ $x = \frac{Q_{CZ0}\lvert\bar{E}\rvert^2}{{P_{CZ0}}^2+{Q_{CZ0}}^2}$
Constant current	$\lvert\bar{I}_0\rvert = I_{x,CI}^2 + I_{y,CI}^2$ $E_y I_{x,CI} - E_x I_{y,CI} = (E_x I_{x,CI} + E_y I_{y,CI})\frac{Q_{CI0}}{P_{CI0}}$	$\lvert\bar{I}_0\rvert = \frac{\sqrt{(P_{CI0})^2+(Q_{CI0})^2}}{\sqrt{(E_{x0})^2+(E_{y0})^2}}$
Shunt Capacitor	$I_x = \frac{sc}{n_c}\frac{+E_y}{x}$ $I_y = sc\frac{-E_x}{x}$	$r = 0$ and $x < 0$ $sc \in \{0, 1, ..., n_c\}$
Shunt Reactor	$I_x = sr\frac{+E_y}{x}$ $I_y = sr\frac{-E_x}{x}$	$r = 0$ and $x > 0$ $sr \in \{0/n_c, 1/n_c, ..., n_c/n_c\}$

Then, the following equalities can be used to model constant power load:

$$I_x = \frac{PE_x + QE_y}{E_x^2 + E_y^2} \tag{C.1}$$

$$I_y = \frac{PE_y - QE_x}{E_x^2 + E_y^2} \tag{C.2}$$

In this thesis, Eqs. (C.1) and (C.2) are the equality contraints of a constant-power load.

C.1.2 Constant-Impedance Load

For a constant-impedance load, $\bar{Z} = r + jx$, resistance r and reactance x are assumed to be constant. Their values can be calculated as follows

$$\begin{aligned}
\bar{Z}_p &= \frac{|\bar{E}_{p-n0}|^2}{\bar{S}_{p0}^*} \\
&= \frac{|\bar{E}_{p-n0}|^2}{P_0 - jQ_0} \\
&= \frac{|\bar{E}_{p-n0}|^2}{P_0 - jQ_0} \times \frac{P_0 + jQ_0}{P_0 + jQ_0} \\
&= \frac{P_0|\bar{E}_{p-n0}|^2}{{P_0}^2 + {Q_0}^2} + j\frac{Q_0|\bar{E}_{pn}|^2}{{P_0}^2 + {Q_0}^2} \\
&= r + jx
\end{aligned}$$

where $|\bar{E}_{p-n0}|$ is the rated line-to-ground voltage magnitude. Hence, the resistance and reactance can be calculated using

$$r = \frac{P_0|\bar{E}_{p-n0}|^2}{{P_0}^2 + {Q_0}^2}, \text{ and} \tag{C.3}$$

$$x = \frac{Q_0|\bar{E}_{p-n0}|^2}{{P_0}^2 + {Q_0}^2}. \tag{C.4}$$

The complex current flowing into a constant-impedance load then can be calculated as follows

$$\begin{aligned}
\bar{I} &= \frac{\bar{E}}{\bar{\bar{Z}}} \\
&= \frac{E_x + jE_y}{r + jx} \\
&= \frac{E_x + jE_y}{r + jx}\frac{r - jx}{r - jx} \\
&= \frac{(E_x r + E_y x) + j(E_y r - E_x x)}{r^2 + x^2}
\end{aligned}$$

Hence, the real and reactive current can be written as

$$I_x = \frac{E_x r + E_y x}{r^2 + x^2} \tag{C.5}$$

$$I_y = \frac{E_y r - E_x x}{r^2 + x^2} \tag{C.6}$$

In this thesis, Eqs. C.5 and (C.6) are the equality constraints for a constant-impedance load.

C.1.3 Shunt Capacitor and Reactor

A shunt capacitor can be modeled as a constant-impedance load with zero impedance $r = 0$ and negative reactance $x < 0$. Similarly, a shunt reactor can also be modeled as a constant-impedance load with zero impdance $r = 0$ and positive reactance $x > 0$. This means that Eqs. (C.5) and (C.6) reduce into

$$I_x = \frac{+E_y x}{x^2} = \frac{+E_y}{x} \tag{C.7}$$

$$I_y = \frac{-E_x x}{x^2} = \frac{-E_x}{x} \tag{C.8}$$

As expected, if $x < 0$ ($x > 0$) then Eqs. (C.7) and C.8 indicate that the complex current, $I_x + jI_y$, is leading (lagging) the complex voltage, $E_x + jE_y$ by 90^0. In addition, $I_x \neq 0 \iff E_y \neq 0$ and $I_y \neq 0 \iff E_x \neq 0$.

Note that pure reactance load does not consume real power as shown below in Eq. (C.9).

$$\begin{aligned}
\bar{S} &= \bar{E}\bar{I}^* \\
&= (E_x + jE_y)(I_x + jI_y)^* \\
&= (E_x + jE_y)(I_x - jI_y) \\
&= (E_x + jE_y)(\frac{E_y}{x} - j(\frac{-E_x}{x})) \\
&= (E_x + jE_y)(\frac{E_y}{x} + j\frac{E_x}{x}) \\
&= \frac{E_x E_y - E_x E_y}{x} + j\frac{E_x E_x + E_y E_y}{x} \\
&= j\frac{E_x E_x + E_y E_y}{x}
\end{aligned} \tag{C.9}$$

However, this does not mean $I_x = 0$ as indicated by (C.7).

For a capacitor bank have n_c uniform capacitors, the currents can be calculated using

$$\begin{aligned} I_x &= sc\frac{+E_y}{x} && \text{(C.10)} \\ I_y &= sc\frac{-E_x}{x} && \text{(C.11)} \\ sc &\in \{0/n_c, 1/n_c, ..., n_c/n_c\} && \text{(C.12)} \end{aligned}$$

Note that the reactance x is calculated based on the total capacitance of the bank. For example, if $n_c = 5$ then $sc \in \{0, 0.125, 0.25, ..., 1\}$. In general, sc has $n_C + 1$ possible discrete values.

In these thesis, Eqs. (C.10) and (C.11) are the equality constraints of a capacitor bank.

C.1.4 Constant Current

In a constant current load model, $\bar{I} = |\bar{I}|\angle(\delta - \theta)$, the magnitude $|\bar{I}|$ and load power factor angle θ are assumed to be constant. The voltage angle δ varies in such a way the the magnitude of current and the power factor of load are constant. Given the rated power of constant current load $P_{CI0} + jQ_{CI0}$, the two constants can be calculated using

$$\begin{aligned} |\bar{I}_0| &= \sqrt{I_x^2 + I_y^2} \\ &= \sqrt{\frac{(P_{CI0}E_{x0} + Q_{CI0}E_{y0})^2 + (P_{CI0}E_{y0} - Q_{CI0}E_{x0})^2}{((E_{x0})^2 + (E_{y0})^2)^2}} \\ &= \frac{\sqrt{(P_{CI0}E_{x0} + Q_{CI0}E_{y0})^2 + (P_{CI0}E_{y0} - Q_{CI0}E_{x0})^2}}{(E_{x0})^2 + (E_{y0})^2} \\ &= \frac{\sqrt{((P_{CI0})^2 + (Q_{CI0})^2)((E_{y0})^2 + (E_{x0})^2)}}{(E_{x0})^2 + (E_{y0})^2} \\ &= \frac{\sqrt{(P_{CI0})^2 + (Q_{CI0})^2}}{\sqrt{(E_{x0})^2 + (E_{y0})^2}} \end{aligned} \qquad \text{(C.13)}$$

and

$$\theta_0 = \arctan\left(\frac{Q_0}{P_0}\right) = \text{constant.}$$

Furthermore, using the above constants, the following equalities follows:

$$\begin{aligned} \bar{I} &= I_x + jI_y \\ |\bar{I}_0| &= I_x^2 + I_y^2 && \text{(C.14)} \end{aligned}$$

$$
\begin{aligned}
E_y I_x - E_x I_y &= (E_x I_x + E_y I_y) \tan\theta_0 \\
&= (E_x I_x + E_y I_y) \frac{Q_o}{P_0} \qquad \text{(C.15)}
\end{aligned}
$$

In this thesis, Eqs. (C.14), (C.15) are the equality constraints of a contant-current load.

C.2 Delta Connected Loads

Delta-connected loads have similar equations as wye-connected loads. The main different is that here the voltages are line-to-line voltages. For example, for a constant-power load connected between phase a and phase b of bus, the real and reactice currents can be calculated using

$$
I_{xab} = \frac{P E_{xab} + Q E_{yab}}{E_{xab}^2 + E_{yab}^2} \qquad \text{(C.16)}
$$

$$
I_{yab} = \frac{P E_{yab} - Q E_{xab}}{E_{xab}^2 + E_{yab}^2}. \qquad \text{(C.17)}
$$

The current enthering a delta connected load can be calculated using

$$
\begin{bmatrix} \bar{I}_a \\ \bar{I}_b \\ \bar{I}_c \end{bmatrix} = \begin{bmatrix} 1 & 0 & -1 \\ -1 & 1 & 0 \\ 0 & -1 & 1 \end{bmatrix} \begin{bmatrix} \bar{I}_{ab} \\ \bar{I}_{bc} \\ \bar{I}_{ca} \end{bmatrix} \qquad \text{(C.18)}
$$

Similar approach can be applied for constant-impedance and constant-current loads, shunt capacitors, shunt reactors, and distributed generation connected in delta.